



Production of autoclaved aerated concrete with silica raw materials of a higher solubility than quartz

Taban Shamshejani

Vollständiger Abdruck der von der TUM School of Engineering and Design der Technischen Universität München zur Erlangung des akademischen Grades einer

Doktorin der Ingenieurwissenschaften (Dr.-Ing.)

genehmigten Dissertation.

Vorsitz:

Prof. Dr. Alisa Machner

Prüfende der Dissertation:

1. Prof. Dr.-Ing. Detlef Heinz
2. Prof. Dr.-Ing. Karl-Christian Thienel

Die Dissertation wurde am 20.06.2022 bei der Technischen Universität München eingereicht und durch die TUM School of Engineering and Design am 29.09.2022 angenommen.

This is a version of the above-named Dissertation that is optimized for digital use. It provides internal cross-references (Chapters, Figures, References, etc) and redirection of web links (URLs and DOIs).

Abstract

If the silica raw material used in autoclaved aerated concrete (AAC) requires a lower level of energy for dissolution, a lower autoclaving temperature might be applied to reach the required product performance. Accordingly, the raw material quartz sand within the AAC mixture was replaced with calcined diatomaceous earth (C-DE) and rice husk ash (RHA) which have a higher solubility of silica at elevated temperatures in alkaline binder systems.

The autoclaving process was conducted using an autoclave at various temperatures of $T = 134\text{--}192\text{ }^{\circ}\text{C}$ and a corresponding steam pressure of $P = 2\text{--}12$ bar with a total autoclaving duration of 9 hours. Quantitative X-ray diffraction (XRD) analysis according to Rietveld refinement, qualitative XRD analysis, scanning electron microscopy (SEM), differential thermal analysis (DTA), and thermogravimetric analysis (TGA) were carried out to investigate the resultant phase compositions and microstructures of the hardened AAC samples. Additionally, the compressive strength, dry bulk density, A-value, and total drying shrinkage of AAC samples were determined.

The results of this study showed that the C-DE-based AAC and the RHA-based AAC behaved differently than the quartz-based AAC at different autoclaving temperatures. In contrast to the quartz-based AAC, the properties of the C-DE-based AAC and RHA-based AAC were improved by applying a lower autoclaving temperature than the typical temperature used for industrial production of AAC, i.e. $192\text{ }^{\circ}\text{C}$. The most favorable properties of the quartz-based were observed at the autoclaving temperature of $T = 192\text{ }^{\circ}\text{C}$. However, for the C-DE-based AAC, this temperature range was $T = 152\text{--}165\text{ }^{\circ}\text{C}$. Interestingly still, the performance of the C-DE-based AAC autoclaved at $134\text{ }^{\circ}\text{C}$ was greater than that autoclaved at $192\text{ }^{\circ}\text{C}$. In the case of the RHA-based AAC, the optimum properties were observed at the autoclaving temperature of $T = 165\text{--}175\text{ }^{\circ}\text{C}$.

Moreover, the C-DE-based AAC autoclaved at $165\text{ }^{\circ}\text{C}$ exhibited an A-value which was 54 % higher than that of the quartz-based AAC autoclaved at $192\text{ }^{\circ}\text{C}$. The RHA-based AAC autoclaved at $165\text{ }^{\circ}\text{C}$ exhibited almost the same A-value as that of the quartz-based AAC autoclaved at $192\text{ }^{\circ}\text{C}$. However, a higher total drying shrinkage was observed for the C-DE-based AAC and RHA-based AAC autoclaved at $165\text{ }^{\circ}\text{C}$ compared to that for the quartz-based AAC autoclaved at $192\text{ }^{\circ}\text{C}$. This was due to the higher portion of non-crystalline C-S-H in those AAC samples compared to the quartz-based AAC autoclaved at $192\text{ }^{\circ}\text{C}$.

From a general point of view, the results showed that the optimum temperature for autoclaving AAC has a direct dependency on the dissolution behavior of silica raw materials used in the mixture. In the case of using a silica material with different dissolution properties from that of quartz sand in the AAC mixture, applying the typical autoclaving temperature will not necessarily lead to the optimum properties and indeed an adequate adaptation of the autoclaving temperature is required to achieve the optimum performance of the product.

Zusammenfassung

Wenn das für Porenbeton verwendete Kieselsäure-Rohstoffen einen geringeren Energieaufwand zur Auflösung benötigt, kann eine niedrigere Autoklaventemperatur angewendet werden, um die erforderliche Produktleistung zu erreichen. Dementsprechend wurde der Rohstoff Quarzsand in der Porenbetonmischung durch kalzinierte Diatomeenerde (C-DE) bzw. Reishülsenasche (RHA) ersetzt, die in alkalischen Bindemittelsystemen eine höhere Löslichkeit von Kieselsäure bei erhöhten Temperaturen aufweisen.

Der Autoklavierprozess wurde in einem Autoklaven bei verschiedenen Temperaturen von $T = 134\text{--}192\text{ °C}$ und einem entsprechenden Dampfdruck von $P = 2\text{--}12\text{ bar}$ mit einer Gesamtautoklavierdauer von 9 Stunden durchgeführt. Quantitative Röntgenbeugungsanalyse (XRD) mittels Rietveld-Verfeinerung, qualitative XRD-Analyse, Rasterelektronenmikroskopie (REM), Differentialthermoanalyse (DTA) und thermogravimetrische Analyse (TGA) wurden angewandt, um die resultierenden Phasenzusammensetzungen und das Gefüge der gehärteten Porenbetonproben zu untersuchen. Außerdem wurden die Druckfestigkeit, die Trockenrohichte, die A-Zahl und die Gesamttrockenschwindung der hergestellten Porenbetonproben bestimmt.

Die Ergebnisse dieser Studie zeigten, dass Porenbeton auf C-DE-Basis und Porenbeton auf RHA-Basis bei unterschiedlichen Autoklavierungstemperaturen ein anderes Verhalten als Porenbeton auf Quarzbasis aufweisen. Im Gegensatz zur quarzbasierten Mischung verbesserten sich die Porenbetoneigenschaften mit den Mischungen auf C-DE-Basis und RHA-Basis bei Anwendung einer niedrigeren Autoklavierungstemperatur als der für die industrielle Produktion üblichen Temperatur von 192 °C . Die günstigsten Eigenschaften der Porenbetonmischung auf Quarzbasis wurden bei einer Autoklaviertemperatur von $T = 192\text{ °C}$ beobachtet. Bei der Porenbetonmischung auf C-DE-Basis lag dieser Temperaturbereich jedoch bei $T = 152\text{--}165\text{ °C}$. Interessanterweise war die Leistung der bei 134 °C autoklavierten Porenbetonmischung auf C-DE-Basis besser als die bei 192 °C autoklavierte. Bei der Porenbetonmischung auf RHA-Basis wurden die optimalen Eigenschaften bei einer Autoklavierungstemperatur von $T = 165\text{--}175\text{ °C}$ beobachtet.

Außerdem wies die bei 165 °C autoklavierte Porenbetonmischung auf C-DE-Basis eine A-Zahl auf, die 54 % höher war als der bei 192 °C autoklavierten Porenbetonmischung auf Quarzbasis. Die bei 165 °C autoklavierte Porenbetonmischung auf RHA-Basis wies fast die gleiche A-Zahl auf wie die bei 192 °C autoklavierte Porenbetonmischung auf Quarzbasis. Allerdings wurde bei der bei 165 °C autoklavierten Porenbetonmischung auf C-DE-Basis und der Porenbetonmischung auf RHA-Basis eine höhere Gesamttrockenschwindung gegenüber der bei 192 °C autoklavierten Porenbetonmischung auf Quarzbasis beobachtet. Dies ist auf den höheren Anteil an nicht kristallinem C-S-H in diesen Porenbetonproben im Vergleich zu der bei 192 °C autoklavierten Porenbetonmischung auf Quarzbasis zurückzuführen.

Generell haben die Ergebnisse gezeigt, dass die optimale Temperatur für das Autoklavieren von Porenbeton direkt vom Auflösungsverhalten der in der Mischung verwendeten Silica-Rohstoffe abhängt. Bei der Verwendung eines Kieselsäure-Rohstoffes mit einer anderen Auflösungsrate und Löslichkeit als die des Quarzsandes in der Porenbetonmischung führt die Anwendung der typischen Autoklavierungstemperatur nicht unbedingt zu optimalen

Eigenschaften, und in der Tat ist eine angemessene Anpassung der Autoklavierungstemperatur erforderlich, um die optimalen Eigenschaften des Produkts zu erreichen.

Acknowledgments

Here I would like to acknowledge some of the people who made it possible and easier for me to start, do, and finish my PhD. My sincere appreciation goes to my wise team of supervisors. I would like to give my supervisor Prof. Detlef Heinz my gratitude for his great guidance, support, and all his valuable feedbacks. My special thanks go to Dr. Georg Schober for passing his many years of experience in the field of autoclaved aerated concrete to me. His dedication to this study and the very fruitful discussions are highly appreciated. I would like to thank my mentor, Dr. Severin Seifert, for his temperate arrangement and all his help and time spent assisting me.

I would like to thank all members of the Department of Inorganic Materials & Recycling of IBP group, who were always warm, friendly, and ready to help, especially, Dr. Volker Thome, Dr. Sebastian Dittrich, Christine Kalina, Katrin Scherer, and Florian Heß.

Importantly, I would like to thank, my dear parents who always support me without any expectation with their unconditional love and my siblings, Taravat, Paridokht, and Behniya who always think and believe in me. My special gratitude goes to my husband, Ali, for all of his never-ending support, dedication, and especially his encouragement which was very motivating for me.

Content

1 Introduction	1
2 Literature Review.....	3
2.1 Autoclaved Aerated Concrete	3
2.1.1 History.....	3
2.1.2 Manufacture	3
2.1.3 Constituent materials.....	3
2.1.4 Mix design.....	4
2.1.5 Process of production	6
2.2 Chemical transformations during the production of ACC	9
2.2.1 Chemical reactions before autoclaving	9
2.2.2 Chemical reactions at the beginning of the autoclaving process	10
2.2.3 Phases present in the final product.....	11
2.3 Structure of AAC	13
2.4 Properties of AAC.....	15
2.4.1 Bulk density.....	15
2.4.2 Thermal conductivity	16
2.4.3 Compressive strength	16
2.4.4 Shrinkage.....	20
2.5 Opportunity to save energy during hydrothermal treatment of AAC	21
2.5.1 Dissolution of silica.....	22
2.5.2 Lime-silica system.....	23
2.5.3 Behavior of various types of silica materials in AAC.....	27
2.5.4 Limitation of knowledge	30
2.6 Aims and research objectives	32
2.7 Thesis outline	33
3 Material and Methods.....	36
3.1 Characterization of the raw materials.....	36
3.1.1 Materials sources.....	36
3.1.2 Chemical compositions and physical properties	37
3.1.3 Mineral composition and microstructure	39
3.2 Procedure of producing AAC samples.....	41
3.3 Issues during the production of samples	44
3.4 Methods.....	45

3.4.1	Compressive strength	45
3.4.2	X-ray diffraction (XRD) analysis	46
3.4.3	X-ray fluorescence (XRF) analysis	47
3.4.4	Scanning Electron Microscope (SEM)	48
3.4.5	Thermal analyses	49
3.4.6	Laser diffractometry	49
3.4.7	Shrinkage	49
3.4.8	Bulk density	51
4	Results and Discussion	53
4.1	Behavior of C-DE and RHA in AAC	53
4.1.1	Influence of C-DE and RHA on the mineralogical composition of AAC.....	53
4.1.2	Influence of C-DE and RHA on the performance of AAC characterized by the compressive strength and shrinkage behaviors	54
4.2	Performance of the quartz-based AAC, C-DE-based AAC, and RHA-based AAC under different autoclaving temperatures	57
4.2.1	Mineralogical phase composition of the quartz-based AAC, C-DE-based, and RHA-based AAC at various autoclaving temperatures	57
4.2.2	Compressive strength and shrinkage behaviors of the quartz-based AAC, C-DE-based AAC, and RHA-based AAC at various autoclaving temperatures	61
5	Conclusion and Outlook.....	65
5.1	Conclusion	65
5.1.1	Possibility to reduce energy consumption in AAC production	66
5.1.2	Properties of raw materials which can be used as silica materials of a higher solubility than quartz to meet the objectives of this study	69
5.2	Outlook for future research.....	69
A	Supporting Information on Chapter 4.....	71
A.1	Publication 1	71
A.2	Publication 2	88
A.3	Publication 3	100
B	Permission to Reprint Figures in Chapter 2.....	129
	List of Figures	131
	List of Tables.....	133
	References.....	134

Glossary

Autoclaving

The final step of AAC production is autoclaving which is carried out in an autoclave under saturated steam conditions.

A-value

A-value is a dimensionless parameter of compressive strength that is used to compare the compressive strength of the AAC products with different bulk densities from 400 to 750 kg/m³. A-value is between 600 and 1400 for standard AAC products.

Blowing out

The blowing out begins after ending the expansion by appearing small openings on the surface of the mass. Hydrogen gas, which accumulates below the surface, escapes through those small openings on the surface which induces a sinking back of the expanded volume for a certain amount depending on its height.

Cake, green cake

The expanded solid cake-like block obtained by storing the expanded mixture for a couple of hours is called cake or green cake which is composed of different amounts of gas bubbles depending on its density.

Cement chemistry notation

In this study, cement chemistry notation is used in which C, S, A, H, and F stand, respectively, for CaO, SiO₂, Al₂O₃, H₂O, and Fe₂O₃.

Dwell time

The duration in which the sample is being autoclaved at constant maximum temperature (or pressure) is called dwell time which usually takes from 5 to 9 h.

Expanding process

The expanding process begins immediately after casting by swelling of the mixture in the mold due to the reaction of aluminum under alkaline conditions which produces hydrogen gas. The expansion process could take only 15 minutes or up to 60 minutes depending on the type of the mixture, i.e. lime-rich or cement-rich, casting temperature, the specific surface area of aluminum particles, and other circumstances.

Expansion crack

The expansion crack can occur in AAC at the end of the expanding process due to the accumulation of gases that could not escape out of the green cake.

Macro-pores

The air pores are generated due to the reaction of aluminum under alkaline condition and the formation of hydrogen gas as the reaction product. In this study, these large air pores are called macro-pores which are defined as roughly spherical pores with a diameter of $D > 100 \mu\text{m}$.

Micro-pores

The porosity in the solids material structure surrounding the macro-pores is made up of mostly irregular pores which are referred to as micro-pores in this study.

Introduction

Climate change and global warming have led topics such as the “ecology movement” or the “Green movement” to become the highest of priorities in recent years. The building materials field is also strongly affected because of its huge extent and its great demand for energy and raw materials. Consequently, “Sustainable building” or “Green building” has attracted more attention. Autoclaved Aerated Concrete (AAC) is a lightweight cellular material which has great potential for use in the “Sustainable building” due to its environmentally friendly properties such as excellent thermal insulation [1, 2] and lower embodied energy compared to other building materials, e.g. ordinary concrete and brick [4, 6]. Moreover, it provides an opportunity for the application of recycled and waste materials in large quantities. Therefore, a better understanding of AAC is essential in order to develop it into a more sustainable building material for the future.

An improvement in the sustainability of AAC products can mainly be achieved by reducing energy consumption along with the carbon dioxide emission related thereto. Around 25–27 % of the total energy consumption in AAC production is associated with the autoclaving process [7–10]. The autoclaving process includes the hydrothermal treatment of AAC mixture at elevated temperature, typically around 180–200 °C and a corresponding pressure of 9–14 bar in a saturated steam condition. The autoclaving process is an essential step in the production of AAC since it affects the product properties significantly [11, 12]. A reduction in the required autoclaving temperature and/or time would provide subsequent environmental and economic advantages. Moreover, around 45–50 % of the total energy consumption in AAC production is associated with the embodied energy of raw materials which is mainly determined by the content of binder, i.e. cement and lime in the AAC mixture [7–10]. Accordingly, if a reduction in the required autoclaving temperature and/or time is accompanied by a reduction in the binder content, the total energy consumption in the production of AAC will be reduced considerably.

Introduction

Declaration: The content of chapter 2 is partially identical to the scientific articles published by the author.

Literature Review

2.1 Autoclaved Aerated Concrete

2.1.1 History

AAC is a lightweight building material used in buildings for specific applications such as insulation and structural purposes [11, 13]. The method for producing AAC was first patented by the Swedish inventor Dr. Johan Axel Eriksson in 1924. In 1929, the production of AAC on large scale was started in Sweden. Shortly afterward AAC became an accepted building material and was manufactured in other European countries such as Germany and the Netherlands [14, 16].

2.1.2 Manufacture

AAC products are mainly manufactured as blocks for masonry and prefabricated slabs for walls, floors, and roofs. The prefabricated panels of AAC could be steel-reinforced or fiber-reinforced. The steel-reinforced AAC includes internal reinforcement with either ripped or smooth structural steel bars. However, fiber-reinforced AAC contains fibers such as polypropylene, carbon, basalt, and glass fiber [17–19].

AAC products are manufactured in a wide density range of 200–1000 kg/m³ with different qualities [20]. The production of AAC with density grades of below 200 kg/m³, e.g. 100 kg/m³ and 150 kg/m³, was reported as well [21]. Among AAC products with various densities, those with a bulk density of higher than 350 kg/m³ can be used for load-bearing purposes. Depending on the bulk density, around 30–85 % of the total volume of AAC is composed of air pores resulting in high porosity of the products [21]. High porosity is a prominent property of AAC which provides the main advantages of the product, i.e. low density and excellent thermal insulation.

2.1.3 Constituent materials

The main components used to produce AAC are quartz sand as a SiO₂ source, lime and cement as a CaO source, and a small amount of aluminum powder or paste as a pore-forming agent [12]. However, almost all of the current produced AAC contains sulfate carriers (i.e. gypsum and anhydrite) as well [21]. Sulfates in the AAC mixture regulate the setting of the mixture and improve the properties of this material. Reducing the sulfate content in the AAC mixture leads to increased shrinkage and reduced compressive strength [21–24]. In addition to the raw materials mentioned, ground recycled AAC (GRA) obtained from grinding waste AAC is effectively used as an environmentally friendly and economical filler in the industrial production of AAC [25]. GRA is the waste resulting from the manufacturing process of AAC

Literature Review

which is already steam cured or returned from construction sites. In some countries, returned AAC materials from demolished AAC buildings are also used as GRA.

In addition to quartz sand, waste industrial by-products such as fly ash and oil shale combustion residue are frequently used as silica materials for AAC production. Oil shale was the first material used as a silica source in the AAC mixture when the production of AAC was started in Sweden [26]. However, one of the main reasons for using fly ash in AAC production is that fly ash does not need to be ground. Although some cleaning, drying, or sieving processes might be necessary for fly ash, the process of grinding quartz sand is still much more expensive [27, 28]. On the other hand, impurities and additional ingredients which are present in fly ash could reduce the compressive strength of AAC. It was also reported that using a high amount of fly ash increases the shrinkage of AAC as a result of increasing proportions of semi-crystalline C-S-H phases [29–32].

The porous structure of AAC is obtained by the chemical reaction of aluminum powder/paste under an alkaline condition which generates hydrogen gas as a reaction product. This causes an expansion of the mixture to a higher volume depending on the desirable bulk density. After escaping from the mixture, hydrogen gas is replaced by air and as a result, a highly porous structure is left [22, 33, 20, 14].

2.1.4 Mix design

AAC mix designs are characterized by comparing some characteristic parameters including water to solid ratio (W/S), the total amount of binder, molar CaO/SiO₂-ratio (C/S), and cement/lime (c/l) of the starting materials. These aforementioned factors have a determining effect on the final properties of AAC. Therefore, they should be taken into consideration while determining AAC mix design.

The water content in the AAC mixture is represented by the W/S. Unlike ordinary concrete, W/S is more critical than the water-to-cement ratio (W/C) for AAC. The W/S should be adjusted according to the consistency of the fresh mix to obtain the proper viscosity of the mixture. Adjusting the W/S to too high values may cause an expansion (rising) of the AAC mixture with a very high speed which results in a green body with low stability and ruptured air pores structure. On the other hand, in the case of using a very low W/S, the generation of air pores would be hindered significantly due to the high viscosity of the AAC mixture. It should be noted that adjustment of characteristic parameters for obtaining a proper expanding process is always a matter of trial-and-error as there are a high number of influencing parameters, e.g. fineness of powders, the reactivity of lime, and aluminum, W/S, and the temperature of components, in this process step.

The temperature of the AAC mixture can be adjusted by adjusting the temperature of the mixing water. The appropriate water temperature can be demonstrated experimentally [26, 34, 35].

The binder content, which includes the amount of lime and cement, determines the quantity and crystallinity of tobermorite and other C-S-H formed in the AAC. Tobermorite is a crystallized C-S-H phase with a favorable cementation property which could be obtained by the hydrothermal treatment of the AAC mixture. This hydrothermal product appears as the main binding phase in AAC offering strength and durability [20, 36, 37]. The high compressive strength of AAC could be achieved by a high quantity of tobermorite with a

high degree of crystallinity [38–42]. However, this is not the only factor that affects the mechanical properties of AAC significantly. Therefore, the required amount of binder in the AAC mixture mainly depends on the desirable strength-density grade of the product.

The molar C/S of the starting material is defined by the ratio of the molar amount of active CaO in raw materials which are present in the mix design, e.g. lime and cement, to the molar amount of SiO₂ contributed by the existing raw materials, e.g. quartz sand, fly ash and cement. The C/S of the starting material influences phase formation and the micro-morphology of crystalline phases significantly [43–49]. Thus, it is needed to adjust the C/S of the starting in a way that leads to optimum final properties for AAC products. However, it is almost impractical to define a specific range as the optimum C/S of the starting materials since the C/S ratio of the starting materials is influenced significantly by some other circumstances, e.g. type of silica sources, type of CaO sources, the temperature of the environment, etc. For this reason, the reported ranges for the optimum C/S ratio are not in agreement with each other in all cases [41, 43, 44, 50]. On the other hand, most researchers have studied the C/S ratio in the synthesized C-S-H system [51–55]. However, the results of the works on the synthesized C-S-H system might not be directly applied to AAC products in practice. Assarsson [56–58] studied the hydrothermal reactions of calcium hydroxide with both amorphous and crystalline silica comprehensively. Based on Assarsson's studies, starting materials with C/S of 0.67–1.25 might lead to tobermorite. In another study [43], Sato et al. observed that C-S-H synthesized with C/S > 1 crystallized into tobermorite, while those with C/S < 1 did not transform into tobermorite. On the contrary, Taylor [50] stated that C-S-H is crystallized to tobermorite only when it is prepared with C/S < 1. Most studies have reported the formation of tobermorite from C-S-H with a synthesizing C/S of 0.8–1 [39, 51, 52, 59]. However, the starting C/S of 0.8–1 does not necessarily result in the formation of tobermorite. Mitsuda et al. [44] reported that a mixture of quartz sand and lime with a starting C/S of 0.8 led to the formation of initial C-S-H with C/S of 1.69 which crystallized into tobermorite with a C/S of 0.9. In comparison, for a mixture of silicic acid and lime with the same starting C/S, the initial C-S-H reached the C/S of 0.8 very fast and does not crystallize to tobermorite in the next steps. Therefore, in determining the starting C/S of AAC all the influencing parameters, such as the type of silica source should be considered.

Previous studies [52, 60–63] have reported that the introduction of aluminum to the AAC mixture has a significant effect on tobermorite formation, its structure, and cell parameters. Therefore, in the case of introducing aluminum-containing materials into the AAC mixture, e.g. fly ash and slag, the molar C/ (A+S) and A/ (A+S) might also be used to characterize the AAC mix design. The molar C/ (A + S) of 0.48–0.83 have been mostly adopted in the literature [12, 64–67]. The minimum A/ (A+S) used to investigate the influence of aluminum on calcium silicate hydrate was 0.05. However, significant changes in tobermorite structure can be observed at A/ (A+S) ≥ 0.1 [52, 68–70].

Different production technologies are used for the manufacture of AAC products. As a consequence, it is needed to adapt AAC mix designs to the certain type of production technology used in each factory. For the type of production technology which is necessary to lift the green cake after demolding, the green cake must have a certain hardness to be transported. Accordingly, higher content of cement is required to use in AAC mix design in order to reach a proper hardness of the green cake. In this case, the mix design is

Literature Review

characterized as cement-based or cement-rich, i.e. cement/lime ratio (c/l) > 1 . On the other hand, for some other types of production technology, there is no need to make the green cake harder for displacing or cutting process. The mix designs adapted to this type of production technology contain less cement and could be lime-based or lime-rich, i.e. $c/l < 1$. Therefore, c/l is an important ratio to characterize AAC mix designs. Nowadays, AAC mix designs are mostly cement-rich with c/l above 1 up to 5. For most of the lime-based mix designs, a c/l ratio of 0.7 is applied. However, a c/l ratio of 0.4 could also be used for the mix designs with an especially high content of lime [34].

2.1.5 Process of production

In the factories, preparing the mixtures is performed automatically according to the mix design. The first step is dosing and adding the constituent materials into the mixer. In the beginning, the mixing water with a temperature calculated to attain the required mixture temperature is added to the mixer. In addition to the mixing water, the return slurry and sand slurry are also added to the mixer at this step. The return slurry refers to the mixture of water and waste resulting from the manufacturing process of AAC, e.g. residues from the cutting process, which are returned to the manufacturing process. The sand slurry is obtained from the wet grinding of quartz sand using a wet production ball mill.

Afterward, quartz sand, fillers, and binders including cement and lime are added which produces a water-based slurry with a low viscosity. Aluminum paste/powder is the last raw material that is added to the mixer 20 to 40 seconds before ending of the mixing process. In general, the whole mixing process takes between 3 to 4 minutes [20, 34, 71].



Figure 2.1 Casting the AAC mixture into the molds. This figure is reprinted with permission from Schober [72].

The slurry should be cast into the oiled molds immediately (**Figure 2.1**). A mixture temperature of around 40 °C is recommended while casting. However, casting temperatures up to 55 °C might also work well. Generally, a high casting temperature makes the expanding processes sensitive, especially in the lime-rich mixtures, since the mixture temperature is already increasing due to the quick reaction of lime [14, 34].

Soon after casting, the “expanding process” begins by “swelling” the mixture in the mold due to the reaction of aluminum under alkaline conditions which produces hydrogen gas. The expansion of the AAC mixture could take only 15 minutes or up to 60 minutes depending on the type of the mixture, i.e. lime-rich or cement-rich, casting temperature, the specific surface area of aluminum particles, and other circumstances. Moreover, the mixture temperature is increasing constantly due to the ongoing occurrence of chemical reactions during this period [11, 34].

At the end of the expanding process, a foam-like material, which is still not hard, is obtained. The “blowing out” begins after ending the expansion by appearing small openings on the surface of the mass. Hydrogen gas, which accumulates below the surface, escapes through those small openings on the surface which induces a sinking back of the expanded volume for a certain amount depending on its height.



Figure 2.2 Storing the AAC mixture. This figure is reprinted with permission from Schober [72].

The expanded mixture is stored in chambers or tunnels with elevated temperatures (**Figure 2.2**) for a couple of hours until gaining sufficient hardness for the demolding process. Although the storing period depends on the type of the mixture, after about 2 hours (h) the expanded mixture will typically gain a certain stiffness. During this time, the expanded mixture turns from a liquid phase into a solid cake-like block. This expanded block is called “cake” or “green cake” which is composed of different amounts of gas bubbles depending

Literature Review

on its density. In the course of the demolding process, the green cake is cut into masonry units or slabs in desirable dimensions using wires (**Figure 2.3**) [34].



Figure 2.3 Demolding (left) and cutting (right) the AAC green cake. This figure is reprinted with permission from Schober [72].

In the next step, the green cake which is cut into desirable dimensions is autoclaved under a saturated steam condition. The autoclaving process, which is the hydrothermal treatment of the green cake, includes different steps of evacuation, steaming up, “dwell time”, and steaming down.

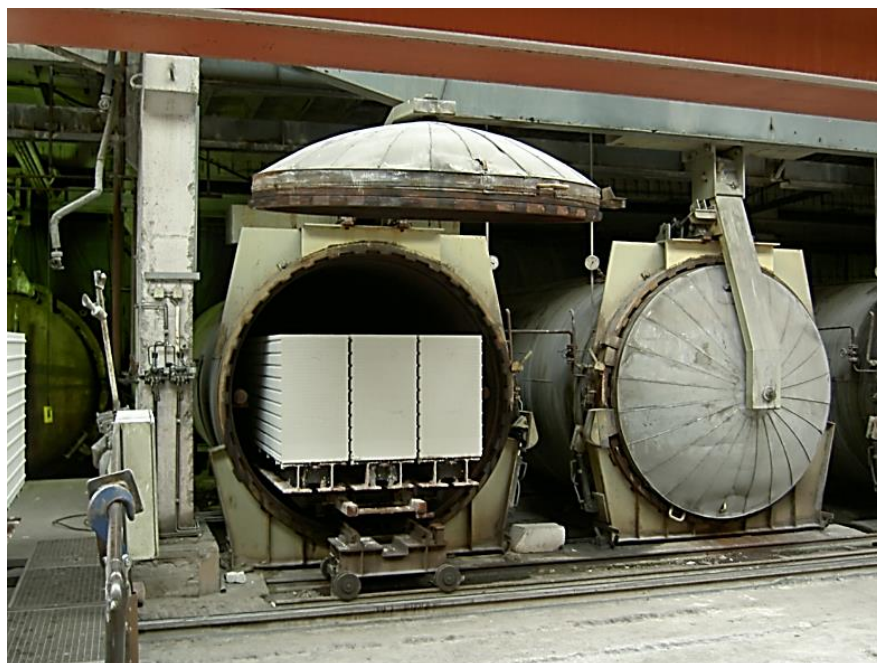


Figure 2.4 Removing the AAC blocks out of the autoclave. This figure is reprinted with permission from Schober [72].

During the evacuation, the pressure is reduced as a result of the extraction of air. The typical duration for the steaming up is 2 h which is the same as that for the steaming down. The duration in which the sample is being autoclaved at maximum temperature, typically around 180–200 °C and a corresponding pressure of 9–14 bar, is called dwell time which usually takes from 5 to 9 h. Therefore, the duration of the whole autoclaving process is between 8 h and 12 h [73]. In this thesis, the pressure is expressed in relative values (gauge pressure).

The final properties of AAC, e.g. compressive strength, depend on the maturity of the binding phases which is expressed by the quantities of formed C-S-H. The formed C-S-H including tobermorite act as the binding agent in AAC [1, 74–76]. The autoclaving process is necessary for establishing the conditions under which the formation of sufficient C-S-H including tobermorite can take place [12]. During autoclaving at maximum temperature the formation of C-S-H, which started previously, proceeds more rapidly. Additionally, after 1-2 h at maximum temperature, complex hydrothermal transformations affecting the CaO-SiO₂-H₂O (C-S-H) system start which leads to the formation of semi-crystalline C-S-H phases, e.g. C-S-H (I) and crystalline C-S-H phases, e.g. tobermorite [22, 39].

Finally, after removing out of the autoclave (**Figure 2.4**), AAC units and slabs are separated and then packed for being sold.

2.2 Chemical transformations during the production of ACC

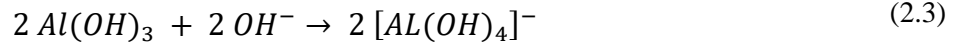
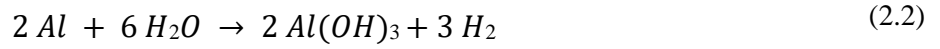
A lot of research works have been carried out on the determination of the reaction kinetics and the development of the phases in the lime-silica system during hydrothermal treatment [43, 44, 47, 77]. However, the results of those research works might not be directly applicable to understanding phase transformation during the production of AAC. The phase transitions during the production of AAC were investigated by Schober [22]. Additionally, Mitsuda et al. conducted several studies on phase transformation and tobermorite formation in AAC [12, 38, 39, 62, 78]. Matsui et al. [75, 24] and Kikuma et al. [79, 80] carried out similar studies as well. In this thesis, the main chemical reactions which occur during different steps of AAC production are described according to the above-mentioned studies. Accordingly, subsections 2.2.1, 2.2.2, and 2.2.3 are based on those aforementioned studies [22, 38, 12, 62, 39, 78, 80, 79, 24, 75].

2.2.1 Chemical reactions before autoclaving

Hydration of lime and reaction of aluminum are the first chemical reactions that occur simultaneously in the initial step of producing AAC, i.e. mixing the raw materials. Hydration of lime, which occurs according to reaction Eq. (2.1), leads to the formation of calcium hydroxide, i.e. Ca(OH)₂ with a mineral name of portlandite.

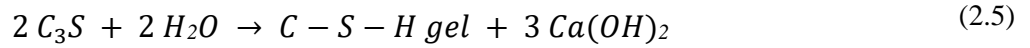


The reaction of aluminum with water produces hydrogen gas (H₂) and aluminum hydroxide (Al(OH)₃) according to reaction Eq. (2.2). Subsequently, aluminum hydroxide transforms into dissolved aluminate due to its high solubility under alkaline conditions. This transformation is described by reaction Eq. (2.3).



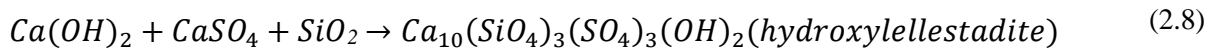
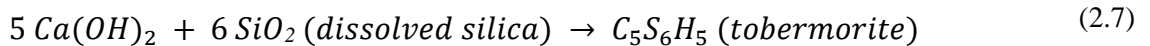
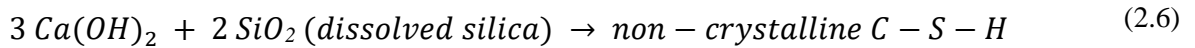
The generation of hydrogen gas is followed by the expansion of the mixture and the creation of the pores in the AAC mixture as described in section 2.1.3. The generation of pores and formation of portlandite, i.e. reaction Eqs. (2.1-3) takes place during the first few hours of the production process.

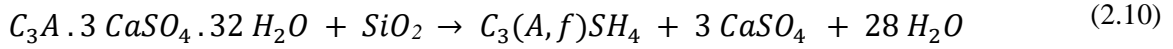
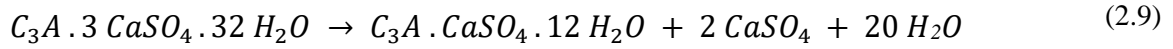
Cement has a lower reactivity compared to lime and aluminum. Therefore, the hydration of cement happens after the hydration of lime and the reaction of aluminum. According to reaction Eqs. (2.4) and (2.5), ettringite, portlandite, and C-S-H gel are the main reaction products of cement hydration.



2.2.2 Chemical reactions at the beginning of the autoclaving process

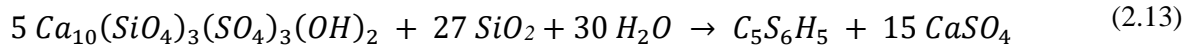
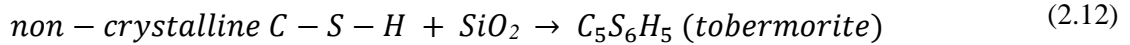
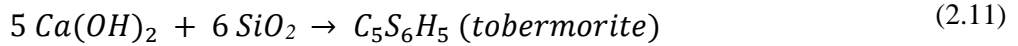
The main influence of hydrothermal treatment is dissolving silica and speeding up ongoing reactions, such as the C-S-H formation according to reaction Eq. (2.6). At this stage, the formed C-S-H are mainly calcium-rich and non-crystalline. Nevertheless, tobermorite could also be formed according to reaction Eq. (2.7). Moreover, hydrothermal treatment leads to the formation of new phases including hydroxyllellstadite. Hydroxyllellstadite is a high-lime product that is formed through the reaction of the sulfate materials (gypsum or anhydrite) with lime and dissolved silica according to reaction Eq. (2.8). Moreover, ettringite transforms into tricalcium monosulfate ($C_3A \cdot CaSO_4 \cdot 12 H_2O$) and hydrogarnet ($C_3(A, F)SH_4$) due to the increased temperature. The attributed reactions to this transformation are presented as reaction Eqs. (2.9) and (2.10).



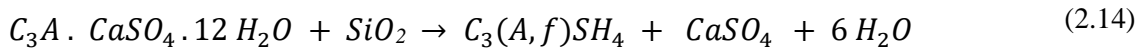


2.2.3 Phases present in the final product

Autoclaving at constant temperature for several hours promotes silica dissolution and, as a result, tobermorite formation in the AAC green cake. In this step, tobermorite is formed through different pathways including the reaction of dissolved silica with calcium hydroxide (reaction Eq. (2.11)), crystallization of the non-crystalline C-S-H formed at the initial stages of the hydrothermal treatment (reaction Eq. (2.12)), and the reaction of hydroxylellestadite with dissolved silica (reaction Eq. (2.13)).



Moreover, tricalcium monosulfate, formed in the previous step through reaction Eq. (2.9), reacts with dissolved silica and produces hydrogarnet and anhydrite as the reaction products according to the reaction Eq. (2.14).



Based on the reaction Eqs. (2.1-14), phases that are present in the final AAC products are tobermorite, non-crystalline C-S-H, sulfate phases i.e. anhydrite and/or bassanite, and hydrogarnet. In the case of applying comparatively a short autoclaving duration and introducing a high enough content of sulfate carrier to the mixture, hydroxylellestadite could also be present in the final products.

Figure 2.5 and **Figure 2.6** present an overview of changes in the phase composition of AAC during different steps of the production process and autoclaving process, respectively. The vertical line at 90 min indicates the time at which the dwell time started (autoclaving at a constant value of 190 °C). **Figure 2.5** shows semi-quantitative phase determination using powder diffractometry as well as calculation from the consumption of source materials [21]. However, **Figure 2.6** was obtained by the results of in situ X-ray diffraction analysis [75]. Moreover, AAC samples used to make those figures contained quartz sand as the main silica source.

Literature Review

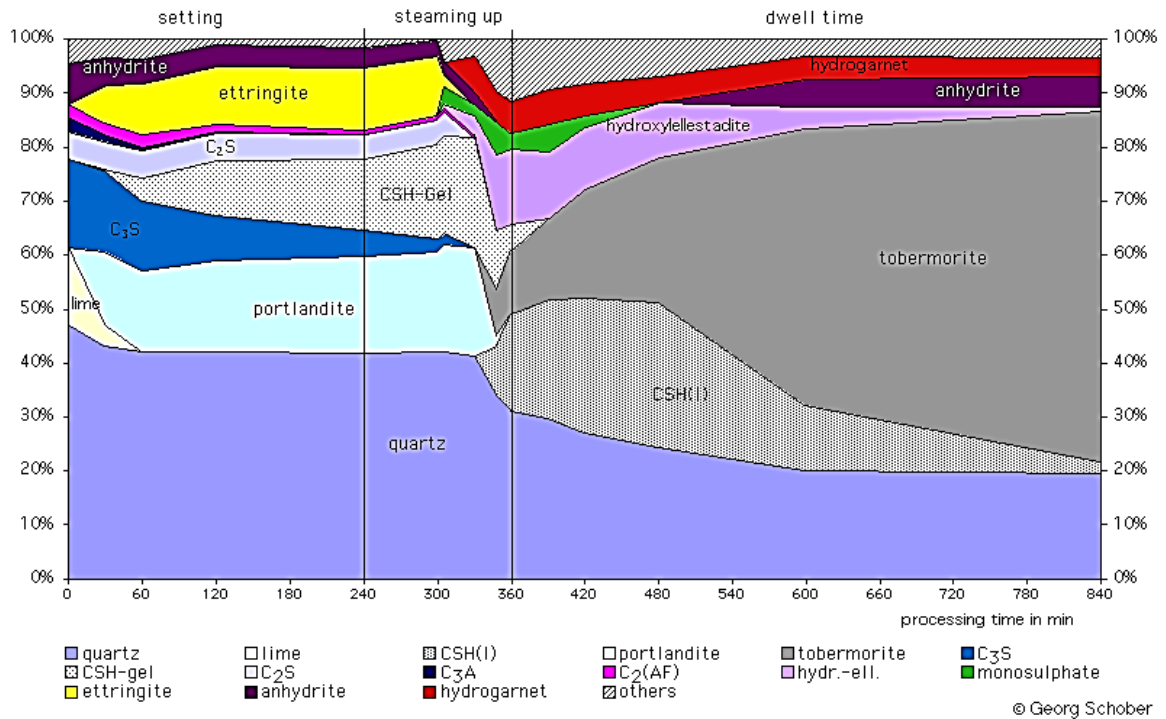


Figure 2.5 Phase transformation during different steps of the AAC production process [81, 21].

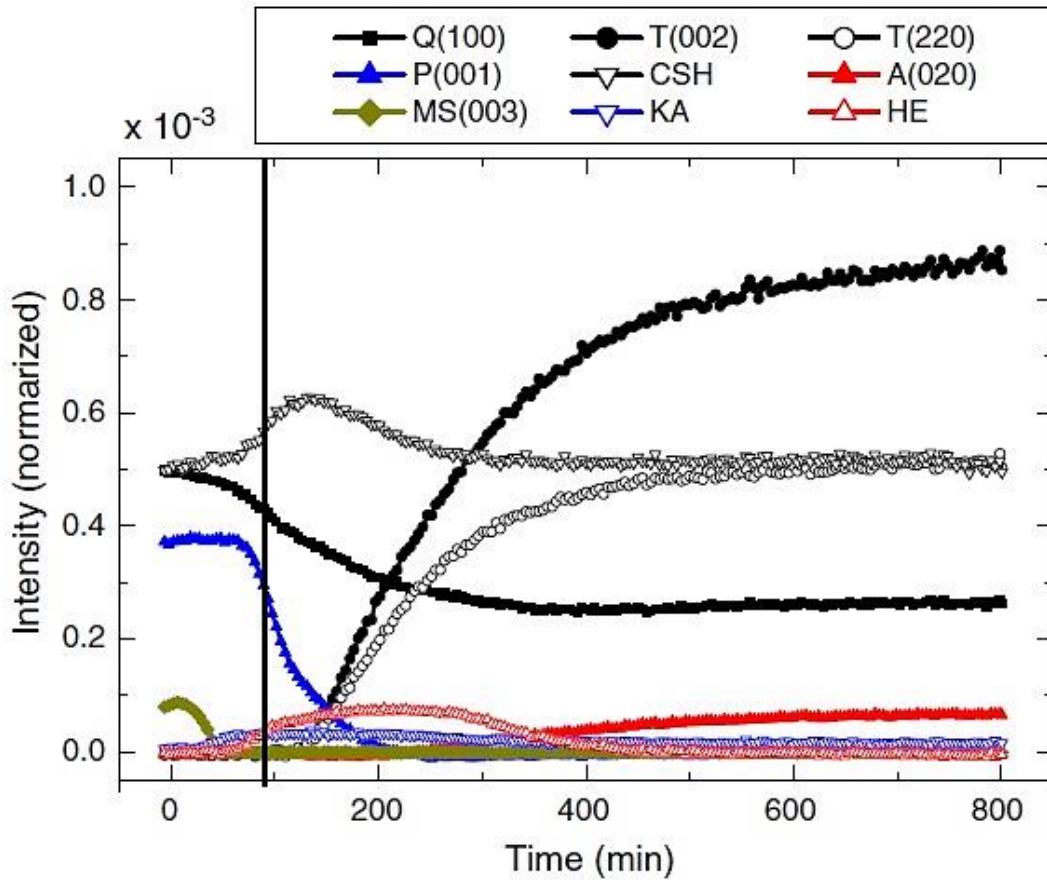


Figure 2.6 Variations in peak intensities of main phases formed in AAC during the autoclaving process. T: tobermorite; P: portlandite; Q: quartz; MS: monosulfate; KA: katoite; HE: hydroxyllellastadite; A: anhydrite; C-S-H: non-crystalline calcium silicate hydrate. [75].

The mineralogical composition of AAC varies depending on the quality, C/S, and proportion of the starting materials, as well as the temperature and duration of the autoclaving process. However, AAC could generally contain 40–80 wt. % tobermorite, 10–40 wt. % residual quartz, 1–7 wt. % anhydrite, and 1–7 wt. % hydrogarnet [73]. There is no reliable estimation for the content of non-crystalline C-S-H since it is not easy to detect amorphous and semi-crystalline C-S-H. However, several studies have confirmed that in AAC, the main hydrothermal product is C-S-H including semi-crystalline C-S-H phases such as C-S-H (I), amorphous C-S-H, and crystalline C-S-H phases such as tobermorite [12, 39, 40, 82].

2.3 Structure of AAC

AAC is an extremely porous material that is mainly composed of air. This fact provides its main favorable property, i.e. excellent thermal insulation. **Figure 2.7** shows the porous structure of AAC including pores and crystals of tobermorite formed on the wall of the pores.

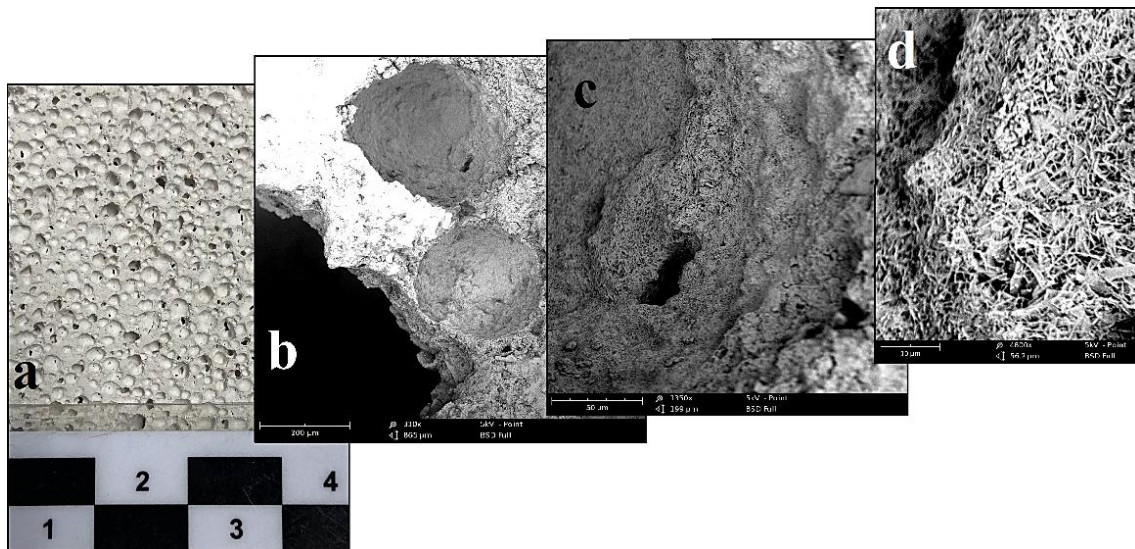


Figure 2.7 Porous structure of AAC, (a: eye observation of pores on the surface of AAC, line: 4 cm), (b: SEM image of pores on the surface of AAC, line: 200 μm), (c: SEM image of pore wall, line: 50 μm), (d: SEM image of tobermorite crystals formed on the wall of the pore, line: 10 μm).

In general, the AAC volume is composed of 27–83 vol. % air pores and 17–73 vol. % solid matrix (or solid structure) corresponding to a density range of 100–800 kg/m^3 [21]. The AAC volume comprising air pores and the solid structure is represented schematically in **Figure 2.8**. The air pores are generated due to the reaction of aluminum under alkaline condition and the formation of hydrogen gas as the reaction product. These large air pores are called “macro-pores” which are defined as roughly spherical pores with a diameter of $D > 100 \mu\text{m}$ [83–85] or $D > 60 \mu\text{m}$ according to other research [86].

The solid matrix around the air pores consists of solid material and mostly irregular pores which are referred to as “micro-pores” [73]. In another word, the solid matrix contains another part of the total porosity in its microstructure which makes up from 13 to 41 % of the total volume. Therefore, the total portion of pore volume in AAC, i.e. volume of (macro-

Literature Review

pores + micro-pores), reaches an approximate range of 68–96 vol.% corresponding to a density range of 100–800 kg/m³ [21, 83, 87].

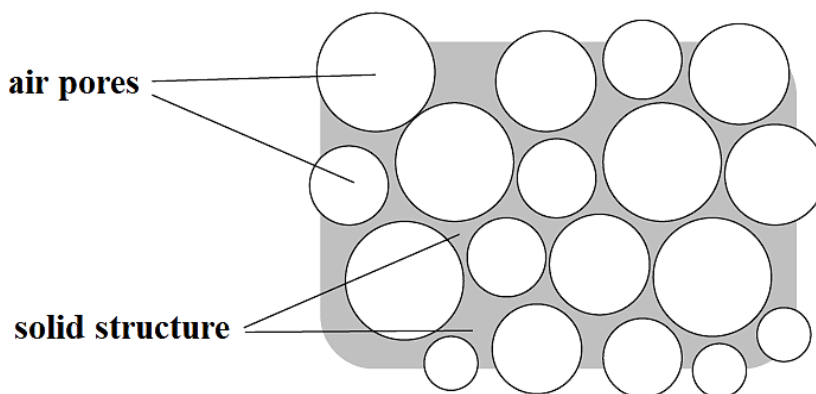


Figure 2.8 Schematic representation of the air pores and the solid structure. This figure is reprinted with permission from Schober [73].

The micro-pores volume is mainly determined by the content of mixing water or W/S. The average pore size of the micro-pores before autoclaving the green cake is within the range of $D = 1\text{--}10\ \mu\text{m}$ [39, 78] which changes to $D = 0.05\text{--}0.1\ \mu\text{m}$ after autoclaving [78, 39, 31]. This is due to the growth of crystalline and semi-crystalline C-S-H as well as intermediate reaction products during hydrothermal treatment [21].

The solid materials are composed of the final phases formed during AAC production including tobermorite, non-crystalline C-S-H, and other phases which were described in section 2.2.3. In the case of curing the AAC mixture at room temperature, the solid material would be composed of C-S-H gel which is typically found in ordinary concrete and cement-based materials. However, curing the AAC mixture under saturated steam condition leads to the formation of solid materials with a micro-crystalline structure and a significantly lower specific surface compared to that of ordinary concrete [11].

The pore structure is mainly controlled by the macro-pores rather than the micro-pores which are formed in the area between the macro-pores. The average contribution of the macro-pores on the compressive strength and bulk density is much higher than that of the micro-pores. Therefore, the aluminum content has a more decisive role in determining compressive strength and bulk density compared to the water content represented by the W/S [73, 21].

In addition to the classification of pores into macro and micro, there exist other classification methods introduced in other research works [89]. In some studies, the pores are categorized in terms of diameter rather than the way of formation. In this method, pores are classified into three groups; macro-pores which are defined as pores with $D > 50\ \text{nm}$, micro-pores which are referred to as the pores with $D < 2\ \text{nm}$, and meso-pores which includes the pores within the range of $2\text{--}50\ \text{nm}$ [83]. In this thesis, the first classification method in which the air pores are considered as the macro-pores and all the other pores in the solid structure are called micro-pores is used.

The pore structure of AAC is usually characterized using different parameters of total porosity, pore size distribution, and pore shape [11, 90]. The total porosity, which is usually determined using a helium pycnometer, can be obtained by Eq. (2.15) [84, 17].

$$P = \left(1 - \frac{q_b}{q}\right) \times 100 \quad (2.15)$$

In Eq. (2.15), P represents the total porosity, q_b is bulk density, and q represents skeletal density or true density.

To calculate the total porosity of AAC, the skeletal density must be measured. In AAC, there is indeed no significant difference in the density of the skeletal material. Although the skeletal material is composed of different sets of C-S-H phases, the densities of C-S-H phases are too close to each other which leads to almost the same skeletal material or true density. The true density of AAC was measured to be around 2.6 kg/m^3 [84, 91]. **Table 2.1** shows the pore structure characteristics of AAC products with different bulk densities.

Table 2.1 The pores volume and the total porosity of AAC with different bulk densities [21].

bulk density (kg/m^3)	macro-pores (vol.%)	micro-pores (vol.%)	total porosity (vol.%)
100	83	13	96
150	77	17	94
300	70	16	86
400	65	19	84
600	45	31	76
800	27	41	68

The total porosity is mainly the function of aluminum content. However, the W/S and the proportion of the raw materials influence the total porosity as well.

The final properties of AAC such as compressive strength, bulk density, and drying shrinkage are significantly affected by pore structure which will be explained in the following sections.

2.4 Properties of AAC

2.4.1 Bulk density

The bulk density of AAC is mainly determined by the type, quantity, as well as fineness of the aerating agent, i.e. aluminum paste or powder. Nevertheless, other factors such as the W/S and the specific gravity of the starting materials could also influence the density of the product [1, 34]. Moreover, in order to obtain a certain density grade, it is necessary to consider the volume of the mold used for casting and adjust the quantities of the components based on that.

As it was mentioned earlier, the density of AAC is closely related to its pore structure. In order to produce a homogenous AAC with a uniform density, the formed pores must be dispersed homogeneously in the product. In general, the bulk density of AAC reduces with an increase in the total volume of air in the mass, i.e. an increase in porosity [17, 86, 40]. An

Literature Review

increase in the total volume of air can occur by an increase in the number of macro-pores or an increase in the size of individual pores [31].

It has been reported that changing the autoclaving temperature and time did not influence the bulk density of AAC significantly [42, 92].

2.4.2 Thermal conductivity

The porous structure of AAC is responsible for its excellent thermal insulation. The thermal conductivity of AAC blocks with a bulk density of 400–700 kg/m³ is within the range of 0.07–0.21 W/(m·K), while that of ordinary concrete is within the range of 1.6–1.8 W/(m·K) which is 7–25 times higher [93, 17]. The thermal conductivity of AAC is a function of its pore structure and as a result its bulk density [94–99]. In particular, the total quantity of pores, pore size distributions, and thickness of walls between air pores have a significant impact on the thermal conductivity of AAC [98].

The higher porosity or the lower density implies a higher total volume of air which provides effective heat insulation. Therefore, one general way to improve thermal conductivity is to increase porosity. However, almost all of the building materials including AAC contain moisture when they are in use. This implies that some pores are filled with moisture rather than air which influences the thermal insulation behavior. Therefore, in determining the thermal conductivity of AAC, the moisture content should be taken into account [100, 83, 101].

Comparison of the results of several studies [102–104] shows that a reduction of 100 kg/m³ in density leads to an approximate reduction of 0.02–0.04 W/(m·K) in the thermal conductivity. It has also been reported that the autoclaving process did not influence thermal conductivity considerably [1].

2.4.3 Compressive strength

The compressive strength of AAC is controlled by the porosity properties, e.g. pore volume, and structure of the solid matrix, e.g. the types, quantities, morphology, and distribution of hydrothermal products [1, 38, 105, 107]. The porosity properties have a more determining effect on compressive strength compared to the structure of the solid matrix [108, 109]. For the same pore structure, the compressive strength of AAC depends on the phases present in the solid matrix [109].

2.4.3.1 Influence of the pore structure

As was mentioned in section 2.3, the pore structure is mainly controlled by macro-pores, i.e. air pores, rather than micro-pores in the skeletal material. Therefore, changes in compressive strength of AAC are, first of all, contributed by the macro-pores [83]. However, changing the micro-pores would influence the compressive strength as well. Increasing the W/S generates more micro-pores in the skeletal material which may lead to a reduction in compressive strength [21].

It has been reported that the compressive strength of AAC showed an exponential correlation with its total porosity [21, 108, 110]. In addition to the total porosity, the thickness of walls between the air pores, and the size distribution of air pores could affect compressive strength

as well [105, 86]. A thin thickness of walls between air pores resulted in a high total porosity which reduces strength significantly [21].

First, it was reported that an increase in air pore size resulted in lower compressive strength [31]. However, it was then demonstrated by FEM simulations that the decisive factor was indeed not the pore size but the thickness of pore walls. For the same air pore porosity, an increase in the size of air pores resulted in thicker walls between the air pores which provided higher compressive strength. Moreover, AAC samples with broad air pore size distribution as well as single air pore size exhibited a lower strength compared to those with a narrow distribution of air pore size. [21].

2.4.3.2 Influence of the skeletal material structure

In general, C-S-H is well-known for being responsible for favorable cementation properties due to its high surface charge density. Therefore, in AAC, different types of formed C-S-H act as the binding agent in skeletal material holding all present phases in the matrix [41, 111–113].

Among the C-S-H phases formed in the lime-silica system, well-crystallized tobermorite has been found to have the highest strength which improves the compressive strength of AAC and reduces its shrinkage [114, 82, 42]. In addition to tobermorite, C-S-H (I) was reported to be a high-strength C-S-H phase that could be present in commercial calcium silicate products [13, 115, 116]. On the other hand, xonotlite and α -C₂S hydrate exhibited poor “space-filling” ability and as a result, were expected to attribute low compressive strength [13]. Therefore, the transformation of tobermorite to other C-S-H phases, e.g. xonotlite could cause a reduction in the compressive strength of AAC products [39, 117]. Moreover, the stress-strain curve showed that tobermorite 11 Å had the highest strength among the tobermorite family [118].

According to the relevant literature, to obtain an AAC with ideal properties, crystalline tobermorite should be the main final phase formed in the solid matrix. Moreover, several studies have reported that the final properties of AAC significantly depend on tobermorite quantity as well as its crystallinity [40, 12, 74, 39]. However, the results of some other studies have shown that in addition to a high content of tobermorite, a homogeneous distribution of the tobermorite crystals in the solid structure is required to obtain optimum strength properties [119, 38]. It has also been revealed that optimum compressive strengths can be achieved when the maximum fraction of volume is occupied by tobermorite and other C-S-H together [76].

Therefore, to produce AAC with high compressive strength, all the influencing parameters should be adjusted in a way that supports the formation of C-S-H including tobermorite with a high degree of crystallinity in skeletal material. The formation of tobermorite and other C-S-H in skeletal material strongly depends on the constituent materials, especially binder content, and the autoclaving process. The effect of the binder content on C-S-H formation was described in section 2.1.4 and the following section deals with the impact of the autoclaving process.

2.4.3.3 Influence of the autoclaving process

In general, the autoclaving process has a favorable effect on the compressive strength of AAC such as it increases the quantity of crystallized C-S-H including tobermorite [38, 39]. During the autoclaving process, non-crystalline C-S-H, which are loosely packed and spatially disordered, are being transformed into crystallized C-S-H phases with a lower specific volume and high “space-filling” ability. This results in a denser solid structure which improves the compressive strength, drying shrinkage, and in general the quality of the material [21, 13].

Figure 2.9 shows the influence of the autoclaving process on the specific surface area of AAC. As it is shown, the specific surface area of the AAC samples decreases when the autoclaving duration increases. This implies a denser matrix as a result of autoclaving for a longer time which is accompanied by a higher strength. Additionally, for each autoclaving duration, the AAC sample which contains anhydrite in its mixture exhibited a lower specific surface and as a result a denser matrix [21]. The influence of anhydrite on compressive strength is explained in detail in the following section.

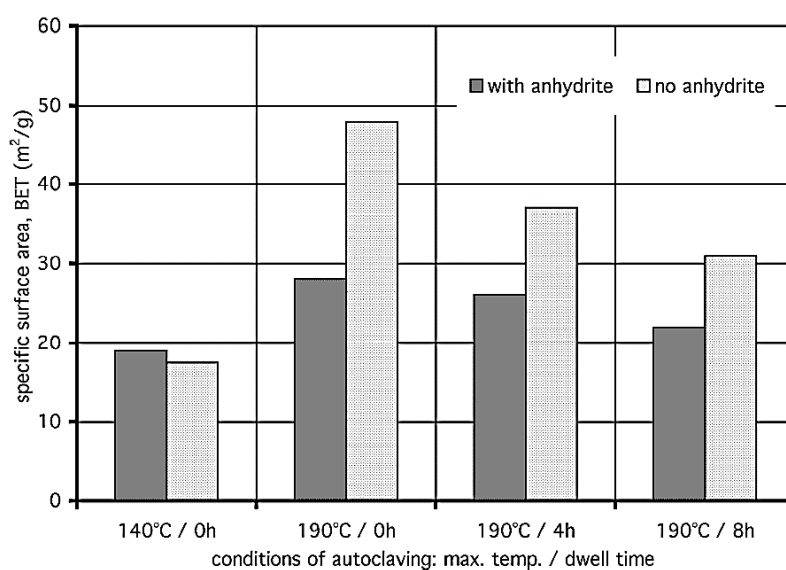


Figure 2.9 Influence of the autoclaving process on the specific surface area of AAC [21].

2.4.3.4 Influence of sulfate carriers addition

In addition to autoclaving, anhydrite addition improves the compressive strength of AAC as well.

The pieces of evidence [119, 22, 120, 121] show that the addition of sulfate carrier has a significant effect on the solution equilibrium at the beginning of the hydrothermal treatment which affects strength properties favorably. This positive effect was attributed to the formation of tobermorite and other C-S-H phases in a way that leads to a higher density of the solid matrix in AAC. However, the mechanism of forming a denser matrix by the addition of sulfate carriers has not been investigated in detail. An important work referring

to the influence of sulfate on AAC properties has recently been performed by Mesecke [119]. The findings of this study [119] have demonstrated that in the AAC samples without the addition of sulfate carriers, the solution is saturated with Ca^{2+} at the beginning of the autoclaving process. At this stage, the concentration of SiO_4^{4-} is low. As the temperature increases, the solubility of Ca^{2+} decreases, and that of SiO_2 increases slowly. At the approximate temperature of 170°C , the solvated SiO_4^{4-} ions react with the Ca^{2+} -saturated solution parallel to the quartz grain surface. Therefore, the calcium silicate hydrates preferentially form on the surface of quartz grains. Subsequently, further diffusion of SiO_4^{4-} can hardly occur from the quartz surface. As long as the hydrothermal solution is largely dominated by Ca^{2+} , SiO_4^{4-} can diffuse only up to a limited extent. Therefore, in the absence of sulfate carriers, nucleation of C-S-H mainly takes place on the surface of quartz grains, and in the rest of the structure, the formation of C-S-H is low. This will lead to a porous structure that influences the compressive strength negatively because the C-S-H and tobermorite predominantly grow around quartz grains, and the micro-pores and micro-cracks, formed in the green cake, remain unfilled and act as weak points in the final product.

However, in AAC with the addition of sulfate carriers, those small pores are filled by larger tobermorite crystals at the beginning steps of the hydrothermal treatment. In fact, the addition of sulfate carrier leads to the formation of hydroxyllestadite at the beginning of the hydrothermal treatment which significantly consumes Ca^{2+} as hydroxyllestadite has a C/S of 3.3. This would prevent the formation of the initially formed C-S-H with a too high C/S and provide a more favorable distribution of SiO_4^{4-} in the matrix which results in a more homogeneous distribution of C-S-H and corresponding tobermorite. Therefore, a homogeneous distribution of C-S-H phases including tobermorite grows in micro-pores and micro-cracks and fills them quite soon, i.e. at the beginning steps of the hydrothermal treatment.

Moreover, the SEM images showed that for the AAC samples without the addition of sulfate carriers, the solid matrix contains a significantly higher number of micro-pores within the range of $D < 10\ \mu\text{m}$ [119] which affects the strength properties negatively. Therefore, the hydroxyllestadite formation and later on its decomposition develops the formation of a more homogenous and denser microstructure resulting in higher strength of AAC.

2.4.3.5 Relation with the bulk density

Although the fact that the compressive strength of AAC increases with increasing its density is widely known [11, 1, 122, 17, 40], extracting a precise relation would be more favorable.

First, the researchers simply made a regression between the strength and density using the values of a large database. The best fit was found to be a parabola which indicated a quadratic relation between compressive strength and bulk density of AAC.

Based on the above concept a figure of merit so-called A-value (A-Zahl in German) of AAC was extracted by the YTONG company in Germany during the 1980ies which is defined by Eq. (2.16) [21].

$$A - \text{value} = \frac{\text{compressive strength}}{\text{bulk density}^2 \times 0.016} \quad (2.16)$$

Literature Review

Where compressive strength is given in N/mm^2 and bulk density in kg/dm^3 .

A-value is a dimensionless parameter of compressive strength that is used to compare the compressive strength of the AAC products with different bulk densities from 400 to 750 kg/m^3 . In fact, when it is not possible to compare a set of samples with each other because of different bulk density values, this relation can be used to control the quality of samples. A-value is between 600 and 1400 for standard AAC [73, 21].

2.4.3.6 Anisotropy

It has been observed that AAC shows different compressive strength when it is submitted to the loading with a parallel or perpendicular direction to the expansion direction [123, 124, 90]. This difference which is an anisotropy in strength could be within the range of 5–25%. The stress-strain curves of the AAC samples with a loading direction of parallel and perpendicular to expanding direction are displayed in **Figure 2.10** [21].

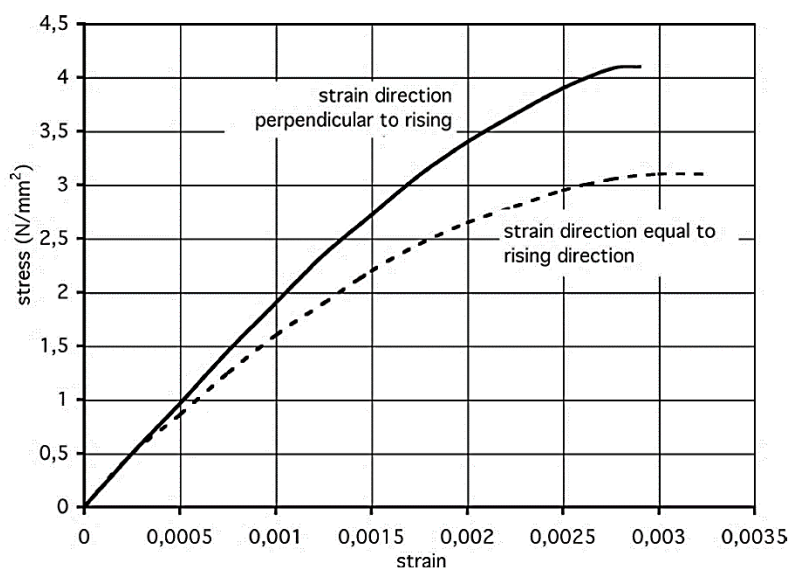


Figure 2.10 Stress-strain curves of the AAC samples with a loading direction of parallel and perpendicular to expanding direction [21].

It has been reported that the anisotropy in strength is due to the horizontal cracks which appear in the pore walls at the end of the expanding process. During this process step, the air pores rupture because of the high viscosity of the mixture which produces horizontal cracks in the wall of the pores. These horizontal cracks propagate until bridging the nearby air pores. Therefore, AAC shows a higher strength when is loaded perpendicularly to the expansion direction. Because in this state, the loading direction is parallel to the direction of the crack which cancels the negative effect of the cracks on the compressive strength [90, 123, 21].

2.4.4 Shrinkage

The relative change in dimensions, during storage in the air not saturated with humidity, is known as drying shrinkage [125–127] which is one of the current issues in the development

of AAC products. In AAC, all microstructure regions which contain capillaries partly filled with water are compressed by the air pressure as a consequence of loss of moisture. This leads to capillary suction which eventually could result in cracks [128]. In general, AAC has a higher shrinkage compared to ordinary concrete since its mixture contains a minor amount of only fine aggregates.

It has been reported that the shrinkage of AAC mainly depends on the volume and the specific surface of micro-pores [129, 130]. The high porosity and the high specific surface of the pores are responsible for the high drying shrinkage of AAC [129, 125]. On the other hand, increasing the degree of crystallinity is accompanied by a lower specific surface and a lower porosity of micro-pores. Therefore, a high degree of crystallinity leads to a low shrinkage [40, 89]. On the contrary, a high proportion of non-crystalline C-S-H increases the drying shrinkage of AAC [29, 40]. In 2000, Ramamurthy et al. [125] reported that the shrinkage of the fly ash-based AAC was 5-7 times higher than that of the quartz-based AAC. The reason was attributed to the reduction in the degree of crystallinity as the result of replacing quartz sand with fly ash in the AAC mixture.

The autoclaving process, which supports the formation of well-crystallized C-S-H, reduces shrinkage by up to 80% [89]. Moreover, cement-rich AAC shows lower shrinkage compared to lime-rich AAC [26, 125].

By comparing the reactions in section 2.2, it might be assumed that removing anhydrite from the reaction mixture would not lead to any change in the formation of the required bonding phases, i.e. tobermorite and other C-S-H phases since it would only simplify the reaction equations. Although the addition of the anhydrite does not change the formation of the binding phases, it changes microporosity positively by causing a denser microstructure and indeed has a decisive effect on the shrinkage and strength properties of AAC [21–23, 75, 120, 126]. It has been revealed that sulfate favored the formation of well-crystallized tobermorite with a house-of-cards structure which resulted in a low shrinkage [131]

However, the results of a study that has been carried out by Mesecke [119] showed that the drying shrinkage of AAC depends only slightly on the addition of sulfate carriers. It has been reported that the drying shrinkage of AAC is mainly controlled by the content and crystallinity of tobermorite which did not change significantly by changing sulfate addition. On the contrary, the compressive strength of AAC is indeed a sulfate addition-dependent property. In AAC samples without the addition of sulfate carriers, the maximum A-value value was only around 1100, regardless of the cement to lime ratio. However, this value is around 1600 in AAC samples with sulfate addition due to the development of a finer and denser microstructure [119].

2.5 Opportunity to save energy during hydrothermal treatment of AAC

As it was explained in section 2.4.3, the autoclaving process improves the mechanical properties of AAC significantly because of establishing a condition under which C-S-H, i.e. binding phases, can be formed. C-S-H forms through the reaction of the solvated SiO_4^{4-} ions with the Ca^{2+} -saturated solution. Lime (CaO) is the most reactive component in the AAC mixture. Therefore, hydration of lime occurs in the initial step of producing AAC, i.e. mixing

Literature Review

of the solid raw materials with water. However, the dissolution of silica requires the autoclaving process. In another word, the formation of C-S-H can take place only when dissolved silica (SiO_4^{4-}) diffuses into the solution to an adequate extent, and indeed the main role of the autoclaving process is dissolving silica resulting in the formation of C-S-H phases [22]. This implies that if a lower level of energy is required for the dissolution of the silica raw material, a lower autoclaving temperature and/or a shorter autoclaving duration could be applied.

Currently, the use of quartz sand as a SiO_2 source for AAC production is well-established. Quartz has relatively low solubility in water and the rate of dissolution is relatively slow as well. Therefore, when quartz sand is the main silica source in the AAC mixture, a relatively high autoclaving temperature, i.e., greater than $T > 180\text{ }^\circ\text{C}$ is required [75, 132]. However, compared to quartz, some other forms of silica, such as amorphous silica and cristobalite exhibit a higher solubility and as a result require less energy to be dissolved [133, 135, 136]. Therefore, it can be assumed that replacing quartz sand with silica materials of a higher solubility in the AAC mixture offers the advantage of reducing autoclaving temperature and/or time.

2.5.1 Dissolution of silica

The formation of binding phases, i.e. tobermorite and other C-S-H, has several sources in which reactions occur only in the presence of dissolved silica. According to reaction Eqs. (2.6), (2.11)–(2.13), dissolved silica reacts with other phases, e.g., calcium hydroxide, non-crystalline C-S-H, and hydroxyllestadite to form tobermorite and other C-S-H [22, 75]. In all of those reactions, the formation of binding phases is controlled by the dissolution of silica, as long as sufficient calcium is available. Therefore, the process of dissolution of silica is the rate-determining step in the formation of binding phases [48, 41, 12].

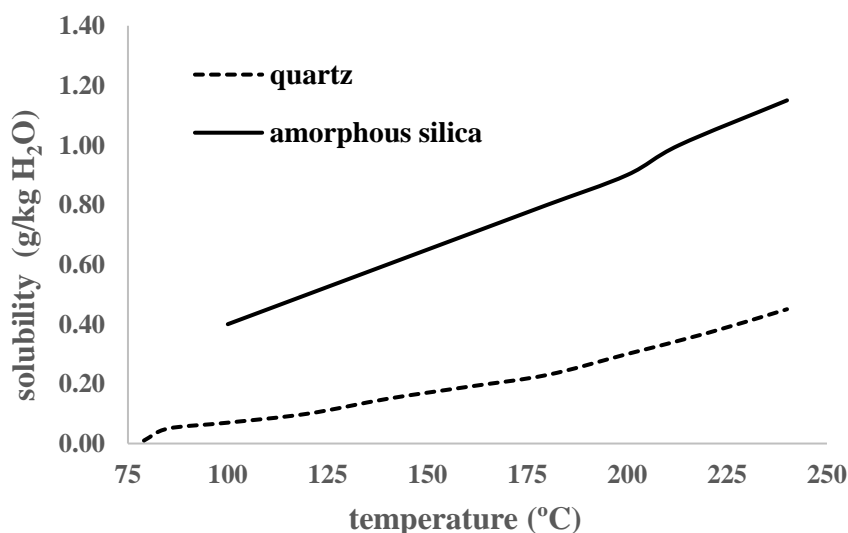


Figure 2.11 Solubility of amorphous silica and quartz in water at different temperatures (modified from source [136]).

There exist various forms of silica with different dissolution properties in water. The difference in their dissolution properties is mainly due to their different solubility (in this study, solubility specifically refers to water solubility). It is well known that amorphous silica shows a higher solubility than quartz at all temperatures (**Figure 2.11**). Additionally, some other crystalline modifications of silica, e.g. cristobalite, tridymite, and stishovite exhibit higher solubility than quartz [133, 135, 136].

As can be seen in **Table 2.2**, quartz has a lower rate of dissolution compared to fused silica, which is a type of amorphous silica, and other crystalline modifications such as tridymite and cristobalite [133]. Accordingly, it comparatively requires a higher level of energy to decompose.

Table 2.2 Relative rate of dissolution for different forms of silica in water at a temperature of 25 °C and a pH of 8.5 [133].

type of silica	rate of dissolution ($10^{-6} \text{ g ml}^{-1} \text{ day}^{-1}$)
quartz	2.8
cristobalite	6.0
tridymite	4.5
stishovite	11.0
fused silica (amorphous)	39.0

The solubility and dissolution rate of silica significantly increase with an increase in the temperature and pH of the solution [13]. Therefore, it is expected that the concentration of dissolved silica increases significantly with increasing temperatures in alkaline binder systems at the initial stages of the autoclaving process, particularly in the case of applying high autoclaving temperatures.

Besides solubility, the second factor which affects the rate of hydrothermal reactions is the specific surface area of the silica materials. A higher specific surface area leads to a faster dissolution of silica materials. Therefore, silica materials with a porous microstructure show a higher dissolution rate compared to quartz sand which contains solid particles without cavities.

2.5.2 Lime-silica system

In 2003, Garbev [137] studied the influence of synthesis conditions on the formation of C-S-H phases in the CaO-SiO₂-H₂O system. In the above-mentioned study, C-S-H gels with various C/S ratios within the range of 0.5–2.0 were synthesized under CO₂-free conditions. Afterward, the synthesized C-S-H gels were autoclaved at different temperatures to obtain stable crystalline states. **Figure 2.12** shows the stability ranges of the resultant phases.

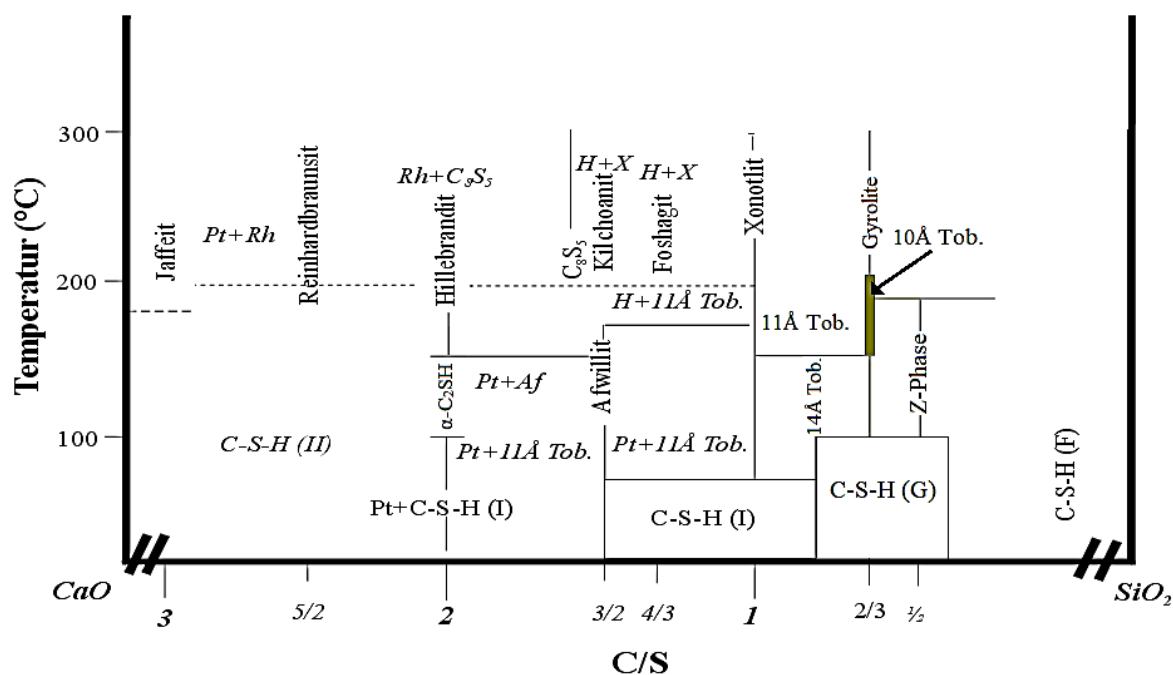


Figure 2.12 Stability ranges of different synthesized C-S-H phases under the saturated steam condition as a function of temperature and C/S of initial synthesized C-S-H gels (modified from source [137]). Pt: portlandite; Rh: pure reinhardbraunsit; H: H₂O; X: xonotlite, C-S-H (G): gyrolite-gel, C-S-H (F): faujasite-gel.

A similar representation of stability of synthesized C-S-H phases was previously derived by Taylor [107]. **Figure 2.12** is based on Taylor's graph and indeed an expanded version of that.

The stability of the formed C-S-H phases depends on the C/S as well as the autoclaving condition. For instance, at the autoclaving temperature of 180 °C and the C/S of 1, tobermorite would be the most stable C-S-H phase, while at 210 °C and the same C/S, xonotlite would be the reaction product with the highest stability.

Figure 2.12 shows that autoclaving the synthesized C-S-H gel with the C/S between 0.67 and 2 led to the formation of C-S-H (I) and gyrolite-gel (C-S-H (G)) at a temperature below 100 °C. The formed C-S-H (I) and C-S-H (G) transformed to tobermorite as the temperature increased to T= 100–200 °C. For the temperature above 200 °C, the formed tobermorite transformed to xonotlite, hillebrandite, and other phases. Therefore, the C/S within the range of 0.67–2 and the autoclaving temperature of T= 100–200 °C with enough duration would likely lead to tobermorite formation.

Moreover, according to **Figure 2.12**, a general pathway of phase evolution in the lime-silica system, which is similar to what was described in section 2.2, could be summarized in the following steps.

- The formation of non-crystalline C-S-H including semi-crystalline C-S-H from the reaction of dissolved silica and lime.
- The formation of tobermorite and other crystalline C-S-H phases from crystallization of non-crystalline C-S-H.

However, **Figure 2.12** provides no information on the influence of the type of silica on the phase evolution and the mechanism of C-S-H formation. Moreover, the C/S of 0.67–2 can be obtained at different autoclaving temperatures depending on the dissolution properties of the silica raw material. Therefore, the dissolution properties of silica affect the kinetics of hydrothermal reactions significantly.

The influence of different types of silica in the lime-silica system was comprehensively investigated by Assarsson [56–58]. In the aforementioned studies, the hydrothermal reactions of lime with both amorphous silica and quartz were studied. For the lime-amorphous silica system, the autoclaving temperatures of $T= 120\text{--}160\text{ }^{\circ}\text{C}$ and $T= 180\text{--}220\text{ }^{\circ}\text{C}$ with a different duration from several hours to days were used. In general, for the lime-amorphous silica system, the formation of phases was classified into three stages. In the first stage, the reaction product was called phase B which was a poorly crystallized and unstable phase. In the second step, phase B transformed into different phases depending on the preparation (starting) molar ratio of calcium hydroxide to silicon dioxide, i.e. molar C/S of the starting mixture. However, these ratios were not the same for the different ranges of the autoclaving temperatures, i.e. $T= 120\text{--}160\text{ }^{\circ}\text{C}$ and $T= 180\text{--}220\text{ }^{\circ}\text{C}$. For the autoclaving temperature of $T= 120\text{--}160\text{ }^{\circ}\text{C}$, phase B transformed to Z-phase at the C/S of 0–0.67. The C/S of 0.67–1.25 led to tobermorite and in the mixture with C/S of 1.25–2, α -dicalcium silicate was formed. For the autoclaving temperature of $T= 180\text{--}220\text{ }^{\circ}\text{C}$, these ratios changed to C/S of 0–1, 0.67–2, and above 2, respectively. For the C/S of 1–2, uncombined lime was observed. In the third stage, the metastable phases formed in the second stage crystallized into stable phases. Accordingly, Z-phase transformed to gyrolite, tobermorite crystallized to xonotlite, and dicalcium silicate transformed to hillebrandite [56, 57].

In the lime-quartz system, the hydrothermal reaction was investigated within the range of $T= 120\text{--}220\text{ }^{\circ}\text{C}$ for different periods of time which varied from a couple of hours to several days. In the aforementioned study, it was mentioned that the phase formation was controlled by the amount of calcium hydroxide per unit area of the grain surface, autoclaving temperature, and time. For the lime-quartz system, the general reactions pathway included the formation of the B-phase in the first stages similar to what was observed for amorphous silica. However, the phases formed in the next steps differed from the lime-amorphous silica system. In the next step, tobermorite and α -dicalcium silicate were formed in poor in lime and rich in lime mixtures, respectively. Subsequently, the formed tobermorite and α -dicalcium silicate acted as the source of lime and reacted with silica ions which were gradually diffused from the quartz surface. The reaction products of those mentioned reactions were gyrolite, xonotlite, and Z-phase [58]. In the contrast to the lime-amorphous silica system, phases with comparatively high silica content such as Z-phase did not appear in the second stages but rather presented only in the last stages. Moreover, in the lime-quartz system, gyrolite was always formed by the reaction of tobermorite and dissolved silica, while in the lime-amorphous silica system it appeared from the crystallization of the Z-phase.

The hydrothermal reactions were examined for both the lime-quartz system and the lime-amorphous silica system by Kalousek [53]. In the lime-amorphous silica system, silicic acid was used as the amorphous silica. **Figure 2.13** shows a schematic representation of the reaction pathway for lime-quartz and lime-amorphous silica systems at the autoclaving temperature of $175\text{ }^{\circ}\text{C}$. According to **Figure 2.13**, a similar general pathway of the phase formation was observed for quartz and amorphous silica, whereas rates of formation and

Literature Review

stability of C-S-H phases were different. The main difference was that at the temperature of 175 °C, the consumption of lime required several hours in the quartz system, while this stage occurred rapidly within 40 minutes in the amorphous silica system at the same temperature. Therefore, for the lime-amorphous silica system, non-crystalline C-S-H formed rapidly within 2–3 hours due to the high solubility and dissolution rate of amorphous silica at the initial stages. However, the transition of non-crystalline C-S-H into well-crystallized tobermorite was slow which was considered unexpected by Kalousek. In opposition to lime-amorphous silica, the poorly crystallized C-S-H formed in the lime-quartz system was completely transformed into well-crystallized tobermorite.

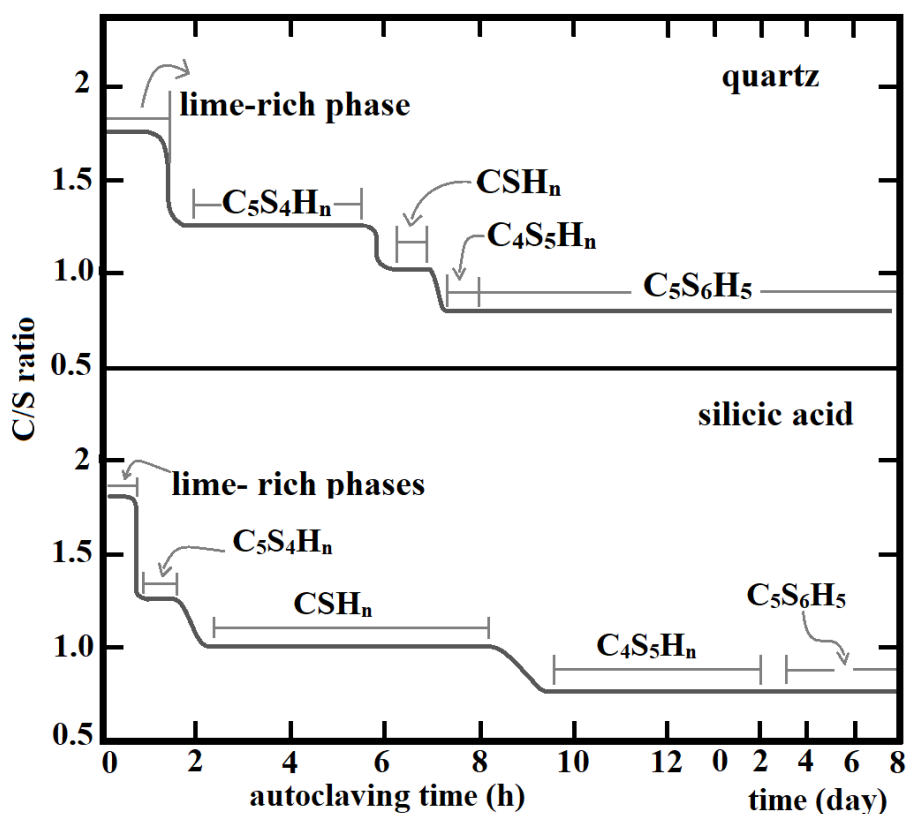


Figure 2.13 Reaction pathway of quartz and amorphous silica with calcium hydroxide at the autoclaving temperature of 175 °C (modified from source [53]).

Several other studies also reported similar results as those which were considered surprising by Kalousek. However, this time the results were interpreted by examining the structure of C-S-H gel formed at the initial stages of hydrothermal treatment. Sato et al. [43] studied the effect of starting materials on the synthesis of tobermorite. In their study, mixtures of lime-quartz and lime-colloidal silica with a C/S of 0.8 were hydrothermally treated at the temperature of 180 °C. The results showed the formation of well-crystallized tobermorite in the lime-quartz system in 4 h which gained its highest amount in 8 h. On the other hand, in the mixture of lime with amorphous silica, i.e. colloidal silica, semi-crystalline C-S-H formed very rapidly in 2 h. Nevertheless, they did not crystallize to well-crystallized tobermorite even after 24 h. Moreover, the result of NMR spectroscopy revealed that semi-crystalline C-S-H formed in the lime-colloidal system had a high Q_2/Q_1 plus Q_3 and as a result contained long and cross-linked silicate chains. However, low Q_2/Q_1 was observed for

the initial C-S-H formed in the mixture of lime-quartz which implies short silicate chains. Eventually, it was concluded that in the lime-colloidal silica system, C-S-H was hardly rearranged to tobermorite since they contained long and cross-linked silicate chains. In the case of the lime-quartz system, the transition of initially formed C-S-H to tobermorite occurred easily due to the short silicate chains of the initial C-S-H.

The parallel results as those mentioned above were observed by Mitsuda et al. [44, 46, 47, 138]. The outcome of their studies indicated that utilization of silica materials of high solubility in the hydrothermally treated lime-silica mixture led to the formation of initial C-S-H with a high degree of polymerization and long silicate chains which hindered the rearrangement to tobermorite.

2.5.3 Behavior of various types of silica materials in AAC

Studying the hydrothermal chemistry of the lime-silica system is insufficient to understand the performance of the various types of silica materials in AAC.

Mitsuda et al. [39] investigated phase evolution during autoclaving process of AAC. In their study, the AAC samples were produced according to the factory recipes in which quartz sand was used as the silica source in the AAC mixture. The autoclaving process was conducted at 180 °C for various curing times of 1 h, 2 h, 3 h, 5 h, 8 h, 16 h, 32 h, and 64 h. For the curing time of 1 h, the hydrothermal products contained Ca-rich C-S-H with a low degree of crystallinity and a small amount of poorly-crystalline tobermorite. Increasing the autoclaving time led to an increase in the amount and crystallinity of tobermorite which increases compressive strength. Highly crystalline tobermorite was achieved only by autoclaving for more than 8 h. However, prolonged autoclaving, i.e. for 32–64 h, causes a decrease in the compressive strength of AAC samples as a result of the decomposition of tobermorite to xonotlite. In the above-mentioned study, only the influence of autoclaving time was evaluated. Moreover, the performance of other types of silica materials was not examined.

The influence of autoclaving time, as well as temperature on the properties of quartz-based AAC, was studied by Chen et al. [42]. The various autoclaving temperatures between 160 °C and 208 °C with corresponding steam pressure between 5 bar and 17 bar were applied. The autoclaving time was adjusted between 2 h and 24 h. It was observed that under the autoclaving pressure of 12 bar (corresponding to around 192 °C), the compressive strength of the AAC samples increased when the autoclaving duration increased to 12 h. However, extending the autoclaving time to 16 h did not change the compressive strength significantly. Moreover, it was reported that the improvement in the compressive strength was accelerated when the autoclaving pressure increased from 12 bar to 18 bar (corresponding to around 210 °C). For the autoclaving pressure of 18 bar, the compressive strength grew as the autoclaving time increased to 5 h. However, autoclaving for 8 h and 12 h did not make any further development in compressive strength. The compressive strength of AAC samples autoclaved under 18 bar for 5 h was higher than that autoclaved under 12 bar and 15 bar for 12 h. It was concluded that applying a high autoclaving pressure would reduce the required autoclaving time, although it could increase expenses related to the equipment. The phase formation was investigated only under 12 bar for 5 h, 12 h, and 16 h. Progress in the tobermorite formation was observed as the autoclaving duration increased from 5 h to 16 h which is similar to what was observed by Mitsuda [39].

Literature Review

Isu et al. [12, 38] investigated the influence of different particle sizes of quartz sand on the chemical reactions and mechanical properties of AAC blocks which were prepared at 180 °C under saturated steam pressure for various times from 0.5 h to 64 h. It was observed that all the mixtures had almost the same composition before autoclaving. At this stage, the green bodies of all samples contained C-S-H, Ca(OH)₂, alite, belite, and almost all the quartz which remained unreacted. However, the composition of samples became different after autoclaving. They found that with finer quartz sand (mean particle diameters < 32.3 μm and specific surface area of 1.65 m²/g) tobermorite was formed only after 0.5 h autoclaving, indicating that finer quartz sand could reduce the autoclaving processing time. However, it was also observed that the tobermorite formed with finer quartz sand had small crystals indicating low crystallinity. For the AAC samples with the coarser quartz sand (mean particle diameters of 32.3 μm and specific surface area of 0.91 m²/g), highly crystalline tobermorite with large crystals formed after 2 h autoclaving.

The reason was attributed to the high specific surface of the finer quartz sand which led to a high degree of supersaturation as a result of supplying a high amount of dissolved silica to the solution. In such cases, a high quantity of nuclei prevents the growth of crystals, thus yielding the formation of small crystals with low crystallinity.

For the AAC samples with coarser quartz sand, the compressive strength, fracture energy, and Young's modulus increased as the tobermorite formation increased. However, the compressive strength of AAC samples containing fine quartz sand decreased as the autoclaving time increased to 64 h. Therefore, AAC samples with coarser quartz exhibited higher mechanical strength compared to those with finer quartz. It was mentioned that in AAC samples with coarser quartz, higher amounts of well-crystallized tobermorite yielded a lower maximum pore size (0.02 μm) in solid matrix compared to that with finer quartz (0.05 μm).

Moreover, it was observed that the compressive strength of AAC samples with finer quartz decreased considerably when the autoclaving time increased from 32 h to 64 h which was suggested to be the result of the decomposition of tobermorite to gyrolite after 64 h autoclaving.

Similar results were observed by Matsui et al. [75] who investigated the influence of quartz reactivity on tobermorite formation in AAC samples produced at the autoclaving temperature of 190 °C with different duration. Two types of quartz sand with different fineness which led to different reactivity were used. It was reported that in the experiments using quartz of a higher reactivity (small quartz crystals with a grain size of several micrometers), tobermorite formed quickly in the initial steps of the hydrothermal treatment. Nevertheless, the rate of formation dropped in the following steps. Thus, non-crystalline C-S-H and katoite, which is a type of hydrogarnet, were left in the final sample. On the contrary, for the system with quartz of a lower reactivity (large quartz crystals with a grain size of several hundred micrometers), tobermorite formation lasted up to the final stages of the autoclaving process. It was concluded that using two different types of quartz with different reactivity yielded the formation of two different types of C-S-H at the initial steps of the autoclaving. The type formed in AAC containing quartz of higher reactivity did not rearrange to tobermorite whereas, another type formed in AAC with quartz of a lower reactivity transformed to tobermorite easily.

Several studies investigated the influence of different types of fly ash, e.g. fluidized fly ash, on the properties of AAC [29–31, 139]. Among different types of fly ashes, pulverized fly ash (PFA) stands as a source of reactive silica composed of amorphous silicate and/or aluminosilicate which could be used for AAC production. In addition to amorphous silicate, crystalline inclusions of sulfates, mullite, and quartz are present [140]. Carroll [13, 141, 142] conducted a comprehensive study on the hydrothermal reactions of PFA and the production of PFA-based AAC. The results revealed the formation of the semi-crystalline C-S-H phase and hydrogarnet phase at the initial stages of the hydrothermal treatment. The crystallization extent of semi-crystalline C-S-H to tobermorite was found difficult to determine, but it was reported that a large quantity of semi-crystalline C-S-H did not crystallize to tobermorite and remain in the final product. In the aforementioned study, autoclaving conditions comparable to those in the industrial manufacture of AAC were used. The hydrothermal reactions of PFA were investigated at the temperature of 184 °C for different periods of up to 21 hours.

Mostafa [74] studied the effect of air-cooled slag (AS) on AAC properties by replacing quartz sand and lime with AS. The autoclaving process was conducted under a pressure of 10 bar and a corresponding temperature of 183 °C. It was noted that up to 50% replacement of quartz sand with AS in the low-lime mixture (10% CaO) led to the formation of tobermorite after only 2 h autoclaving. Nevertheless, the intensity of the tobermorite peak remained constant with increasing the autoclaving time to 24 h. The author mentioned that this occurred due to the faster consumption of lime by AS as a result of its higher reactivity compared to quartz sand. Moreover, the combined water increased as a result of substituting AS for quartz sand which implies a higher rate of hydration reaction in the slag-based AAC compared to the quartz-based AAC. Therefore, in those mixes, the C-S-H formed after a short autoclaving time and then transformed into tobermorite due to its suitable C/S. However, continuing the autoclaving process for a longer time reduced the value of C/S to very low values corresponding to a long silicate chain and a high Q_2/Q_1 plus Q_3 . It was mentioned that tobermorite cannot be formed from C-S-H with a very low C/S ratio (Si-rich) neither by a long autoclaving time nor by the addition of accelerators such as aluminum and sulfate ions [143]. Thus, the amount of tobermorite remained constant even after a longer autoclaving time. The author declared that the replacement of quartz sand with AS in the AAC mixture might lead to optimization of the autoclaving time.

Kunchariyakun et al. [122] examined the properties of AAC containing rice husk ash (RHA) as a silica source. The AAC mixtures in which quartz sand was replaced with RHA, were autoclaved at the temperature of 180 °C for 8 h and 18 h. RHA contained cristobalite which has a higher solubility than quartz. The results showed that compressive strength decreased when quartz sand was replaced with RHA in the AAC mixture. It was also reported that compressive strength slightly changed with the increasing autoclaving time. The results of qualitative XRD analysis confirmed the results of compressive strength. They observed that increasing the autoclaving time did not affect the intensity of tobermorite peaks and thus concluded that the use of RHA in AAC led to a reduction in the required autoclaving time. These results are in line with the previously mentioned results observed by Mostafa [74]. In both aforementioned studies [74, 122], only the effect of autoclaving time was discussed, and the autoclaving temperature was kept constant.

In 2018, Kunkarchiyan et al. [92] carried out a similar study with black rice husk ash (BRHA) and bagasse ash (BA) in which in addition to the autoclaving time, the influence of

Literature Review

the autoclaving temperature was also examined. However, in that study, they did not observe a trend to decrease the autoclaving time or temperature. The results of their study imply that under different autoclaving conditions, more-soluble silica-based AAC exhibits a behavior similar to quartz-based AAC. It appeared that the compressive strengths of the AAC samples containing BRHA and BA increased as the autoclaving temperature and time increased, whereas it was reported earlier that the compressive strength for rice husk ash replacements of greater than 25% remained stable after a longer curing time.

2.5.4 Limitation of knowledge

Many efforts have been made in the use of by-products as well as secondary and waste materials such as air-cooled slag, silica fume, fly ash, bottom ash, zeolite, iron ore tailings, and waste glass in the AAC mixture to make it more environmentally friendly and economical [2, 74, 32, 29, 145–147]. However, there are still quite a few studies related to a reduction in energy consumption during the autoclaving process through the utilization of silica materials of a higher solubility than quartz in the AAC mixture.

Table 2.3 displays the summary of the investigations and the current knowledge on the behavior of silica materials in the lime-silica system and AAC mixture.

Table 2.3 Overview of research studies on the behavior of different silica materials in the lime-silica system (red) and AAC mixture (blue).

year	researcher(s)	outcome
1955	Kalousek [53]	<p>Lime-amorphous silica mixture: Rapid formation of non-crystalline C-S-H within 2–3 h, the slow transition of non-crystalline C-S-H into well-crystallized tobermorite</p> <p>Lime-quartz mixture: The complete transformation of poorly crystallized C-S-H into well-crystallized tobermorite</p> <p>Autoclaving condition: T= 175 °C with different duration</p>
1978–1994	Chan et al. [47] Mitsuda et al. [138] Okada et al. [46] Sato et al. [43]	<p>lime-amorphous silica mixture: Initially formed C-S-H with very low C/S, high Q₂/Q₁ plus Q₃, long and cross-linked silicate chains, difficult to transform to tobermorite</p> <p>lime-quartz mixture: Initially formed C-S-H with enough high C/S, low Q₂/Q₁, short silicate chains, transform to tobermorite readily</p> <p>Autoclaving condition: T= 180 °C with different duration</p>
1995	Isu et al. [12, 38]	<p>AAC with finer quartz sand: Tobermorite was formed quickly, small crystals with lower crystallinity, a high degree of supersaturation.</p> <p>AAC with the coarser quartz sand: Highly crystalline tobermorite with large crystals, higher compressive strength, and Young's modulus due to the denser solid matrix</p> <p>Autoclaving condition: T= 180 °C with different duration</p>

1996	Carroll [13, 141, 142]	<p>AAC containing pulverized fly ash (PFA): A large quantity of semi-crystalline C-S-H did not crystallize to tobermorite and remain in the final product. Autoclaving condition: T= 184 °C with different duration</p>
2005	Mostafa [74]	<p>AAC containing air-cooled slag (AS) (up to 50% replacement of quartz sand with AS in the low-lime mixture): After a short autoclaving time: Quick formation of tobermorite, formation of C-S-H with suitable C/S for tobermorite formation. Further autoclaving: Constant intensity of the tobermorite peak, reduction of C/S to very low values corresponding to a long silicate chain, and a high Q₂/Q₁ plus Q₃. It was emphasized that tobermorite can not be formed from C-S-H with a very low C/S ratio (Si-rich) neither by a long autoclaving time nor by the addition of accelerators such as aluminum and sulfate ions. General outcome: the replacement of quartz sand with AS in the AAC mixture might lead to optimization of the autoclaving time. Autoclaving condition: T= 183 °C with different duration</p>
2011	Matsui et al. [75]	<p>AAC with quartz sand of a higher reactivity: Tobermorite formed quickly in the initial steps of the hydrothermal treatment, initially formed C-S-H did not rearrange to tobermorite in the last stages of autoclaving, and non-crystalline C-S-H and katoite were left in AAC. AAC with quartz sand of a lower reactivity: Tobermorite formation lasted up to the final stages of the autoclaving process, the higher total amount of tobermorite. Main outcome: using two different types of quartz with different reactivity yielded the formation of two different types of C-S-H at the initial steps of the autoclaving. Autoclaving condition: T= 190 °C with different duration</p>
2015	Kunchariyakun et al. [122]	<p>AAC containing rice husk ash (RHA) as silica source: Compressive strength and tobermorite formation did not change significantly with increasing the autoclaving time. The compressive strength and tobermorite formation decreased when quartz sand was replaced with RHA. General outcome: there might be a possibility to reduce the required autoclaving time by replacing quartz sand with RHA in the AAC mixture. Autoclaving condition: T= 180 °C for 8 h and 18 h</p>
2018	Kunchariyakun et al. [92]	<p>AAC containing black rice husk ash (BRHA) and bagasse ash (BA) : A trend to decrease the autoclaving time or temperature was not observed. The compressive strengths and tobermorite formation increased as the autoclaving temperature and time increased. Main outcome: under different autoclaving conditions, more-soluble silica-based AAC exhibits a behavior similar to quartz-based AAC. Autoclaving condition: T= 140 °C, 160 °C and 180 °C for 4 h, 8 h and 12 h.</p>

Literature Review

As it is shown in **Table 2.3**, previous studies revealed the determining role of C/S in the equilibrium of the formed C-S-H. Moreover, the results of previous studies have generally shown that utilization of the silica materials of a higher solubility in either the lime-silica system or the AAC mixture hinders the final rearrangement of C-S-H to tobermorite [43, 47, 75, 74, 13] and decreases the compressive strength of AAC samples. However, as stated earlier, the replacement of quartz sand with silica materials of a higher solubility is expected to have the advantage of reducing the autoclaving temperature and/or time without affecting the performance of AAC negatively.

This is likely because, in all of those studies, the applied autoclaving temperature for the system composed of lime and more soluble silica was relatively high at a level of $T \geq 180$ °C similar to that used for the quartz system. However, high autoclaving temperatures, similar to those used for autoclaving the quartz-based AAC, are probably not the optimum temperatures for autoclaving systems containing silica materials of high solubilities. According to section 2.5.1, the solubility and dissolution rate of silica significantly increase with an increase in temperature. Therefore, applying a high autoclaving temperature makes the dissolution of silica materials of higher solubility even faster which affects the equilibrium of the initially formed C-S-H and its transformation to tobermorite. This could be the reason why previous studies have reported inhibition of tobermorite formation in a more soluble system which is not desirable.

According to sections 2.5.2 and 2.5.3, the performance of the quartz-based AAC under different autoclaving conditions is within the scope of knowledge. It is widely known that the optimum properties of the quartz-based AAC can be obtained at the autoclaving temperatures of $T > 180$ °C and a total duration of 8–12 h, depending on the size of the samples [75, 132]. However, the performance of more soluble silica-based AAC at different autoclaving temperatures has only been examined by Kunkarchiyan et al. [92] who did not observe a trend to decrease the autoclaving time and/or temperature.

Therefore, with regard to silica materials known to have a higher solubility than quartz, the expected advantages for AAC production, e.g. obtaining the same level of quality by applying a lower autoclaving temperature and/or shorter autoclaving time have not been achieved to a sufficient extent so far.

2.6 Aims and research objectives

The question arises whether it is possible to control the dissolution of silica materials of a higher solubility in a way that leads to a reduction in the autoclaving temperature and/or time without a deterioration in the performance of AAC products. Since the dissolution of silica materials is strongly dependent on temperature, the dissolution of more soluble silica might be controlled by using a lower autoclaving temperature compared to that used for the dissolution of quartz which might avoid progressive polymerization of silicate chains. This thesis addresses this gap by applying low temperatures for autoclaving the more soluble silica-based AAC.

Thus, using silica materials of a higher solubility than quartz as the silica source in AAC while the autoclaving temperature is adjusted might present an opportunity to produce AAC products that require less energy for the hydrothermal process.

From a general point of view, the goal of this thesis is formalized as the following.

Thesis objective:

This study was intended to reduce the required autoclaving temperature in the production of AAC in a way that does not influence its properties negatively.

For this purpose, quartz sand within the AAC mixture was replaced with calcined diatomaceous earth (C-DE) and rice husk ash (RHA) as silica raw materials of higher solubility. Therefore, the first research question in this dissertation can be mentioned as the following.

Research question I:

How is the behavior of C-DE and RHA in AAC?

This question was answered by examining the possibility of producing AAC samples using C-DE and RHA as the silica source in the mixture.

Furthermore, the gap seen in the current knowledge related to achieving the expected advantages of using silica materials of high solubility is addressed by the following two research questions.

Research question II:

Is the performance of the C-DE-based and RHA-based AAC under different autoclaving temperatures similar to that of the quartz-based AAC?

Research question III:

Is a lower autoclaving temperature required to reach the specific properties of AAC when C-DE or RHA is used as the silica material in the AAC mixture?

To answer the above research questions, first, the performances of the quartz-based AAC and more soluble silica-based AAC under different autoclaving conditions were evaluated. Finally, the possibility of reducing the autoclaving temperature in AAC production by using silica raw materials of a higher solubility than quartz as the silica source in the mixture was discussed.

2.7 Thesis outline

The contribution of this cumulative thesis is mainly based on the following three articles published in international peer-reviewed journals.

Shams T, Schober G, Heinz D, Seifert S, “Production of autoclaved aerated concrete with silica raw materials of a higher solubility than quartz part I: Influence of calcined diatomaceous earth” *Construction and Building Materials*, V. 272, 2021. <https://doi.org/10.1016/j.conbuildmat>

Shams T, Schober G, Heinz D, Seifert S, “Production of autoclaved aerated concrete with silica raw materials of a higher solubility than quartz Part II: Influence of autoclaving

Literature Review

temperature” *Construction and Building Materials*, V. 287, 2021.
<https://doi.org/10.1016/j.conbuildmat>

Shams T, Schober G, Heinz D, Seifert S, “Rice husk ash as a silica source for the production of autoclaved aerated concrete – a chance to save energy during the hydrothermal treatment” *Journal of Building Engineering*, 2022 (accepted).

This dissertation is categorized into five chapters. A short introduction is presented in **chapter 1**. The literature review and goals of this thesis are given in **chapter 2** which is the present chapter. In **chapter 3**, Materials, laboratory experiments, methods, and procedures are presented. **Chapter 4** provides a synopsis of the results of the above-mentioned papers with relevant discussions. In this chapter, all results are not presented to avoid repetition mainly in discussion sections. This makes it more comfortable for readers to understand the topic while providing an option for them to refer to the publications for possible additional information. Conclusion and outlook are presented in **chapter 5**. Finally, the publications as supplements for chapter 4 are included in **appendix A**.

Declaration: The contents of Chapters 3 to 5 are largely identical to the scientific articles published by the author.

Material and Methods

In this chapter, the properties of materials, procedures of producing samples, issues during the production of samples, and methods used in the study are presented, respectively.

3.1 Characterization of the raw materials

3.1.1 Materials sources

In this study, three types of silica sources, quartz sand, calcined diatomaceous earth (C-DE), and rice husk ash (RHA) were used (**Figure 3.1**). Quartz sand, which was extracted from an open-pit mine in Germany, was provided by Dorfner GmbH, Germany. C-DE was provided by Apj GmbH, Germany. However, it was manufactured in the western region of the USA from raw diatomaceous earth (DE).



Figure 3.1 Silica materials used in this study. From left to right, quartz sand, C-DE, and RHA.

DE is a siliceous, sedimentary rock consisting of fossilized skeletal remains of diatoms. DE is an attractive material offering broad application in the industry owing to its properties of a low bulk density, high chemical and thermal resistance, high porosity, and a high specific surface area. As a natural mineral raw material, DE is convenient and promising with respect to the production of porous building materials such as AAC due to its natural porosity, low density, and mineralogical composition [148]. Moreover, DE is much softer than quartz sand eased the grinding process. This fact can provide considerable energy savings in the milling operations of AAC production. C-DE is obtained from treating DE at a temperature range of 700–900 °C. Usually, DE is calcinated before being sold to remove impurities and undesirable volatile contents. The purpose of this approach is also specific industrial applications such as further hardening the skeletons of the diatoms in order to create better filtering agents. Since DE is mostly used for filtration and C-DE provides a higher flow rate in filtration, most DE available in the market are in the form of C-DE. The total consumption of DE in Germany is about 100,000 tons per year which produces a large amount of waste.

Although a kind of non-waste C-DE was used in this study, it could present an opportunity for incorporating these solid wastes into construction uses. There were regular efforts in the past to recalcine C-DE after it was used as a filter. In Germany, a lot of DE producers, e.g. brewery plants, have worked on the recycling processes of C-DE because the disposal of the consumed filter cakes becomes more and more a matter of concern. C-DE could be reused in the filtration processes but only in a limited quantity. In this case, it is needed to use a fresh DE in addition to recycled material, i.e. a mixture of fresh and recycled DE [149–152].

RHA was provided by Ackermann VDL, Germany which imported RHA from South America. For most plants, RHA is a worthless by-product that the expenses of its disposal should even be borne. However, it might be utilized as a substitute for by-products from coal-fired power plants, e.g. fly ash and bottom ash due to the decommissioning of the coal power plants by 2030 in Europe [153].

Rice husk, which is known as a favorable source of dry biomass, is a secondary product derived from the milling process of rice [154]. Based on the reported values, the global production of rice husk is 137 million tons per year [156]. However, this value is increasing rapidly due to the increased demand for rice production in order to feed a growing population. Rice husk produced in the milling process has been mainly used as a fuel in parboiling plants. The thermal energy obtained from burning rice husk is used for the milling process of rice. Additionally, the process of burning rice husk in the parboiling plants produces RHA as a waste residue which is usually about 20% of the primary fuel weight. RHA contains up to 95% silica in the form of crystalline and amorphous particles. The degree of crystallinity of RHA depends mainly on the temperature of the burning process as well as calcination parameters, e.g. calcination temperature and heating rate [157, 158]. RHA is calcined to remove impurities which could be unfavorable for its pozzolanic properties. RHA used in this study was calcined at a temperature range of 700–800 °C. Due to the high content of silica and also the fact that the quantity of these waste residues has been considerably increasing, there is an opportunity to use these waste residues as silica materials in the AAC mixture.

A type of soft-burnt quicklime (CL 90-Q) was used as a lime raw material which was provided by the Fels-Werke GmbH (Germany). Portland cement type I (CEM I 42.5), which was provided by Dornburger cement GmbH (Germany), was used. Anhydrite used in this study is from natural anhydrite which is finely ground and free of any additives (from Krone-Gips, Germany). GRA which was obtained by grinding waste AAC was provided by Xella Technologie- und Forschungsgesellschaft mbH, Germany.

3.1.2 Chemical compositions and physical properties

The chemical compositions and physical properties of the materials used in this study are given in **Table 3.1** and **Table 3.2**, respectively. In this study, the X-ray fluorescence (XRF) technique was used to determine the chemical compositions. However, the chemical compositions of some of the materials were provided by suppliers. The details of the measurement are described in section 3.4.3. In **Table 3.2**, density was determined according to DIN 66137-2 [159] using a gas pycnometer.

Figure 3.2 and **Table 3.3** show the particle size distribution of quartz sand, C-DE, and RHA which were determined by Laser particle size distribution (Malvern Mastersizer 3000).

Material and Methods

Table 3.1 Chemical composition of raw materials (wt. %).

sample	SiO ₂	CaO	Al ₂ O ₃	Fe ₂ O ₃	MgO	TiO ₂	Na ₂ O	K ₂ O	SO ₃	P ₂ O ₅	L.O.I	total
sand	98.8	0.0	0.8	0.0	0.0	0.0	0.0	0.3	-	-	0.2	100.2
C-DE	92.8	0.6	4.2	1.6	0.3	0.1	0.1	0.2	-	-	0.3	100.2
RHA	89.6	1.0	0.3	0.3	0.8	0.1	0.3	1.6	0.0	0.5	5.7	99.9
lime	0.8	1.0	0.3	0.2	0.5	-	-	-	0.2	-	3.0	100.0
cement	20.4	62.9	4.9	2.5	1.7	-	0.2	1.0	3.8	-	3.0	100.5
GRA	41.2	37.4	2.0	1.3	-	0.1	-	0.7	5.7	-	12.0	100.4
anhydrite	-	47.5	-	0.2	-	-	-	-	52.2	-	-	99.9

Table 3.2 Physical properties of raw materials.

sample	density (g/cm ³)	bulk density (g/cm ³)
quartz sand	2.63	0.93
C-DE	2.41	0.19
RHA	2.30	0.45

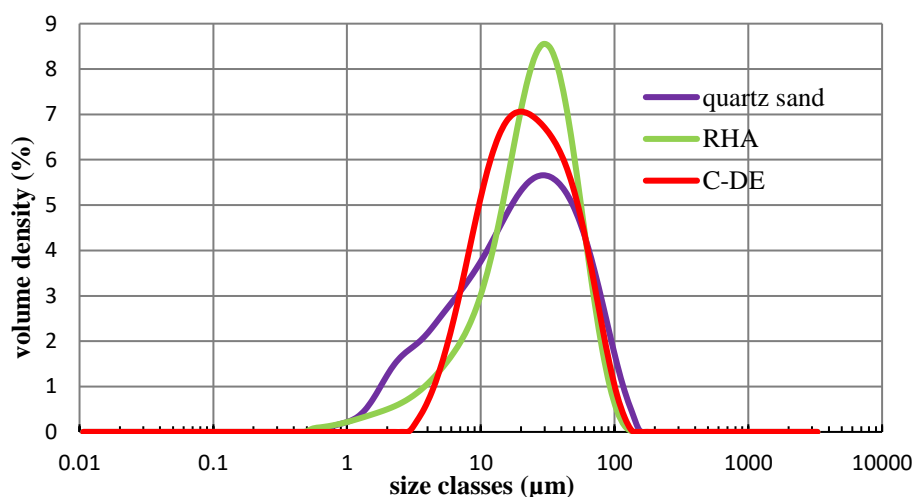


Figure 3.2 Comparison of the particle size distribution of silica raw materials.

Table 3.3 Particle size distribution of silica materials.

sample	D(10) μm	D(50) μm	D(90) μm
quartz sand	3.7	20.4	65.6
C-DE	8.0	21.9	59.1
RHA	6.5	25.0	56.2

3.1.3 Mineral composition and microstructure

Figure 3.3 shows the XRD patterns of quartz sand, C-DE, and RHA. The XRD pattern of quartz sand includes sharp peaks of quartz while C-DE and RHA consist of cristobalite which has a higher solubility than quartz [133, 135]. Additionally, a comparatively broad peak of cristobalite shows a lower degree of crystallinity of C-DE and RHA compared to quartz sand. This can also be understood by comparing the values in **Table 3.4**.

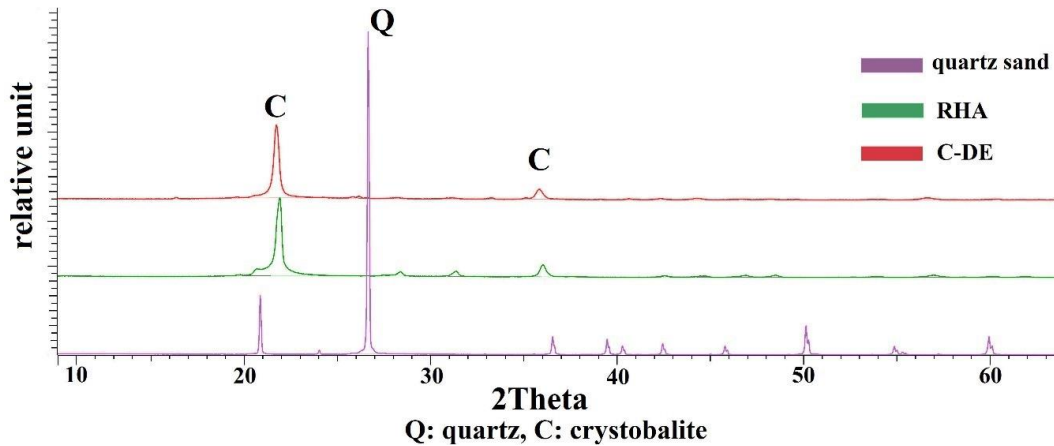


Figure 3.3 XRD pattern of quartz sand, C-DE, and RHA.

Table 3.4 shows the amorphous and crystalline content of these materials as provided by DIFFRAC.EVA and DIFFRAC.TOPAS software. EVA software calculates the crystalline content by dividing the total area of crystalline peaks by the total area under the diffraction curve, i.e., crystalline peaks plus amorphous reflections [160]. The degree of crystallinity calculations in TOPAS software requires the definition of at least two phases to describe the intensity contributions coming from the crystalline and the amorphous parts of the sample. Different techniques can be used for modeling crystalline and amorphous parts of the sample [161].

Table 3.4 Amorphous and crystalline content of quartz sand, C-DE, and RHA.

sample	crystalline %		amorphous %	
	EVA	TOPAS	EVA	TOPAS
quartz sand	94	98	6	2
C-DE	71	66	29	34
RHA	75	77	25	23

SEM micrographs of quartz sand, C-DE, and RHA are shown in **Figure 3.4**, **Figure 3.5**, and **Figure 3.6**, respectively. According to **Figure 3.4** quartz sand is composed of dense particles without any internal pores. However, as can be observed in **Figure 3.5** C-DE has a porous structure including internal pores on the micrometer scale leading to a cellular microstructure. The SEM images of RHA (**Figure 3.6**) display a structure composed of

Material and Methods

different sizes of cavities and layered appearances resulting in an interconnected microstructure.

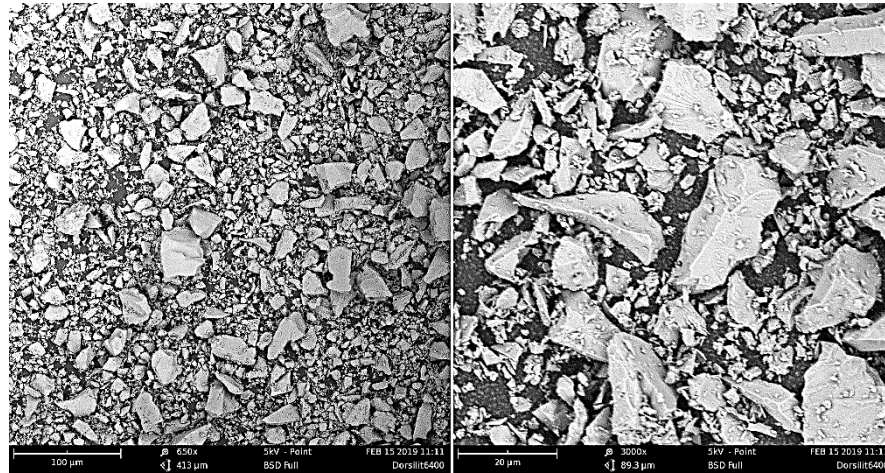


Figure 3.4 SEM micrographs of quartz sand.

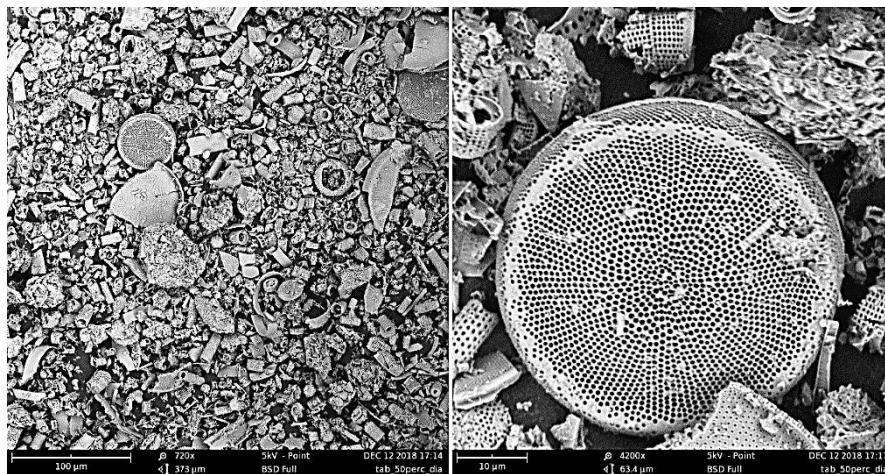


Figure 3.5 SEM micrographs of C-DE.

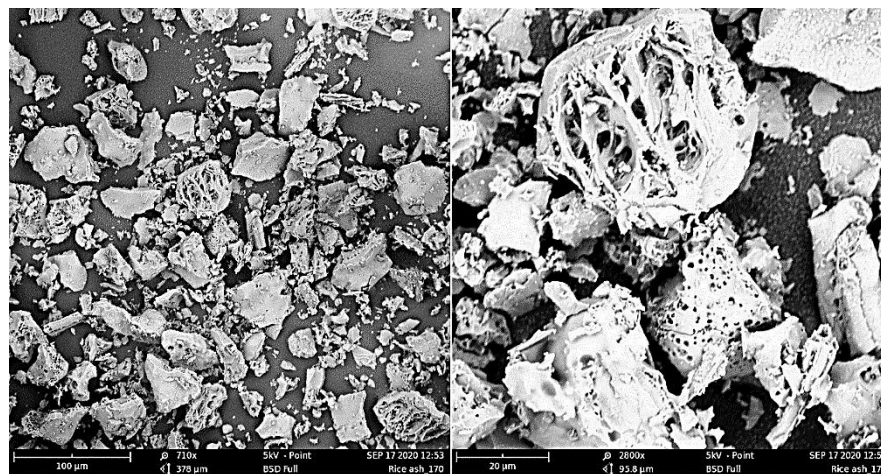


Figure 3.6 SEM micrographs of RHA.

Moreover, the specific surface areas of quartz sand, C-DE, and RHA were determined by the BET (Brunauer, Emmett, and Teller) method. Accordingly, the values of 0.79 m²/g, 2.90 m²/g, and 1.80 m²/g were obtained for quartz sand, C-DE, and RHA, respectively, which shows higher specific surface areas for C-DE and RHA compared to that for quartz sand.

3.2 Procedure of producing AAC samples

The referenced mix design (Q100), which was similar to the mix proportion of AAC produced in the industry, was adjusted to the P4-500 grade. The P4-500 is a German grade for AAC which refers to AAC with a density range of 450–500 kg/m³ and compressive strength of greater than 4.9 MPa. Quartz sand in the Q100 mix was replaced by C-DE for 25 wt. %, 50 wt. %, and 75 wt. % to produce DE25, DE50, and DE75, respectively. A stable AAC sample could not be obtained when the whole quartz sand was replaced with C-DE. Therefore, the DE100 mix was not produced.

Experience in experimental work with C-DE and relevant results showed that the quantity of C-DE has to be large enough to influence the AAC properties. Therefore, for subsequent experiments, RHA was used as the main silica material in the AAC mixture. Accordingly, R75 and R100 mixes were produced by replacing 75 wt. % and 100 wt. % of quartz sand with RHA in the reference mix, respectively. The mix proportions are shown in **Table 3.5**.

Table 3.5 Mix proportions of AAC samples (wt. %).

mixture	sand	C-DE	RHA	cement	lime	anhydrite	GRA	C/S*	W/S**	Aluminum***
Q100	41.0	-	-	31.0	10.0	6.0	12.0	0.635	0.70	3.35
DE25	31.0	11.0	-	31.0	10.0	6.0	11.0	0.633	0.80	3.07
DE50	20.5	22.0	-	31.0	10.0	6.0	10.5	0.636	0.95	2.62
DE75	10.0	33.0	-	31.0	10.0	6.0	10.0	0.640	1.20	1.87
R75	10.0	-	34.5	31.0	10.0	6.0	8.5	0.640	0.80	3.03
R100	-	-	45.5	31.0	10.0	6.0	7.5	0.642	0.83	2.92

* Molar ratio of CaO/SiO₂

** Water to solids ratio

*** Aluminum values are in g

Water-to-solids ratio (W/S) and aluminum paste values were set in a way to obtain almost the same bulk density for all mixes. The mixtures containing C-DE and RHA required higher water content, which is represented by the higher W/S, because of their porous structure compared to quartz sand. In such a case which was necessary to increase the W/S, a higher water quantity was compensated by a lower quantity of aluminum paste (the last two columns in **Table 3.5**) to obtain a similar bulk density.

To be able to observe the effect of C-DE and RHA on the final properties of AAC all the other parameters influencing the final properties must have been kept constant. Accordingly, it was needed to use similar particle size distribution for silica sources and also almost the

Material and Methods

same C/S of the starting materials for all mixes. In this study, an almost similar particle size distribution for silica sources was used (**Figure 3.2**).

The C/S of starting materials influences the matrix structure strongly. In order to compare the effect of C-DE and RHA directly on the AAC properties, it was, therefore, necessary to keep the C/S of starting material constant for all samples. However, replacing quartz sand with C-DE or RHA reduced the C/S of the starting materials since C-DE and RHA contained a lower SiO₂ content compared to quartz sand. Therefore, to keep the C/S of the starting materials constant for all mixes, it was needed to change the mix design adequately. For this purpose, there was a precondition that needed to be satisfied before changing the mix design; the total amount of reactive CaO must have not been changed otherwise the total possible amount of C-S-H would have changed. Thus, the portion of lime and cement could not be changed unless both components were changed in a way that the total reactive CaO remained constant. The simple alternative solution (in the author's opinion) was that after replacing quartz sand with C-DE or RHA for the aforementioned replacement ratios, the amount of C-DE or RHA were increased for a minor quantity and the quantity of GRA was decreased adequately. All the aforementioned changes were in a range of 1–4.5 wt. % which was not a severe change in the mix design since GRA, which acts only as a filler, is not reactive during the process. Subsequently, the C/S molar ratio of the starting material for all mixes was adjusted at 0.63–0.64 by applying the above-mentioned approach.

Quartz sand, C-DE, RHA, and GRA were mixed with water. In this study, a water temperature of 38 °C was used. Lime, cement, and anhydrite were then added, and the mixture was stirred for 2 minutes. Finally, the aluminum suspension was added and the mixing continued for 30 seconds (**Figure 3.7**). In general, the whole mixing process took between 3 to 4 minutes.



Figure 3.7 The mixing process. This figure is reprinted from Fraunhofer IBP archive.

The slurries were poured into 22 cm cubic Styrofoam molds. The samples were then stored at room temperature for 3 h (**Figure 3.8**). After demolding, the samples were steam cured in the autoclave at different temperatures for a constant duration.

In industrial production, the duration of the whole autoclaving process including evacuating before steaming, steaming up, dwell time, and steaming down is around 12 h. The autoclaving steps of evacuation, steaming up, and steaming down usually take 3–4 h. Thus,

the autoclaving time in which the sample is under desired pressure (or temperature), i.e. dwell time, is around 8–9 h. However, the autoclaving time is optimized with respect to the sample size and density of the samples. Lower densities and smaller samples need less autoclaving time. Therefore, for AAC production on the laboratory scale in which the smaller sample size is used a rather shorter dwell time could be applied.

In this study, the autoclaving time in which the sample is under desired temperature (or pressure) was 6 h. The evacuation and steaming up steps took around 1.5 h and steaming down took another 1.5 h. Thus, the total duration of the autoclaving process was around 9 h. The duration of the autoclaving process was kept constant for all samples.



Figure 3.8 From left to right, molding, rising to the final volume, and demolding.

The autoclave used in this study has been specially produced similar to autoclaves used for industrial production of AAC. This autoclave has a volume of 1.5 m³ with an external steam supply (**Figure 3.9**).

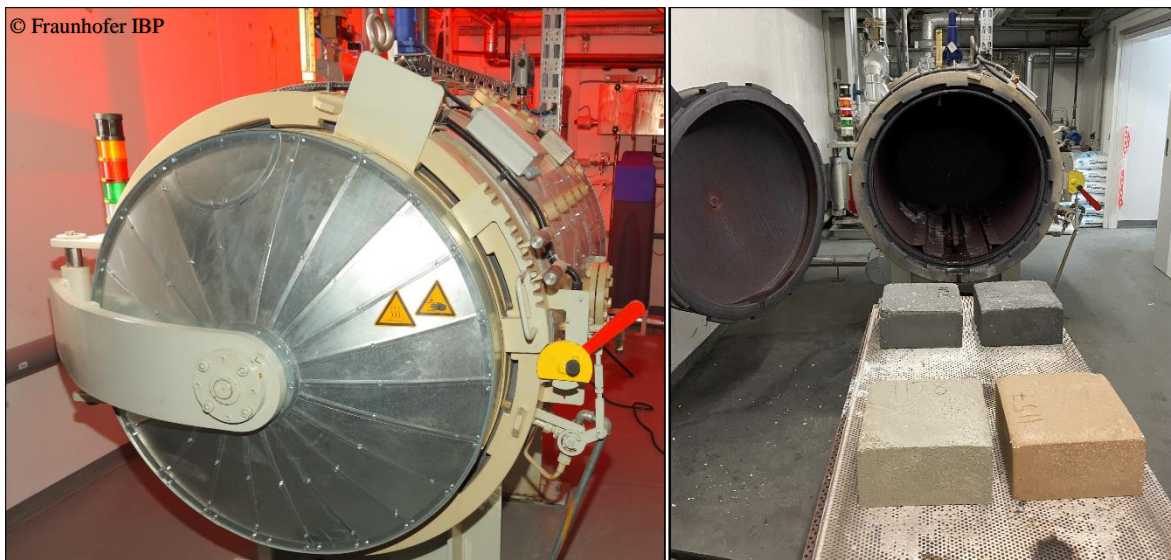


Figure 3.9 The autoclave used in this study. The left figure is reprinted from Fraunhofer IBP archive.

After removing the samples from the autoclave, the samples were cut into 10 × 10 × 10 cm³ cubes (**Figure 3.10**) and 4 × 4 × 16 cm³ prisms.

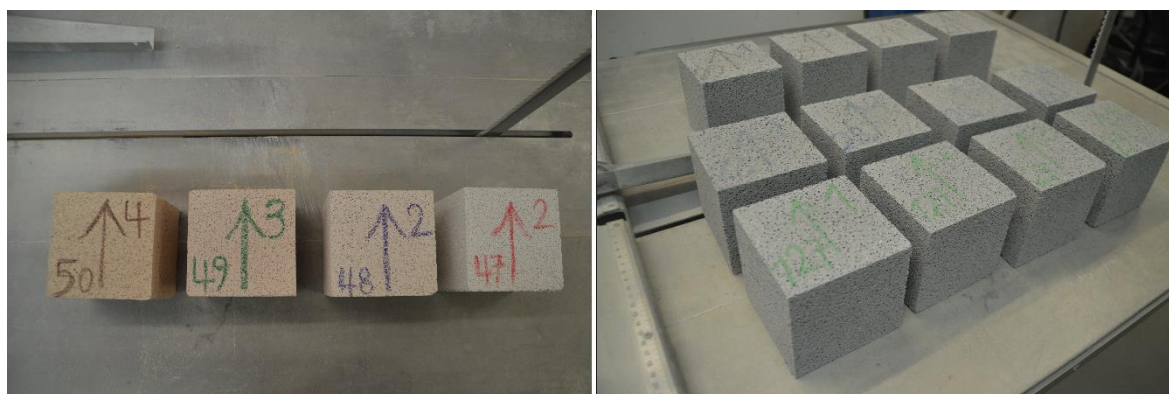


Figure 3.10 AAC cubes after the cutting process.

3.3 Issues during the production of samples

In the course of the first trials to produce AAC samples containing C-DE, an internal horizontal crack was observed in most of the samples. This crack was discovered during the cutting process when the samples were cut in half (**Figure 3.11**). For all of the samples, the crack appeared in an almost horizontal direction at about one-third of the sample height from the top of the surface. This implies that in all of the samples, the crack occurred due to the same reason.

This kind of crack, which is called expansion crack, can occur in AAC at the end of the expanding process due to the accumulation of gases that could not escape out of the green cake. The mechanism of occurring this type of crack was studied by Aono et al. [162]. According to the aforementioned study, expansion crack is occurred due to the difference in setting time of the top and bottom of the sample. The bottom part is set earlier compared to the top part. Therefore, the bottom part includes interconnected pores enabling gas to escape out of the sample through the solid structure. However, the gas passing through the top part is blocked in the sample since an interconnected structure has not been formed in the matrix. The accumulation of gas in the top part generates open cracks as a result of internal pressure. In this study, this crack might happen due to the high water content of AAC samples containing C-DE which delayed the setting of the mixture.

Utilization of a type of aluminum powder or paste with an elongated gas generation process, increased number of coarse particles, and wrinkled surface shape could prevent the generation of expansion cracks. Because in this case, the process of producing gas lasts longer when the setting of the top part has already started. Therefore, the produced gas enables to escape from the sample which avoids the formation of expansion cracks. In addition to using an optimum type of aluminum powder or paste, other solutions such as decreasing W/S might be effective [162].

In this study, this issue was handled by changing the type of aluminum paste. For this purpose, different aluminum pastes were tested, and finally, the aluminum paste Hydropor V 300 with an active metal content of $\geq 90\%$, D (50) of $35\ \mu\text{m}$, and D (90) of $100\ \mu\text{m}$ provided by ECKART GmbH was found to be compatible. The samples which were produced with this type of aluminum did not contain any expansion crack.



Figure 3.11 Expansion crack which was observed in the samples.

3.4 Methods

3.4.1 Compressive strength

The compressive strength was determined according to DIN EN 772-1 [163]. For this purpose, $10 \times 10 \times 10 \text{ cm}^3$ cubes were dried at $50 \text{ }^\circ\text{C}$ for several days until a moisture content of $6 \pm 2 \text{ wt. } \%$ was reached. The measurement was performed on four $10 \times 10 \times 10 \text{ cm}^3$ cubes per AAC block.

The compressive strength was determined using Zwick Roell Z 100 compression test machine (**Figure 3.12**) with the measurement parameters listed in **Table 3.6**. Due to the anisotropy of the specimens, the load was applied perpendicular to the expanding direction for all samples.



Figure 3.12 Measuring the compressive strength with Zwick Roell Z 100.

Material and Methods

Table 3.6 Measurement parameters used for determination of the compressive strength.

measurement parameter	value
loading speed	0.1 (N / mm ²) / s
force threshold for fracture investigation	10,000 N

After measuring compressive strength, a small but representative part of the broken sample was weighted and used for XRD analyses, SEM images, and thermal analyses. The broken sample was then collected in a bowl in order to determine the dry bulk density. In the following sections, the aforementioned measurements are described in detail.

3.4.2 X-ray diffraction (XRD) analysis

The XRD analysis was performed using a D2 Phaser diffractometer from Bruker (**Figure 3.13**) with Cu-K α radiation and a LynxEye silicon strip detector. All samples were measured with a step size of 0.02° 2 θ and a duration of 4 s/step over the range of 5–65° 2 θ . A summary of the measurement parameters is presented in **Table 3.7**.

The qualitative XRD analysis was performed using DIFFRAC.EVA software (Ver. 4.2) according to the International Center for Diffraction Data (ICDD) Powder Diffraction File (PDF). The Associated reference pattern numbers used for phase identification are given in **Table 3.8**.

Rietveld quantitative phase analysis was carried out using the internal standard method [164–166] to determine absolute phase contents including amorphous content. For this purpose, DIFFRAC.TOPAS software (Ver. 4.2) was used.

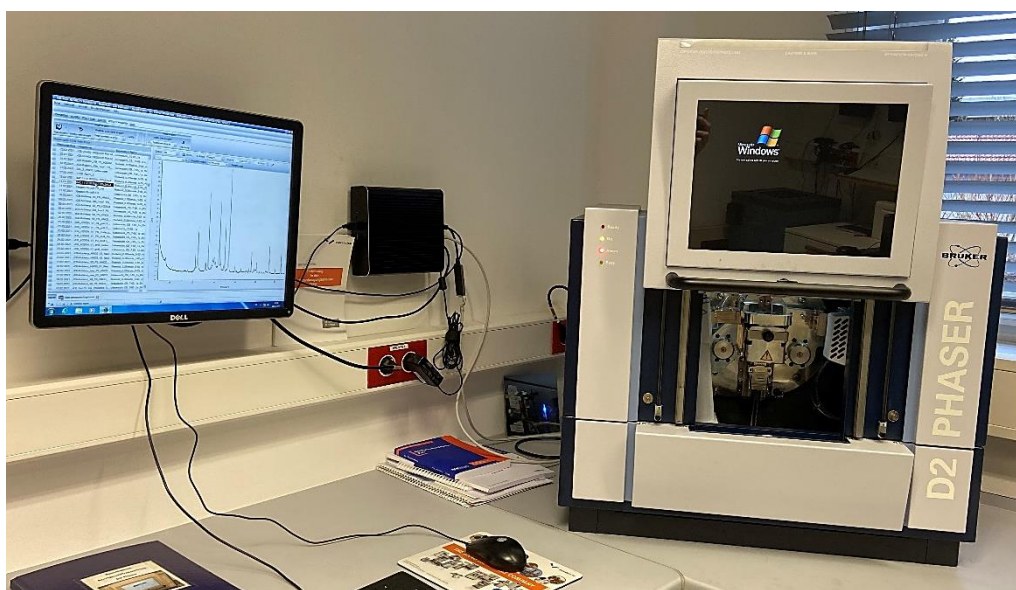


Figure 3.13 D2 Phaser diffractometer (from Bruker) which was used to record XRD patterns.

Table 3.7 Measurement parameters and settings of the Bruker D2 phaser diffractometer.

measurement parameter	value
wavelength	Cu-K α ($\lambda = 1.54 \text{ \AA}$)
voltage	30 kV
amperage	10 mA
measuring range	5–65° 2 θ
step size	0.02° 2 θ
measurement time per step	4 s
sample rotation speed	15 rpm
divergence diaphragm	0.2 mm
monochromator	Ni-Filter
detektor	silicon strip detektor (LynxEye)

Table 3.8 PDF number of compounds used for phase identification.

compound name	chemical composition	PDF number
quartz	SiO ₂	PDF 00-046-1045
cristobalite	SiO ₂	PDF 00-039-1425
tobermorite-11 \AA	Ca ₅ Si ₆ (O, OH, F) ₁₈ · 5 H ₂ O	PDF 00-045-1480
tobermorite-9 \AA	5 CaO · 6 SiO ₂ · 2.5 H ₂ O	PDF 00-010-0374
anhydrite	CaSO ₄	PDF 00-037-1496
bassanite	Ca (SO ₄) · 0.5 (H ₂ O)	PDF 01-072-4535
calcite	CaCO ₃	PDF 01-085-1108
katoite	Ca ₃ Al ₂ (SiO ₄) (OH) ₈	PDF 00-038-0368

For quantitative phase analysis, a grain size of < 10 μm is required. To avoid the amorphization of the sample during grinding, wet milling was used in XRD-Mill McCrone (from RETSCH). Before grinding in the McCrone Mill, the sample was crushed and passed through a 500-micron sieve. The standard material was then mixed with the sample by hand before grinding to produce a homogeneous mixture with reproducible results [167]. 10 wt. % addition of Zincite (ZnO) as the standard material was used. The mixture of the weighted sample and 10% ZnO was then carefully transferred to McCrone Mill. In the next step, 5 ml of ethanol as a grinding agent was added. This mixture was ground for 3 min. After micronizing, the sample was recuperated in cups by using ethanol and was dried for one-two days under a fume hood. Dried samples are gently disaggregated and passed through a 250-micron sieve. Eventually, frosted glass was used to fill sample holders and make a flat surface. To minimize the effect of preferential orientation, the surface was disordered with rough-texture glass. In this study, each sample was measured three times and the results were then averaged.

3.4.3 X-ray fluorescence (XRF) analysis

In this study, the X-ray fluorescence (XRF) technique was used to determine the chemical composition. XRF analysis was performed using Epsilon 3XLE spectrometer and Omnian software. For this purpose, samples were prepared as pressed tablets. To produce the tablets, the samples were first ground to a powder by using a planetary mill (FRITSCH Pulverisette

Material and Methods

6) with tungsten carbide balls. The ground samples were then mixed in a ratio of 4:1 with a binder (micro powder C, $C_{38}H_{76}N_2O_2$). The sample and binder must be mixed homogeneously. Thus, the mixture of the sample and binder was shaken together with iron balls for one minute. The mixture was then pressed using a tablet press machine at a pressure of 200 kN for about one minute to obtain a pressed tablet of 4-5 mm thick.

3.4.4 Scanning Electron Microscope (SEM)

The SEM was performed using a Phenom Pro X (**Figure 3.14**) made with a CeB6 electron source with acceleration voltages of 5 and 15 kV. For this purpose, a small flat piece of the AAC was fixed on an aluminum stub (12.5 mm). The prepared sample was then coated with a thin layer of gold as a conductive material (**Figure 3.15**). The compressed air was then blown on prepared samples in order to prevent drawing particles into the pump during the chamber evacuation.



Figure 3.14 Phenom Pro X, used to examine the microstructure of samples.



Figure 3.15 SEM sputter coater.

3.4.5 Thermal analyses

The thermal analyses including, differential thermal analysis (DTA) and thermogravimetric analysis (TGA), were performed using NETZSCH STA 409 CD over the temperature range of 23–1200 °C at a heating rate of 10 °C /min. Before starting the measurement, the samples were stored at 50 °C for 24 h.

3.4.6 Laser diffractometry

Laser diffractometry is used to determine the particle size distribution of samples, i.e. silica sources. The measurement was carried out with a Mastersizer 3000 (from Malvern) and the Hydro MV wet dispersion unit (**Figure 3.16**). Distilled water was used as the dispersant. At least 30 measurements were carried out per sample in order to observe possible changes. In this study, the results were reported as volume distribution.



Figure 3.16 Malvern Mastersizer 3000, used for determination of particle size for powders.

3.4.7 Shrinkage

The shrinkage of AAC samples was measured according to DIN EN 680: 2005 [168] on three $4 \times 4 \times 16 \text{ cm}^3$ prisms per AAC block **Figure 3.17** (left). To avoid incorrect readings, the measuring points should be marked on both sides of the prisms **Figure 3.17** (right).

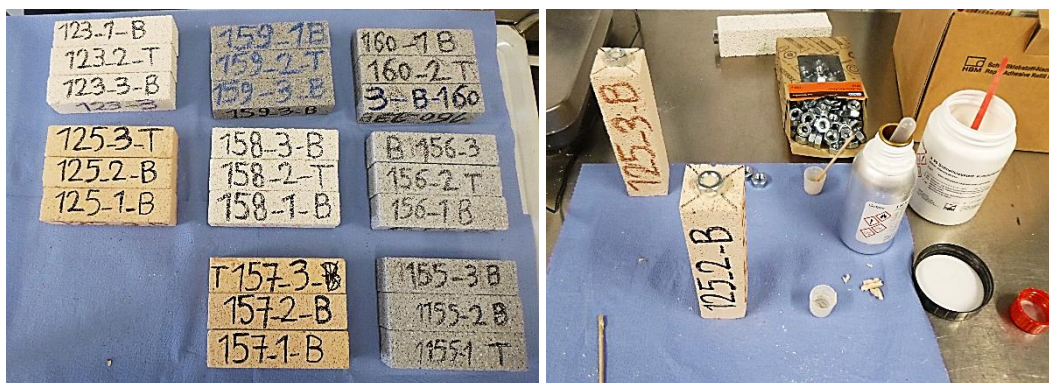


Figure 3.17 AAC prisms for measuring shrinkage (left). Marking measuring points on prisms (right).

Material and Methods

Subsequently, the prisms were placed in water with a temperature of 20 ± 2 °C for a period of 72 h (**Figure 3.18**); one-third of their thickness during the first 24 hours, two-thirds of their thickness during the second 24 hours, and completely submerged during the last 24 hours.



Figure 3.18 Conditioning AAC prisms in water with a temperature of 20 ± 2 °C for 72 h.

They were then stored in plastic wrap for 24 h. At this step, the first measurement of length (L_{c0}) and mass (m_0) should be carried out (**Figure 3.19**).

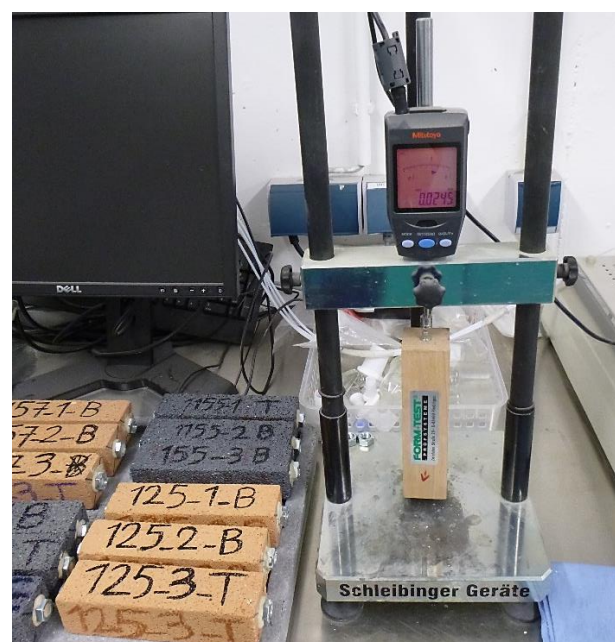


Figure 3.19 First measurements of length (L_{c0}).

In the next step, they were stored in a climatic chamber at a temperature of 20 ± 2 °C and relative humidity of 45 ± 5 % until a constant length is reached. The last measurement of the specimens should be carried out after 28 days of storage in the specified standard climate. If the relative change in length increases by more than 0.02 mm/m between 21 and 28 days, then the storage of specimens should be continued. Subsequently, additional measurements and weighing should be performed until the increase in length change within 7 days no longer exceeds 0.02 mm/m.

For each measurement time (t_i), the values of relative change in length (ϵ_{csi}) and moisture content, (μ_{mi}) should be recorded. These values will be linked by associated graphs. According to DIN EN 680: 2005 [168], the total drying shrinkage ($\epsilon_{cs, tot}$) refers to the relative change in length between the end of the conditioning time at time t_0 and the end of the shrinkage storage at time t_e .

3.4.8 Bulk density

The dry bulk density was determined according to DIN EN 772-13 [169]. For this purpose, the cubes were dried at a temperature of 105 ± 5 °C in the oven until reaching a constant weight. This was achieved when the weight loss in two consecutive weighings in an interval of 24 hours did not exceed 0.2% of the total weight.

Material and Methods

The content of this chapter is published in the following three peer-reviewed articles:

Shams T, Schober G, Heinz D, Seifert S, “Production of autoclaved aerated concrete with silica raw materials of a higher solubility than quartz part I: Influence of calcined diatomaceous earth” *Construction and Building Materials*, V. 272, 2021. <https://doi.org/10.1016/j.conbuildmat>

Shams T, Schober G, Heinz D, Seifert S, “Production of autoclaved aerated concrete with silica raw materials of a higher solubility than quartz Part II: Influence of autoclaving temperature” *Construction and Building Materials*, V. 287, 2021. <https://doi.org/10.1016/j.conbuildmat>

Shams T, Schober G, Heinz D, Seifert S, “Rice husk ash as a silica source for the production of autoclaved aerated concrete – a chance to save energy during the hydrothermal treatment” *Journal of Building Engineering*, 2022 (accepted).

Results and Discussion

In this chapter, the synopsis of the results of three peer-reviewed papers, which are given in the appendix, with relevant discussions is introduced in a general context.

4.1 Behavior of C-DE and RHA in AAC

This section presents functional relationships between the properties of the silica raw materials used in this study and the resulting hydration products and the performance of obtained AAC characterized by the compressive strength and the shrinkage behaviors. The results and discussions presented in this section are according to the typical autoclaving condition, i.e. the autoclaving temperature of 192 °C (corresponding to the pressure of 12 bar) with a total duration of 9 h. The performances of AAC samples at different autoclaving temperatures are described in section 4.2

The results of this thesis demonstrate that RHA and C-DE showed a compatible behavior with the AAC compositions. It is feasible to produce stable AAC samples using RHA and C-DE, although some adaptations in the mix design might be needed such as quantity and types of aluminum paste/powder.

4.1.1 Influence of C-DE and RHA on the mineralogical composition of AAC

Replacing quartz sand with C-DE or RHA in the AAC mixture did not change the type of resultant phases present in the final product, but indeed their proportions. As an example, the phase compositions of AAC samples containing C-DE with different substitution ratios are presented in **Table 4.1**. In the following table, DE25, DE50, and DE 75 represent AAC samples in which quartz sand was replaced with C-DE for 25 wt. %, 50 wt. % and, 75 wt. %, respectively.

Substitution of quartz sand with C-DE or RHA for more than 50 wt. % in the AAC mixture promoted the formation of poorly and non-crystalline C-S-H with low C/S and prevented the formation of tobermorite in a great amount. This might be due to the suppression in the crystallization of non-crystalline C-S-H to tobermorite which was evidenced by an increase in the amorphous content and a reduction in the total quantity of tobermorite. In addition, the amount of unreacted or residual cristobalite was much lower than the residual quartz, which confirms the higher solubility of C-DE and RHA compared to quartz sand. In general, increasing the content of C-DE or RHA led to a decrease in the amount of unreacted SiO₂. This could imply a lower C/S of the initially formed C-S-H for the C-DE-based or RHA-based AAC compared to that of the quartz-based AAC. The reason for this is probably that C-DE or RHA, which contained cristobalite, had a higher solubility and dissolution rate than quartz sand. Additionally, the porous and interconnected microstructure of C-DE and RHA

Results and Discussion

promoted their dissolution rate, as well. At the same autoclaving temperature, the C/S ratio of the initially formed C-S-H in the more soluble silica system was, therefore, lower (higher SiO_4^{4-} concentration) than that of the quartz system [75, 43]. Moreover, it has been reported that C-S-H with a low C/S ratio tends to have long and cross-linked chains of tetrahedral [46, 77, 170–172]. This implies that the transformation of non-crystalline C-S-H to tobermorite can hardly occur [74, 43, 46], whereas C-S-H with a high C/S contains short silicate chains and could readily crystallize into tobermorite. Moreover, the formation of polymerized C-S-H with low C/S in the C-DE-based AAC was evidenced by an increase in the wollastonite formation temperature and an increase in OH groups in the C-S-H structure obtained by differential thermal analysis (DTA) and thermogravimetric analysis (TGA), respectively. This explains why tobermorite formation was suppressed in the more soluble silica system, whereas it was promoted in the quartz system. Several studies have also reported similar results that replacing quartz sand with amorphous silica enhances the polymerization of C-S-H, which prevents the final rearrangement of C-S-H into tobermorite [48, 43, 46].

Table 4.1 Absolute contents (wt. %) of main phases existing in AAC samples autoclaved under the typical autoclaving condition (192 °C, 9 h). The results were determined by Rietveld refinement using the internal standard method. Standard deviations of the measurement which was repeated 3 times per specimen are given in parentheses.

phases	Q100	DE25	DE50	DE75
anhydrite	3.4 (0.3)	3.5 (0.2)	4.1 (0.2)	3.3 (0.2)
calcite	2.8 (0.5)	3.0 (0.4)	4.4 (0.5)	4.5 (0.4)
cristobalite	-	0.0 (0.0)	0.0 (0.0)	1.0 (0.1)
hydroxyllestadite	3.0 (0.3)	2.3 (0.1)	2.1 (0.3)	1.9 (0.2)
quartz	15.3 (1.8)	15.2 (0.7)	12.6 (0.9)	7.4 (0.5)
tobermorite-9 Å	4.7 (0.1)	4.0 (0.3)	7.2 (0.1)	5.8 (0.3)
tobermorite-11 Å	36.6 (0.6)	37.6 (0.5)	27.2 (0.6)	6.3 (0.9)
amorphous content	27.9 (3.2)	26.6 (1.5)	33.3 (1.8)	64.2 (1.7)

4.1.2 Influence of C-DE and RHA on the performance of AAC characterized by the compressive strength and shrinkage behaviors

Changing the proportions of resultant hydrothermal products, affected the determining properties of AAC, e.g. compressive strength. In order to compare the compressive strength of several samples with each other, it is needed to consider the effect of density. In general, the bulk density of all of the samples remained in the range of 450–495 kg/m³ corresponding to the P4-500 grade as the mix designs were adjusted for that density range. The bulk densities of the AAC samples containing C-DE were almost the same as that of the reference sample which contained only quartz sand as the silica source. As can be seen in **Table 4.2**, the difference in bulk densities of the C-DE-based AAC, i.e. DE75 mix, and the quartz-based AAC, i.e. Q100 mix, was less than 2 % which is insignificant. Therefore, the compressive strength of AAC samples containing C-DE can directly be compared with that of quartz-based AAC without requiring the determination of A-values. Under the typical autoclaving

condition, the C-DE-based AAC reached a compressive strength slightly higher than that of the quartz-based AAC despite its substantially lower tobermorite content (70.7 % lower). In this case, the high strength was probably related to the thickness of the pore walls, the microstructure, and the proportion of ingredients. The C-DE-based AAC had almost the same bulk density and, as a result, almost the same total porosity [84, 86, 102, 90, 173] compared to the quartz-based AAC. However, the C-DE-based AAC contained less aluminum in the mixture compared to the quartz-based AAC (**Table 3.5**). The lower quantity of aluminum paste was compensated by a higher water quantity, which is represented by the higher W/S. This implies that despite having a similar total porosity, the C-DE-based AAC and the quartz-based AAC did not contain the same number of air pores. Compared to the quartz-based AAC, the porosity of the C-DE-based AAC was made up of a lower number of air pores (macro-pores) and a higher number of small-size pores in the solid structure (micro-pores). Therefore, the solid structure of the C-DE-based AAC had likely a lower strength than that of the quartz-based AAC. However, a decrease in the number of air pores resulted in thicker pore walls which predominated over the effect of solid structure and favored the compressive strength of the C-DE-based AAC [83, 100]. Moreover, the interconnection and intermixture of C-S-H phases, which are expected to be mainly non-crystalline Si-rich C-S-H with grass-like microstructure, might influence the compressive strength of the AAC positively. In terms of the ingredients and mixture composition, the proportion of C-DE with respect to other solid materials and water mixture might have reached a beneficial size in the C-DE-based AAC which could improve the compressive strength. The aforementioned results could suggest that the porosity properties, microstructure, e.g. the proportion and interconnection of different C-S-H, would have a positive effect on compressive strength just as significant as the effect of tobermorite content alone.

Table 4.2 Characteristic properties of AAC samples under the typical autoclaving condition (192 °C, 9 h). Values in parentheses represent standard deviations of repeated samples.

properties	Q100	DE75	R75	R100
compressive strength (MPa)	4.2 (0.2)	4.4 (0.1)	3.2 (0.1)	3.2 (0.2)
bulk density (kg/m ³)	493 (3)	484 (1)	464 (1)	459 (2)
A-value	1080	1174	929	949
total drying shrinkage (mm/m)	0.58	1.84	1.41	1.72

Since the bulk densities of the RHA-based AAC and the quartz-based AAC were not equal to each other (**Table 4.2**), the A-value was used to compare the quality of the samples considering compressive strength. As can be seen in **Table 4.2**, the average A-value of the RHA-based AAC was about 13 % lower than that of the quartz-based AAC under the typical autoclaving condition. This implies that under the typical autoclaving condition, the compressive strength to density ratio of the RHA-based AAC tends to be lower than that of the quartz-based AAC. Moreover, it can be inferred that the existing difference in the compressive strength of those samples is not because of the difference in bulk density since comparison with the subtraction of density effect, i.e. A-value comparison, still indicates different values.

Results and Discussion

Obtaining different compressive strengths for the RHA-based AAC and the quartz-based AAC under the typical autoclaving condition could be due to the different solid structures. The maximum tobermorite content of the RHA-based autoclaved under the typical condition was around 12 wt. % whereas this value was more than 3 times higher (around 41 wt. %) for the quartz-based AAC. A lower tobermorite content and/or different C-S-H phases which are less crystalline in RHA-based AAC may cause somewhat lower strength. However, under the typical autoclaving condition, the C-DE-based AAC with almost the same tobermorite content (12 wt. %) showed a slightly higher compressive strength than that of the quartz-based AAC. It should be noted that the C-DE-based AAC and the RHA-based AAC are different in terms of porosity properties.

The RHA-based AAC and the quartz-based AAC have nearly the same porosity properties caused by the close content of aluminum and W/S in those mixes. However, for the C-DE-based AAC, obtaining slightly higher compressive strength could be due to the different porosity properties, i.e. thicker pore walls, which predominated over the effect of significantly different skeletal material structures and favors the compressive strength.

Although the low content of tobermorite did not cause a decrease in compressive strength for all cases, it did lead to higher drying shrinkage. A high proportion of non-crystalline C-S-H increased the drying shrinkage of AAC products [40, 29]. The variations of relative change in length with time under the typical autoclaving condition for the C-DE-based AAC (DE75 mix), RHA-based AAC (R75 mix), and quartz-based AAC (Q100 mix) are shown in **Figure 4.1**.

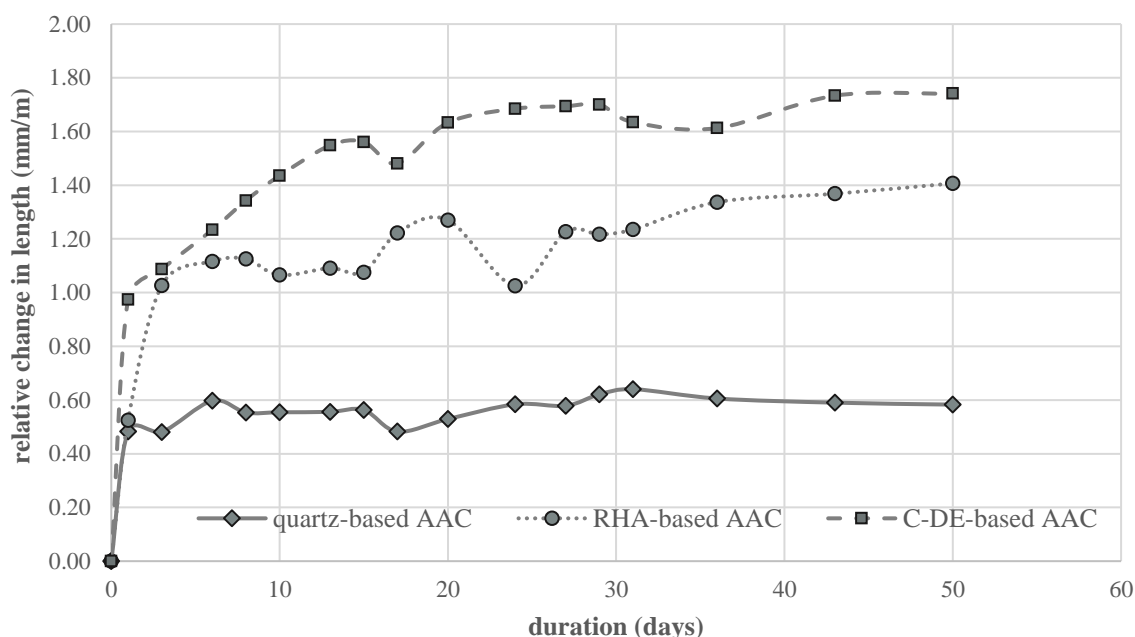


Figure 4.1 Variation of the relative change in length (ϵ_{csi}) with time for AAC samples autoclaved under the typical condition (192 °C, 9 h) during storage at a temperature of 20 ± 2 °C and relative humidity of 45 ± 5 %.

In general, a comparison of values shows a higher drying shrinkage of the C-DE-based AAC and RHA-based AAC compared to the quartz-based AAC. The reason attributes to a reduction in the degree of crystallinity as a result of replacing quartz sand with C-DE or

RHA in the AAC mixture. A decrease in the degree of crystallinity was evidenced by an increase in the content of non-crystalline C-S-H and a decrease in tobermorite quantity. It has been reported that the shrinkage of AAC mainly depends on the volume and the specific surface of micro-pores [129, 130]. The high porosity and the high specific surface area of the pores are responsible for the high drying shrinkage of AAC [129, 125]. On the other hand, increasing the degree of crystallinity is accompanied by a lower specific surface area and a lower portion of micro-pores. Therefore, a higher degree of crystallinity and a lower content of non-crystalline C-S-H lead to a lower shrinkage [40, 89, 29]. In general, replacing 75 wt. % of quartz sand with C-DE and RHA in the AAC mixture increased the total value of drying shrinkage, respectively, to 3 and 2.5 times higher than that of the quartz-based AAC. Similar observations have been reported by Ramamurthy et al. [125], where the shrinkage of the fly ash-based AAC was 5–7 times higher than that of the quartz-based AAC.

4.2 Performance of the quartz-based AAC, C-DE-based AAC, and RHA-based AAC under different autoclaving temperatures

In this section, the performances of the quartz-based AAC and the more soluble silica-based AAC, i.e. C-DE-based AAC and RHA-based AAC, under different autoclaving conditions are introduced.

As mentioned in section 2.5.4, in contrast to the quartz-based AAC, the performance of the more soluble silica-based AAC under different autoclaving conditions has rarely been studied. Moreover, the only published finding [92] implies similar behaviors of those AAC under different autoclaving conditions. However, the results of this study have demonstrated that the C-DE-based AAC and the RHA-based AAC behaved differently than the quartz-based AAC at different autoclaving temperatures. In contrast to the quartz-based AAC, the properties of the C-DE-based AAC and the RHA-based AAC have been improved by applying a lower autoclaving temperature than the typical temperature used for industrial production of AAC, i.e. 192 °C.

The quartz-based exhibited its most favorable properties at the autoclaving temperature of $T = 192$ °C which is in accordance with the current state of knowledge [132, 75, 42, 39, 174, 38]. However, for the C-DE-based AAC, this temperature range was $T = 152$ – 165 °C. In the case of the RHA-based AAC, the optimum properties were observed at the autoclaving temperature of $T = 165$ – 175 °C.

4.2.1 Mineralogical phase composition of the quartz-based AAC, C-DE-based, and RHA-based AAC at various autoclaving temperatures

Applying different autoclaving temperatures affected reactions kinetics and the development of the phases during hydrothermal treatment which altered the characteristic properties of AAC samples. For the C-DE-based AAC and the RHA-based, higher tobermorite content was obtained by autoclaving samples at lower temperatures. For both aforementioned AAC mixes, the autoclaving temperature of 165 °C led to the highest tobermorite content. A promotion in tobermorite formation was always accompanied by a reduction in amorphous content. However, an opposite variation pattern was observed for the quartz-based AAC.

Results and Discussion

Applying the autoclaving temperatures lower than 192 °C suppressed the tobermorite formation and increased amorphous content in AAC containing quartz sand as the only silica source.

As an example, the influence of the autoclaving temperature on the phase composition of the RHA-based AAC, e.g. R100 mix, and the quartz-based AAC, i.e. Q100 mix are given in **Table 4.3** and **Table 4.4**, respectively. As shown in **Table 4.3**, for the R100 mix, the tobermorite content, i.e. the sum of tobermorite-11Å and tobermorite-9Å, increased (by 12 wt. %) and the amorphous content decreased (by 8.4 wt. %) when the autoclaving temperature of 165 °C was applied instead of 192 °C. This is possibly caused by promoting the transition from non-crystalline C-S-H to tobermorite according to reaction Eq. (2.12) [22].

Table 4.3 Absolute contents (wt. %) of main phases existing in the R100 mix autoclaved at different temperatures. The results were determined by Rietveld refinement using the internal standard method. Standard deviations of the measurements which were repeated 3 times per specimen are given in parentheses.

Phases in the R100 mix	192 °C	175 °C	165 °C	152 °C
anhydrite	1.6 (0.1)	1.4 (0.1)	1.0 (0.0)	0.2 (0.0)
bassanite	0.9 (0.1)	2.0 (0.1)	2.9 (0.1)	0.7 (0.0)
calcite	3.9 (0.3)	3.4 (0.1)	3.3 (0.1)	3.6 (0.1)
cristobalite	8.6 (0.8)	8.3 (0.3)	8.4 (0.2)	12.0 (0.2)
hydroxyllellstadite	5.6 (0.2)	4.2 (0.1)	3.5 (0.1)	7.7 (0.1)
quartz	1.2 (0.2)	1.2 (0.1)	1.3 (0.1)	1.3 (0.1)
tobermorite-9 Å	2.6 (0.4)	2.7 (0.1)	2.5 (0.1)	1.0 (0.4)
tobermorite-11 Å	6.5 (0.4)	15.6 (0.3)	18.6 (0.1)	4.3 (0.0)
amorphous content	63.1 (2.3)	56.2 (0.3)	54.7 (0.2)	64.7 (1.0)

The reason for promoting the above-mentioned transformation could trace back to a change in the dissolution behavior of RHA as a result of autoclaving samples at a lower temperature of 165 °C instead of 192 °C [133]. As was expected, applying a lower autoclaving temperature affected the dissolution properties of RHA in a way that reduced the diffusion of SiO_4^{4-} to the matrix and avoided progressive polymerization of silicate chains. Subsequently, C/S of non-crystalline C-S-H which are formed at the initial stages of the hydrothermal treatment increased. This means that initial non-crystalline C-S-H formed at the autoclaving temperature of 165 °C had likely higher C/S compared to those formed at the autoclaving temperature of 192 °C. On the other hand, according to literature, C-S-H phases with a higher C/S have short silicate chains and a lower degree of polymerization which implies that they could rearrange to tobermorite more easily [43, 170, 171]. Therefore, the RHA-based AAC autoclaved at 165 °C contained a higher quantity of tobermorite and a lower amorphous content compared to that autoclaved at 192 °C. The above interpretation is valid for the C-DE-based AAC as well.

Table 4.4 Absolute contents (wt. %) of main phases existing in the Q100 mix autoclaved at different temperatures. The results were determined by Rietveld refinement using the internal standard method. Standard deviations of the measurements which were repeated 3 times per specimen are given in parentheses.

Phases in the Q100 mix	192 °C	175 °C	165 °C	152 °C
anhydrite	3.4 (0.3)	0.3 (0.2)	0.0 (0.0)	0.0 (0.0)
bassanite	0.8 (0.1)	1.4 (0.2)	1.2 (0.2)	1.0 (0.0)
calcite	2.8 (0.5)	2.0 (0.2)	1.7 (0.1)	2.4 (0.0)
hydroxyllellstadite	3.0 (0.3)	7.4 (0.0)	7.5 (0.5)	7.7 (0.2)
quartz	15.3 (1.8)	16.6 (1.1)	22.0 (3.3)	25.6 (2.3)
tobermorite-9 Å	4.7 (0.1)	5.4 (0.0)	2.9 (0.5)	3.4 (0.0)
tobermorite-11 Å	36.6 (0.6)	29.0 (0.9)	20.6 (0.3)	6.3 (0.1)
amorphous content	27.9 (3.2)	33.4 (2.3)	36.8 (5.6)	47.0 (2.3)

There exist other pathways for tobermorite formation which might also be favored by autoclaving RHA-based AAC at lower temperatures, i.e. $T < 192$ °C. For the R100 mix, an increase in the total content of tobermorite was also accompanied by a reduction in the quantity of hydroxyllellstadite and an increase in the total quantity of the sulfate phases, i.e. the sum of bassanite and anhydrite quantities. This might be due to promoting the reaction of dissolved silica with hydroxyllellstadite which generates tobermorite and either or both of the sulfate phases, i.e. bassanite and anhydrite, which can be described by the reaction Eq. (2.13) [22, 120].

This is another pathway for crystallization of tobermorite under hydrothermal conditions which might be promoted in the R100 mix as the lower autoclaving temperature of 165 °C was applied instead of 192 °C. However, tobermorite formation might not be favored through this pathway for the R75 and DE75 mixes since in those cases, the hydroxyllellstadite quantity and the total quantity of the sulfate phases did not significantly vary as the autoclaving temperature was adjusted to 165 °C instead of 192 °C. The probable cause is that the R100 mix contains a higher amount of more soluble silica compared to the R75 and DE75 mixes. Thus, there will be more dissolved silica (SiO_2) available to react with hydroxyllellstadite in the R100 mix.

Tobermorite formation was promoted through the crystallization of non-crystalline C-S-H to tobermorite and also the decomposition of hydroxyllellstadite when the R100 mix was autoclaved at the temperature of 165 °C instead of 192 °C. However, for the R75 mix formation of tobermorite was favored only through crystallization of C-S-H. This can be a possible reason for a higher increase in tobermorite content for the R100 mix (131.9 %) compared to that for the R75 mix (105 %). Moreover, autoclaving the C-DE-based AAC at the autoclaving temperature of 165 °C instead of 192 °C caused an increase of 60 % in the total content of tobermorite which is lower than that in the RHA-based AAC. The reason could be attributed to the different dissolution properties of the C-DE and RHA. Comparing amorphous content, SEM images, specific surface areas, as well as water demand of RHA with those of C-DE, indicates that C-DE had a higher solubility and dissolution rate than

Results and Discussion

RHA. This could cause a greater concentration level of SiO_4^{4-} at the initial stage of the hydrothermal treatment in the C-DE-based AAC compared to that in the RHA-based AAC. Lower unreacted cristobalite which remained in the C-DE-based AAC compared to the RHA-based at all autoclaving temperatures could confirm the aforementioned understanding. A higher level of SiO_4^{4-} concentration would lead to the initially formed C-S-H with a higher degree of polymerization and as a result, a lower increase in tobermorite content for the C-DE-based AAC compared to that for the RHA-based AAC. This could also be another reason for the observation mentioned earlier that the decomposition of hydroxyllestadite to tobermorite was not promoted for the C-DE-based AAC. A higher solubility and dissolution rate of C-DE compared to RHA could cause a fast consumption of dissolved silica by calcium oxide and the formation of polymerized C-S-H. This implies that most dissolved silica might contribute to the C-S-H structure and, as a result, there might not exist enough dissolved silica available for the decomposition of hydroxyllestadite.

For the RHA-based AAC, temperatures below 165 °C might lead to a silica dissolution which does not support the transition to tobermorite. A higher quantity of quartz and cristobalite which remained unreacted in the R75 and R100 samples autoclaved at the temperature of 152 °C, supports the aforementioned explanation. For the C-DE-based AAC, the same temperature range, i.e. $T < 165$ °C, led to a slight reduction in the total content of tobermorite. However, unlike the RHA-based AAC, autoclaving at temperatures below 165 °C did not affect cristobalite content considerably. This indicates a higher solubility of C-DE compared to RHA used in this study.

The above results demonstrate that for the C-DE-based AAC and the RHA-based AAC, an adequate adaptation of the autoclaving temperature is required to achieve the optimum tobermorite formation.

Autoclaving the quartz-based AAC at temperatures below 192 °C led to suppression in the crystallization of non-crystalline C-S-H to tobermorite according to reaction Eq. (2.12). This is in accordance with the result of studies carried out by Mitsuda et al. [39] and Chen et al. [42] in which the amount of 1.1-nm tobermorite and crystallinity increased with further autoclaving. The reason for this is probably that when the autoclaving temperature was adjusted to $T < 192$ °C, the dissolution properties of quartz were influenced significantly, leading to the formation of initially C-S-H with a C/S beyond those suitable for tobermorite crystallization according to reaction Eq. (2.12). Therefore, autoclaving the quartz-based AAC at $T < 192$ °C was followed by a decrease in tobermorite and an increase in the amorphous content. However, decomposition of quartz did not occur at temperatures below 152 °C. The quartz and lime, therefore, remained unreacted in the sample, resulting in a lower amorphous content due to the reduction in C-S-H formation. The presence of portlandite and a high quantity of residual quartz in the reference sample autoclaved at 134 °C confirms the above explanation

Moreover, a decrease in the total content of tobermorite occurred simultaneously with an increase in the quantity of hydroxyllestadite and a decrease in the total quantity of the sulfate phases. The possible cause attributed to this is similar to what was discussed earlier. The decomposition of hydroxyllestadite (reaction Eq. (2.13)) was suppressed since the quartz was not dissolved to a sufficient extent at low autoclaving temperatures. A higher amount of quartz which was left unreacted and did not react with hydroxyllestadite confirms this understanding.

4.2.2 Compressive strength and shrinkage behaviors of the quartz-based AAC, C-DE-based AAC, and RHA-based AAC at various autoclaving temperatures

The variations in compressive strength were correlated with the hydrothermal reactions kinetics, types, and proportions of hydration products. The results revealed that autoclaving the C-DE-based and the RHA-based AAC at temperatures lower than the typical temperature improved the compressive strength of those samples. However, for the quartz-based AAC, a deterioration in compressive strength was observed. **Table 4.5** shows the variation in the compressive strength, bulk density, A-value, and total drying shrinkage of the AAC samples at autoclaving temperatures of 165 °C and 192 °C.

Table 4.5 Characteristic properties of AAC samples at autoclaving temperatures of 192 °C and 165 °C. Values in parentheses represent standard deviations of repeated samples.

mix	Q100		DE75		R75		R100	
	192 °C	165 °C						
autoclaving temperature	192 °C	165 °C						
compressive strength (MPa)	4.2 (0.2)	3.3 (0.1)	4.4 (0.1)	6.6 (0.2)	3.2 (0.1)	3.6 (0.1)	3.2 (0.2)	3.9 (0.1)
bulk density (kg/m ³)	493 (3)	488 (3)	484 (1)	498 (4)	464 (1)	459 (3)	468 (1)	465 (2)
A-value	1080	866	1174	1663	929	1027	949	1127
total drying shrinkage (mm/m)	0.58	0.92	1.74	1.35	1.41	0.95	1.72	1.40

The bulk density of samples of each mix, e.g. samples of R100 mix autoclaved at various autoclaving temperatures, did not change significantly when different autoclaving temperatures were applied. Therefore, the difference in the compressive strength values of samples of each mix is not because of the difference in bulk densities but rather due to changes in the solid structures. This agrees with the XRD results where changing the autoclaving temperature affected the formation of hydrothermal products, which existed in the solid structure, for all mixes.

Autoclaving the C-DE-based AAC at a temperature of 58 °C lower than the typical temperature, i.e. 192 °C, resulted in an increase in the compressive strength from 4.4 MPa to 5.7 MPa (by 30%). Moreover, a reduction of 27 °C and 40 °C in the applied autoclaving temperature increased the compressive strength of the C-DE-based AAC from 4.4 MPa to 6.6 MPa (by 50 %) and 6.4 MPa (by 45 %), respectively. On the other hand, the requirement corresponding to the P4-500 grade, i.e. compressive strength \geq 4.9 MPa, could still be fulfilled by obtaining lower compressive strengths. One advantage of obtaining an AAC product with higher strength than technical requirements is the opportunity to reduce binder content in the mixture.

Results and Discussion

The optimum compressive strength of the C-DE-based AAC occurred at an autoclaving temperature range of $T = 152\text{--}165\text{ }^{\circ}\text{C}$. Interestingly, the compressive strength of the C-DE-based AAC autoclaved at $134\text{ }^{\circ}\text{C}$ was still higher than that autoclaved at $192\text{ }^{\circ}\text{C}$. For the RHA-based AAC, the highest compressive strength was obtained at the autoclaving temperature of $T = 165\text{--}175\text{ }^{\circ}\text{C}$. This implies that for the C-DE-based and RHA-based AAC, the microstructure, e.g. the proportions and types of different C-S-H might approach the optimum effectiveness when the autoclaving temperature is in the range of $T = 152\text{--}165\text{ }^{\circ}\text{C}$ and $T = 165\text{--}175\text{ }^{\circ}\text{C}$, respectively.

The above observations are in opposition to what occurred with AAC which contained only quartz sand as the SiO_2 source. For the quartz-based AAC, the compressive strength decreased by 85 % when the autoclaving temperature was adjusted to $134\text{ }^{\circ}\text{C}$ instead of $192\text{ }^{\circ}\text{C}$. It, therefore, appears that for the quartz-based AAC, the optimum microstructure might be acquired by autoclaving at $T = 192\text{ }^{\circ}\text{C}$.

For all specimens, an increase in compressive strength occurred with an increase in the total content of tobermorite which is in accordance with the results of numerous studies [1, 11, 38, 174, 39].

The C-DE-based AAC autoclaved at $165\text{ }^{\circ}\text{C}$ exhibited an A-value of 54% higher than that of the quartz-based AAC autoclaved at $192\text{ }^{\circ}\text{C}$ regardless of having a lower tobermorite content. Moreover, the A-value of the RHA-based AAC autoclaved at $165\text{ }^{\circ}\text{C}$ appeared to be almost the same as that of the quartz-based AAC autoclaved at $192\text{ }^{\circ}\text{C}$. This shows that the existing difference in the compressive strength of these samples is simply due to the difference in density since comparison with the subtraction of density effect, i.e. A-value comparison, shows almost equal strength quality. Thus, the strength to density ratio of the RHA-based AAC autoclaved at $165\text{ }^{\circ}\text{C}$ is almost the same as that of the quartz-based AAC autoclaved at $192\text{ }^{\circ}\text{C}$ in spite of the distinct difference in tobermorite content.

For the C-DE-based AAC autoclaved at $165\text{ }^{\circ}\text{C}$, the solid materials consist of 19.4 wt. % tobermorite and 52 wt. % amorphous content. Under the same autoclaving condition, close quantities of tobermorite and amorphous content were obtained for the RHA-based AAC. The R75 and R100 mixes (RHA-based AAC samples) autoclaved at $165\text{ }^{\circ}\text{C}$ contain 24.4 wt. % and 21.1 wt. % tobermorite, respectively. However, the tobermorite content of the quartz-based AAC autoclaved at $192\text{ }^{\circ}\text{C}$ is about two times higher (41.3 wt. %).

The above results indicate that the tobermorite content might not be the only determining factor for compressive strength. Although in many cases an increase in tobermorite content favors the compressive strength by providing a denser microstructure and a higher proportion of large crystals, the existence of a microstructure composed of a low portion of tobermorite compared to non-crystalline C-S-H does not necessarily lead to low compressive strength. In addition to tobermorite, other types of C-S-H act as the binding phases in the microstructure. The interconnection and intermixture of tobermorite with some of those C-S-H, e.g. non-crystalline Si-rich C-S-H, might provide a high space-filling ability as well. Thus, the microstructure, types, proportions, and morphologies of C-S-H and tobermorite, and the way they are interconnected to each other might affect compressive strength considerably. This is in line with the outcomes of other studies [119, 38] and results mentioned earlier in section 4.1 which have shown that in addition to a high content of

tobermorite, a homogeneous distribution of the tobermorite crystals in the solid structure is required to obtain optimum strength properties.

For the C-DE-based and the RHA-based AAC autoclaved at 165 °C, around 20–25 wt. % tobermorite and 50–55 wt. % amorphous content resulted in a microstructure which led, respectively, to a higher and equal strength to density ratio compared to that provided by the microstructure of the quartz-based AAC (Q100 mix) autoclaved at 192 °C which contains around 41 wt. % tobermorite and 28 wt. % amorphous content. It should be noted that different silica materials lead to the formation of different non-crystalline C-S-H with different morphologies, C/S ratios, and degrees of crystallinity. Therefore, the amorphous content which exists in the C-DE-based AAC or the RHA-based AAC is not of the same type as that in the quartz-based AAC. This is also valid for tobermorite formed in mixes with different silica raw materials. For instance, in the RHA-based AAC autoclaved at 165 °C, lath-like tobermorite was formed while tobermorite formed in the quartz-based AAC autoclaved at 192 °C was a type of needle-like.

This could imply that there might exist an optimum proportion of C-S-H for each type of the mix which leads to the high compressive strength of the AAC product. The intermixture of around 50 wt. % non-crystalline C-S-H, which are expected to be Si-rich C-S-H, and 20 wt. % tobermorite might be close to the optimum proportion for compressive strength of AAC products containing silica materials of a higher solubility, e.g. C-DE and RHA, as the main silica sources. This optimum proportion will be achieved by applying adequately low autoclaving temperature, i.e. a temperature which is significantly lower than that required for autoclaving the quartz-based AAC.

The suggested optimum proportion of tobermorite and non-crystalline C-S-H are according to the mix designs (C/S of 0.63–0.64), materials, approaches (the total autoclaving duration of 9 h), and the equipment used in this study. Other research situations might lead to a more optimized proportion.

Changing the autoclaving temperature affected the shrinkage of samples for all mixes. The drying shrinkage of the quartz-based AAC autoclaved at 165 °C was approximately 59 % higher than that autoclaved at 192 °C. This is an expected result since the quartz-based AAC autoclaved at 165 °C contained a lower quantity of tobermorite and a higher amorphous content compared to that autoclaved at 192 °C. It is widely known that the autoclaving process reduces the shrinkage of quartz-based AAC by supporting the formation of well-crystallized C-S-H [89, 175, 176, 1]. The C-DE-based AAC and RHA-based AAC demonstrated contrary shrinkage behaviors to that of the quartz-based AAC. According to **Table 4.5**, the C-DE-based AAC and the RHA-based AAC autoclaved at the temperature of 165 °C showed a lower drying shrinkage compared to those autoclaved at 192 °C. The total values of drying shrinkage of the R75 and R100 mixes autoclaved at 165 °C were, respectively, around 33 % and 19 % lower than those autoclaved at 192 °C. For the C-DE-based AAC, the total drying shrinkage decreased by 22 % as the autoclaving temperature was adjusted to 165 °C instead of 192 °C. This improvement in shrinkage behavior of the C-DE-based and the RHA-based AAC is due to the increased tobermorite content as a result of curing at the optimum autoclaving temperature.

In general, a comparison of values shows a higher drying shrinkage of the C-DE-based AAC and the RHA-based AAC compared to the quartz-based AAC. Although the total drying

Results and Discussion

shrinkage of the C-DE-based AAC and the RHA-AAC decreased by virtue of applying lower autoclaving temperature, similar shrinkage values as that of the quartz-based AAC autoclaved at 192 °C could not be achieved. For the C-DE-based AAC and the RHA-based AAC, the optimum values of drying shrinkage were obtained at the autoclaving temperature of 165 °C which were, respectively, 2.3 times and 1.6 times higher than that of the quartz-based AAC autoclaved at 192 °C. The reason attributes to the increase in the content of non-crystalline C-S-H phases as the result of replacing quartz sand with C-DE or RHA in the AAC mixture. However, regardless of having a higher content of non-crystalline C-S-H, the C-DE-based AAC and the RHA-based AAC autoclaved at 165 °C, respectively, exhibited a higher and almost the same A-value than that of the quartz-based AAC autoclaved at 192 °C.

According to the above findings, it could be concluded that the drying shrinkage of AAC would mainly be controlled by the content of non-crystalline C-S-H phases while for the compressive strength, the microstructure, e.g. distribution and interconnection of the hydrothermal products, all kinds of C-S-H phases, in the solid structure is more determining. This outcome is in line with the results of the study carried out by Mesecke [119] in which the drying shrinkage of AAC was reported to be a function of the content and crystallinity of tobermorite while the compressive strength depends mainly on the properties of the microstructure.

Conclusion and Outlook

In this chapter, a conclusion is drawn and an outlook of the work is presented. The possibility of reducing energy consumption in AAC production by using C-DE and RHA as the main silica source and the decisive properties of materials which can be used as silica raw materials of a higher solubility to meet the objectives of this study are discussed. The suggestions for further research are made at the end of the chapter.

5.1 Conclusion

The present study demonstrated that the C-DE-based AAC and RHA-based AAC, which, respectively, contained calcined diatomaceous earth (C-DE) and rice husk ash (RHA) as the main silica material, exhibited different behaviors from that of the quartz-based AAC at different autoclaving temperatures. In contrast to the quartz-based AAC, autoclaving the C-DE-based AAC and RHA-based AAC at lower temperatures than the typical temperature used for industrial production of AAC, i.e. 192 °C, improved their performances characterized by the compressive strength and shrinkage behaviors.

For the C-DE-based AAC and RHA-based AAC, a maximum increase of 50 % and 22 % in the compressive strength, 60 % and 132 % in the total content of tobermorite, 42 % and 19 % in the A-value, and a maximum decrease of 27 % and 33 % in the total value of drying shrinkage were, respectively, observed as the autoclaving temperature was adjusted to 165 °C instead of 192 °C. The above observations are in opposition to what occurred with AAC which contained only quartz sand as the SiO₂ source. For the quartz-based AAC, the total content of tobermorite, the compressive strength, and the A-value decreased by 43 %, 21 %, and 20 %, respectively, and the total value of drying shrinkage increased by 59 % when the autoclaving temperature was set to 165 °C instead of 192 °C.

The results showed that applying an autoclaving temperature of 192 °C with a total duration of 9 hours, which is a typical autoclaving condition in industrial AAC production, inhibited tobermorite formation in the C-DE-based AAC and RHA-based AAC. However, for the quartz-based AAC, applying the aforementioned autoclaving condition promoted tobermorite formation. This probably resulted from the varying dissolution behaviors of silica raw materials. In the next steps, applying relatively low autoclaving temperatures avoided progressive polymerization of silicate chains by affecting the dissolution properties of C-DE and RHA. This led to an increase in tobermorite formation for the C-DE-based and RHA-based AAC that mainly occurred through promoting the crystallization of non-crystalline C-S-H to tobermorite. However, in the end, a higher portion of non-crystalline C-S-H was obtained for the C-DE-based AAC and RHA-based AAC compared to the quartz-based AAC.

Conclusion and Outlook

The optimum performance of the C-DE-based AAC and the RHA-based AAC occurred at an autoclaving temperature range of $T = 152\text{--}165\text{ }^{\circ}\text{C}$ and $T = 165\text{--}175\text{ }^{\circ}\text{C}$, respectively. However, for the quartz-based AAC, the optimum properties were acquired by autoclaving at $T = 192\text{ }^{\circ}\text{C}$.

From a general point of view, the results have shown that the optimum temperature for autoclaving AAC has a direct dependency on the dissolution behavior of silica raw materials used in the mixture. In the case of using a silica material with different dissolution properties from those of quartz sand in the AAC mixture, applying the typical autoclaving temperature will not necessarily lead to the optimum properties and indeed an adequate adaptation of the autoclaving temperature is required to achieve the optimum performance of the product.

The C-DE-based AAC autoclaved at $165\text{ }^{\circ}\text{C}$ exhibited a compressive strength and A-value which were, respectively, 57 % and 54 % higher than those of the quartz-based AAC autoclaved at $192\text{ }^{\circ}\text{C}$. Moreover, the RHA-based AAC autoclaved at $165\text{ }^{\circ}\text{C}$ exhibited almost the same A-value as that of the quartz-based AAC autoclaved at $192\text{ }^{\circ}\text{C}$. However, a higher total drying shrinkage was observed for the C-DE-based AAC and RHA-based AAC autoclaved at $165\text{ }^{\circ}\text{C}$ compared to that for the quartz-based AAC autoclaved at $192\text{ }^{\circ}\text{C}$ which was due to the higher portion of non-crystalline C-S-H in those AAC samples compared to the quartz-based AAC autoclaved at $192\text{ }^{\circ}\text{C}$. Similarly, it has been reported that fly ash-based AAC exhibited higher drying shrinkage compared to quartz-based AAC as well. This might be an issue for some applications in which it is needed to fulfill shrinkage requirements in addition to the strength and density grades.

5.1.1 Possibility to reduce energy consumption in AAC production

Using C-DE as the main silica material in the AAC mixture results in the conservation of quartz sand resources as the quarried natural resources, and a reduction in the electricity consumption by removing the milling process of quartz sand. C-DE is much softer than quartz sand which eased the grinding process and provides considerable energy savings in the milling process of AAC production. It should be noted that the milling process of quartz sand is one of the energy-intensive steps in AAC production which is one of the main reasons for substituting quartz sand with fly ash in the industry [27, 28].

In the case of using RHA, which is an agricultural waste product, as the main silica source in the AAC mixture, in addition to the above-mentioned advantages material efficiency of AAC products can also be improved. C-DE used in this study was a kind of non-waste, nevertheless, it could present an opportunity for incorporating waste C-DE into construction uses.

The results have revealed that when C-DE or RHA are used as the main silica material in the AAC mixture, a lower autoclaving temperature is required to meet the specific strength-to-density ratio (A-value) of the AAC product.

Autoclaving the C-DE-based AAC at a temperature $40\text{ }^{\circ}\text{C}$ lower than the typical temperature increased the compressive strength by 45 %, which exceeds technical requirements. One advantage of obtaining an AAC product with higher strength than technical requirements is the opportunity to reduce binder content in the mixture. Alternatively, there is a possibility to extend the density grades of AAC products, e.g. a specific compressive strength could be obtained by a lower density, which has the advantage of an improved thermal insulation

property. Thus, the subsequent advantages of reducing autoclaving temperature could be accompanied by the economic and environmental benefits of reducing binder content or improving thermal insulation properties.

On the other hand, for the C-DE-based AAC, a reduction of 58 °C in the applied autoclaving temperature led to a compressive strength which still fulfills the requirement. This implies that there is a compromise between applying around 58 °C lower temperature and autoclaving at a 40 °C lower temperature which would be followed by a possibility to reduce binder content or improve thermal insulation properties. In such cases, it is needed to determine which of those aforementioned situations would lead to lower total energy consumption.

In general, a lower reduction in the autoclaving temperature was observed for the RHA-based AAC compared to the C-DE-based AAC. For the RHA-based AAC, a maximum reduction of 27 °C in the autoclaving temperature was obtained. However, the R75 mix, in which 75 wt. % of quartz sand was replaced with RHA, showed a lower drying shrinkage compared to the DE75 mix.

From a general point of view, the results of this study could be associated with the following benefits:

- AAC products of a lower density, with improved thermal insulation properties
- AAC products of a higher compressive strength in each of the density grades
- AAC products with less binder (cement and lime) in the recipes
- Energy consumption during the autoclaving process would be reduced
- Energy consumption during the grinding process would be reduced
- CO₂ emissions would be reduced due to the lower energy consumption in the autoclaving and grinding processes, and less binder consumption. In case of improved thermal insulation properties, CO₂ emissions would be reduced through decreased energy consumption in AAC buildings
- A wider range of silica materials could be used, and in particular, industrial wastes containing silica in highly soluble form could be reused
- Resources of quartz sand would be saved

The question arises as to how much energy would totally be saved in the production of AAC as a result of such reductions, e.g. 58 °C, in the autoclaving temperature. Giving an accurate answer to this question needs carrying out a complete life cycle analysis (LCA) which is beyond the scope of this study. However, a rough estimation can be made based on the quantitative relationship between heat transfer and temperature change and using the information provided in a few studies [7, 10].

The energy reduction during the hydrothermal process can be estimated using Eq. (5.1).

$$Q = mc\Delta T \quad (5.1)$$

Conclusion and Outlook

Where Q is the symbol for heat transfer, m is the mass of the substance, and ΔT is the change in temperature. The symbol c stands for specific heat capacity and depends on the material and state of matter.

The autoclaving process is carried out using a saturated steam generator having a pressure some bars above the maximum pressure inside the curing vessel during dwell time. The main heat effect during autoclaving is the heating up of AAC green cakes and the vessel equipment which are made of iron and steel. The temperature levels are around 80 °C when autoclaves are opened to be loaded or emptied, and 192 °C or 134 °C (equivalent to a reduction of 58 °C), when curing is running in the dwell time interval. To overcome the temperature differences only steam is used, in one case there is a temperature difference (ΔT) of 192 °C – 80 °C = 112 °C and in the other 134 °C – 80 °C = 54 °C which have to be leveled. The difference between these temperature steps, i.e. $(112 - 54) / 112 = 51.8 \%$, gives simply a figure of around 52 % as a rough estimation for the opportunity of energy saving during the autoclaving process. This is equivalent to a reduction of 13–14 % in the total energy consumption needed for AAC production by assuming that autoclaving process makes up around 25–27 % of the total energy consumption in AAC production [7, 10]. This means that using C-DE as the main silica material in the AAC mixture could offer an opportunity for a reduction of 58 °C in the autoclaving temperature which leads to a total energy reduction of 52 % and 13–14 % in the autoclaving process and the whole process of AAC production, respectively.

In the case of autoclaving C-DE-based AAC at a 40 °C lower temperature, the energy consumption associated with the autoclaving process would be reduced by 35 % which is equivalent to a reduction of 9-10 % in the total energy consumption during the production of AAC. However, in this case, the energy consumption would also be reduced through the possibility of reducing binder content. It is difficult to estimate the reduction of energy consumption associated with reducing binder content because it is not clear how much of the cement and lime amounts can be decreased when the C-DE-based AAC is autoclaved at a 40 °C lower temperature. Nevertheless, it is an additional opportunity for a reduction in energy consumption.

For the RHA-based AAC, a maximum reduction of 27 °C contributes to an energy reduction of 24 % and 6–7 % during the autoclaving process and the whole process of AAC production, respectively.

Moreover, energy reduction through saving electricity in the grinding process should also be considered. In general, around 8–12 % of the total energy consumption in AAC production is associated with electricity [10, 7] which is mainly consumed through the grinding process of quartz sand.

It should be considered that the above estimations for energy reduction in cases of C-DE-based and RHA-based AAC are accompanied by differences in the property of drying shrinkage compared to quartz-based. This situation concerning drying shrinkage is similar to what has been observed for the fly ash-based AAC which shows a higher total drying shrinkage compared to the quartz-based AAC.

5.1.2 Properties of raw materials which can be used as silica materials of a higher solubility than quartz to meet the objectives of this study

Calcined diatomaceous earth (C-DE) and rice husk ash (RHA) used in this study contained around 90–93 % silica mainly in the form of cristobalite which has a higher solubility than quartz. The degree of crystallinity was between 65 % and 75 %. Moreover, they had a porous and interconnected microstructure with corresponding specific surface areas of 2.90 m²/g and 1.80 m²/g, respectively, which affected the dissolution rate.

At the beginning of the study, only C-DE was used as the silica material of a higher solubility than quartz and it was not clear whether the obtained advantages were limited to C-DE or other silica raw materials of high solubilities could lead to similar results and advantages as well. As the study progressed, it was revealed that using RHA as the silica material of a high solubility resulted in similar outcomes as the previously performed studies with C-DE. This implies that in addition to C-DE and RHA, other silica materials with comparable dissolution properties in alkaline systems can potentially lead to a reduction in energy consumption during hydrothermal treatment.

The potentially appropriate materials to meet the objectives of this study can have properties similar to the aforementioned properties, i.e. above 85 wt. % silica mainly in the form of cristobalite, a degree of crystallinity of 65–75 %, and an interconnected microstructure with a specific surface area of 1.80–2.90 m²/g. However, all of the materials with the above-mentioned properties will not necessarily lead to similar results as those obtained in this study. For instance, the same outcome might not be achieved by using raw materials with a relatively high alkali content or other substances which are not compatible with the AAC mixture. On the other hand, silica materials mainly composed of amorphous silica might be compatible with the purposes of this study and, as a result, can possibly be used as a silica material of high solubility. Preliminary results of a few experiments carried out by the author have shown that the advantages of reducing required autoclaving temperature and binder content could also be achieved using natural diatomaceous earth (N-DE) which exhibited a degree of crystallinity as low as 30 %.

5.2 Outlook for future research

Further research can be conducted as follows:

- Using longer dwell times in order to increase the degree of crystallinity and/or crystallite sizes of C-S-H. Moreover, assessing the possibility of obtaining more optimized autoclaving conditions by applying various autoclaving duration and considering the autoclaving duration as a variable parameter.
- Introducing fine aggregates as a filler such as a limestone powder or similar minerals which do not react significantly during autoclaving.
- Examining the influence of a higher C/S of the starting materials, e.g. C/S of 0.8, on the compressive strength and shrinkage behaviors of AAC containing silica materials of high solubility as the main silica source.
- Investigating the role of sulfate addition on the drying shrinkage of AAC containing silica materials of a higher solubility as the main silica source. The findings of the study performed by Mesecke [119] have demonstrated that the addition of sulfate

Conclusion and Outlook

carriers prevents the formation of the initially formed C-S-H with a too high C/S and provides a more favorable distribution of SiO_4^{4-} which results in a more homogeneous distribution of C-S-H and corresponding tobermorite. However, this effect might not be applicable for the AAC containing silica materials of high solubility since in this case, the initially formed C-S-H have already a relatively low C/S due to the high solubility and dissolution rate of silica. In another word, in the initial stages of the hydrothermal process, the concentration of SiO_4^{4-} is not so low as to require the consumption of Ca^{2+} in an indirect way, i.e. hydroxyllestadite formation. This implies that the silica materials of high solubility might cancel the effect of the sulfate addition in AAC. This introduces the possibility to produce AAC products with low content of sulfate using silica materials of high solubility which improves the sustainability and recyclability of AAC products.

Supporting Information on Chapter 4

In this chapter, the publication archive is presented in order to provide detailed information on the results discussed in chapter 4.

A.1 Publication 1

Construction and Building Materials, V. 272, No. 122014, February 2021.
<https://doi.org/10.1016/j.conbuildmat.2020.122014>

Reprinted (adapted) with permission from Elsevier
(<https://www.elsevier.com/about/policies/copyright/permissions>).

Summary

In this paper, we examined the influence of calcined diatomaceous earth (C-DE) as a silica raw material of a higher solubility than quartz, on the mechanical and microstructural properties of autoclaved aerated concrete (AAC). Accordingly, quartz sand within an AAC mixture was replaced at various replacement ratios by C-DE. The results and discussions presented in this paper are according to the typical autoclaving condition, i.e. the autoclaving temperature of 192 °C (corresponding to the pressure of 12 bar) with a total duration of 9 h. The performances of AAC samples at different autoclaving temperatures are described in the second paper. The results showed that applying an autoclaving temperature of 192 °C with a total duration of 9 hours, which is a typical autoclaving condition in industrial AAC production, inhibited tobermorite formation in the C-DE-based AAC. However, for the quartz-based AAC, applying the aforementioned autoclaving condition promoted tobermorite formation. This probably resulted from the varying dissolution behavior of quartz sand and C-DE.

Author contributions to the three research papers presented in this chapter

Conceptualization, Methodology, Software, Data Curation, Investigation, Formal analysis, Writing - Original Draft, Writing - Review & Editing, Visualization.

The author conceived the idea, developed the theory, and performed almost all of the measurements and analyses. Moreover, the author designed the experiments and analytical methods and processed the experimental data. The author interpreted and discussed the results, drafted the original manuscript, applied comments, and wrote the final version of the manuscript.

Production of autoclaved aerated concrete with silica raw materials of a higher solubility than quartz

Part I: influence of calcined diatomaceous earth

Taban Shams ^{a, b, 1}, Georg Schober ^c, Detlef Heinz ^b, Severin Seifert ^a

^aFraunhofer Institute for Building Physics IBP, Inorganic Materials and Recycling Department, Building Materials Technology Group, Fraunhoferstr. 10, 83626, Valley, Germany

^bTechnical University of Munich, Department of Civil, Geo and Environmental Engineering, Centre for Building Materials cbm, Baumbachstr. 7, 81245, Munich, Germany

^cEngineering office for materials development and process technology, Marbstraße 6, 94405 Landau a.d. Isar, Germany

Abstract

This study examines the effects of calcined diatomaceous earth (C-DE) as a silica raw material of a higher solubility than quartz, on the mechanical and microstructural properties of autoclaved aerated concrete (AAC) produced at the steam curing temperature of 192 °C for 6 hours. Quartz within an AAC mixture was replaced at various replacement ratios by C-DE. The resultant phases were characterized using quantitative and qualitative X-ray diffraction (XRD), scanning electron microscopy (SEM), differential thermal analysis (DTA), and thermogravimetric analysis (TGA). In the mixtures with more than 50% substitution of quartz with C-DE, the autoclaving temperature of 192 °C with a duration of 6 hours prevented the crystallization of amorphous calcium silicate hydrate (C-S-H) to tobermorite. The optimum strength was obtained at the substitution ratio of 75% despite having the lowest tobermorite content. By substituting quartz with C-DE for higher than 50%, plate-like tobermorite was changed to grass-like and amorphous C-S-H with low CaO/SiO₂.

Keywords: autoclaved aerated concrete, diatomaceous earth, steam curing temperature, calcium silicate hydrate (C-S-H), tobermorite

1. Introduction

Climate change and global warming have led topics such as the “ecology movement” or the “Green movement” to become the highest of priorities in recent years. The building materials field is also strongly affected because of its huge extent and its great demand for energy and raw materials. Compared with normal concrete and bricks, Autoclaved Aerated Concrete (AAC) consumes less energy [1] and raw materials [2, 3]. Due to this fact and primarily given its excellent thermal insulation [2, 4, 5], AAC has great potential for use as an element in the buildings of the future. Currently, one major issue in the development of AAC production is energy consumption along with the carbon dioxide emission related thereto. The steam curing process and the embodied energy of raw materials, i.e. lime and cement, require most of the primary energy in the process for producing AAC [3, 6–9]. The main components used to produce AAC are silica sand as a SiO₂ source, lime, and cement as a CaO source, and a small amount of aluminium powder or paste as a pore-forming agent [10]. However, almost all of the current produced AAC contains sulfate carriers (i.e. gypsum and anhydrite) as well. Sulphates in the AAC mixture regulate the setting of the mixture and improve the properties of this material. Reducing the sulfate content in the AAC mixture leads to increased shrinkage and reduced compressive strength [11–14]. In addition to the raw materials mentioned, ground recycled AAC (GRA) is effectively used as an eco-friendly and cheap filler in the industrial production of AAC [15]. GRA is the waste resulting from the manufacturing process of AAC, e.g., residues from the cutting process or rejects, which is returned to the manufacturing process. The autoclaving process includes the hydrothermal treatment of a mixture at elevated

¹ Corresponding author. Tel.: +49 8024 643-637.

E-mail address: taban.shamshafshejani@tum.de

temperature, typically around 180–200 °C and a corresponding pressure of 12–13 bar in a saturated steam condition [16, 17]. The autoclaving process affects the mechanical properties of AAC significantly and is an essential step in the production of AAC [10, 18]. During the autoclaving process, complex hydrothermal reactions affecting the CaO-SiO₂-H₂O (C-S-H) system occur which leads to the formation of tobermorite and other C-S-H phases [11, 19–24]. Among hydrothermal products, tobermorite is the main binding phase in AAC which improves compressive strength and reduces shrinkage [16, 25]. Therefore, in order to optimize the autoclaving process, tobermorite formation should happen under optimized curing conditions to decrease energy, time, and also cost requirements. The formation of tobermorite has several sources in which reactions occur only in the presence of dissolved silica. Dissolved silica reacts with other phases, e.g., calcium hydroxide, non-crystalline C-S-H, hydroxylellestadite, etc. to form tobermorite [11, 17]. Therefore, the process of dissolving silica is the rate-determining step in tobermorite formation [10, 21, 26]. Different forms of silica have different solubilities and dissolution rates. It is well known that amorphous silica is more soluble than quartz at all temperatures [27–29]. Additionally, some other types of silica, e.g., cristobalite, tridymite, and stishovite exhibit higher dissolution rates than quartz [27, 30]. Therefore, it can be assumed that replacing quartz with all the aforementioned silica offers the advantage of reducing curing temperature and/or time because they have a higher solubility and require lower energy to dissolve and form tobermorite [24, 31]. Currently, the use of quartz as a SiO₂ source for AAC production is well-established, but it must first be finely ground, which requires additional energy. Quartz has relatively low solubility in water, and the rate of dissolution is also relatively slow. Therefore, when quartz is the main silica source in the AAC mixture, saturated steam curing at a relatively high temperature, i.e., greater than $T > 180$ °C is required. However, when silica sources of a higher solubility are used, a lower steam curing temperature might be needed. Many efforts have also been made in the use of by-products as well as secondary and waste materials in the AAC mixture to make it environmentally friendly and economical [5, 22, 32–34]. However, detailed studies related to an optimization of the curing condition leading to a reduction in energy consumption are still quite limited in number. Isu et al. [10, 35] investigated the chemical reactions in the hardening of AAC block using ground quartz of different particle sizes. The samples were prepared at 180 °C under saturated steam pressure for various times from 0.5 to 64 h. They found that with finer quartz tobermorite was formed after 0.5 h autoclaving, indicating that finer quartz reduces the autoclaving processing time. However, it was also observed that the tobermorite formed had lower crystallinity with finer quartz. The reason was attributed to a higher degree of supersaturation caused by the higher specific surface area of finer quartz. Matsui et al. [17] investigated the effects of quartz reactivity on tobermorite formation. It was observed that in the experiments using quartz of a higher reactivity, tobermorite crystallized rapidly in the early stage of the autoclave process. Kunchariyakun et al. [24] and Mostafa [31] studied the effect of rice husk ash (RHA) and air-cooled slag (AS) respectively on AAC properties. They found that increasing the autoclaving time has no effect on the tobermorite peak intensity and thus concluded that the use of RHA and AS in AAC led to a reduction in the required autoclaving time. In both studies, only the autoclaving time was changed, and the curing temperature remained constant. In 2018, Kunkarchiyan et al. [36] investigated the influence of rice husk ash on AAC properties at various times as well as temperatures. It was stated that the compressive strengths of the AAC samples containing RHA increased with further increasing autoclaving temperatures and times, whereas it was reported earlier that the compressive strength for rice husk ash replacements of greater than 25% remained stable after longer curing time. Therefore, with regard to silica materials known to have a higher solubility than quartz, the expected advantages for AAC production, e.g., shorter curing times or temperatures, higher strength values, or a lower binder content in recipes, have not been achieved to a sufficient extent so far. Accordingly, the object of the whole study is to optimize autoclaving temperature by means of substituting quartz with calcined diatomaceous earth (C-DE) as silica of a higher solubility than quartz. For this purpose, first the possibility of using C-DE as a substituent of quartz in the AAC mixture was examined. Diatomaceous earth (DE) is a siliceous, sedimentary rock consisting of the fossilized skeletal remains of diatoms. DE is an attractive material offering broad application in the industry owing to its properties of a low bulk density, high chemical and thermal resistance, high porosity, and a high specific surface area. As a natural mineral raw material, DE is convenient and promising with respect to the production of porous building materials such as AAC due to its natural porosity, low density, and mineralogical composition [37]. Moreover, DE is much softer than quartz eased the grinding process. This fact can provide considerable energy savings in the milling operations of AAC production. C-DE is obtained from treating DE at a temperature of 700–900 °C. Usually, DE is calcinated

before being sold to remove impurities and undesirable volatile contents. The purpose of this approach is also specific industrial applications such as further harden the skeletons of the diatoms in order to create better filtering agents. Since DE is mostly used for filtration and C-DE provides a higher flow rate in filtration, most DE available in the market are in the form of C-DE. The total consumption of DE in Germany is about 100,000 tons per year, thus producing a large amount of waste [38]. Although a kind of non-waste C-DE was used in this study, it could present an opportunity for incorporating these solid wastes into construction uses. This study is being presented in two parts. Part I, which is the present paper, deals with research regarding the possibility of using C-DE as a silica material of a higher solubility in the AAC mixture. Moreover, the influences of C-DE substitution on the mechanical, chemical, and thermal properties of AAC produced at a typical autoclaving temperature of 192 °C for 6 hours were studied. The purpose of part I is to investigate the influences of replacing quartz within an AAC mixture with C-DE at various replacement ratios and a typical autoclaving condition. Part II regards the effect of autoclaving temperature on the mechanical and microstructural properties of C-DE-substituted AAC produced the same way as in part I.

2. Materials and methods

In this study, two types of silica sources, Dorsilit as the quartz, and Calcined Diatomaceous Earth (C-DE) as the silica of a higher solubility than quartz were used. Dorsilit was obtained from a quartz sand refining company (Dorfner, Germany). C-DE was provided by the apj GmbH company, Germany. As a lime raw material, a type of soft-burnt quicklime (CL 90-Q) was used and obtained from the Fels-Werke Company. Portland cement type I (CEM I 42.5) obtained from the Dornburger cement company was used. The chemical compositions and physical properties of materials used in this study are given in Tables 1 and 2 respectively. In this study, the X-ray fluorescence (XRF) technique was used to determine the chemical composition. XRF analysis was performed using Epsilon 3XLE spectrometer and Omnian software. For this purpose, samples were prepared as pellets. To produce the pellets, samples were mixed in a ratio of 4: 1 with a binder (micro powder C, C38H76N2O2). Sample and binder must be mixed homogeneously. The mixture was then pressed using a tablet press at a pressure of 200 kN for about one minute to obtain a pellet of 4-5 mm thick. In Table 2, density was determined according to DIN 66137-2 [39] using a gas pycnometer. The other values in Table 2 were provided by suppliers.

Table 1 Chemical composition of raw materials (wt %)

sample	SiO ₂	CaO	Al ₂ O ₃	Fe ₂ O ₃	MgO	TiO ₂	Na ₂ O	K ₂ O	SO ₃	L.O.I	total
Dorsilit	98.8	0.02	0.8	0.02	0.01	0.03	0.01	0.3	-	0.21	100.2
C-DE	92.8	0.6	4.2	1.6	0.3	0.05	0.1	0.2	-	0.3	100.2
lime	0.8	95	0.3	0.2	0.5	-	-	-	0.2	3	100
cement	20.4	62.9	4.9	2.5	1.7	-	0.2	1.0	3.8	3.0	100.5
GRA	41.2	37.4	2.0	1.3	-	0.1	-	0.7	5.7	12.0	100.4
anhydrite	-	47.5	-	0.2	-	-	-	-	52.2	-	99.9

Table 2 Physical properties of raw materials

sample	density (g/cm ³)	bulk density(g/cm ³)	pH value
Dorsilit	2.63	0.93	6.1
C-DE	2.41	0.19	6.5

Fig. 1 shows the XRD pattern of Dorsilit and C-DE. The XRD pattern of Dorsilit includes sharp peaks of quartz while C-DE consists of cristobalite which is more soluble than quartz [27, 30]. Additionally, it has broad peaks compared to quartz which shows a higher amorphous content of C-DE rather than Dorsilit. This can also be understood by comparing the values in Table 3. Table 3 shows the amorphous and crystalline content of these materials as provided by DIFFRAC.EVA and DIFFRAC.TOPAS software. EVA software calculated the crystalline content by dividing the total area of crystalline peaks by the total area under the diffraction curve,

i.e., crystalline peaks plus amorphous reflections [40]. The degree of crystallinity calculations in TOPAS software requires the definition of at least two phases to describe the intensity contributions coming from the crystalline and the amorphous parts of the sample. Different techniques, e.g. using structures of Rietveld refinement, can be used for modeling crystalline and amorphous parts of the sample [41].

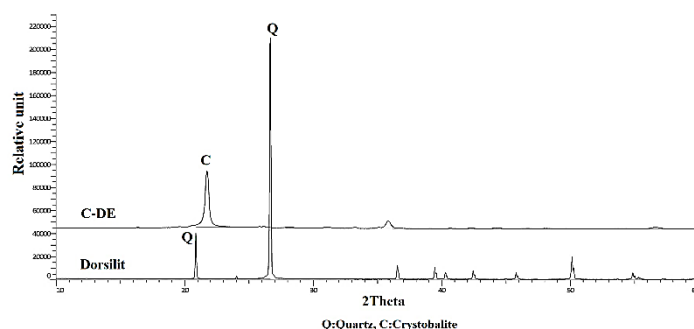


Fig. 1 XRD pattern of Dorsilit and C-DE

Table 3 Amorphous and crystalline content of Dorsilit and C-DE

sample	crystalline%		amorphous%	
	EVA	TOPAS	EVA	TOPAS
Dorsilit	94	98	6	2
C-DE	71	66	29	34

SEM micrographs of C-DE and Dorsilit are shown in Fig. 2a and b, respectively. C-DE has a porous structure including pores on the micrometer scale, while quartz contains dense solid particles.

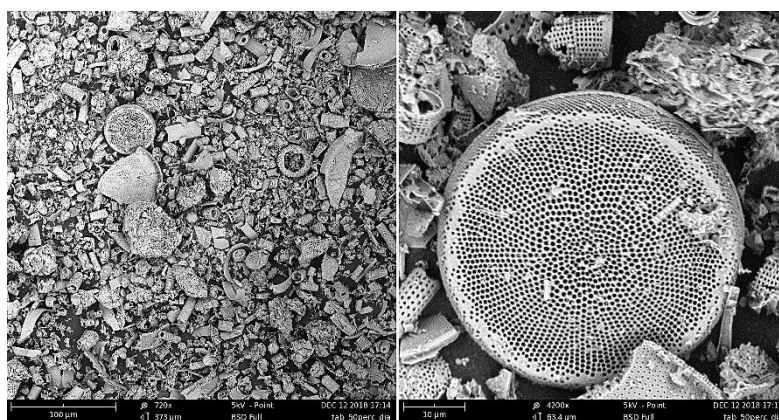


Fig. 2a SEM micrographs of C-DE

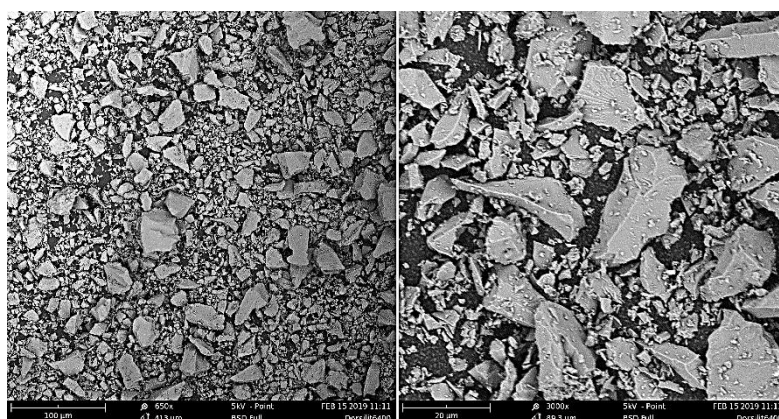


Fig. 2b SEM micrographs of Dorsilit

Fig. 3 and Table 4 show the particle size distribution of quartz and C-DE, which were determined by Laser particle size distribution (Malvern Mastersizer 3000).

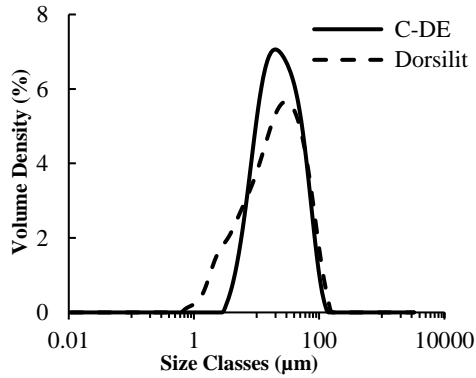


Fig. 3 Particle size distribution of Dorsilit and C-DE

Table 4 Particle size distribution of Dorsilit and C-DE

sample	D(10) μm	D(50) μm	D(90) μm
Dorsilit	3.69	20.4	65.6
C-DE	8.01	21.9	59.1

The referenced recipe, i.e. Q100, was adjusted to P4-500 grade, which is similar to the mix proportion of AAC produced in the industry. P4-500 is a German grade for AAC, which refers to AAC with a density range of 450-500 kg/m³ and compressive strength of greater than 4 MPa. Quartz in the reference recipe was replaced by C-DE for 25 wt%, 50 wt%, and 75 wt% to produce DE25, DE50, and DE75, respectively. The mix proportions are shown in Table 5. Water to solids ratio (W/S) and aluminum paste values were set in a way to have the same bulk density for all recipes. The high porous nature of C-DE compared to quartz required the mixtures containing C-DE to contain more mix water, which is represented by the higher W/S. Therefore, in order to have the same bulk density, a higher water quantity was compensated by a lower quantity of aluminum paste (the last two columns in Table 5).

Table 5 Mix proportions of aerated concrete with C-DE (wt %)

mixture	quartz	C-DE	cement	lime	anhydrite	GRA	C/S*	W/S	Aluminum**
Q100	41	-	31	10	6	12	0.635	0.7	0.23
DE25	31	11	31	10	6	11	0.633	0.8	0.21
DE50	20.5	22	31	10	6	10.5	0.636	0.95	0.18
DE75	10	33	31	10	6	10	0.640	1.2	0.13

*molar ratio

**Aluminum values are in the percentage of binder content

To be able to observe the effect of C-DE as a silica material of a higher solubility on the final properties, all the other parameters influencing the final properties must be kept constant. Accordingly, it is needed to have similar particle size distribution for quartz and C-DE as silica sources and also almost the same CaO/SiO₂ (C/S) of the starting materials for all recipes. In this study, an almost similar particle size distribution for silica sources, i.e., C-DE and Dorsilit were used (Fig. 3). The C/S molar ratio of the starting material for all mixes was adjusted at 0.63-0.64, and a low-lime mixture type was used. For this purpose, after replacing 25%, 50%, and 75% of quartz with C-DE, GRA, and C-DE changed in a range of 1-2%, and the other components remained constant to obtain nearly the same C/S for all recipes. C-DE, quartz, and GRA were mixed with water. Lime, cement, and anhydrite were then added, and the mixture was stirred for 2 minutes. Finally, the aluminum suspension was added and the mixing continued for 30 seconds. The slurries were poured into 22 cm cubic styrofoam molds. The samples were then stored at room temperature (RT) for 3 hours. After demolding, the cubes were steam cured in the autoclave at a temperature of 192 °C and a corresponding steam pressure of 12 bar for 6 hours. The autoclave used was the size of 1.5 m³ which is comparable to industrial autoclaves having an external steam supply. After removing the samples from the autoclave, the samples were cut into 10x10x10 cm³ cubes and dried at 50 °C for several days until a moisture content of 6 ± 2 wt.% was reached. Subsequently, various measurements were performed, including compressive strength according to DIN EN 772-1 [42], X-ray diffraction (XRD) analyses, as well as Scanning Electron Microscope (SEM), and

thermal analyses. The XRD analyses were performed using a Bruker D2 Phaser diffractometer with Cu-K α radiation and a LynxEye silicon strip detector. All samples were measured with a step size of 0.02° and 4 s/step over the range of 5-65° 2 θ . The qualitative XRD analysis was performed using DIFFRAC.EVA software based on the International Center for Diffraction Data (ICDD) database. The XRD quantitative analysis was performed using DIFFRAC.TOPAS software based on the Rietveld method and 10% of ZnO as the internal standard. A grain size of < 10 micron is required for quantitative X-ray diffraction (Rietveld). To avoid the amorphization of the sample during grinding, wet milling was used in XRD-Mill McCrone (from RETSCH). Before grinding in the McCrone Mill, the sample was crushed and passed through a 500 micron sieve. The mixture of weighted sample and 10% ZnO was then carefully transferred to McCrone Mill and 5 ml of ethanol as a grinding agent was added. This mixture was ground for 3 min. After micronizing, the sample was recuperated in cups by using ethanol and was dried for one-two days under a fume hood. Dried samples are gently disaggregated and passed through a 250 micron sieve. Frosted glass was used to fill sample holders and make a flat surface. To minimize the effect of preferential orientation, the surface was disordered with a rough texture glass. In this study, each sample was measured three times and the results were then averaged. The SEM was performed using a Phenom Pro X made with a CeB₆ electron source with acceleration voltages of 5 and 15 kV. For this purpose, A small flat piece of the AAC was fixed on an aluminum stub (12.5 mm). The prepared sample was then coated with a thin layer of gold as a conductive material. The thermal analysis including, DTA-TGA measurements, was performed using NETZSCH STA 409 CD over the temperature range of 23-1200 °C at a heating rate of 10 °C /min. The samples were stored at 50 °C for at least 24 h before analysis. In the next step, the dry bulk density was determined according to DIN EN 772-13 [43]. For this purpose, the cubes were dried at a temperature of 105 +/- 5 °C in the oven until reaching a constant weight.

3. Results and Discussion

3.1 Phase and microstructural analyses

The mineralogical phase composition and microstructures of the samples were examined using XRD and SEM. The diffraction patterns are presented in Fig. 4.

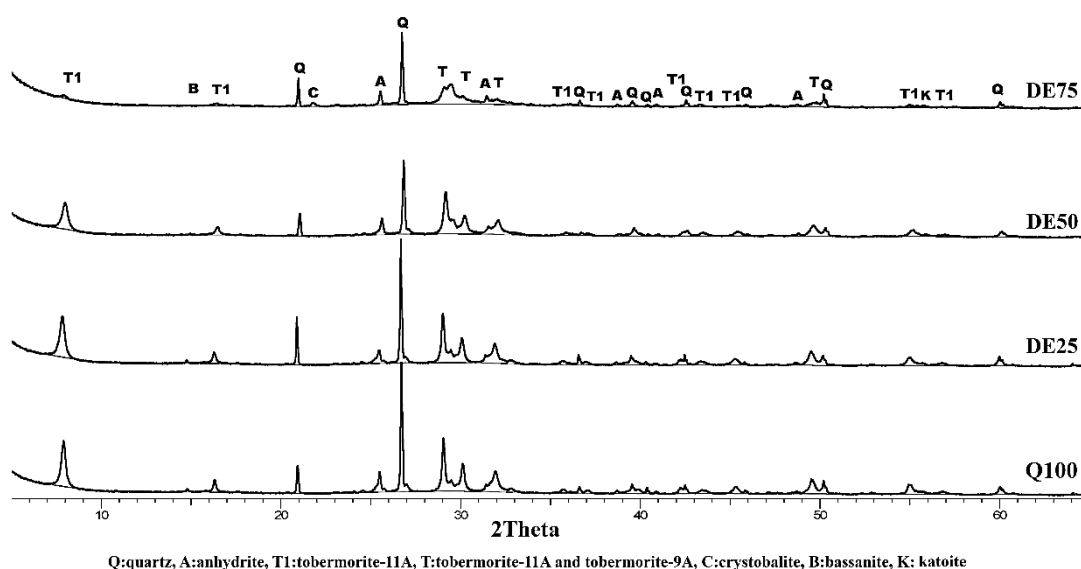


Fig. 4 XRD patterns of AAC with different substitution ratio autoclaving at 192 °C

By incorporating C-DE into the AAC mixture, a broad reflection appeared in the XRD spectra of the DE75 sample at around 29.5° 2 θ . Fig. 5 shows the XRD spectra of reference and DE75 samples around this broad reflection. The asymmetry of the reflection is caused by the integration of two different peaks with close d-

values. The peak at $29.30^\circ 2\theta$ or 3.04 d-scale is related to semi-crystalline C-S-H [44] or C-S-H gel [45] which overlaps with the calcite peak at $29.44^\circ 2\theta$ or 3.03 d-scale.

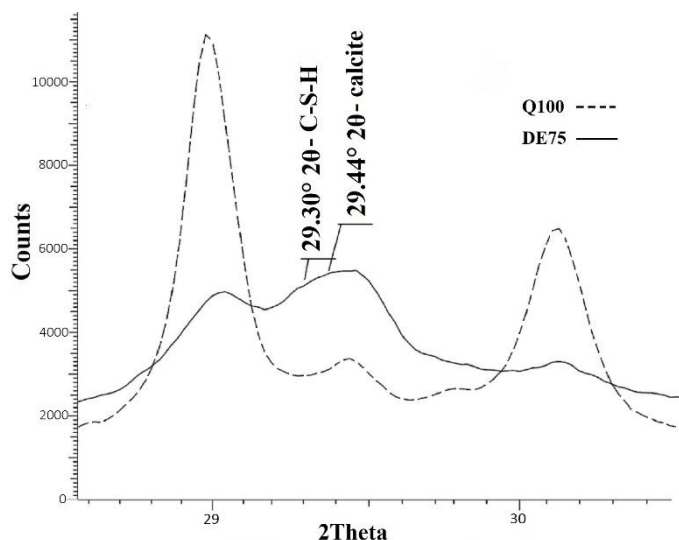


Fig. 5 XRD patterns of reference and DE75 samples around $29.5^\circ 2\theta$

In the XRD pattern of the reference sample, sharp peaks of tobermorite with high intensity can be seen, which implies that the existing tobermorite in the sample has a high degree of crystallinity. By replacing quartz with C-DE, the intensity of the tobermorite peaks weakened and became wider, which means that tobermorite had formed in a poorly crystalline type. In general, the tobermorite peak intensity decreased with increasing C-DE content. The phase contents determined by the Rietveld method are shown in Table 6.

Table 6 Rietveld quantitative analysis results (wt %)

sample	tobermorite-11A	tobermorite-9A	quartz	cristobalite	amorphous	anhydrite	calcite
Q100	36.6 (0.6)	4.7 (0.07)	15.3 (1.8)	-	27.9 (3.2)	3.4 (0.3)	2.8 (0.5)
DE25	37.6 (0.5)	4 (0.3)	15.2 (0.7)	0 (0)	26.6 (1.5)	3.5 (0.2)	3.0 (0.4)
DE50	27.2 (0.6)	7.2 (0.1)	12.6 (0.9)	0 (0)	33.3 (1.8)	4.1 (0.1)	4.4 (0.5)
DE75	6.3 (0.9)	5.8 (0.3)	7.4 (0.5)	1(0.04)	64.2 (1.7)	3.3 (0.2)	4.5 (0.4)

Values in parentheses represent standard deviations of repeated measurement

The tobermorite content decreased with increasing C-DE content. The amorphous content has an opposite trend compared to tobermorite, i.e., an increase in amorphous content was accompanied by a decrease in tobermorite content. It is therefore most likely that changes in the tobermorite content are related to changes in the amorphous content. On the other hand, the obtained amorphous content includes the amorphous C-S-H present in the mixture. This might be due to an inhibition in the crystallization of amorphous C-S-H to tobermorite. The appearance of the peak related to semi-crystalline C-S-H or C-S-H gel confirms the above result as well. Because it shows the presence of non-crystalline C-S-H in the mixture which did not transform to tobermorite and remained in the final product. In fact, by increasing C-DE in the AAC mixture, the amorphous C-S-H remained in the sample and did not crystallize to tobermorite, thus leading to an increase in the amorphous content and a reduction in the tobermorite content. In addition, the amount of unreacted or residual cristobalite was much lower than the residual quartz, which confirms the higher solubility of C-DE compared to quartz. In general, increasing the C-DE content led to a decrease in the amount of unreacted SiO_2 . This implies that there was a lower C/S in the matrix of the C-DE system than that of the quartz system. The reason for this is probably that C-DE, which is partly amorphous and contains cristobalite, had a higher solubility than quartz and dissolved more quickly. So, at the same steam curing temperature (i.e., 192°C), the C/S ratio of the initially formed C-S-H in the more soluble silica system was lower (higher Si content) than that of the quartz system [17, 44]. Moreover, it has been reported that C-S-H with a low C/S ratio tends to have long and cross-linked chains of tetrahedral [21, 46–50]. So, it would be difficult to be transformed into tobermorite [31, 44, 46],

whereas C-S-H with a high C/S contains short silicate chains and readily crystallizes into tobermorite. This explains why tobermorite formation was inhibited in the more soluble silica system at a high autoclaving temperature with a regular duration, whereas it was promoted in the quartz system. Several studies have also reported similar results that replacing quartz with amorphous silica enhances the polymerization of C-S-H, which prevents the final rearrangement of C-S-H into tobermorite [26, 44, 46]. The SEM results were in good agreement with the above findings. Fig. 6 shows the microstructure of the samples examined using SEM. A plate-like tobermorite was formed in the reference sample (Fig. 6a). By substituting 25% of quartz with C-DE, the microstructure of the reference sample did not change significantly (Fig. 6b). This outcome can also be interpreted by comparing the XRD pattern and phase contents of the reference and DE25 samples (Fig. 4). There was no great difference in the tobermorite and amorphous content of reference and DE25 samples. This might show that 25% C-DE as a replacement ratio is not high enough to influence the phase formation and microstructure of AAC. Further increases in the C-DE replacement ratio up to 50% led to the formation of tobermorite and a grass-like C-S-H structure in the matrix (Fig. 6c). It is likely that the tobermorite formed due to the reaction of dissolved quartz with the other components, whereas grass-like C-S-H appeared in the presence of dissolved C-DE. It is also expected that the formed grass-like C-S-H is a type of C-S-H with a low C/S ratio (Fig. 6c) because C-DE has a higher rate of Si supply to the matrix. A similar result was observed by Kunchariyakun et al. [24] and by Mostafa [31], who used rice husk ash and slag respectively as amorphous silica in the AAC mixture. Both of the aforementioned studies have reported the formation of a grass-like C-S-H structure with a very low Ca/Si ratio in the mixtures with a high degree of quartz substitution by amorphous silica. As can be seen in Fig. 6c, it appears that using both quartz and C-DE in equal amounts as silica sources in the AAC mixture leads to the formation of C-S-H phases with a different microstructure and morphology, i.e., tobermorite and grass-like C-S-H. Fig. 6d shows that almost no tobermorite was formed in the DE75 sample rather, amorphous and grass-like C-S-H formed which again is expected to be a type with a low C/S. The reason could be that C-DE as the main silica source in the DE75 mixture dissolved quickly at the steam curing temperature of 192 °C and formed C-S-H with a very low C/S ratio which is out of the appropriate range for tobermorite formation. In other words, the C/S of C-S-H formed at the end of the hydrothermal process differed from values reported for tobermorite i.e. 0.66, 0.75, and 0.83 [45]. Therefore, the tobermorite percentage reduced, and the grass-like, and amorphous C-S-H increased. This observation is in good agreement with the XRD result of DE75. Previous studies [51–54, 19] have reported that the introduction of aluminium to the AAC mixture has a significant effect on tobermorite formation. In this study, the Al/(Al+Si) molar ratio is 0.035 which is not expected to influence tobermorite structure and/or cell parameters. The minimum Al/(Al+Si) used to investigate the influence of aluminium on calcium silicate hydrate was 0.05. However, significant changes in the tobermorite structure can be observed at $Al/(Al+Si) \geq 0.1$ [51, 55-57]. Therefore, in this study the quantity of aluminium is not high enough to influence the C-S-H structure. This is also confirmed by the XRD result of DE75. It should be noted that in the quartz system, the duration of 6 hours at a temperature of 192 °C is long enough for tobermorite formation and compressive strength development. However, in the case of the C-DE system, at a high autoclaving temperature a longer duration might be needed to obtain tobermorite in a large portion. It has been reported that when colloidal silica fume, which has a higher solubility than quartz, was used as a starting material, it was difficult to produce highly crystalline tobermorite even after 24 hours of autoclaving at 180 °C [44]. In this study, the obtained results are corresponding to a duration of 6 hours and another duration might not lead to the same result.

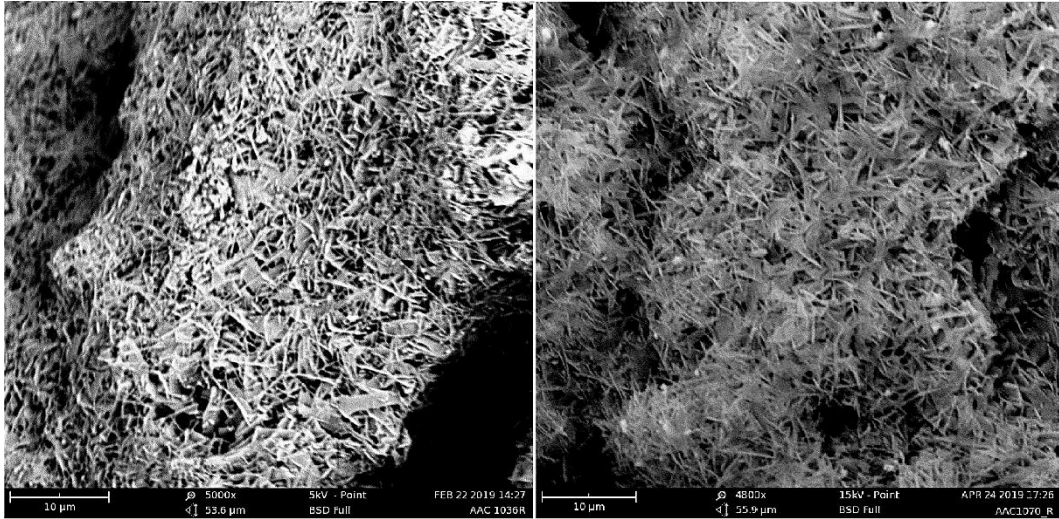


Fig. 6a. SEM micrographs of the reference mixes

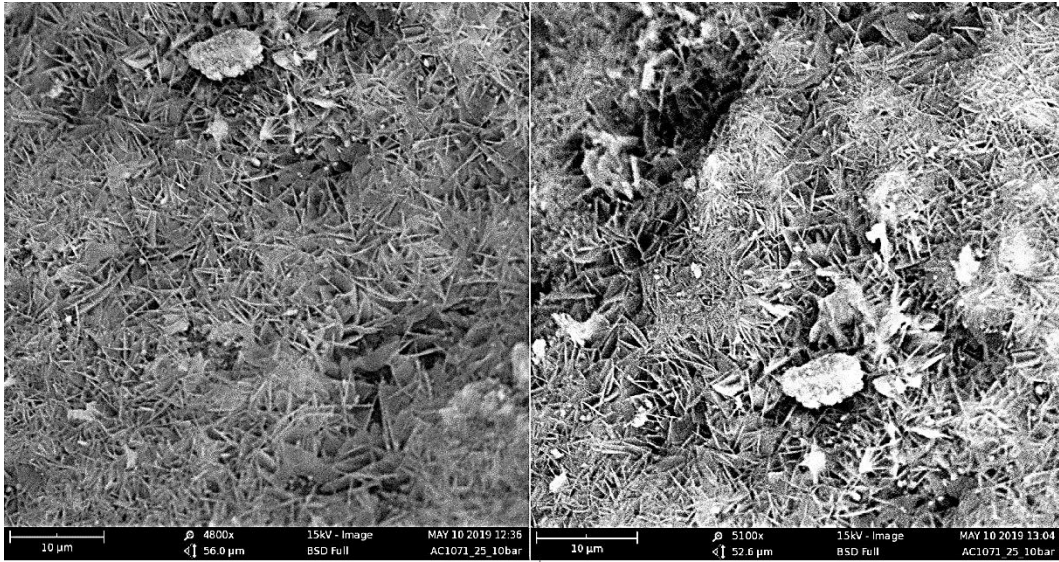


Fig. 6b. SEM micrographs of the DE25 mixe

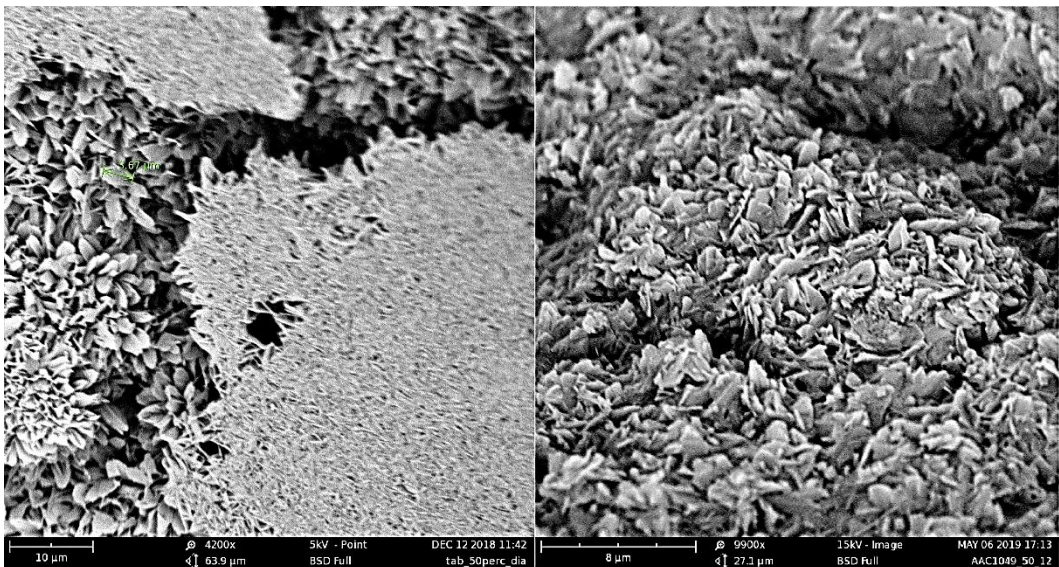


Fig. 6c. SEM micrographs of the DE50 mixes

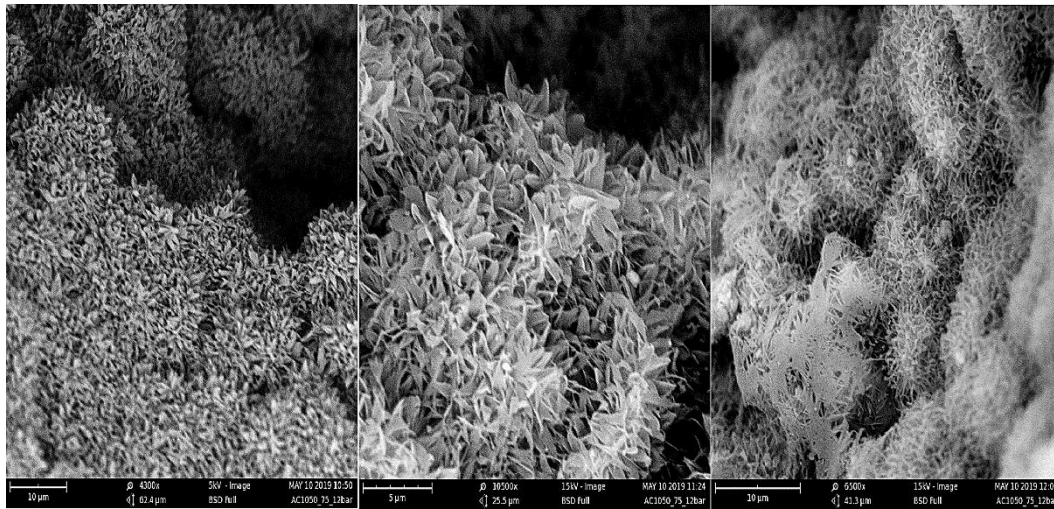


Fig. 6d. SEM micrographs of the DE75 mixes

3.2 Mechanical properties

The compressive strength and bulk density of the samples are presented in Fig. 7. The compressive strength decreased by increasing the substitution of quartz by C-DE by up to 50%, whereas it increased and even slightly exceeded the compressive strength of the reference sample for the substitution rate of 75%. In fact, the compressive strength of the DE25 and DE50 samples dropped by 14% and 28%, respectively, compared to that of the reference sample. However, the DE75 sample reached a strength slightly higher than and almost the same as the reference. The reduction in compressive strength of the DE25 and DE50 samples compared to the reference sample might be due to the reduced tobermorite formation. However, the reason for the additional reduction in the compressive strength of DE50 compared to DE25 is probably that using two different silica sources with an equal amount in the AAC mixture might lead to the formation of C-S-H phases with different microstructure and morphology in the matrix (Fig. 6c), meaning that they were not fully locked into each other, and the spaces between crystals would not fill, which may have had a negative effect on the compressive strength of the DE50 samples. The optimum strength was obtained by DE75 samples despite its lowest tobermorite content. In this case, the high strength was probably related to the pore size, the microstructure, and the proportion of ingredients.

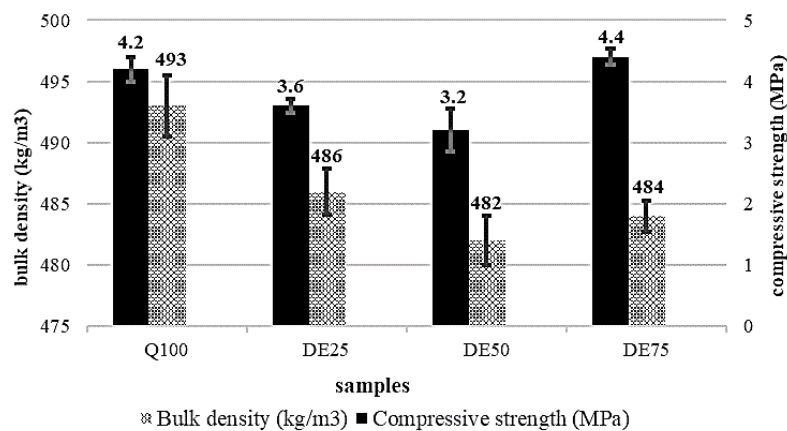


Fig. 7 Compressive strength and bulk density of AAC samples

The DE75 mixture had almost the same bulk density and, as a result, almost the same total porosity [58–62] compared to the other mixes. Despite having a similar total porosity, an increment of small-size pores in the DE75 samples might have led to a higher compressive strength [63]. The increment in the small-size pores i.e.

micropores was caused by less aluminum content in the DE75 mixture compared to other mixes (Table 5) [64, 4, 18]. The lower aluminum paste quantity was compensated by a higher water quantity, which is represented by the higher W/S. Moreover, the combination and intermixture of C-S-H phases, which are expected to be Si-rich C-S-H, might influence the compressive strength of the AAC positively. In terms of the ingredients and mixture composition, the proportion of C-DE with respect to other solid materials and water in the DE75 mixture might have reached a beneficial size which resulted in a compressive strength improvement. The bulk density of the samples containing C-DE was slightly lower than that of the reference sample. However, the maximum difference was only 2%. In general, the bulk density of all of the samples remained in the range of 480-495 kg/m³, which corresponds to the P4-500 grade.

3.3 Thermogravimetric analysis (TGA)

The DTA-TGA curves and the corresponding results of the thermogravimetry analysis for reference and the DE75 samples are shown in Fig. 8 and 9 respectively. The TGA curves reveal a non-steady weight loss from RT to 1200 °C. Looking closer at the data, the result of thermogravimetry analysis shows weight loss over the different temperature ranges.

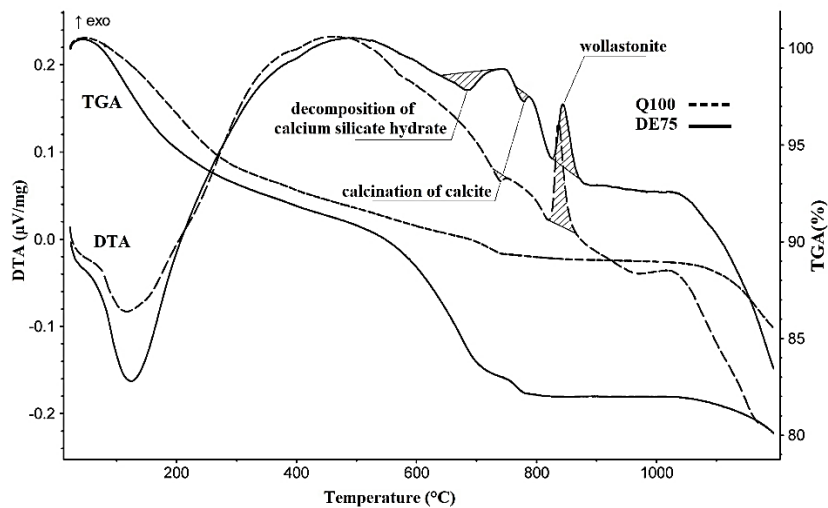


Fig. 8 DTA-TGA curves of reference and DE75 samples

According to Figs. 8 and 9, the DE75 sample had a higher total weight loss than the reference sample. The total weight loss increased from 14.5% to 19.9% by replacing 75% of quartz with C-DE in the reference sample. This increase in total weight loss is mainly ascribed to increased weight loss between 600 and 800 °C. The maximum weight loss for the reference sample occurred between 220 to 600 °C whereas it occurred between 600 and 800 °C for the DE75 sample. On the other hand, it has been reported that molecular water is lost at up to 600 °C and all weight losses above 600 °C may be ascribed to OH groups [65]. Therefore, the increase in weight loss was probably due to an increase in OH groups. H atoms can be attached to bridging tetrahedron to form a Si-OH linkage [44, 66], which implies an increase in Si-OH groups in the C-S-H structure. It has also been reported that the concentration of Si-OH bonds decreases with an increase of the C/S ratio [66, 67]. This shows that an increase in the concentration of Si-OH might be caused by decreasing the C/S of the formed C-S-H. This observation is in good agreement with both the XRD and SEM results, in which the C-DE effect can be explained best by a high rate of silicate polymerization and long silicate chains as a result of decreasing the C/S of the formed C-S-H.

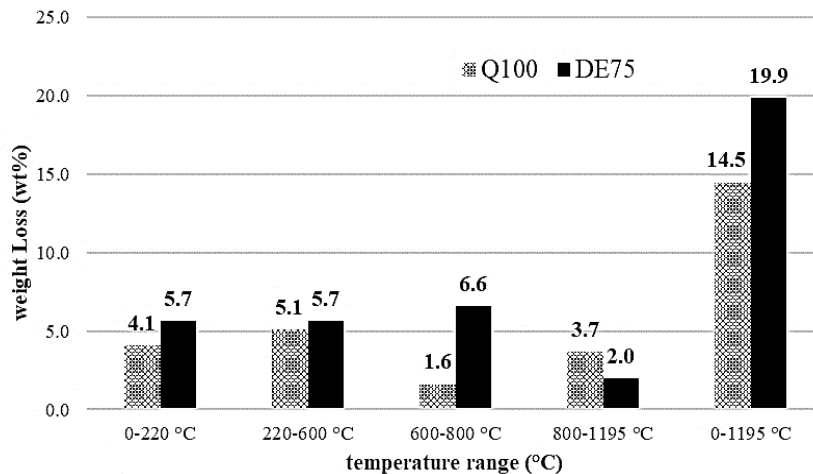


Fig. 9 Weight loss of reference and DE75 samples over the different temperature ranges

3.4 Differential thermal analysis (DTA)

Examples of the endothermic and exothermic reactions observed during the differential thermal analysis of the reference and DE75 samples are shown in Fig. 8. The largest exothermic peak appeared at approximately 840 °C in both groups is related to the formation of wollastonite from C-S-H and tobermorite. This peak was observed at 836 °C and 844 °C for the reference and DE75 samples, respectively. The transformation temperature increased by replacing 75% of quartz with C-DE. This may be explained by the higher stability and a higher degree of polymerization of DE75 compared to the reference sample. In fact, it seems that the formation of wollastonite in the DE75 sample required more structural rearrangement of the silicate anions than in the reference sample. Accordingly, wollastonite formation requires more energy, as manifested by an increase in the formation temperature. Similar interpretations were reported by Stumm et al. [65] and Klimesch et al. [68], who studied the effect of zinc on calcium silicate hydrates and quartz surface areas on the autoclaved cement respectively. They suggested that higher formation temperatures of wollastonite could be due to stacking disorder [68] and the high degree of polymerization [65]. This finding confirms the obtained results from XRD and SEM. Moreover, the DTA curve of the DE75 sample shows a broad endothermic peak at 688 °C, whereas no peak was observed in this area for the reference sample. This broad endothermic peak at 688 °C is related to the decomposition of calcium silicate hydrate bonding which occurs in the range of 600-750 °C. This peak is superimposed with a small endothermic peak located around 750 °C which is attributed to the calcination of calcite [69]. The appearance of the peak at around 688 °C in the DTA curve of DE75 may have resulted from the decomposition of OH bonds in the calcium silicate hydrate since the TGA results suggested an increment in OH bonds in the DE75 sample compared to that of the reference. In Fig. 8, the exothermic peak related to wollastonite became smaller by substituting quartz with C-DE. On the other hand, it was indicated that the increase in exotherm area and/or height can be attributed to the development of increasing quantities of calcium silicate hydrate phases, including 1.1 nm tobermorite [70, 71]. This suggests that there should be a higher amount of tobermorite in the reference sample compared to the DE75 sample, which is in agreement with the XRD and SEM results.

4. Conclusion

The present study has shown that applying a steam curing temperature of 192 °C for 6 hours, which is a typical figure in industrial AAC production, inhibits tobermorite formation in the more soluble silica system while promoting that in the quartz system. This might result from the varying dissolution behavior of silica raw materials. Quartz has relatively low solubility, and the rate of dissolution is also relatively slow. Therefore, the use of quartz as a silica source in AAC requires steam curing at a quite high temperature, i.e., more than 180 °C. However, silica sources with a higher solubility dissolve faster at the same steam curing temperature, thus

preventing tobermorite formation. It seems that, in the case of using more soluble silica than quartz, a lower steam curing temperature might be needed to achieve optimum tobermorite formation. Therefore, the possibility exists that the dissolution of C-DE could be controlled by means of applying a lower steam curing temperature in a way that promotes tobermorite formation. This will be accounted for in a subsequent study. Out of the results of the present study, the following conclusions can be drawn:

- The optimum strength was obtained by a replacement level of 75%, despite having the lowest tobermorite content. This might imply that the pore size, microstructure, i.e., the formed C-S-H conglomerate, and the proportion of different C-S-H would have a positive effect on compressive strength just as significant as the effect of tobermorite alone.
- At a high steam curing temperature with a duration of 6h, a high degree of C-DE substitution by quartz in the AAC mixture promoted the formation of poorly and non-crystalline C-S-H and prevented tobermorite formation, which might be due to inhibiting the crystallization of amorphous C-S-H to tobermorite. This may be caused by the quick dissolution of C-DE at a common autoclaving condition that leads to the formation of polymerized C-S-H with low C/S and a long silicate chain, thus resulting in a more difficult rearrangement to tobermorite.
- A high degree of C-DE substitution in the AAC mixture resulted in the formation of grass-like and amorphous C-S-H with low C/S, an increase in the wollastonite formation temperature, an increase in OH groups in C-S-H structure all of which imply a high rate of polymerization caused by the high rate of Si supply to the matrix at a relatively high steam curing temperature.

Acknowledgments

The authors wish to thank Dr. Volker Thome, Head of mineral materials and building material recycling department at the Fraunhofer Institute for Building Physics, Germany and Dr. Liudvikas Urbonas Head of AG binding agents and additives Laboratory at Centre for Building Materials, Technical University of Munich for their help and useful discussions. Funding: This work was supported by the Fraunhofer Institute for Building Physics IBP; Inorganic Materials and Recycling Department and Iran Ministry of Science.

References

- [1]. Nuneze E, Nunez SA, Fouad FH, "Sustainability in Autoclaved Aerated Concrete (AAC) construction,". 4th International Conference on Autoclaved Aerated Concrete-Innovation and Development, Taylor & Francis Group, London, 8 pp., Kingston University, London. Jan, 2005.
- [2]. Thongtha A, Maneewan S, Punlek C, Ungkoon Y, "Investigation of the compressive strength, time lags and decrement factors of AAC-lightweight concrete containing sugar sediment waste," *Energy and Buildings*, V. 84, pp. 516–525, 2014.
- [3]. Kohler N, "Global Energetic Budget of Aerated Concrete." In Autoclaved Aerated Concrete, Moisture and Properties: Ed. F. H. Wittmann," Elsevier, Amsterdam, 1983.
- [4]. Qu X, Zhao X, "Previous and present investigations on the components, microstructure and main properties of autoclaved aerated concrete – A review," *Construction and Building Materials*, V. 135, pp. 505–516, 2017.
- [5]. Karakurt C, Kurama H, Topçu İB, "Utilization of natural zeolite in aerated concrete production," *Cement and Concrete Composites*, V. 32, No. 1, pp. 1–8, 2010.
- [6]. Aroni S, "On energy conservation characteristics of autoclaved aerated concrete," *Materials and Structures*, V. 23, No. 1, pp. 68–77, 1990.
- [7]. Frey E, Briesemann D, "Neuere Berechnungen zum Primärenergieinhalt von Gasbeton," *Betonwerk+Fertigteil-Technik*, V. 51, No. 7, pp. 468–472, 1985.
- [8]. Lutter J, "New research on the primary energy content of building materials,". 3rd RILEM International Symposium on AAC, Balkema, Zurich, Switzerland. 14-16 October, 1992.
- [9]. Ankele K, Steinfeldt M, "Ökobilanz für typische YTONG-Produktanwendungen," Institut für ökologische Wirtschaftsforschung, Berlin, 1996, ISBN: 3-932092-01-5.
- [10]. Isu N, Ishida H, Mitsuda T, "Influence of quartz particle size on the chemical and mechanical properties of autoclaved aerated concrete (I) tobermorite formation," *Cement and Concrete Research*, V. 25, No. 2, pp. 243–248, 1995.
- [11]. Schober G, "Chemical transformations during the manufacturing of autoclaved aerated concrete (ACC): Cement, lime, gypsum and quartz sand become cellular concrete: Die chemischen Umsetzungen bei der Herstellung von Porenbeton: Aus Zement, Kalk, Gips und Quarzsand wird Porenbeton," *ZKG international*, V. 58, No. 7, pp. 63–70, 2005.
- [12]. Schober G, "The most important aspects of microstructure influencing strength of AAC,". 4th International Conference on Autoclaved Aerated Concrete, Taylor & Francis, 9 pp., Kingston University London. 8 - 9 September, 2005.
- [13]. Stumm A, "Cement and sulphate free autoclaved aerated concrete,". 5th International Conference on Autoclaved Aerated Concrete, Cement Wapno Beton, poland. September 14-17, 2011.
- [14]. Matsui K, Ogawa A, Kikuma J, Tsunashima M, Ishikawa T, Matsuno S, "Influence of addition of Al compound and gypsum on tobermorite formation in autoclaved aerated concrete studied by in situ X-ray diffraction,". 5th International Conference on Autoclaved Aerated Concrete, Cement Wapno Beton, Poland. September 14-17, 2011.
- [15]. Kaminskis R, Barauskas I, "Autoclaved aerated concrete waste as a micro-filler for portland cement," *Romanian Journal of Materials*, V. 49, No. 2, pp. 244–250, 2019.
- [16]. Schober G, "Porenbetonherstellung - Ist-Zustand und mögliche Verbesserungen," *BFT International*, No. 12, pp. 4–11, 2007.
- [17]. Matsui K, Kikuma J, Tsunashima M, Ishikawa T, Matsuno S-y, Ogawa A, Sato M, "In situ time-resolved X-ray diffraction of tobermorite formation in autoclaved aerated concrete: Influence of silica source reactivity and Al addition," *Cement and Concrete Research*, V. 41, No. 5, pp. 510–519, 2011.
- [18]. Narayanan N, Ramamurthy K, "Structure and properties of aerated concrete: a review," *Cem. Concr. Composites*, V. 22, No. 5, pp. 321–329, 2000.
- [19]. Sakiyama M, Mitsuda T, "Hydrothermal reaction between C₂SiH and kaolinite for the formation of tobermorite at 180°C," *Cem. Concr. Res.*, V. 7, No. 6, pp. 681–685, 1977.
- [20]. Mitsuda T, Sasaki K, Ishida H, "Phase evolution during autoclaving process of aerated concrete," *Journal of the American Ceramic Society*, V. 75, No. 7, pp. 1858–1863, 1992.
- [21]. Taylor HFW, "Cement chemistry," Thomas Telford, 1997, ISBN: 0727725920.
- [22]. Hauser A, Eggenberger U, Mumenthaler T, "Fly ash from cellulose industry as secondary raw material in autoclaved aerated concrete," *Cement and Concrete Research*, V. 29, No. 3, pp. 297–302, 1999.
- [23]. Yang J, Shi Y, Yang X, Liang M, Li Y, Li Y, Ye N, "Durability of autoclaved construction materials of sewage sludge–cement–fly ash–furnace slag," *Construction and Building Materials*, V. 48, pp. 398–405, 2013.

- [24]. Kunchariyakun K, Asavapisit S, Sombatsompop K, "Properties of autoclaved aerated concrete incorporating rice husk ash as partial replacement for fine aggregate," *Cement and Concrete Composites*, V. 55, pp. 11–16, 2015.
- [25]. Chen Y, Chang J, Lai Y, Chou M, "A comprehensive study on the production of autoclaved aerated concrete: Effects of silica-lime-cement composition and autoclaving conditions," *Construction and Building Materials*, V. 153, pp. 622–629, 2017.
- [26]. Chan C, Sakiyama M, Mitsuda T, "Kinetics of the CaO.quartz .H2O reaction at 120° to 180°C in suspensions," *Cement and Concrete Research*, V. 8, No. 1, pp. 1–5, 1978.
- [27]. Iler RK, "The Chemistry of Silica: Solubility, Polymerization, Colloid and Surface Properties and Biochemistry of Silica," Wiley, London, 1979, ISBN: 978-0-471-02404-0.
- [28]. Carroll RA, "Hydrothermal performance of pulverised fuel ash and the manufacture of autoclaved aerated concrete," (Doctoral dissertation, © Robert A. Carroll), 1996.
- [29]. Gundlach H, "Dampfgehärtete Baustoffe," Wiesbaden, Berlin, 1973.
- [30]. Stoeber W, "Equilibrium Concepts in Natural Water Systems: Formation of Silicic Acid in Aqueous Suspensions of Different Silica Modifications," *Advances in Chemistry*, 1967, 9780841200685.
- [31]. Mostafa NY, "Influence of air-cooled slag on physicochemical properties of autoclaved aerated concrete," *Cement and Concrete Research*, V. 35, No. 7, pp. 1349–1357, 2005.
- [32]. Černý V, Drochytka R, Šebestová P, "Options for the implementation of new secondary raw materials in autoclaved aerated concrete,". 6th International Conference on Autoclaved Aerated Concrete, ce/papers, University Potsdam. September 4-6, 2018.
- [33]. Wang C, Ni W, Zhang S, Wang S, Gai G, Wang W, "Preparation and properties of autoclaved aerated concrete using coal gangue and iron ore tailings," *Construction and Building Materials*, V. 104, pp. 109–115, 2016.
- [34]. Song Y, Li B, Yang E, Liu Y, Ding T, "Feasibility study on utilization of municipal solid waste incineration bottom ash as aerating agent for the production of autoclaved aerated concrete," *Cement and Concrete Composites*, V. 56, pp. 51–58, 2015.
- [35]. Isu N, Teramura S, Ishida H, Mitsuda T, "Influence of quartz particle size on the chemical and mechanical properties of autoclaved aerated concrete (II) fracture toughness, strength and micropore," *Cement and Concrete Research*, V. 25, No. 2, pp. 249–254, 1995.
- [36]. Kunchariyakun K, Asavapisit S, Sinyoung S, "Influence of partial sand replacement by black rice husk ash and bagasse ash on properties of autoclaved aerated concrete under different temperatures and times," *Construction and Building Materials*, V. 173, pp. 220–227, 2018.
- [37]. Reka AA, Pavlovski B, Makreski P, "New optimized method for low-temperature hydrothermal production of porous ceramics using diatomaceous earth," *Ceramics International*, V. 43, No. 15, pp. 12572–12578, 2017.
- [38]. Gock E, Vogt V, Leußner T, Hoops G, Knauf H, "Mineralische Nebenprodukte und Abfälle: Einführung des Recyclings von Kieselgur in die Praxis der Bierherstellung," Thomé-Kozmiensky Verlag GmbH, Neuruppin, Germany, 2014, 978-3944310114.
- [39]. DIN 66137-2, *Determination of solid state density - Part 2: Gaspycnometry: Bestimmung der Dichte fester Stoffe - Teil 2: Gaspyknometrie*, 2004.
- [40]. Bruker AXS GmbH, "DIFFRAC.EVA Tutorial,".
- [41]. Bruker AXS GmbH, "TOPAS Tutorial," 2016.
- [42]. DIN EN 772-1, *Prüfverfahren für Mauersteine – Teil 1: Bestimmung der Druckfestigkeit*, 2016.
- [43]. DIN EN 772-13, *Prüfverfahren für Mauersteine Teil 13: Bestimmung der Netto- und Brutto-Trockenrohichte von Mauersteinen (außer Natursteinen)*, 2000.
- [44]. Sato H and Grutzeck M, "Effect of Starting Materials on the Synthesis of Tobermorite | MRS Online Proceedings Library (OPL) | Cambridge Core," *Material research society*, V. 245, pp. 235–240, 1992.
- [45]. Garbev K, "Struktur, Eigenschaften und quantitative Rietveldanalyse von hydrothermal kristallisierten Calciumsilikathydraten (C-S-H-Phasen)," Dissertation, Universität Heidelberg, Heidelberg, Germany, 2003.
- [46]. Okada Y, Ishida E. H., Mitsuda T, "²⁹Si NMR spectroscopy of silicate anions in hydrothermally formed CSH," *Journal of the American Ceramic Society*, V. 77, No. 3, pp. 765–768, 1994.
- [47]. Chen J, Thomas J, Taylor HWF, Jennings H, "Solubility and structure of calcium silicate hydrate," *Cement and Concrete Research*, V. 34, No. 9, pp. 1499–1519, 2004.
- [48]. Richardson I, "Tobermorite/jennite- and tobermorite/calcium hydroxide-based models for the structure of C-S-H: applicability to hardened pastes of tricalcium silicate, β-dicalcium silicate, Portland cement, and blends of Portland cement with blast-furnace slag, metakaolin, or silica fume," *Cement and Concrete Research*, V. 34, pp. 1733–1777, 2004.

- [49]. Nonat A, "The structure and stoichiometry of C-S-H," *Cement and Concrete Research*, V. 34, No. 9, pp. 1521–1528, 2004.
- [50]. Grutzeck M, Benesi A, Fanning B, "Silicon-29 Magic Angle Spinning Nuclear Magnetic Resonance Study of Calcium Silicate Hydrates," *Journal of the American Ceramic Society*, V. 72, No. 4, pp. 665–668, 1989.
- [51]. El-Hemaly SAS, Mitsuda T, Taylor HFW, "Synthesis of normal and anomalous tobermorites," *Cement and Concrete Research*, V. 7, No. 4, pp. 429–438, 1977.
- [52]. Gabrovsek R, Kurbus B, Lengar Z, "Comparison of unsubstituted and aluminum containing synthetic tobermorite characterized by different methods," *Cement and Concrete Research*, V. 16, No. 3, pp. 325–332, 1986.
- [53]. Barnes MW SBE, "The chemistry of Al-tobermorite and its coexisting phases at 175 C, ". Special Cements with Advanced Properties, Material Research Society Symposium Proceedings, Boston, 1989.
- [54]. Isu N, Sasaki K, Ishida H, Mitsuda T, "Mechanical Property Evolution during Autoclaving Process of Aerated Concrete Using Slag: I, Tobermorite Formation and Reaction Behavior of Slag," *Journal of the American Ceramic Society*, V. 77, No. 8, pp. 2088–2092, 1994.
- [55]. Mitsuda T TH, "Influence of aluminium on the conversion of calcium silicate hydrate gels into 11 Å tobermorite at 90°C and 120°C," *Cement and Concrete Research*, V. 5, pp. 203–210, 1975.
- [56]. Sakiyama M, Maeshima T, Mitsuda T, "Synthesis and crystal chemistry of Al-substituted 11 Å tobermorite," *Journal of the Society of Inorganic Materials*, V. 7, pp. 413–419, 2000.
- [57]. Youssef H, Ibrahim D, Komarneni S, Mackenzie KJD, "Synthesis of 11 Å Al-substituted tobermorite from trachyte rock by hydrothermal treatment," *Ceramics International*, V. 36, pp. 203–209, 2010.
- [58]. Kadashevich I, Schneider HJ, Stoyan D, "Statistical modeling of the geometrical structure of the system of artificial air pores in autoclaved aerated concrete," *Cement and Concrete Research*, V. 35, No. 8, pp. 1495–1502, 2005.
- [59]. Petrov I, Schlegel E, "Application of automatic image analysis for the investigation of autoclaved aerated concrete structure," *Cement and Concrete Research*, V. 24, No. 5, pp. 830–840, 1994.
- [60]. Jerman M, Keppert M, Výborný J, Černý R, "Hygic, thermal and durability properties of autoclaved aerated concrete," *Construction and Building Materials*, V. 41, pp. 352–359, 2013.
- [61]. Cabrillac R, Fiorio B, Beaucour A, Dumontet H, Ortola S, "Experimental study of the mechanical anisotropy of aerated concretes and of the adjustment parameters of the introduced porosity," *Construction and Building Materials*, V. 20, No. 5, pp. 286–295, 2006.
- [62]. H. Weber HH, "Porenbeton Handbuch," Aufl. Bauverlag, 2002.
- [63]. Tada S, "Material design of aerated concrete-An optimum performance design," *Materials and Structures*, V. 19, No. 1, pp. 21–26, 1986.
- [64]. Schober G, "Porosity in autoclaved aerated concrete (AAC): A review on pore structure, types of porosity, measurement methods and effects of porosity on properties," . 5th International Conference on Autoclaved, Cement Wapno Beton, 10 pp., Poland. September 14-17, 2011.
- [65]. Stumm A, Garbev K, Beuchle G, Black L, Stemmermann P, Nüesch R, "Incorporation of zinc into calcium silicate hydrates, Part I: formation of C-S-H(I) with C/S=2/3 and its isochemical counterpart gyrolite," *Cement and Concrete Research*, V. 35, No. 9, pp. 1665–1675, 2005.
- [66]. Yu P, Kirkpatrick RJ, Poe B, McMillan PF, Cong X, "Structure of Calcium Silicate Hydrate (C-S-H): Near-, Mid-, and Far-Infrared Spectroscopy," *J. Am. Ceram. Soc.*, V. 82, No. 3, pp. 742–748, 1999.
- [67]. Dolado JS, Griebel M, Hamaekers J, "A Molecular Dynamic Study of Cementitious Calcium Silicate Hydrate (C-S-H) Gels," *J Am Ceram Soc*, V. 90, No. 12, 3938-3942, 2007.
- [68]. Klimesch DS, Ray A, "DTA-TGA evaluations of the CaO–Al₂O₃–SiO₂–H₂O system treated hydrothermally," *Thermochimica Acta*, V. 334, pp. 115–122, 1999.
- [69]. Niedersen K, Malorny W, "Thermally induced changes in microstructure and their effects on the mechanical parameters of AAC," *Zement Kalk Gips international*, V. 64, No. 4, pp. 62–72, 2011.
- [70]. Alexanderson J, "Relations between structure and mechanical properties of autoclaved aerated concrete," *Cement and Concrete Research*, V. 9, No. 4, pp. 507–514, 1979.
- [71]. Connan H, Klimesch D, Ray A, Thomas P, "Thermal characterisation of autoclaved cement made with alumina-silica rich industrialwaste," *Journal of Thermal Analysis and Calorimetry*, V. 84, No. 2, pp. 521–525, 2006.

A.2 Publication 2

Construction and Building Materials, V. 287, No. 123072, June 2021.
<https://doi.org/10.1016/j.conbuildmat.2021.123072>

Reprinted (adapted) with permission from Elsevier
(<https://www.elsevier.com/about/policies/copyright/permissions>).

Summary

In this paper, the performances of the quartz-based AAC and C-DE-based AAC under different autoclaving conditions were introduced. The autoclaving process was conducted using an autoclave at various temperatures of $T = 134\text{-}192\text{ }^{\circ}\text{C}$ and a corresponding steam pressure of $P = 2\text{-}12\text{ bar}$ for 6 hours. This paper demonstrated that the C-DE-based exhibited different behaviors from that of the quartz-based AAC at different autoclaving temperatures. In contrast to the quartz-based AAC, autoclaving the C-DE-based AAC at lower temperatures than the typical temperature used for industrial production of AAC, i.e. $192\text{ }^{\circ}\text{C}$, improved their performances characterized by the compressive strength and shrinkage behaviors.

Production of autoclaved aerated concrete with silica raw materials of a higher solubility than quartz Part II: Influence of autoclaving temperature

Taban Shams ^{a, b, 2}, Georg Schober ^c, Detlef Heinz ^b, Severin Seifert ^a

^aFraunhofer Institute for Building Physics IBP, Inorganic Materials and Recycling Department, Building Materials Technology Group, Fraunhoferstr. 10, 83626, Valley, Germany

^bTechnical University of Munich, Department of Civil, Geo and Environmental Engineering, Centre for Building Materials cbm, Franz-Langinger-Str. 7, 81245, Munich, Germany

^cEngineering office for materials development and process technology, Marbstraße 6, 94405 Landau a.d. Isar, Germany

Abstract

This study examines the effects of autoclaving temperature on the mechanical and microstructural properties of autoclaved aerated concrete (AAC) containing calcined diatomaceous earth (C-DE) as the main silica source. The autoclaving process was conducted using an autoclave at various temperatures of $T = 134\text{-}192\text{ }^{\circ}\text{C}$ and a corresponding steam pressure of $P = 2\text{-}12\text{ bar}$ for 6 hours. The resultant phases were characterized using quantitative and qualitative X-ray diffraction (XRD), differential thermal analysis (DTA) and thermogravimetric analysis (TGA). The compressive strength of samples containing C-DE as the main silica source increased by 30% when the autoclaving temperature decreased by around $60\text{ }^{\circ}\text{C}$. This is in complete opposition to samples containing quartz as the only SiO_2 source. The compressive strength of the latter decreased by 85% when the autoclaving temperature decreased by approximately $60\text{ }^{\circ}\text{C}$. For all samples, changes in compressive strength corresponded with changes in tobermorite formation.

Keywords: autoclaved aerated concrete, calcined diatomaceous earth, autoclaving temperature, tobermorite

² Corresponding author. Tel.: +49 8024 643-637.

E-mail address: taban.shamshafshejani@tum.de

1. Introduction

Currently, one major issue in the development of autoclaved aerated concrete (AAC) production is energy consumption along with the carbon dioxide emission related thereto. Energy consumption during the manufacturing of AAC is strongly determined by the autoclaving process [1–5]. A reduction in autoclaving temperature and/or time would provide relevant economic advantages. Part I [6] of this study discussed the influence of calcined diatomaceous earth (C-DE) as a silica raw material of a higher solubility than quartz, on the mechanical and microstructural properties of AAC produced at the autoclaving temperature of 192 °C for 6 hours. The results showed that silica raw materials of a higher solubility need an appropriate adjustment of autoclaving temperature to attain optimum tobermorite formation. The purpose of this study is to develop properties of C-DE-substituted AAC by adjusting the autoclaving temperature.

The compressive strength of AAC depends on the pore structure and the maturity of the binder, which is expressed by the quantities of hydrothermal products [7]. The mechanical properties of AAC are affected during the autoclaving process such that the compressive strength increases with an increase in the quantity of tobermorite formation [8, 9]. The autoclaving process is necessary for establishing the conditions under which C-S-H including tobermorite formation can take place [10, 11]. This implies that a general way to optimize the autoclaving process could be to optimize the formation of tobermorite with respect to the reaction temperature. The formation of tobermorite is controlled by the dissolution of silica, as long as sufficient calcium is available. Thus, if silica dissolution occurs at a lower temperature, it is more likely to decrease the required autoclaving temperature, resulting in a reduction in the energy demand of the curing process.

Currently, the use of quartz as a SiO₂ source for AAC production is well-established, but quartz has relatively a low solubility in water, and the rate of dissolution is also relatively slow. Therefore, when quartz is the main silica source in the AAC mixture, saturated steam curing at a quite high temperature, i.e., greater than $T > 180$ °C is required [12]. Compared to quartz, some other types of silica, such as amorphous silica and cristobalite exhibit a higher dissolution rate and require less energy to be dissolved [13–16]. For instance, quartz has a solubility of 2.8 ppm in water with a pH of 8.5 at 25°C. While cristobalite has a solubility of 6 ppm under the same condition [13]. Therefore, the replacement of quartz with silica materials of a higher solubility might have the advantage of reducing the autoclaving temperature.

However, the results of Part I of this study [6] as well as several other studies have shown that replacing quartz with silica materials of a higher solubility hinders the final rearrangement of C-S-H to tobermorite [17–19]. This is likely because the same high autoclaving temperature with a typical duration as that of quartz was used in all of those studies. Therefore, silica materials of a higher solubility (more soluble silica) dissolve more quickly than quartz, so at the same autoclaving temperature, the CaO/SiO₂ (C/S) of initially formed C-S-H in a more soluble silica system is lower (has a higher Si content) than that of a quartz system [17, 20]. Moreover, it has been reported that a C-S-H with a low C/S tends to have long chains of tetrahedra [19, 21–25]. It would therefore be difficult to be transformed into tobermorite [17, 19, 26]. This could be the reason why a high autoclaving temperature with a regular duration, inhibits tobermorite formation in a more soluble system while promoting it in a quartz system.

Therefore, with regard to silica materials known to have a higher solubility than quartz, the expected advantages for AAC production, e.g., shorter autoclaving times or temperatures, higher strength values, or a lower binder content in recipes, have not been achieved to a sufficient extent so far.

The challenge is therefore to ascertain whether it is possible to control the dissolution of silica material of a higher solubility in a way that leads to an optimum silica dissolution rate for tobermorite formation. Since the dissolution of silica materials is strongly dependent on temperature, the dissolution of more soluble silica might be controlled by using a lower autoclaving temperature compared to that used to decompose quartz. In fact, by decreasing the autoclaving temperature, silica with a higher solubility might dissolve more slowly at a lower dissolution rate [13, 14, 27] which leads to a reduction in the Si supply and causes an increase in the C/S of initially formed C-S-H phases. Thus, the rearrangement of C-S-H to tobermorite can occur more easily [17, 22–25].

As stated above, a C-S-H with a low C/S can hardly be transformed to tobermorite, while a C-S-H with a high C/S crystallizes readily to tobermorite. This means that tobermorite formation depends on the C/S of the C-S-H. The C/S of the C-S-H depends on two factors. The first is the autoclaving temperature i.e. a lower autoclaving temperature leads to a higher C/S of the C-S-H. The second is the C/S of the starting materials i.e. a higher C/S of starting material causes a higher C/S of the C-S-H. This implies that if a high C/S of starting material and a low autoclaving temperature would be used at the same time, then the C/S of the C-S-H could reach a too high value, which would not be conducive to tobermorite formation. In other words, for a lower autoclaving temperature, the C/S of starting material could be adjusted to a lower value. Based on the literature [28, 29], starting mixtures with a C/S of < 0.67 lead to a C-S-H with a low C/S, and those with $C/S > 0.67$ lead

to a C-S-H with a high C/S. Thus, to avoid the formation of a C-S-H with an excessively high C/S during autoclaving at low temperature, a starting material with a C/S of < 0.67 could be used. Therefore, in more soluble silica systems, not only the autoclaving temperature but also the C/S of the starting material has a determining effect that should be taken into consideration.

It thus seems that using silica materials of a higher solubility as the main silica source in AAC while the autoclaving temperature and the C/S of the starting material are low enough might present an opportunity to produce a high quality AAC product that requires less curing energy and less binder. The results of Part I [6] of this study showed that when more soluble silica than quartz is used, a lower autoclaving temperature might be needed to attain optimum tobermorite formation. Accordingly, Part II of the study, which is the object of the present paper, deals with improving tobermorite formation in the AAC containing C-DE as the main silica source by applying a low autoclaving temperature while the C/S of the starting material is adjusted to low values. The AAC samples were produced the same way as in part I. The purpose of this study is to improve the properties of C-DE-substituted AAC by adjusting the autoclaving temperature. Accordingly, the influence of autoclaving temperature on the mechanical and microstructural properties of C-DE-substituted AAC autoclaved at various temperatures of $T = 134\text{-}192\text{ }^{\circ}\text{C}$ for a duration of 6 hours was investigated.

2. Materials and methods

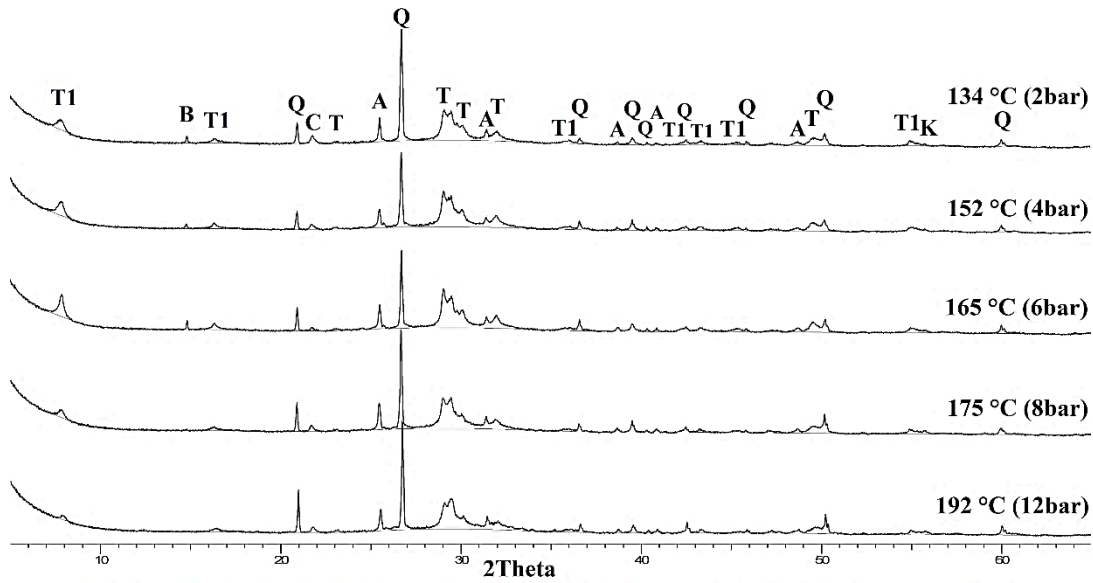
Material characterizations, mix proportions, preparations, all measurements (including XRD, DTA, TGA analyses, compressive strength and bulk density measurements), and other details were described in Part I of this study [6]. Part I of this study investigated two types of silica source: Dorsilit as a form of quartz and calcined diatomaceous earth (C-DE) as a form of silica of a higher solubility than quartz. The quartz in the reference mix was replaced with C-DE for 25 wt%, 50 wt%, and 75 wt% to produce DE25, DE50, and DE75, respectively. The molar C/S of starting material for all mixes was adjusted at 0.63-0.64 and a low-lime mixture was used. The optimum compressive strength was obtained by a C-DE substitution ratio of 75%, based on the result of Part I of this study [6]. From the DE-substituted AAC produced in Part I, the DE75 mix was selected as the AAC which contained C-DE as the main silica source to investigate the influence of the autoclaving temperature. The DE75 and reference (Q100) samples were made based on the method described in the previous paper [6]. The autoclaving process was conducted using an autoclave at various temperatures of $T = 134\text{-}192\text{ }^{\circ}\text{C}$ and corresponding steam pressures of $P = 2\text{-}12$ bar for a duration of 6 hours. The duration of the autoclaving process was constant for all samples.

3. Results and Discussion

3.1 X-ray diffraction analysis (XRD)

The hydration products were examined at different autoclaving temperatures using XRD. Figs. 1 and 2 show the effect of the autoclaving temperature on the diffraction pattern and phase formation of the DE75 sample, respectively. The diffraction patterns of the DE75 sample show the formation of poorly crystalline tobermorite at the typical autoclaving temperature of $192\text{ }^{\circ}\text{C}$. By decreasing the autoclaving temperature, the intensity of the tobermorite peaks increased and became sharper.

The results of phase contents obtained by the Rietveld method (Fig. 2) show that the tobermorite content increased from 6.3% to 14% when the autoclaving temperature decreased from $192\text{ }^{\circ}\text{C}$ to $165\text{ }^{\circ}\text{C}$. With a further reduction from $165\text{ }^{\circ}\text{C}$ to $134\text{ }^{\circ}\text{C}$, tobermorite content decreased with a lower slope from 14% to 10.3%. However, the quantity of tobermorite formed at $134\text{ }^{\circ}\text{C}$ was still higher than at $192\text{ }^{\circ}\text{C}$. This implies that a reduction in the autoclaving temperature led to an increase in tobermorite formation in the AAC containing C-DE as the main silica source. Amorphous content showed the opposite trend to tobermorite i.e. a decrease in amorphous content was accompanied by an increase in tobermorite content. The increase in tobermorite and decrease in amorphous content might therefore be due to the crystallization of amorphous C-S-H to tobermorite. The reason for this might be that by decreasing the autoclaving temperature, the C-DE, which is partly amorphous and contains cristobalite, might dissolve more slowly at a lower dissolution rate [13, 16, 27], which causes a reduction in the Si supply and increases the C/S of the initially formed C-S-H phases. A higher C/S implies a higher residual negative charge on the silicate tetrahedra. This results in increasing screening and relaxation of the silicon atoms, inducing lower binding energies [30–32].



Q: quartz, A: anhydrite, T1: tobermorite-11A, T: tobermorite-11A and tobermorite-9A, C: cristobalite, B: bassanite, K: katoite

Fig. 1 Diffraction patterns of the DE75 samples cured at different autoclaving temperatures

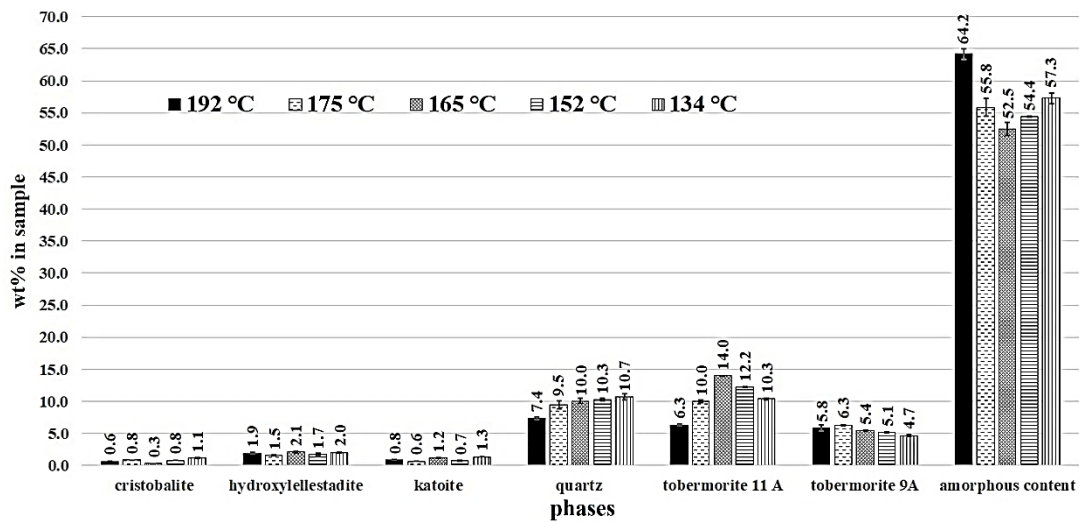


Fig. 2 Rietveld quantitative analysis results of the DE75 mix cured at different autoclaving temperatures

Rupturing of the tetrahedral chains can therefore occur between bridging and non-bridging silicon atoms [33], which generates a lower rate of polymerization and a short silicate chain [31]. Thus, it would be more likely to rearrange to tobermorite [17, 22–25]. This shows that C-DE dissolution might be controlled by using a lower autoclaving temperature, which results in an optimum silica dissolution rate for tobermorite formation. The above results also suggest that when C-DE is the main SiO₂ source in the AAC mixture, optimum tobermorite formation can occur when the autoclaving temperature and C/S of the starting materials are low enough. This finding is also supported by the results of Part I [6], in which applying high autoclaving temperature influenced tobermorite formation negatively in the C-DE system.

A reduction in the autoclaving temperature from 165 to 134 °C resulted in a decrease in tobermorite content and an increase in amorphous content of the DE75 sample. This may be because at temperatures T < 165 °C, the quartz did not dissolve and remained unreacted and/or the dissolution of C-DE might have become too slow. This would cause the formation of an initial C-S-H with a too high C/S, which does not promote rearrangement to tobermorite. However, the decreasing of the autoclaving temperature did not lead to any significant decrease in the cristobalite content, and there was no sign of portlandite in the XRD pattern of the DE75 sample, even at 134 °C. This might indicate that the C-DE dissolved and was consumed at all temperatures, even at T < 140 °C, and that the hydration reactions were promoted between various components to form C-S-H.

Figs. 3 and 4 show the effect of autoclaving temperature on the diffraction pattern and phase formation of the reference sample, respectively. In the reference sample, at a typical autoclaving temperature of 192 °C, the formed tobermorite had a high crystallinity. By decreasing autoclaving temperature the tobermorite diffraction peaks became smaller and wider until they eventually almost disappeared. The result of the Rietveld method shows a significant reduction in tobermorite content as a result of lowering the autoclaving temperature. This indicates that a reduction in the autoclaving temperature led to a decrease in tobermorite formation of the AAC containing quartz as the main silica source.

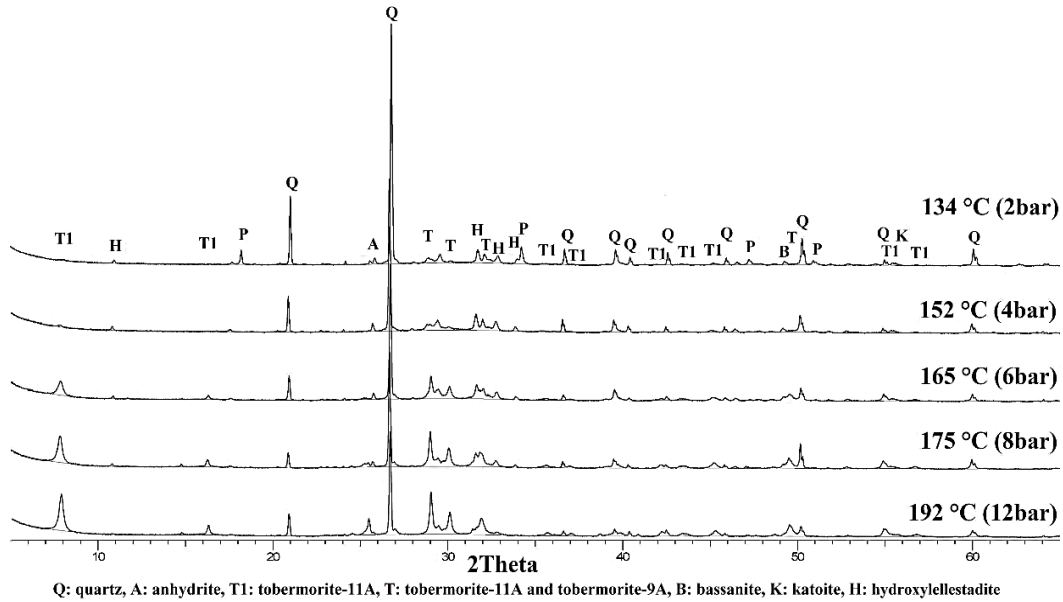


Fig. 3 Diffraction patterns of the reference samples (Q100) cured at different autoclaving temperatures

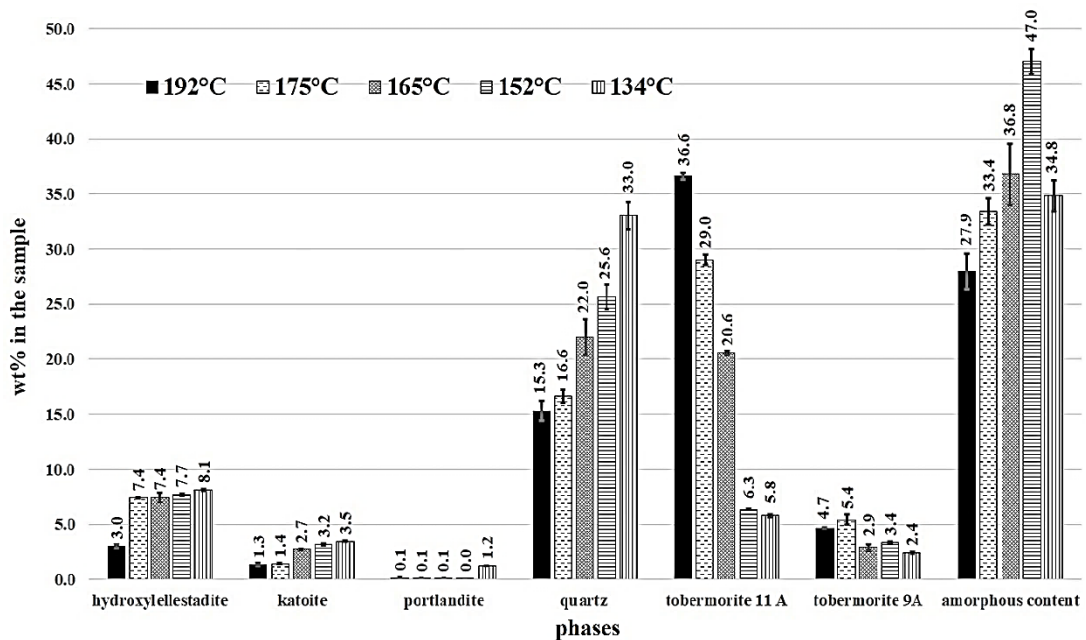


Fig. 4 Rietveld quantitative analysis results of the Q100 mix cured at different autoclaving temperatures

Additionally, by decreasing the autoclaving temperature from 192 °C to 152 °C, the amorphous content increased and then decreased when the temperature was further reduced to 134 °C (Fig. 4). The reason for this is probably that when the autoclaving temperature was lowered from 192 °C to 152 °C, the quartz dissolved too slowly, leading to the formation of C-S-H with a C/S beyond those suitable for tobermorite formation. Thus, the tobermorite decreased and the amorphous content increased. However, at temperatures below 152 °C decomposition of quartz did not occur. The quartz and lime therefore remained unreacted in the sample,

resulting in a lower amorphous content due to the reduction in C-S-H formation. The presence of portlandite and a high quantity of residual quartz in the reference sample cured at 134 °C confirms the above explanation. Moreover, by decreasing the autoclaving temperature amount of quartz, hydroxyllestadite, and katoite, increased significantly and characteristic peaks associated with portlandite appeared in the XRD pattern of the reference sample. This might show that when quartz is the main silica source in the AAC mixture, decreasing the autoclaving temperature results in increased unreacted quartz and restricted hydration reactions, causing a reduction in tobermorite formation.

In general, for an AAC containing C-DE as the main silica source, optimum tobermorite formation occurs at autoclaving temperatures of $T = 165\text{-}135$ °C for a duration of 6h, while in the case of quartz, it occurs at an autoclaving temperature of 192 °C for the same duration of 6h which is a typical figure in industrial AAC production.

3.2 Mechanical properties

The compressive strength and bulk density of all the samples at various autoclaving temperatures are given in Figs. 5 and 6, respectively. By decreasing the autoclaving temperature than the one typically used in industry (192 °C), the compressive strength of the DE75 sample increased, while that of the reference sample decreased. The compressive strength of the DE75 sample increased by 30% when the autoclaving temperature decreased by 58 °C. Moreover, a reduction of 27 °C in the autoclaving temperature resulted in an optimum compressive strength of 6.6 MPa, which is equivalent to a 50% increase. This is in complete opposition to what occurred with AAC that contained only quartz as the SiO₂ source. Here, the compressive strength decreased drastically by 85% when the autoclaving temperature decreased by 58 °C.

The optimum compressive strength of the DE75 sample occurred at an autoclaving temperature of 165-152 °C. However, the compressive strength of the DE75 sample at 134 °C was still higher than that at 192 °C. This indicates that the energy consumed in the production of AAC could be decreased, which makes AAC a more sustainable and cost-effective product.

Moreover, as stated above, C-DE will have the advantage of reducing the autoclaving temperature only when the C/S of the starting material is sufficiently low. Accordingly, in this study, the C/S of the starting material was adjusted to low values and a low-lime mixture was used. On the other hand, when the autoclaving temperature decreased by 30-60 °C, samples containing C-DE gained a high compressive strength, in excess of the technical requirements. This implies that the total amount of binder can be even more reduced.

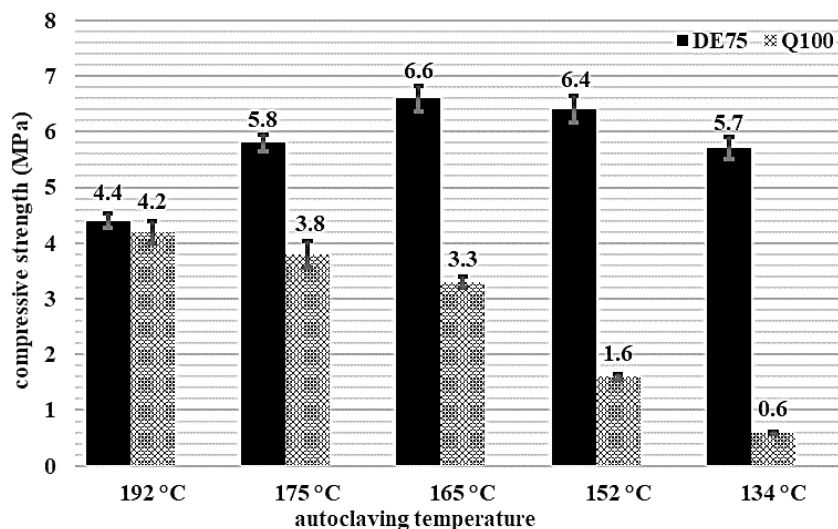


Fig. 5 Compressive strength of the samples cured at various autoclaving temperatures

Moreover, as stated above, C-DE will have the advantage of reducing the autoclaving temperature only when the C/S of the starting material is sufficiently low. Accordingly, in this study, the C/S of the starting material was adjusted to low values and a low-lime mixture was used. On the other hand, when the autoclaving temperature decreased by 30-60 °C, samples containing C-DE gained a high compressive strength, in excess of the technical requirements. This implies that the total amount of binder can be even more reduced.

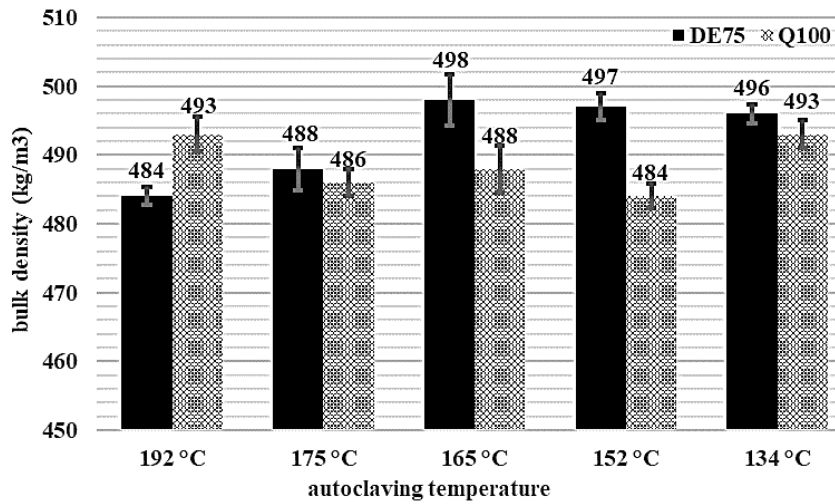


Fig. 6 Bulk density of the samples cured at various autoclaving temperatures

The results of XRD analyses, both quantitative and qualitative, confirmed the above results. For all samples, changes in compressive strength resembled changes in tobermorite formation i.e. an increase in compressive strength was accompanied by the increase in tobermorite formation. Thus, it is more likely that a change in compressive strength, whether a decrease or an increase, can be explained by a change in tobermorite formation.

Changing the autoclaving temperature did not significantly influence the bulk density, which remained in the range of 484-500 kg/m³ for all samples.

3.3 Thermogravimetric analysis (TGA)

The results of the thermogravimetric analysis which shows weight loss over the various temperature ranges are given in Figs. 7 and 8.

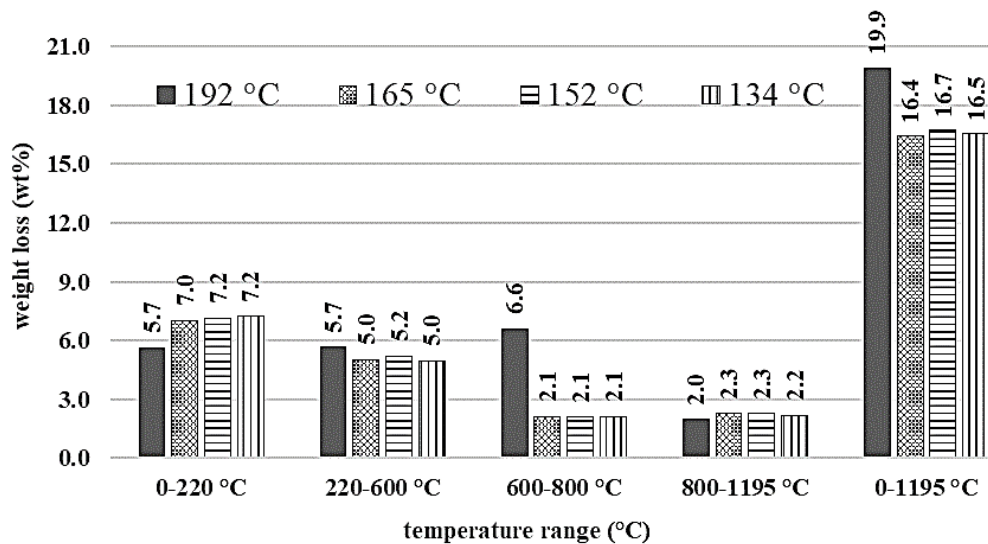


Fig. 7 Weight loss of the DE75 samples cured at different autoclaving temperatures

According to Figs. 7 and 8, the total weight loss decreased from 19.9% to 16.5% and from 14.5% to 10.2% for the DE75 and the reference samples, respectively, when the autoclaving temperature decreased from 192 °C to 165 °C. Therefore, the total weight loss decreased by decreasing the autoclaving temperature for both reference and DE75 samples. However, the reduction in total weight loss occurred at different temperature ranges. For the DE75 sample (Fig. 7), the variation in total weight loss is mainly ascribed to a variation in temperature between 600 °C and 800 °C. In fact, it is the weight loss between 600 °C and 800 °C that decreased by decreasing the autoclaving temperature.

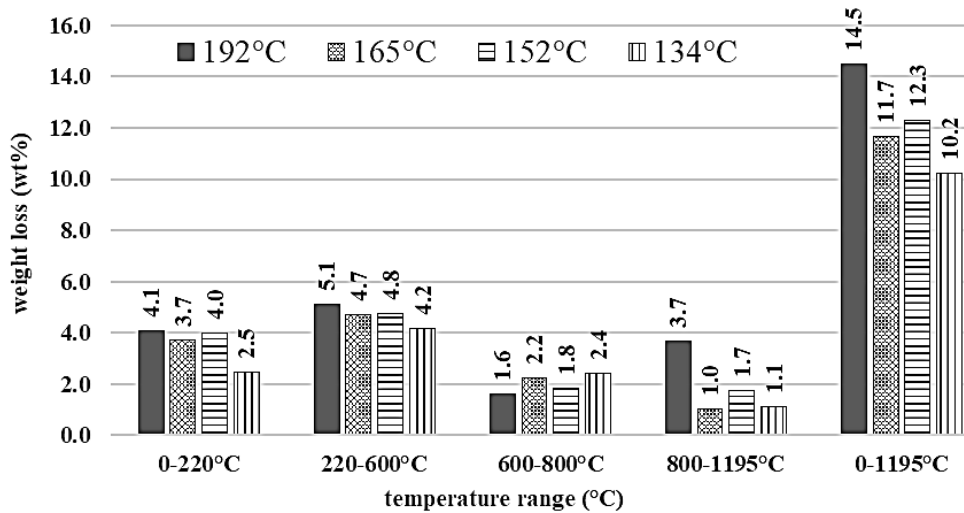


Fig. 8 Weight loss of the Q100 samples cured at different autoclaving temperatures

It has been reported that molecular water is lost up to 600 °C and all weight losses above 600 °C may be ascribed to the OH groups [34]. Therefore, any reduction in weight loss between 600 °C and 800 °C is probably due to a decrease in the OH groups. On the other hand, it is a basic property of the C-S-H structures that bridging tetrahedrons bear OH groups, which form a Si-OH linkage [17, 35]. Thus, a decrease in total weight loss might be due to decreasing the Si-OH bonds in the C-S-H structure. The concentration of the Si-OH decreases with an increase of the C/S in the formed C-S-H [35, 36]. Therefore, a decrease in the autoclaving temperature might lead to a reduction of the Si-OH bonds in the C-S-H structure as a result of increasing the C/S of the formed C-S-H in the DE75 sample. This result is in agreement with the XRD results of the DE75 sample, where the effect of decreasing autoclaving temperature can be best explained by a lower rate of polymerization and short silicate chain resulting from an increase in the C/S of the formed C-S-H.

In the reference sample (Fig. 8), the variation in total weight loss is mainly ascribed to a variation in the range of 800-1195 °C, which corresponds to the wollastonite formation [37, 38]. Therefore, decreasing the autoclaving temperature might induce a reduction in the wollastonite formation, which is probably caused by the decrease in tobermorite formation in the reference sample.

3.4 Differential thermal analysis (DTA)

The DTA curves of the DE75 and reference samples are shown in Figs. 9 and 10, respectively. According to Fig. 9, the DTA curves of the DE75 sample show that the decreasing of the autoclaving temperature from 192 °C to 152 °C led to a decrease in the wollastonite formation temperature from 844 °C to 834 °C. A further reduction in the autoclaving temperature from 152 °C to 134 °C led to an increase in the wollastonite formation temperature from 834 °C to 839 °C. However, the wollastonite formation temperature at 134 °C was still lower than that at 192 °C.

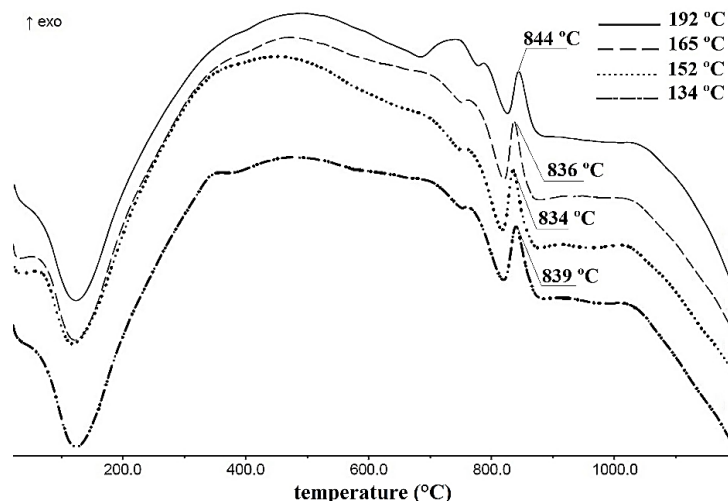


Fig. 9 DTA curves of the DE75 samples cured at different autoclaving temperatures

It was reported that higher wollastonite formation temperatures could be due to a stacking disorder [39] and a high degree of polymerization [34]. Therefore, it seems that DE75 samples cured at a low autoclaving temperature, such as 165-134 °C, are more likely to display a lower degree of polymerization compared to those cured at a high autoclaving temperature, such as 192 °C. This might imply an increase in the C/S of initially formed C-S-H for DE75 samples, due to a decrease in autoclaving temperature. This finding is similar to the XRD and compressive strength results, where a reduction in autoclaving temperature caused an increase in tobermorite and compressive strength, which can be best explained by the increase in the C/S of initially formed C-S-H.

DTA curves of the reference sample (Fig. 10) show that the exothermic peak related to wollastonite formation became smaller when the autoclaving temperature was reduced from 192 to 152 °C. With a further reduction in the autoclaving temperature, i.e. at temperatures below 152 °C, the wollastonite characteristic peak disappeared. Connan et al. [37] indicated that an exothermic reaction occurring at about 800–900 °C was related to the crystallization of beta wollastonite (β -CaSiO₃) from C-S-H and tobermorite. Therefore, the above results suggest that in the reference sample, tobermorite and/or C-S-H formation was inhibited when the autoclaving temperature was reduced. Moreover, at an autoclaving temperature below 152 °C, the endothermic peak at 400-500 °C associated with portlandite (Ca(OH)₂) occurred, which means hydration reactions were restricted. These findings are in accordance with the observation in the XRD analysis.

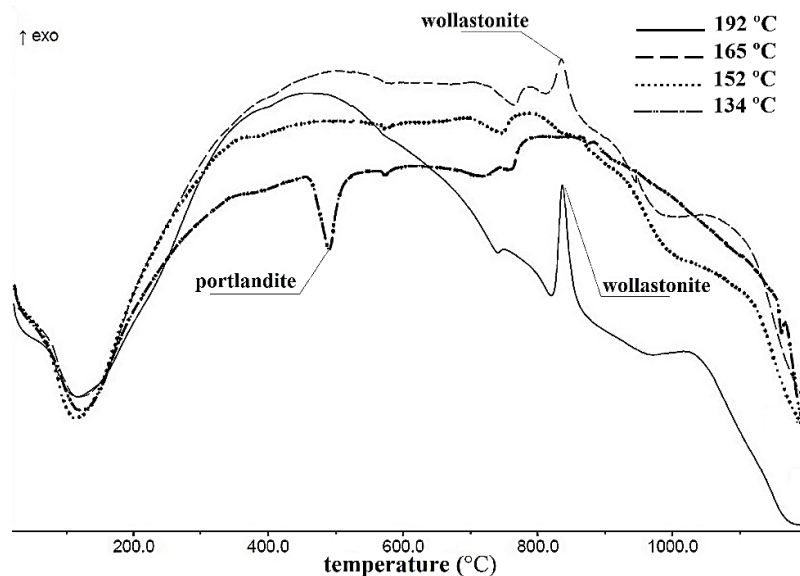


Fig. 10 DTA curves of the reference samples cured at different autoclaving temperatures

4. Conclusion

The present study shows that using C-DE, which has a higher solubility than quartz, as the main silica source in AAC while the autoclaving temperature and the C/S of the starting material are sufficiently low has a high potential to lead to a high-quality AAC product which requires less energy for curing and less binder. This has the advantage of reducing energy consumption, CO₂ emissions, and the cost of producing AAC, and enabling the use of a wider range of raw materials. In this study, the autoclaving temperature was reduced by up to around 60 °C, not only without a reduction in compressive strength but even with an increase of up to 50%, which exceeds technical requirements. This suggests that the total amount of binder could be reduced even further for existing standard AAC products on the market. This will be associated with the following benefits:

- AAC products of a lower density, with improved thermal insulation properties
- AAC products of a higher compressive strength in each of the density grades for masonry and panels
- AAC products with less binder (cement and lime) in the recipes
- Energy consumption during the autoclaving process would be reduced
- CO₂ emissions would be reduced due to the lower energy consumption in the autoclaving process and less binder
- A wider range of silica materials could be used, and in particular, industrial wastes containing silica of high solubility could be reused

- Resources of quartz sand would be saved

The following conclusions can be drawn from the findings of the present study:

- The compressive strength of samples containing C-DE as the main silica source increased by 30% when the autoclaving temperature was decreased by around 60 °C. This is in total opposition to what occurred with samples containing quartz as the only SiO₂ source. Their compressive strength decreased by 85% when the autoclaving temperature decreased by around 60 °C.
- A reduction in the autoclaving temperature promoted tobermorite formation in the C-DE system, while hindering that in the quartz system.
- The DE75 samples cured at temperatures between 165 °C and 134 °C were more likely to have a lower degree of polymerization compared to those cured at 192 °C.
- The optimum autoclaving temperatures were $T < 165$ °C in the C-DE system, while for the quartz systems, the optimum autoclaving temperatures were $T > 165$ °C.

Acknowledgments

The authors wish to thank Dr. Volker Thome, Head of the Mineral Materials and Building Material Recycling Department at the Fraunhofer Institute for Building Physics, Germany and Dr. Liudvikas Urbonas, Head of the Binding Agents and Additives Laboratory at Centre for Building Materials, Technical University of Munich for their help and their useful discussions. Funding: This work was supported by the Fraunhofer Institute for Building Physics IBP, the Inorganic Materials and Recycling Department, and the Iran Ministry of Science.

References

- [1]. Kohler N, "Global Energetic Budget of Aerated Concrete." In *Autoclaved Aerated Concrete, Moisture and Properties*: Ed. F. H. Wittmann," Elsevier, Amsterdam, 1983.
- [2]. Aroni S, "On energy conservation characteristics of autoclaved aerated concrete," *Materials and Structures*, V. 23, No. 1, pp. 68–77, 1990.
- [3]. Frey E, Briesemann D, "Neuere Berechnungen zum Primärenergieinhalt von Gasbeton," *Betonwerk+Fertigteil-Technik*, V. 51, No. 7, pp. 468–472, 1985.
- [4]. Lutter J, "New research on the primary energy content of building materials,". 3rd RILEM International Symposium on AAC, Balkema, Zurich, Switzerland. 14-16 October, 1992.
- [5]. Ankele K, Steinfeldt M, "Ökobilanz für typische YTONG-Produktanwendungen," Institut für ökologische Wirtschaftsforschung, Berlin, 1996, ISBN: 3-932092-01-5.
- [6]. Shams T, Schober G, Heinz D, Seifert S, "Production of autoclaved aerated concrete with silica raw materials of a higher solubility than quartz part I: Influence of calcined diatomaceous earth," *Construction and Building Materials*, V. 272, 2021.
- [7]. Qu X, Zhao X, "Previous and present investigations on the components, microstructure and main properties of autoclaved aerated concrete – A review," *Construction and Building Materials*, V. 135, pp. 505–516, 2017.
- [8]. Isu N, Teramura S, Ishida H, Mitsuda T, "Influence of quartz particle size on the chemical and mechanical properties of autoclaved aerated concrete (II) fracture toughness, strength and micropore," *Cement and Concrete Research*, V. 25, No. 2, pp. 249–254, 1995.
- [9]. Mitsuda T, Sasaki K, Ishida H, "Phase evolution during autoclaving process of aerated concrete," *Journal of the American Ceramic Society*, V. 75, No. 7, pp. 1858–1863, 1992.
- [10]. Isu N, Ishida H, Mitsuda T, "Influence of quartz particle size on the chemical and mechanical properties of autoclaved aerated concrete (I) tobermorite formation," *Cement and Concrete Research*, V. 25, No. 2, pp. 243–248, 1995.
- [11]. Narayanan N, Ramamurthy K, "Structure and properties of aerated concrete: a review," *Cem. Concr. Composites*, V. 22, No. 5, pp. 321–329, 2000.
- [12]. Pachideh Gh GM, "Effect of pozzolanic materials on mechanical properties and water absorption of autoclaved aerated concrete," *Journal of Building Engineering*, V. 26, Article No.100856, 2019.
- [13]. Iler RK, "The Chemistry of Silica: Solubility, Polymerization, Colloid and Surface Properties and Biochemistry of Silica," Wiley, London, 1979, ISBN: 978-0-471-02404-0.
- [14]. Carroll RA, "Hydrothermal performance of pulverised fuel ash and the manufacture of autoclaved aerated concrete," (Doctoral dissertation, © Robert A. Carroll), 1996.
- [15]. Gundlach H, "Dampfgehärtete Baustoffe," Wiesbaden, Berlin, 1973.
- [16]. Stoeber W, "Equilibrium Concepts in Natural Water Systems: Formation of Silicic Acid in Aqueous Suspensions of Different Silica Modifications," *Advances in Chemistry*, 1967, 9780841200685.
- [17]. Sato H and Grutzeck M, "Effect of Starting Materials on the Synthesis of Tobermorite | MRS Online Proceedings Library (OPL) | Cambridge Core," *Material research society*, V. 245, pp. 235–240, 1992.
- [18]. Chan C, Sakiyama M, Mitsuda T, "Kinetics of the CaO.quartz .H2O reaction at 120° to 180°C in suspensions," *Cement and Concrete Research*, V. 8, No. 1, pp. 1–5, 1978.
- [19]. Okada Y, Ishida E. H., Mitsuda T, "²⁹Si NMR spectroscopy of silicate anions in hydrothermally formed CSH," *Journal of the American Ceramic Society*, V. 77, No. 3, pp. 765–768, 1994.
- [20]. Matsui K, Kikuma J, Tsunashima M, Ishikawa T, Matsuno S-y, Ogawa A, Sato M, "In situ time-resolved X-ray diffraction of tobermorite formation in autoclaved aerated concrete: Influence of silica source reactivity and Al addition," *Cement and Concrete Research*, V. 41, No. 5, pp. 510–519, 2011.
- [21]. Taylor HFW, "Cement chemistry," Thomas Telford, 1997, ISBN: 0727725920.
- [22]. Chen J, Thomas J, Taylor HFW, Jennings H, "Solubility and structure of calcium silicate hydrate," *Cement and Concrete Research*, V. 34, No. 9, pp. 1499–1519, 2004.
- [23]. Richardson I, "Tobermorite/jennite- and tobermorite/calcium hydroxide-based models for the structure of C-S-H: applicability to hardened pastes of tricalcium silicate, β-dicalcium silicate, Portland cement, and blends of Portland cement with blast-furnace slag, metakaolin, or silica fume," *Cement and Concrete Research*, V. 34, pp. 1733–1777, 2004.
- [24]. Nonat A, "The structure and stoichiometry of C-S-H," *Cement and Concrete Research*, V. 34, No. 9, pp. 1521–1528, 2004.
- [25]. Grutzeck M, Benesi A, Fanning B, "Silicon-29 Magic Angle Spinning Nuclear Magnetic Resonance Study of Calcium Silicate Hydrates," *Journal of the American Ceramic Society*, V. 72, No. 4, pp. 665–668, 1989.

- [26]. Mostafa NY, "Influence of air-cooled slag on physicochemical properties of autoclaved aerated concrete," *Cement and Concrete Research*, V. 35, No. 7, pp. 1349–1357, 2005.
- [27]. Dietz T and Bohnemann K, "Calcium silicate hydrate in fiber cement sheets and autoclaved aerated concrete (AAC)," 7th International Conference on Inorganic Bonded Wood and Fiber Composite Materials, USA, 2000.
- [28]. Assarsson GO, "Hydrothermal Reactions between Calcium Hydroxide and amorphous Silica: The Reactions between 180 and 220°," *The Journal of Physical Chemistry*, V. 61, No. 4, pp. 473–479, 1957.
- [29]. Assarsson GO, "Hydrothermal Reactions between Calcium Hydroxide and Amorphous Silica. The Reactions between 120 and 160°," *The Journal of Physical Chemistry*, V. 62, No. 2, pp. 223–228, 1958.
- [30]. Seyama H SM, "Bonding-state characterization of the constituent elements of silicate minerals by X-ray photoelectron spectroscopy," *J. Chem. Soc., Faraday Trans*, V. 81, pp. 485–495, 1985.
- [31]. Black L, Garbev K, Stemmermann P, Hallam KR, Allen GC, "Characterisation of crystalline C-S-H phases by X-ray photoelectron spectroscopy," *Cement and Concrete Research*, V. 33, No. 6, pp. 899–911, 2003.
- [32]. Carriere B, Deville JP, Brion D, Escard J, "X-ray photoelectron study of some silicon-oxygen compounds," *Journal of Electron Spectroscopy and Related Phenomena*, V. 10, No. 2, pp. 85–91, 1977.
- [33]. Faucon P, Delaye JM, Virlet J, Jacquinet JF, Adenot F, "Study of the structural properties of the C-S-H(I) BY molecular dynamics simulation," *Cement and Concrete Research*, V. 27, No. 10, pp. 1581–1590, 1997.
- [34]. Stumm A, Garbev K, Beuchle G, Black L, Stemmermann P, Nüesch R, "Incorporation of zinc into calcium silicate hydrates, Part I: formation of C-S-H(I) with C/S=2/3 and its isochemical counterpart gyrolite," *Cement and Concrete Research*, V. 35, No. 9, pp. 1665–1675, 2005.
- [35]. Yu P, Kirkpatrick RJ, Poe B, McMillan PF, Cong X, "Structure of Calcium Silicate Hydrate (C-S-H): Near-, Mid-, and Far-Infrared Spectroscopy," *J. Am. Ceram. Soc.*, V. 82, No. 3, pp. 742–748, 1999.
- [36]. Dolado JS, Griebel M, Hamaekers J, "A Molecular Dynamic Study of Cementitious Calcium Silicate Hydrate (C-S-H) Gels," *J Am Ceram Soc*, V. 90, No. 12, 3938-3942, 2007.
- [37]. Connan H, Klimesch D, Ray A, Thomas P, "Thermal characterisation of autoclaved cement made with alumina-silica rich industrialwaste," *Journal of Thermal Analysis and Calorimetry*, V. 84, No. 2, pp. 521–525, 2006.
- [38]. Chen Y, Chang J, Lai Y, Chou M, "A comprehensive study on the production of autoclaved aerated concrete: Effects of silica-lime-cement composition and autoclaving conditions," *Construction and Building Materials*, V. 153, pp. 622–629, 2017.
- [39]. Klimesch DS, Ray A, "DTA-TGA evaluations of the CaO–Al₂O₃–SiO₂–H₂O system treated hydrothermally," *Thermochimica Acta*, V. 334, pp. 115–122, 1999.

A.3 Publication 3

Journal of Building Engineering, 2022 (accepted).

Reprinted (adapted) with permission from Elsevier
(<https://www.elsevier.com/about/policies/copyright/permissions>).

Summary

In the previous papers, only C-DE was used as the silica material of a higher solubility than quartz and it was not clear whether the obtained advantages were limited to C-DE or other silica raw materials of high solubilities could lead to similar results and advantages as well. In this paper, it was revealed that using RHA as the silica material of a high solubility than quartz resulted in similar outcomes as the previously performed studies with C-DE. However, a higher total drying shrinkage was observed for the RHA-based AAC compared to that for the quartz-based AAC. From a general point of view, the results showed that the optimum temperature for autoclaving AAC has a direct dependency on the dissolution behavior of silica raw materials used in the mixture.

Rice husk ash as a silica source for the production of autoclaved aerated concrete – a chance to save energy and primary resources

Taban Shams ^{a, b, 3}, Georg Schober ^c, Detlef Heinz ^b, Severin Seifert ^a

^a Fraunhofer Institute for Building Physics IBP, Inorganic Materials and Recycling Department, Building Materials Technology Group, Fraunhoferstr. 10, 83626, Valley, Germany

^b Technical University of Munich, Department of Civil, Geo and Environmental Engineering, Centre for Building Materials cbm, Franz-Langinger-Str. 10, 81245, Munich, Germany

^c Engineering office for materials development and process technology, Marbstraße 6, 94405 Landau a.d. Isar, Germany

Abstract

If the silica raw material used in autoclaved aerated concrete (AAC) requires a lower level of energy for dissolution, a lower autoclaving temperature could be applied to reach the required product performance. Accordingly, the raw material quartz sand in the AAC mixture was replaced with rice husk ash (RHA) which has a higher solubility of silica with increasing temperatures in alkaline binder systems. AAC samples were produced at autoclaving temperatures of 152 °C, 165 °C, 175 °C, and 192 °C with an autoclaving time of 6 hours. Quantitative X-ray diffraction (XRD) analysis according to Rietveld refinement, qualitative XRD analysis, and scanning electron microscopy (SEM) were carried out to investigate the microstructure of the hardened AAC samples. Additionally, the compressive strength, dry bulk density, A-value, and total drying shrinkage were determined. In contrast to the quartz-based AAC, the properties of the RHA-based AAC were improved by applying a lower autoclaving temperature than the typical temperature used for industrial production of AAC,

³ Corresponding author. Tel.: +49 8024 643-637.

E-mail address: taban.shamshafshejani@tum.de

i.e. 192 °C. For the RHA-based AAC, a maximum increase of 22 % in the compressive strength, 132 % in the total content of tobermorite, 19 % in the A-value, and a maximum decrease of 33 % in the total value of drying shrinkage were observed as the applied autoclaving temperature was changed from 192 °C to 165 °C. Moreover, the material efficiency of the AAC product can be improved by using RHA as an agricultural waste product in the mixture. The RHA-based AAC autoclaved at 165 °C exhibited a slightly higher compressive strength to density ratio (A-value) than the quartz-based AAC autoclaved at 192 °C. However, a higher total drying shrinkage was observed for the RHA-based AAC autoclaved at 165 °C compared to the quartz-based AAC autoclaved at 192 °C. From a general point of view, the results showed that the optimum temperature for autoclaving AAC has a direct dependency on the dissolution properties of silica raw materials used in the mixture.

Keywords: autoclaved aerated concrete, rice husk ash, autoclaving temperature, compressive strength, drying shrinkage, C-S-H formation

1. Introduction

The main factor to evaluate the sustainability of building materials is embodied energy. Based on the reported values of embodied energy for different construction materials, autoclaved aerated concrete (AAC) has a lower embodied energy compared to other building materials, e.g. concrete and brick. Therefore, it could be a reasonable alternative to those aforementioned materials [1, 2]. AAC is a lightweight cellular material that could potentially be used in sustainable buildings due to its environmentally friendly properties such as outstanding thermal insulation [3, 4].

AAC is mainly composed of calcareous and silica materials. Lime and cement are used as calcareous materials and in most cases, quartz sand is utilized as the silica material. Additionally, sulfate carriers, e.g. anhydrite, are added to the AAC mixture as essential additives to control the setting time and improve the compressive strength and shrinkage properties [5–7]. The porous structure of AAC is obtained by the reaction of aluminum powder/paste under an alkaline condition [8, 9]. Moreover, ground recycled AAC (GRA) obtained from grinding waste AAC is used as an environmentally friendly and economical filler for the production of new AAC [10].

In general, the AAC volume is composed of 30-85 vol. % air pores and 15-70 vol. % solid structure (skeletal structure) depending on the density of the product [11, 12]. The air pores, which are generated due to the reaction of the pore-forming agent under alkaline condition, are defined as roughly spherical pores with a diameter of $D > 100 \mu\text{m}$ [13, 14]. The solid structure around the air pores consists of mostly irregular pores in size of 0.5-50 μm (micro-pores) and solid materials. The solid materials are composed of the final phases formed during AAC production [12]. The composition of solid materials varies depending on the quality, the CaO/SiO₂- ratio (C/S), the proportion of the starting materials, as well as the temperature and duration of the autoclaving process. However, it could generally contain different types of calcium silicate hydrates or C-S-H (in this study, cement chemistry notation is used in which C, S, A, and F stand, respectively, for CaO, SiO₂, Al₂O₃, and Fe₂O₃), residual quartz, anhydrite, and other phases in minor quantities [15]. Several studies have confirmed that in AAC, the main hydrothermal product is C-S-H including crystalline C-S-H such as tobermorite, semi-crystalline C-S-H such as C-S-H (I), and amorphous C-S-H [16–19]. **Figure 1** shows the porous structure of AAC including pores and crystals of tobermorite formed on the wall of the pores.

In AAC, different types of formed C-S-H act as the binding agent in solid materials holding all present phases in the matrix [20–22]. Among the C-S-H phases, well-crystallized tobermorite has been found to have the highest strength which improves the properties of AAC, e.g. compressive strength and shrinkage [18, 23, 24]. Several studies have reported that the final properties of AAC significantly depend on tobermorite quantity as well as its crystallinity [17, 18, 25]. However, the results of some other studies have shown that in addition to a high content of tobermorite, a homogeneous distribution of the tobermorite crystals in the solid structure is required to obtain optimum strength properties [7, 26]. It has also been revealed that optimum compressive strengths can be achieved when the maximum fraction of volume is occupied by tobermorite and other C-S-H together [27].

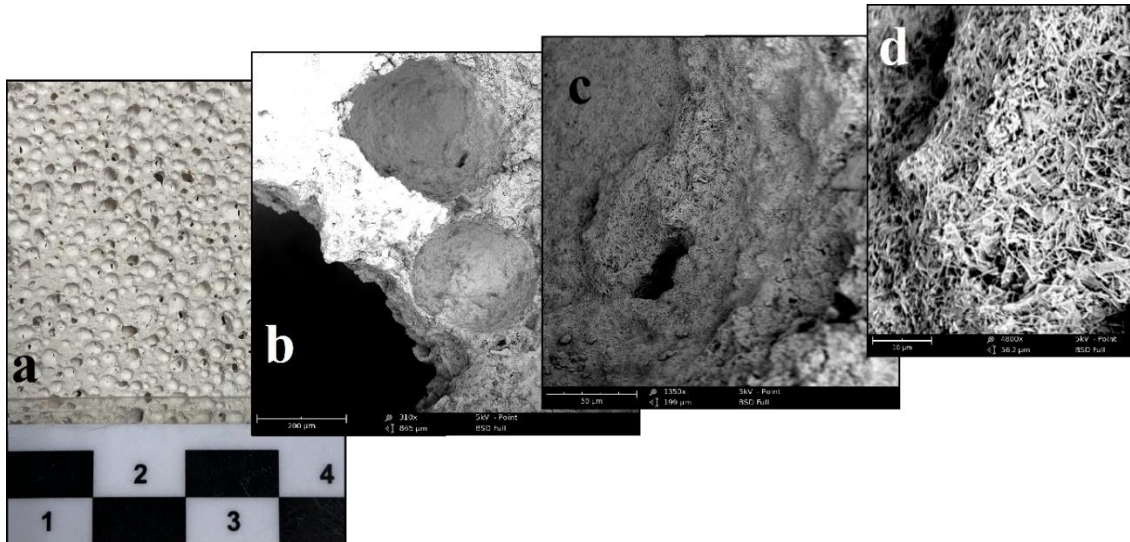


Figure 1 Porous structure of AAC, (a: eye observation of pores on the surface of AAC, line: 4 cm), (b: SEM image of pores on the surface of AAC, scale bar: 200 μm), (c: SEM image of the pore wall, scale bar: 50 μm), (d: SEM image of tobermorite crystals formed on the wall of the pore, scale bar: 10 μm).

The formation of tobermorite and other C-S-H strongly depends on the constituent materials, especially binder content, and the autoclaving process. During the autoclaving process, non-crystalline C-S-H, which are loosely packed and spatially disordered, are being transformed into crystallized C-S-H phases with low specific surface area. This leads to the formation of a dense micro-crystalline structure in the solid structure which improves the properties of AAC [28, 11]. Therefore, the autoclaving process is indispensable to support the formation of sufficient binding phases, i.e. C-S-H including tobermorite with a high degree of crystallinity.

C-S-H forms through the reaction of the solved SiO_4^{4-} ions with the Ca^{2+} -saturated solution. Lime (CaO) is the most reactive component in the AAC mixture. Therefore, hydration of lime occurs in the initial step of producing AAC, i.e. mixing of the solid raw materials with water. However, the dissolution of silica requires the autoclaving process. In another word, the formation of C-S-H can take place only when dissolved silica (SiO_4^{4-}) diffuses into the solution to an adequate extent, and indeed the main role of the autoclaving process is dissolving silica resulting in the formation of the C-S-H-phases [15]. This implies that if a lower level of energy is needed for the dissolution of silica raw material, then a lower autoclaving temperature could be applied.

There exist various forms of silica with different dissolution properties in water. The difference in their dissolution properties is mainly due to their different solubility (in this study, solubility specifically refers to water solubility). As can be seen in **Table 1** [29], quartz has a lower rate of dissolution compared to fused silica, which is a type of amorphous silica, and other crystalline modifications such as tridymite and cristobalite. Accordingly, it comparatively requires a higher level of energy to decompose. Besides solubility, the second factor which affects the rate of hydrothermal reactions is the specific surface area of the silica materials. A higher specific surface area leads to a faster dissolution of silica materials. Therefore, silica materials with a porous microstructure show faster dissolution compared to quartz sand which contains solid particles without cavities.

However, in almost all of the production sites, quartz sand is the firmly established silica raw material used in the AAC mixture. Therefore, the substitution of silica material, which contains a more soluble form of silica, e.g. amorphous silica, stishovite, and cristobalite, for quartz sand in the AAC mixture, might contribute to a reduction in the required autoclaving temperature and/or time without deteriorating the product performance.

The behavior of various types of silica materials in the lime-silica system was investigated in several studies [30–34]. The outcome of those previous studies [30–34] has generally indicated that utilization of silica materials of high solubility in the hydrothermally treated lime-silica mixture led to the formation of initial C-S-H with a high degree of polymerization which crystallized hardly to tobermorite. In fact, in the mixture of lime with silica materials of a higher solubility, e.g. amorphous silica, non-crystalline C-S-H phases formed very rapidly in 1-2 h. Nevertheless, they did not rearrange to well-crystallized tobermorite even after 24 h. In all of the aforementioned studies, the applied autoclaving temperature for the system composed of lime and

more soluble silica was quite high, i.e. $T \geq 180$ °C, similar to that used for the lime-quartz system. According to relevant literature, the solubility of silica significantly increases with an increase in the temperature and pH value of the solution [35, 36]. Therefore, applying a high autoclaving temperature makes the dissolution of silica materials of higher solubility even faster which affects the equilibrium of the formed C-S-H and its transformation to tobermorite negatively. However, applying low autoclaving temperatures might reduce the solubility and dissolution rate which avoids progressive polymerization of silicate chains.

Table 1 Relative rate of dissolution for different types of silica in water at a temperature of 25 °C and a pH of 8.5 [29].

type of silica	rate of dissolution (10^{-6} g ml ⁻¹ day ⁻¹)
quartz	2.8
cristobalite	6.0
tridymite	4.5
stishovite	11.0
fused silica (amorphous)	39.0

Studying the hydrothermal chemistry of the lime-silica system without paying attention to the autoclaving temperature in a wider range is insufficient to understand the performance of the various types of silica materials in AAC products. The performance of the quartz-based AAC under different autoclaving conditions is within the scope of knowledge. It is widely known that the optimum properties of the quartz-based AAC can be obtained at the autoclaving temperatures of $T > 180$ °C and a duration of 6-12 h, depending on the size of the samples [37, 38, 23, 17, 16, 26]. However, the performance of more soluble silica-based AAC at different autoclaving temperatures has only been examined in a few studies [36, 39, 40].

Several studies investigated the influence of different types of fly ash, e.g. fluidized fly ash, on the properties of AAC [41–44]. The main reason for using fly ash in AAC production is that it does not need to be ground. Among different types of fly ashes, pulverized fly ash (PFA) stands as a source of reactive silica composed of amorphous silicate and/or aluminosilicate which could be used for AAC production. In addition to amorphous silicate, crystalline inclusions of sulfates, mullite, and quartz are present [45]. Carroll [36] conducted a comprehensive study on the hydrothermal reactions of PFA and the production of PFA-based AAC. The results revealed the formation of the semi-crystalline C-S-H phase and hydrogarnet phase at the initial stages of the hydrothermal treatment. The crystallization extent of semi-crystalline C-S-H to tobermorite was found difficult to determine, but it was reported that a large quantity of semi-crystalline C-S-H did not crystallize to tobermorite and remain in the final product. In the aforementioned study, autoclaving conditions comparable to those in the industrial manufacture of AAC were used. The hydrothermal reactions of PFA were investigated at the temperature of 184 °C for different periods of up to 21 hours. As it was mentioned earlier, high autoclaving temperatures, similar to those used for autoclaving the quartz-based AAC, are probably not the optimum temperatures for autoclaving systems containing silica materials of a high solubility than quartz.

Kunkarchiyan et al. [39] carried out a study in which quartz sand in the AAC mixture was replaced by bagasse ash (BA) and black rice husk ash (BRHA). The produced AAC samples were subsequently autoclaved at different temperatures for different durations. BRHA contained cristobalite which has a higher solubility than quartz. In that study, a trend to decrease the autoclaving time or temperature was not observed. Indeed, it appeared that the compressive strengths of the AAC samples either containing quartz sand or BRHA increased as the autoclaving temperature and time increased. This implies that under different autoclaving conditions, more soluble silica-based AAC exhibits a behavior similar to quartz-based AAC. However, as was stated earlier, the substitution of more soluble silica materials for quartz sand is expected to contribute to a reduction in the required autoclaving temperature and/or time without affecting the performance of AAC products negatively.

In our previous study [46, 40] calcined diatomaceous earth (C-DE) was used as a silica material, which had a higher solubility and dissolution rate than quartz sand, in the AAC mixture. In that study, the performance of the C-DE-based AAC under different autoclaving conditions was evaluated. The results revealed that the C-

DE-based AAC showed a different behavior than the quartz-based AAC. The tobermorite formation and the compressive strength of the C-DE-based AAC have been improved when a lower autoclaving temperature was applied. However, for the quartz-based AAC, a deterioration in those properties was observed. Moreover, for the C-DE-based AAC, a reduction of 40 °C in the autoclaving temperature increased the compressive strength from 4.4 MPa to 6.4 MPa which was higher than the corresponding requirements, i.e. ≥ 4.9 MPa. One advantage of obtaining an AAC product with higher strength than technical requirements is the opportunity to reduce binder content in the mixture.

Around 25–27 % and 45–50 % of the total energy consumption in AAC production is associated with the hydrothermal treatment and embodied energy of raw materials, respectively [47–49]. Energy consumption during hydrothermal treatment can be reduced through a reduction in the autoclaving time and/or temperature. A reduction in the embodied energy of raw materials can mainly be achieved by decreasing the binder content, i.e. cement and lime in the AAC mixture. If a decrease in the required autoclaving temperature and/or time and a reduction in the binder content occur simultaneously, the total energy consumption in the production of AAC will be reduced considerably. Therefore, our previous studies [40, 46] could offer a possibility for a reduction in the total energy consumption of AAC production since the autoclaving temperature as well as binder content can be reduced at once. However, the C-DE material used in the previous studies was not a waste material but rather a comparatively costly material. It is not clear whether the obtained advantages are limited to C-DE or other silica raw materials of a higher solubility could lead to similar results and advantages as well.

The way that results discussed in those studies [46, 40] show that such advantages might also be achieved by using other silica materials of a higher solubility. In fact, obtaining similar results depends strongly on the dissolution property of silica raw materials. Therefore, it could introduce a possibility for utilization of the waste and recycled materials as the source of more soluble silica in the AAC mixture. It is therefore needed to evaluate the hypothesis of those studies using other silica raw materials with similar dissolution properties which are more economical, energy-efficient and environmentally friendly. Thus, the subsequent advantages of reducing autoclaving temperature would be accompanied by multiple economic and environmental benefits of material efficiency.

Moreover, in those studies [40, 46], C-DE-based AAC contained comparatively lower tobermorite in spite of higher compressive strength and almost similar bulk density. Although the low content of tobermorite did not cause a decrease in compressive strength, it could cause an increase in drying shrinkage. A high proportion of non-crystalline C-S-H increases the drying shrinkage of AAC products [18, 41]. Thus it is needed to evaluate the drying shrinkage of the more soluble silica-based AAC. Consequently, this study was intended to reduce the required autoclaving temperature in the production of AAC using economical and environmentally friendly silica raw materials in a way that does not influence the quality of the product negatively. For this purpose, rice husk ash (RHA) was used as silica raw materials in the AAC mixture.

Rice husk, which is known as a favorable source of dry biomass, is a secondary product derived from the milling process of rice [50]. Based on the reported values, the global production of rice husks is 137 million tons per year [51]. Rice husk produced in the milling process has been mainly used as fuel in parboiling plants. The thermal energy obtained from burning rice husk is used for the milling process of rice. Additionally, the process of burning rice husk in the parboiling plants produces RHA as a waste residue which is usually about 20 % of the primary fuel weight.

RHA contains up to 95 % silica in the form of crystalline and amorphous particles. The degree of crystallinity of RHA depends mainly on the temperature of the burning process as well as calcination parameters, e.g. calcination temperature and heating rate [52, 53]. RHA is calcined to remove substances which could be unfavorable for its pozzolanic properties. Due to the high content of silica and also the fact that the quantity of these waste residues has been considerably increasing, there is an opportunity to use these waste residues as silica materials in the AAC mixture. Additionally, RHA could be composed of cristobalite which has a higher solubility than quartz [29]. C-DE used in the previous studies [46, 40] also contained a high percentage of silica in the form of cristobalite. Therefore, using RHA as the silica material in the AAC mixture could potentially result in similar advantages as in the previous studies while a greater material efficiency can also be achieved. Moreover, replacing RHA with quartz sand in the AAC mixture reduces the consumption of electricity associated with the milling process of quartz sand which is one of the energy-intensive steps in AAC production [54, 55].

A lot of research has been carried out on the utilization of RHA in ordinary concrete and also ultra-high performance concrete as a partial substitute for cement and fine aggregates [52, 53, 56–62]. However, few attempts have been made in the application of RHA in AAC production [63, 39].

From a general point of view, the goal of this study is to reduce the required autoclaving temperature by substituting quartz sand with RHA as a silica material in the AAC mixture. To reach this, the properties of RHA-based AAC including compressive strength, mineralogical composition, shrinkage, and structure of surface under different autoclaving conditions were evaluated.

2. Materials and methods

2.1 Characterization of the raw materials

In this study, soft-burnt quicklime (from Fels-Werke, Germany) and Portland cement type I (from Dornburger Cement, Germany) were used. Anhydrite used in this study is from natural anhydrite which is finely ground and free of any additives (from Krone-Gips, Germany). GRA which was obtained by grinding waste AAC was provided by Xella Technologie- und Forschungsgesellschaft mbH, Germany.

The results of the chemical analysis of all the components of the AAC mixture are presented in **Table 2**. The elemental compositions in **Table 2** were identified using X-ray fluorescence (XRF).

According to the result of density measurement, RHA and quartz sand used in this study had, respectively, a density of 2.3 g/cm³ and 2.6 g/cm³ and a dry bulk density of 0.45 g/cm³ and 0.93 g/cm³. The comparison of the (X-ray diffraction) XRD pattern of RHA and quartz sand is presented in **Figure 2**. Phase identification was performed using EVA software (DIFFRAC. EVA Ver. 4.2). A comparatively broad cristobalite peak was recognized in the XRD pattern of RHA. However, diffraction peaks of quartz with high relative intensity were identified for quartz sand. This shows that RHA contains a more soluble form of silica, i.e. cristobalite, compared to quartz sand [29].

Table 2 Elemental compositions (wt. %).

materials	CaO	SiO ₂	Fe ₂ O ₃	SO ₃	Al ₂ O ₃	MgO	K ₂ O	TiO ₂	P ₂ O ₅	Na ₂ O	LOI*
sand	0.0	98.8	0.0	0.0	0.8	0.0	0.3	0.0	0.0	0.0	0.2
lime	95.0	0.8	0.2	0.2	0.3	0.5	0.0	0.0	0.0	0.0	3.0
GRA	37.4	41.2	1.3	5.7	2.0	0.0	0.7	0.1	0.0	0.0	12.0
RHA	1.0	89.6	0.3	0.0	0.3	0.8	1.6	0.0	0.5	0.3	5.7
cement	62.9	20.4	2.5	3.8	4.9	1.7	1.0	0.0	0.0	0.2	3.0
anhydrite	47.5	0.0	0.2	52.2	0.0	0.0	0.0	0.0	0.0	0.0	0.0

* Loss on ignition

The degree of crystallinity of RHA and quartz sand was calculated by TOPAS software (DIFFRAC.TOPAS Ver. 4.2). According to the results provided by this software, RHA contains 27 % amorphous content which is higher than the quantity of amorphous content in quartz sand, i.e. 2 %. The presence of higher amorphous content in RHA demonstrates its higher solubility compared to quartz sand. It should be considered that the degree of crystallinity of RHA can vary depending on the condition of the burning process and calcination (if applied). RHA used in this study was calcined at a temperature range of 700-800 °C.

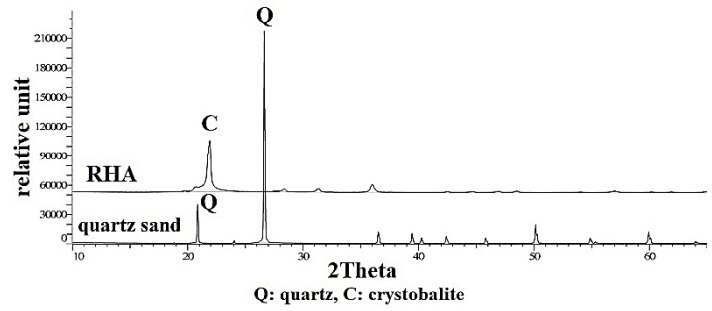


Figure 2 Comparison of the XRD pattern of RHA and quartz sand.

Figure 3 displays scanning electron microscopy (SEM) images of RHA. The SEM images of RHA display a structure composed of different sizes of cavities and layered appearances resulting in a cellular interconnected microstructure whereas quartz sand is composed of dense particles without any internal pores (**Figure 4**).

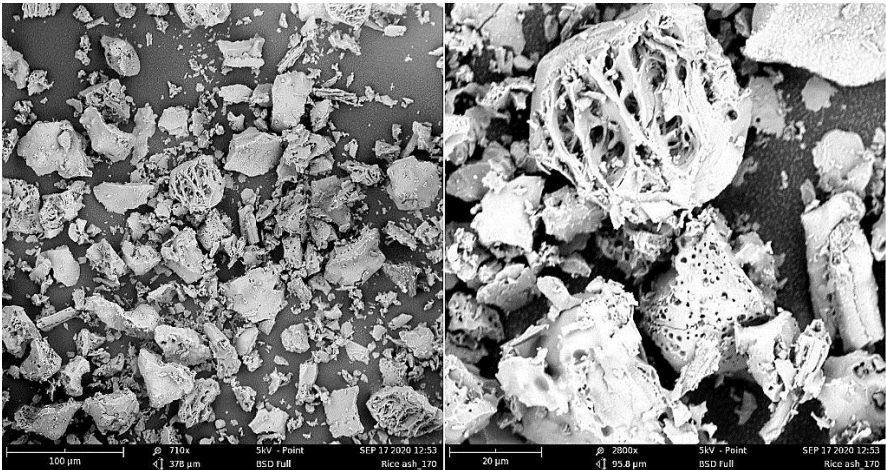


Figure 3 SEM images of RHA. (The left scale bar: 100 µm, The right scale bar: 20 µm).

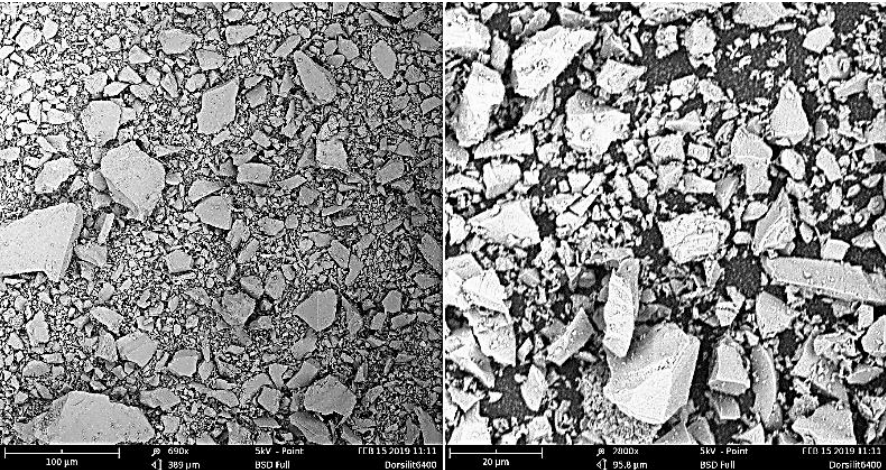


Figure 4 SEM images of quartz sand. (The scale bar of the left figure: is 100 µm, right figure: 20 µm).

The cellular interconnected structure of RHA compared to the solid structure of quartz sand implies a faster dissolution of RHA compared to quartz sand due to its higher specific surface area. Moreover, the specific surface areas of quartz sand and RHA were determined by the BET (Brunauer, Emmett, and Teller) method.

Accordingly, the values of 0.79 m²/g and 1.80 m²/g were obtained for quartz sand and RHA, respectively, which shows a higher specific surface of RHA compared to that of quartz sand.

The laser diffractometry technique is used to determine the particle size distribution of silica sources. The measurement was carried out with a Mastersizer 3000 and the Hydro MV wet dispersion unit. Distilled water was used as the dispersant. A comparison of the particle size distribution of silica sources is displayed in **Figure 5** which shows a close size distribution for RHA and quartz sand. The fineness of silica sources is one parameter which affects the degree of crystallinity, crystal size, and structure of C-S-H forming the solid structure [16, 26]. In order to compare the performance of RHA and quartz sand in AAC mixture, a similar particle size distribution is therefore required. The particle size of GRA used as the filler was between 5 μm to 500 μm.

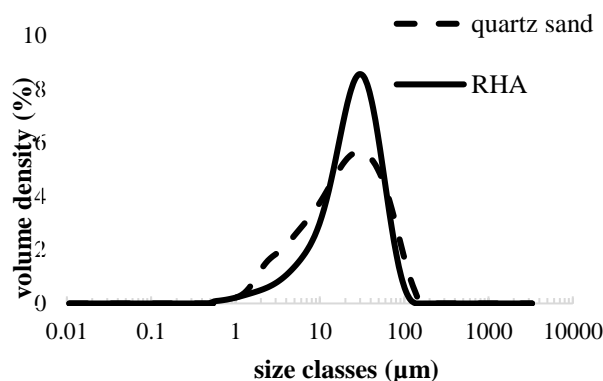


Figure 5 Comparison of the particle size distribution of silica raw materials.

2.2 The procedure of producing AAC samples

Experience in experimental work, as well as results of our previous study on C-DE, showed that the quantity of more soluble silica must be large enough to influence the AAC properties [40, 46]. Additionally, the replacement ratios should be above 50 wt. % to produce RHA-based AAC. Subsequently, R75 and R100 mixes were produced by replacing 75 wt. % and 100 wt. % of quartz sand in the ordinary mix (Q100), respectively.

The proportions of the raw materials are given in **Table 3**. RHA-based mixes required higher water content, i.e. higher water to solids ratio (W/S), because of the cellular structure of RHA compared to quartz. In such cases, the aluminum amount will be reduced adequately to obtain a similar range of bulk density.

Table 3 Autoclaved aerated concrete mixes.

mixture	cement	anhydrite	lime	Aluminum	C/S*	GRA	quartz	RHA	W/S**
units	wt. %	wt. %	wt. %	g	-	wt. %	wt. %	wt. %	-
Q100	31.0	6.0	10.0	3.35	0.635	12.0	41.0	0.0	0.70
R75	31.0	6.0	10.0	3.03	0.640	8.5	10.0	34.5	0.80
R100	31.0	6.0	10.0	2.92	0.642	7.5	0.0	45.5	0.83

* molar ratio of CaO/SiO₂

** water to solids ratio

The molar C/S of the starting material is defined by the ratio of the molar amount of active CaO in raw materials which are present in the mix design, e.g. lime and cement, to the molar amount of SiO₂ contributed by the existing raw materials, e.g. quartz sand and cement. The C/S of the starting material influences the solid structure and micro-morphology of crystalline phases significantly [31, 64, 65]. In order to compare the effect of RHA directly on the AAC properties, it was, therefore, necessary to keep the C/S of starting material constant for all mixes. However, replacing quartz sand with RHA reduced the C/S of the starting material since RHA contained a lower SiO₂ content compared to quartz sand (**Table 2**). Therefore, in order to keep the C/S of the starting materials constant for all mixes, it was needed to change the mix design adequately.

For this purpose, there was a precondition that needed to be satisfied before changing the mix design; the total amount of reactive CaO must have not been changed otherwise the total possible amount of C-S-H would have changed. Thus, the portion of lime and cement could not be changed unless both components were changed in a way that total reactive CaO remained constant. The simple alternative solution was that after replacing quartz sand with RHA for the aforementioned replacement ratios, i.e. 75 wt. % and 100 wt. %, the amount of RHA was increased for a minor quantity and the quantity of GRA was decreased adequately. All the aforementioned changes were in a range of 1- 4.5 wt. % which was not a severe change in the mix design since GRA, which acts only as a filler, is not reactive during the process. Subsequently, the C/S molar ratio of all AAC mixes was adjusted at 0.64 by applying the above-mentioned approach. The C/S of 0.6-0.7 is corresponding to a typical low-lime AAC used in industrial production. The current mix designs used in the industrial production of AAC are mainly low-lime.

Figure 6 displays the process of production of AAC samples. The first step was dosing and adding the constituent materials into the mixer (**Figure 6, b**). In the beginning, the mixing water with a temperature calculated to attain the required mixture temperature was added to the mixer. In this study, the temperature of mixing water was adjusted to 38 °C.

In the next step filler, i.e. GRA and the silica raw materials were added to water which produces a water-based slurry with a low viscosity. The slurry was stirred for 30 s. Afterward, anhydrite and binders, i.e. lime and cement were mixed with the slurry for 2 min. Aluminum paste is the last raw material that was added to the mixer 30 s before ending of the mixing process. In general, the whole mixing process took between 3 to 4 minutes. The slurry was cast into the oiled molds immediately. Soon after casting, the expanding process began by swelling of the mixture in the mold due to the reaction of aluminum under alkaline conditions which produced hydrogen gas. The expanded mixture was stored at room temperature for a couple of hours until gaining sufficient hardness for the demolding process (**Figure 6, c**). Although the storing period depends on the type of the mixture, after about 3 hours (h) the expanded mixture will typically gain a certain stiffness. During this time, the expanded mixture turns from a liquid phase into a solid cake-like block which is called “green cake”. After the demolding process, the green cake was autoclaved at different temperatures between 152 °C and 192 °C for a constant duration (**Figure 6, d**).

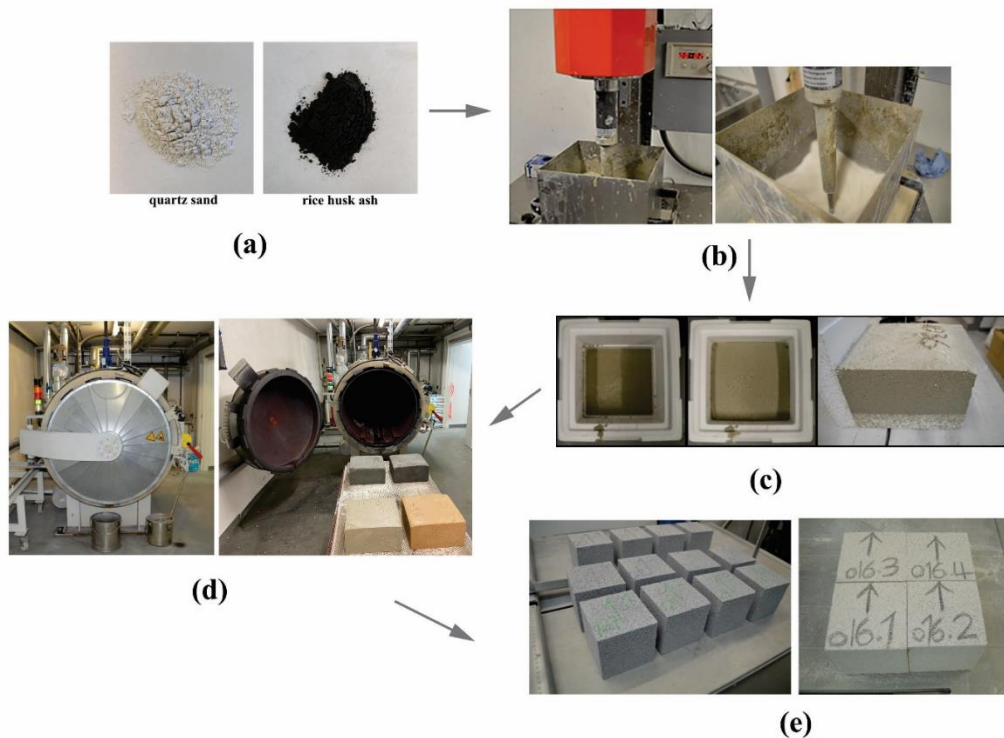


Figure 6 Process of production of AAC samples in this study. (a) silica raw materials (eye observation, dimension of each subfigure: around 5 cm), (b) mixing process, (c) molding, rising to the final volume, and demolding, (d) autoclaving, (e) AAC cubes after cutting process.

The autoclaving temperature of 192 °C (corresponding to the pressure of 12 bar) with a total duration of 8-12 h is a typical condition in industrial AAC production in which the AAC products contain quartz sand as a silica source. As was mentioned in the Introduction section, RHA-based AAC might require lower autoclaving temperatures compared to quartz-based AAC. Therefore the autoclaving temperature was adjusted to be lower than 192 °C. Subsequently, AAC samples were produced at autoclaving temperatures of 152 °C, 165 °C, 175 °C, and 192 °C, corresponding to the pressure of 4 bar, 6 bar, 8 bar, and 12 bar, respectively, with the autoclaving time of 6 hours. The autoclaving time in which the sample was under the desired temperature was 6 h. The evacuation and steaming up steps took around 1.5 h and steaming down took another 1.5 h. Thus, the total autoclaving process took around 9 h. The duration of the autoclaving process was kept constant for all samples. The autoclave used in this study has been specially produced similar to autoclaves used for industrial production of AAC. This autoclave has a volume of 1.5 m³ with an external source (steam generator) for steam supply. In the last step of the production process, the autoclaved samples were cut into prisms and cubes in sizes of 4 × 4 × 16 cm³ and 10 × 10 × 10 cm³, respectively (**Figure 6, e**).

2.3 Methods

The compressive strength was determined based on DIN EN 772-1 [66]. For this purpose, samples were stored in the oven at a temperature of 50 °C to obtain a moisture level of 6 wt. %. The measurement was performed on four 10 × 10 × 10 cm³ cubes per AAC block. The compressive strength was determined using Zwick Roell Z 100 compression test machine (**Figure 7**) with a loading speed of 0.1 (N / mm²) / s. Due to the anisotropy of AAC [67, 68, 11], the load was applied perpendicular to the expanding direction for all samples.

D2 Phaser diffractometer (from Bruker) was used to record XRD patterns. A summary of the measurement parameters is presented in **Table 4**.

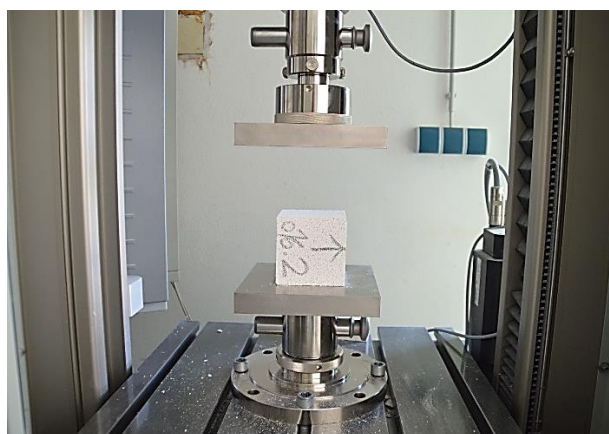


Figure 7 Measuring the compressive strength with Zwick Roell Z 100.

Table 4 Measurement parameters and settings of the Bruker D2 phaser diffractometer.

measurement parameter	value
wavelength	Cu-K α ($\lambda = 1.54 \text{ \AA}$)
measuring range	5-65° 2 θ
step size	0.02° 2 θ
measurement time per step	4 s
monochromator	Ni-Filter
detektor	silicon strip detektor (LynxEye)

After measuring compressive strength, a small but representative part of the broken sample was weighted and used for XRD analyses as well as SEM images. The broken sample, which was collected in a bowl, was then stored in an oven with a temperature of 105 °C to obtain the dry bulk density (DIN EN 772-13). Storing the samples in the oven lasted until the weight loss in two consecutive weighings in an interval of 24 h did not exceed 0.2 % of the total weight. Moreover, Rietveld quantitative phase analysis was carried out using the

internal standard method [69–71] to determine absolute phase contents including amorphous content. For this purpose, 10 wt. % addition of Zincite (ZnO) as the standard material was used. The standard material was mixed with the sample by hand before grinding to produce a homogeneous mixture with reproducible results [72]. Accordingly, the obtained mixture with 5 ml isopropanol was milled using McCrone micronizing for 3 min. After milling, the sample holder was filled with dried samples and measured 3 times. Each reported phase quantity is therefore average of phase content in 3 measurements. TOPAS software (DIFFRAC.TOPAS Ver. 4.2) was used for carrying out Rietveld refinement. EVA software (DIFFRAC. EVA Ver. 4.2) was used to analyze the recorded XRD patterns qualitatively based on ICDD's Powder Diffraction File (PDF). The Associated reference pattern numbers used for phase identification are given in **Table 5**.

Table 5 PDF number of compounds used for phase identification.

compound name	chemical composition	PDF number
quartz	SiO ₂	PDF 00-046-1045
cristobalite	SiO ₂	PDF 00-039-1425
tobermorite-11 Å	Ca ₅ Si ₆ (O, OH, F) ₁₈ · 5 H ₂ O	PDF 00-045-1480
tobermorite-9 Å	5 CaO · 6 SiO ₂ · 2.5 H ₂ O	PDF 00-010-0374
anhydrite	CaSO ₄	PDF 00-037-1496
bassanite	Ca (SO ₄) · 0.5 (H ₂ O)	PDF 01-072-4535
calcite	CaCO ₃	PDF 01-085-1108
katoite	Ca ₃ Al ₂ (SiO ₄) (OH) ₈	PDF 00-038-0368
hydroxyllestadite	Ca ₁₀ (SiO ₄) ₃ (SO ₄) ₃ (OH) ₂	PDF 01-072-9862

SEM was used for high-resolution imaging and microanalysis of the surface of samples. A conductive layer of gold was created on the surface of the sample, i.e. a part of the block sample, using an SEM sputter coater to improve the imaging of samples. The compressed air was then blown on the prepared sample in order to prevent drawing particles into the pump during the chamber evacuation.

The shrinkage of AAC samples was measured according to DIN EN 680: 2005 [73] on three 4 × 4 × 16 cm³ prisms per AAC block **Figure 8** (left). In order to avoid incorrect readings, the measuring points should be marked on both sides of the prisms **Figure 8** (right). The used glue was Superglue X60 which is commonly used for this purpose.

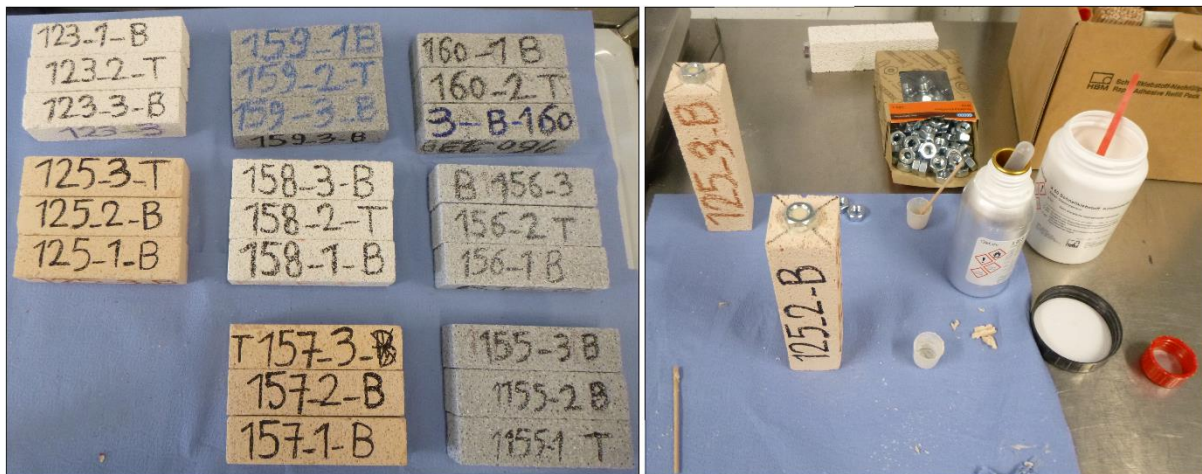


Figure 8 AAC prisms for measuring shrinkage (left). Marking measuring points on prisms (right).

Subsequently, the prisms were placed in water with a temperature of 20 ± 2 °C for a period of 72 h (**Figure 9**); one-third of their thickness during the first 24 h, two-thirds of their thickness during the second 24 h, and completely submerged during the last 24 h.



Figure 9 Conditioning AAC prisms in water with a temperature of 20 ± 2 °C for 72 h.

They were then stored in plastic wrap for 24 h. At this step, the first measurement of length (L_{c0}) and mass (m_0) should be carried out (**Figure 10**). In the next step, they were stored in a climatic chamber at a temperature of 20 ± 2 °C and relative humidity of 45 ± 5 % until a constant length is reached. The last measurement of the specimens should be carried out after 28 days of storage in the specified standard climate. If the relative change in length increases by more than 0.02 mm/m between 21 and 28 days, then the storage of specimens should be continued. Subsequently, additional measurements and weighings should be performed until the increase in length change within 7 days no longer exceeds 0.02 mm/m.



Figure 10 First measurements of length (L_{c0}).

For each measurement time (t_i), the values of relative change in length (ϵ_{csi}) and moisture content, (μ_{mi}) were recorded. These values were then linked by associated graphs. The total drying shrinkage ($\epsilon_{cs, tot}$) refers to the relative change in length between the beginning of the conditioning time at time t_0 and the end of the shrinkage storage at time t_e .

3. Results

3.1 X-ray diffraction analysis (XRD)

Quantitative and qualitative XRD analyses were conducted to study the phase composition of the samples. The XRD patterns of the R75 and R100 samples autoclaved at various temperatures are shown in **Figure 11** and **Figure 12**, respectively.

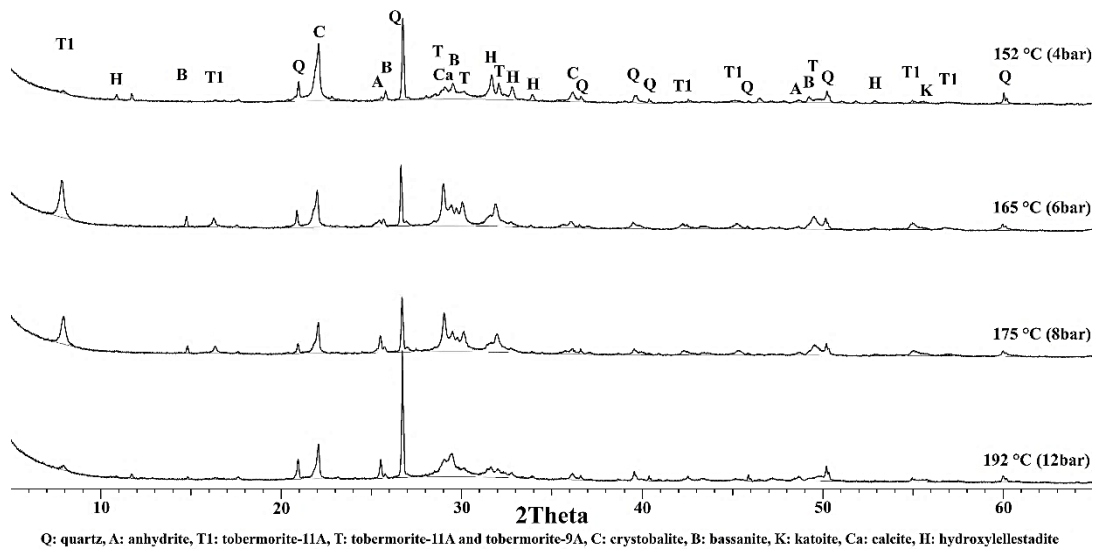


Figure 11 XRD patterns of the R75 mix autoclaved at different temperatures. (The saturated steam pressure corresponding to each temperature is shown in parentheses).

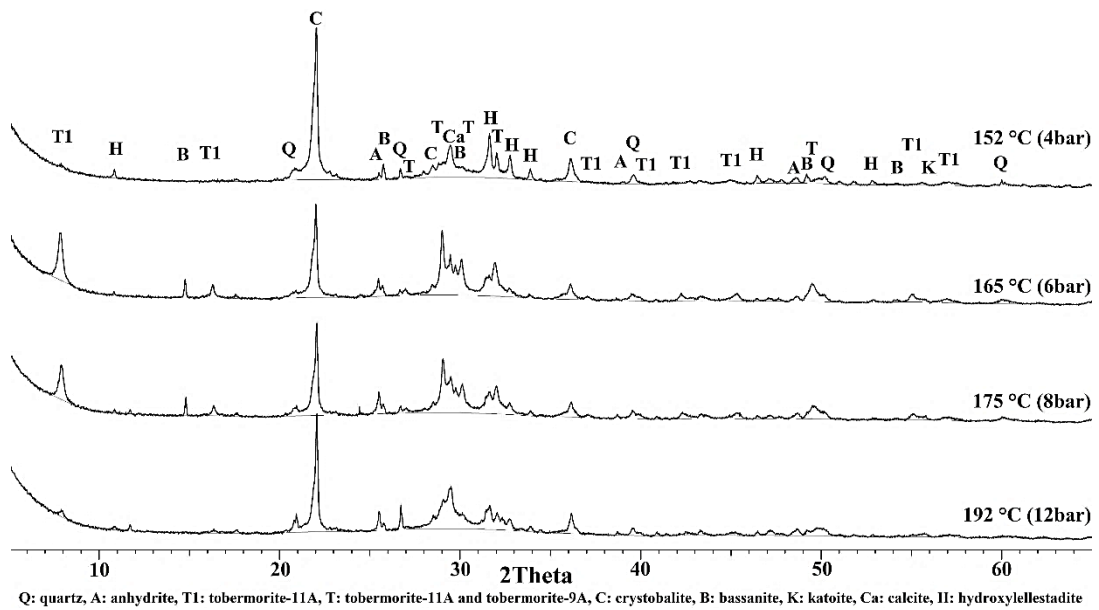


Figure 12 XRD patterns of the R100 mix autoclaved at different temperatures. (The saturated steam pressure corresponding to each temperature is shown in parentheses).

By comparing **Figure 11** and **Figure 12**, it can be implied that the XRD results of the R75 and the R100 mix follow a similar variation pattern. According to those figures, insignificant characteristic peaks of tobermorite can be observed at the autoclaving temperature of 192 °C. For both the R100 and the R75 mixes, clear and significant characteristic peaks of tobermorite were detected as the autoclaving temperature of 165 °C was applied. This suggests that applying the autoclaving temperature of 165 °C instead of 192 °C yielded a higher tobermorite formation and a higher degree of crystallinity in the RHA-based AAC. However, the autoclaving temperature lower than 165 °C, i.e. 152 °C, resulted in a reduction in the intensity of the tobermorite peaks in the R75 and R100 mixes.

Quantitative XRD results determined by Rietveld refinement for the R75 and the R100 mixes are displayed in **Table 6** and **Table 7**, respectively.

Table 6 Absolute contents (wt. %) of main phases existing in the R75 mix autoclaved at different temperatures. The results were determined by Rietveld refinement using the internal standard method. Standard deviations of the measurement which was repeated 3 times per specimen are given in parentheses.

phases	192 °C	175 °C	165 °C	152 °C
anhydrite	1.7 (0.2)	1.5 (0.1)	0.4 (0.1)	0.1 (0.1)
bassanite	1.4 (0.1)	2.7 (0.1)	3.0 (0.1)	1.6 (0.1)
calcite	3.8 (0.0)	2.7 (0.1)	3.7 (0.1)	2.1 (0.3)
crystalite	4.4 (0.2)	4.7 (0.2)	6.2 (0.2)	8.7 (0.2)
hydroxyllestadite	4.1(0.1)	3.2 (0.2)	3.8 (0.2)	8.6 (0.2)
quartz	7.8 (0.6)	7.5 (0.5)	5.8 (0.4)	7.6 (0.5)
tobermorite-9 Å	2.4 (0.1)	3.3 (0.6)	3.5 (0.3)	2.2 (0.2)
tobermorite-11 Å	9.5 (0.5)	19.1 (0.4)	20.9 (0.1)	6.1 (0.3)
amorphous content	57.2 (2.0)	49.5 (0.1)	49.7 (0.3)	58.3 (0.2)

Quantitative XRD results obtained by Rietveld refinement were in line with the results of qualitative XRD. **Table 6** demonstrates that for the R75 mix, the total content of tobermorite, i.e., the sum of tobermorite-11 Å and tobermorite-9 Å increased from 11.9 wt. % to 24.4 wt. % (105 %) when the autoclaving temperature was adjusted to 165 °C instead of 192 °C. However, by autoclaving the samples at a lower temperature, i.e. 152 °C, the total content of tobermorite decreased to 8.3 wt. %. A similar variation pattern was observed for the R100 mix. Based on **Table 7**, the total content of tobermorite formed in the R100 mix autoclaved at 192 °C was 9.1 wt. %. This value increased to 21.1 wt. % (131.9 %) and decreased to 5.3 wt. % when the samples were, respectively, autoclaved at 165 °C and 152 °C. For both R75 and R100 mixes, a promotion in tobermorite formation occurred simultaneously with a reduction in amorphous content. In R100, an increase in the content of tobermorite was also accompanied by a reduction in the quantity of hydroxyllestadite and an increase in the total quantity of the sulfate phases, i.e. sum of bassanite and anhydrite quantities. However, for the R75 mix, the quantity of hydroxyllestadite and the total quantity of sulfate phases did not significantly vary as the autoclaving temperature of 165 °C was applied instead of 192 °C. As can be seen in **Table 6** and **Table 7**, for the R75 and the R100 mixes, the total content of tobermorite decreased, amorphous content increased, hydroxyllestadite quantity increased and the total quantity of the sulfate phases decreased as the applied autoclaving temperature was changed from 165 °C to 152 °C.

Table 7 Absolute contents (wt. %) of main phases existing in the R100 mix autoclaved at different temperatures. The results were determined by Rietveld refinement using the internal standard method. Standard deviations of the measurement which was repeated 3 times per specimen are given in parentheses.

phases	192 °C	175 °C	165 °C	152 °C
anhydrite	1.6 (0.1)	1.4 (0.1)	1.0 (0.0)	0.2 (0.0)
bassanite	0.9 (0.1)	2.0 (0.1)	2.9 (0.1)	0.7 (0.0)
calcite	3.9 (0.3)	3.4 (0.1)	3.3 (0.1)	3.6 (0.1)
crystalite	8.6 (0.8)	8.3 (0.3)	8.4 (0.2)	12.0 (0.2)
hydroxyllestadite	5.6 (0.2)	4.2 (0.1)	3.5 (0.1)	7.7 (0.1)
quartz	1.2 (0.2)	1.2 (0.1)	1.3 (0.1)	1.3 (0.1)
tobermorite-9 Å	2.6 (0.4)	2.7 (0.1)	2.5 (0.1)	1.0 (0.4)
tobermorite-11 Å	6.5 (0.4)	15.6 (0.3)	18.6 (0.1)	4.3 (0.0)
amorphous content	63.1 (2.3)	56.2 (0.3)	54.7 (0.2)	64.7 (1.0)

The XRD patterns and the results of the quantitative XRD analysis of the Q100 mix were given in **Figure 13** and **Table 8**, respectively.

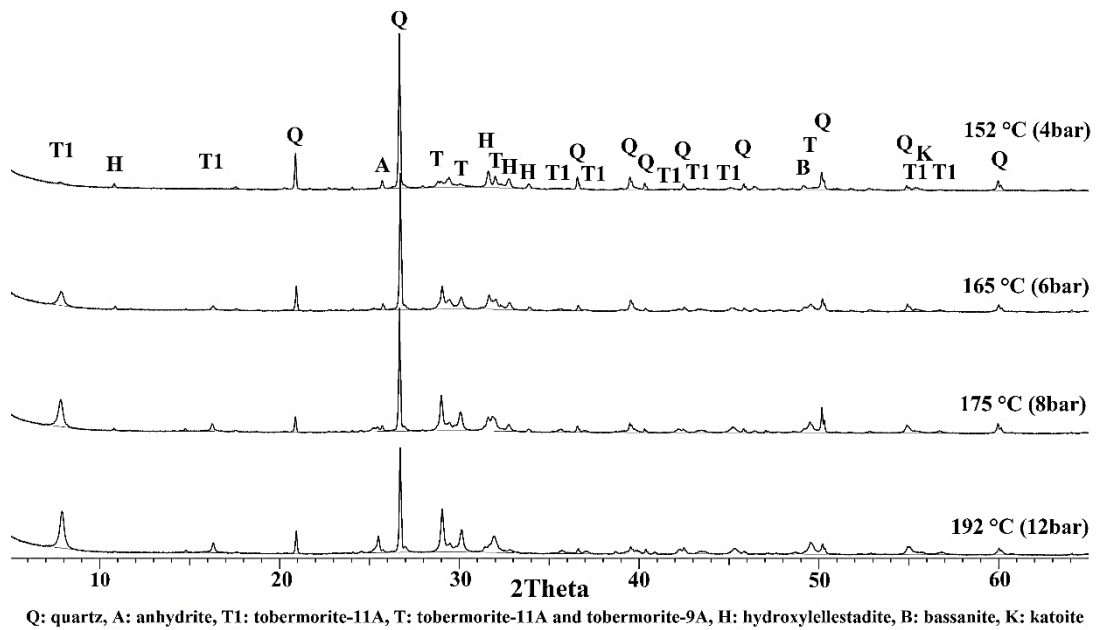


Figure 13 XRD patterns of the Q100 mix autoclaved at different temperatures. (The saturated steam pressure corresponding to each temperature is shown in parentheses).

For the Q100 mix, applying lower autoclaving temperatures than the typical temperature, i.e. 192 °C, affected the intensity of tobermorite diffraction peaks in a significantly negative way. Almost no tobermorite peak can be observed at the temperature of 152 °C. Moreover, according to **Table 8**, the total content of tobermorite decreased from 41.3 wt. % to 9.7 wt. % (76.5 %) and the amorphous content increased from 27.9 wt. % to 47 wt. % (68.5 %), when the samples were autoclaved at the temperature of 152 °C instead of 192 °C. In contrast to the R100 mix, the aforementioned changes were accompanied by an increase in the content of hydroxyllellstadite and a decrease in the total quantity of the sulfate phases.

Table 8 Absolute contents (wt. %) of main phases existing in the Q100 mix autoclaved at different temperatures. The results were determined by Rietveld refinement using the internal standard method. Standard deviations of the measurement which was repeated 3 times per specimen are given in parentheses.

phases	192°C	175°C	165°C	152°C
anhydrite	3.4 (0.3)	0.3 (0.2)	0.0 (0.0)	0.0 (0.0)
bassanite	0.8 (0.1)	1.4 (0.2)	1.2 (0.2)	1.0 (0.0)
calcite	2.8 (0.5)	2.0 (0.2)	1.7 (0.1)	2.4 (0.0)
hydroxyllellstadite	3.0 (0.3)	7.4 (0.0)	7.5 (0.5)	7.7 (0.2)
quartz	15.3 (1.8)	16.6 (1.1)	22.0 (3.3)	25.6 (2.3)
tobermorite-9 Å	4.7 (0.1)	5.4 (0.0)	2.9 (0.5)	3.4 (0.0)
tobermorite-11 Å	36.6 (0.6)	29.0 (0.9)	20.6 (0.3)	6.3 (0.1)
amorphous content	27.9 (3.2)	33.4 (2.3)	36.8 (5.6)	47.0 (2.3)

3.2 Mechanical properties

Figure 14 and **Figure 15** show the variation in the compressive strength and bulk density of the samples after autoclaving at different temperatures, respectively. The compressive strength of the R75 and R100 mixes increased as the autoclaving temperature was set to below 192 °C. On the contrary, the compressive strength of the Q100 mix decreased by applying lower autoclaving temperatures than the typical temperature, i.e. 192 °C. The compressive strength of the R75 mix increased from 3.2 MPa to 3.6 MPa (13 %) when the autoclaving temperature was set to 165 °C instead of 192 °C. For the R100 mix, a higher increase in compressive strength was observed. The compressive strength of the R100 mix increased from 3.2 MPa to 3.9 MPa (22 %) as the

autoclaving temperature decreased from 192 °C to 165 °C. Unlike the RHA-based AAC, the compressive strength of the quartz-based AAC (Q100) decreased from 4.2 MPa to 3.3 MPa (21 %) as the applied autoclaving temperature was changed from 192 °C to 165 °C. A further decrease in the autoclaving temperature from 165 °C to 152 °C caused a decrease in compressive strength for all mixes. For the RHA-based AAC, the autoclaving temperatures of T = 165-175 °C led to the highest compressive strength. However, for the quartz-based AAC, this temperature was T = 192 °C which is within the common range used in the industrial production of AAC.

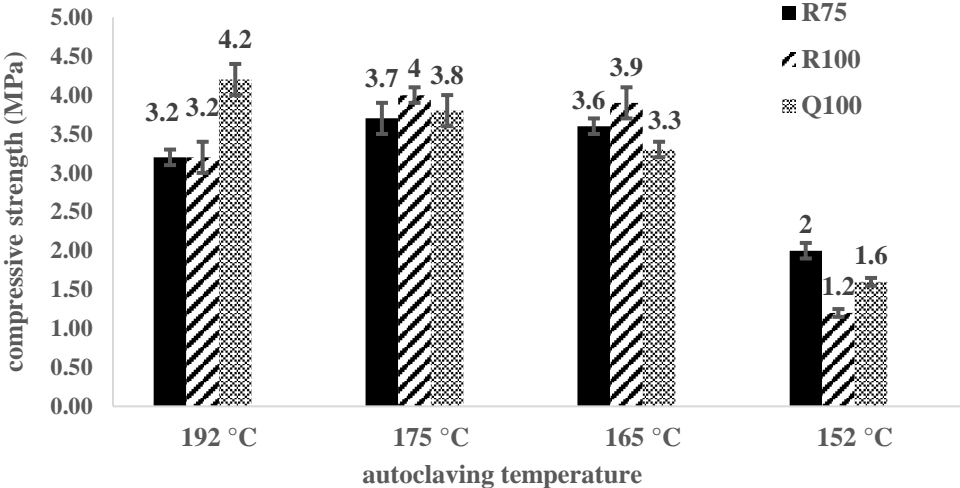


Figure 14 Compressive strength of the AAC specimens autoclaved at different temperatures.

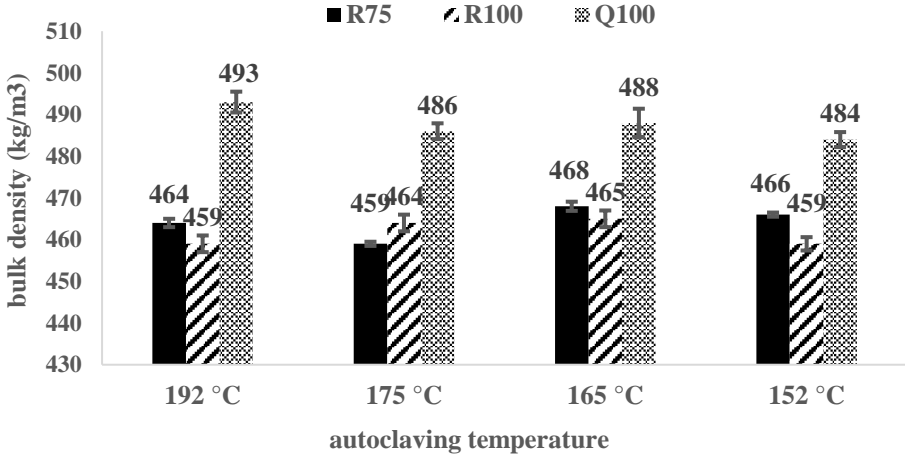


Figure 15 Bulk density of the AAC specimens autoclaved at different temperatures.

The bulk density did not change considerably with applying different autoclaving temperatures between 152 °C to 192 °C. The bulk density of the R75 mix changed by 2 % at the most as the autoclaving temperature decreased from 192 °C to 152 °C. This value was 1.3 % and 1.9 % for the R100 and Q100 mixes respectively.

In order to compare the compressive strength of samples of different mixes, i.e. the compressive strength of samples of the R75 mix with those of the R100 or the Q100 mix, it is needed to use a figure of merit called A-value of AAC which is defined by Eq. (1) [11].

$$A\text{-value} = \frac{\text{compressive strength}}{(\text{bulk density})^2 * 0.016} \quad (1)$$

Where compressive strength is given in N/mm² and bulk density in kg/dm³.

A-value is a dimensionless parameter of compressive strength which is used to compare the compressive strength of the samples with different bulk densities in the range from 400 to 750 kg/m³. In fact, when it is not possible to compare a set of samples with each other because of different bulk density values, this relation can be used to compare the strength quality of samples. The A-value is between 600 and 1400 for standard AAC products [11].

Since the bulk density of samples of the R75, R100 and Q100 mixes are not equal to each other, the A-value is used to compare the quality of the samples considering compressive strength. The A-values of the samples at different autoclaving temperatures are given in **Figure 16**. According to this figure, the A-value of the R75 (1027) and R100 (1127) mixes autoclaved at 165 °C are close to that of the Q100 mix autoclaved at 192 °C (1080). This implies that when RHA, which is an agricultural waste product, is used in the AAC mixture, a lower level of energy could be required to meet the specific A-value of an AAC product.

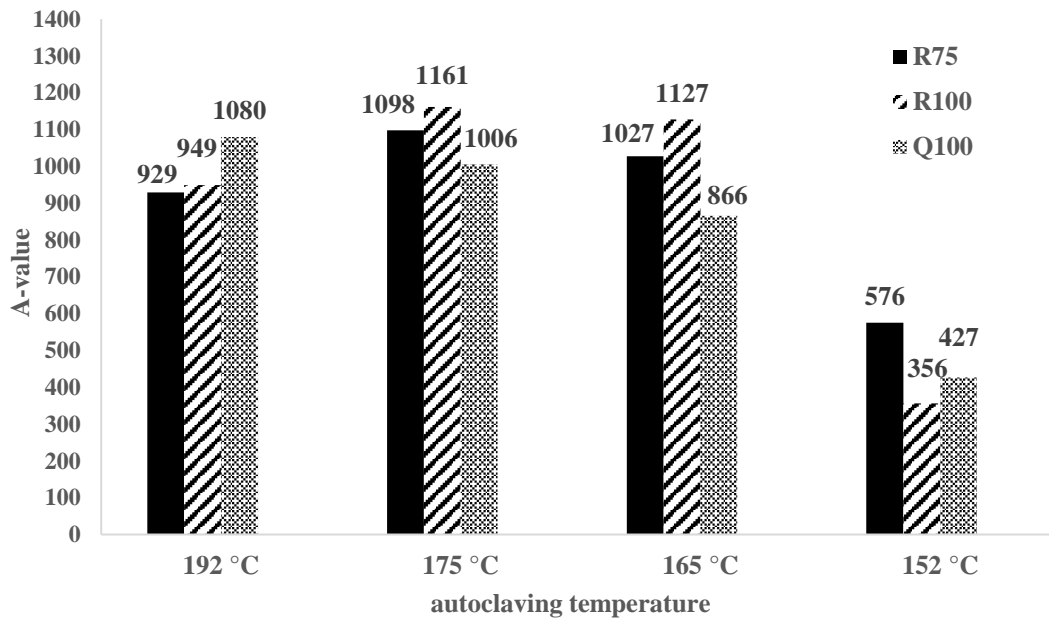


Figure 16 A-values of the AAC specimens autoclaved at different temperatures.

3.3 Scanning electron microscopy (SEM)

Figures 17-19 show changes in the microstructure of the samples as a result of changing the autoclaving temperature. Autoclaving samples at different temperatures led to similar changes in the microstructure of the R75 and R100 mixes. In the SEM image of the R75 and R100 mix autoclaved at 192 °C (**Figure 17, a** and **Figure 18, a**), the non-crystalline C-S-H with a fibrous felted structure can be observed. However, the SEM image of those mixes autoclaved at 165 °C (**Figure 17, b** and **Figure 18, b**) display the appearance of lath-like tobermorite in the samples. The results of quantitative and qualitative XRD are consistent with the above-mentioned results.

According to **Figure 19, a**, needle-like tobermorite was formed in the Q100 mix autoclaved at 192 °C. **Figure 19, b** shows a type of non-crystalline C-S-H which might be one or several steps before tobermorite formation. As can be seen in **Figure 19, b**, this kind of pre-tobermorite phase was mostly not crystallized to tobermorite at the autoclaving temperature of 165 °C except in some small areas in which needle-like tobermorite can be seen. Additionally, unreacted quartz can also be observed in **Figure 19, b**. This is in line with the XRD results

where a decrease in the autoclaving temperature from 192 °C to 165 °C was followed by a decrease in tobermorite and an increase in amorphous content and the quantity of unreacted quartz.

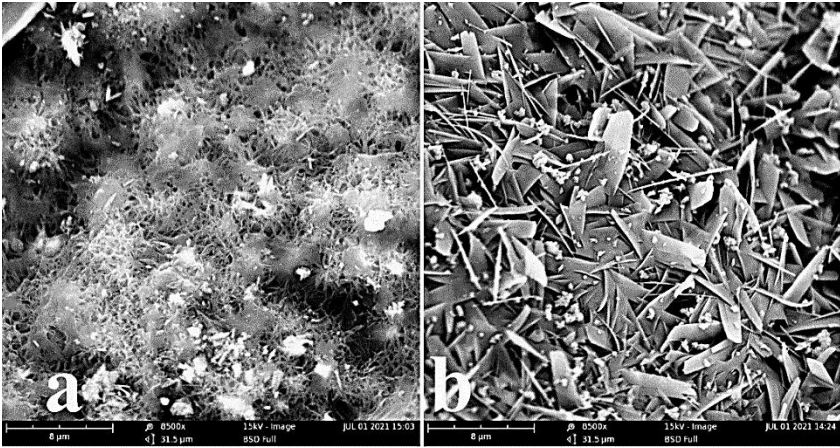


Figure 17 SEM images of the R75 mix autoclaved at 192 °C (a: non-crystalline C-S-H) and 165 °C (b: lath-like tobermorite). The scale bar: 8 μm, magnification level: 8500×

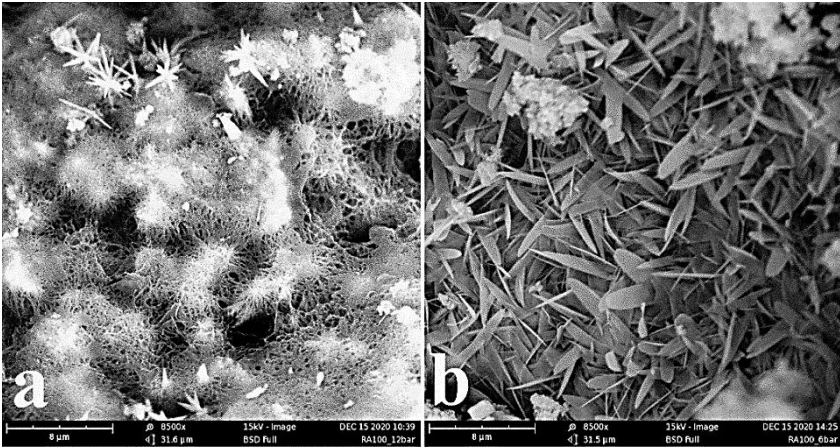


Figure 18 SEM images of the R100 mix autoclaved at 192 °C (a: non-crystalline C-S-H) and 165 °C (b: lath-like tobermorite). The scale bar: 8 μm, magnification level: 8500×

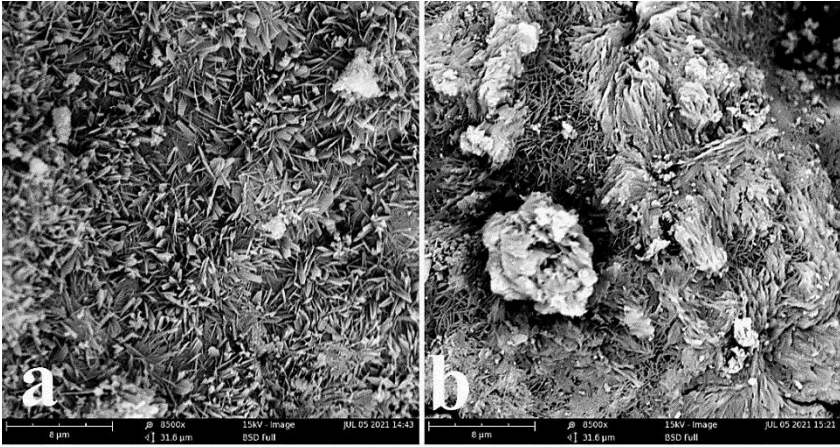


Figure 19 SEM images of the Q100 mix autoclaved at 192 °C (a: needle-like tobermorite) and 165 °C (b: non-crystalline C-S-H). The scale bar: 8 μm, magnification level: 8500×

3.4 Shrinkage

The relative change in dimensions, during storage in the air not saturated with humidity, is known as drying shrinkage [74]. In AAC, all microstructure regions which contain capillaries partly filled with water are compressed by the air pressure as a consequence of loss of moisture. This leads to capillary suction which eventually could result in cracks [75]. In general, AAC has a higher shrinkage compared to ordinary concrete since its mixture contains a minor amount of very fine aggregates.

The Variations of relative change in length with time for the R75, R100, and Q100 mixes are shown in **Figures 20-22**, respectively. According to those figures, R75 and R100 mixes autoclaved at the temperature of 165 °C showed a lower drying shrinkage compared to those autoclaved at 192 °C. On the contrary, the drying shrinkage of the Q100 mix autoclaved at 165 °C was found to be higher than that autoclaved at 192 °C.

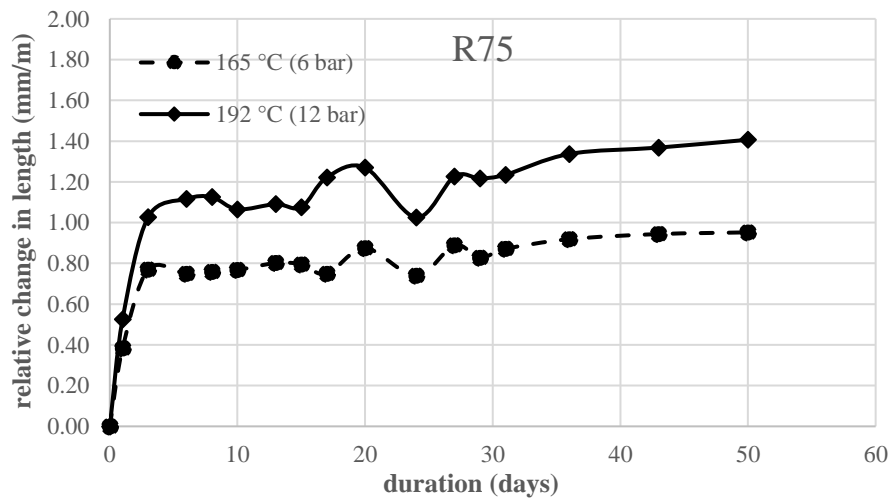


Figure 20 Variation of the relative change in length (ϵ_{csi}) with time for the R75 mix.

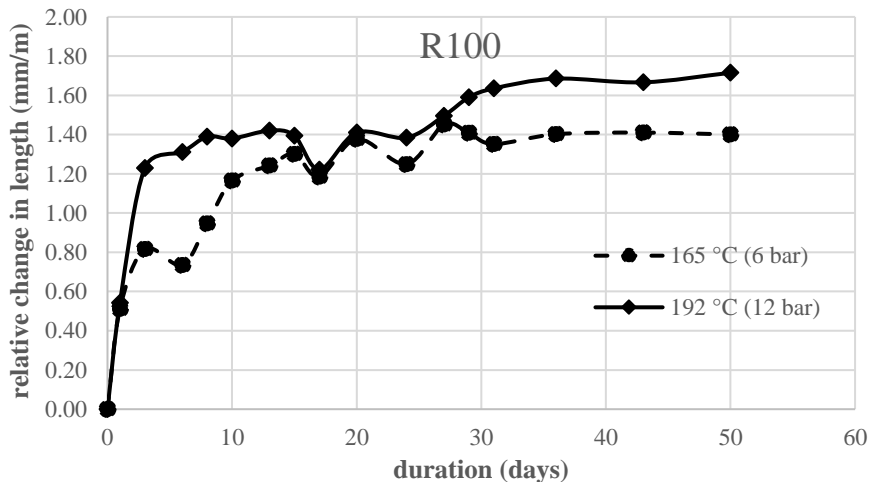


Figure 21 Variation of the relative change in length (ϵ_{csi}) with time for the R100 mix.

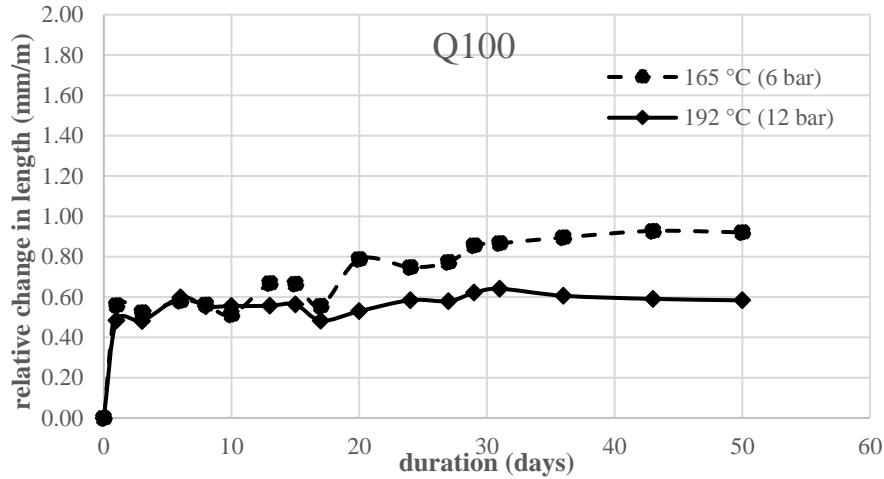


Figure 22 Variation of the relative change in length (ϵ_{csi}) with time for the Q100 mix.

The total values of drying shrinkage are given in **Table 9**. For the R75 mix, the total drying shrinkage decreased from 1.41 mm/m to 0.95 mm/m (33 %) when the samples were autoclaved at 165 °C instead of 192 °C. For the R100 mix, a smaller reduction in total dry shrinkage was observed. The total drying shrinkage of the R100 mix decreased from 1.72 mm/m to 1.40 mm/m (19 %) as the applying autoclaving temperature was changed from 192 °C to 165 °C.

Table 9 Total value of drying shrinkage, $\epsilon_{\text{cs, tot}}$ (mm/m).

mix	Q100		R75		R100	
	192 °C	165 °C	192 °C	165 °C	192 °C	165 °C
$\epsilon_{\text{cs, tot}}$	0.58	0.92	1.41	0.95	1.72	1.40

Although the drying shrinkage of R75 and R100 mixes decreased as the result of applying a lower autoclaving temperature, the values were still higher than that of the Q100 mix autoclaved at 192 °C which is conventionally produced in the industry. The Q100 mix autoclaved at 192 °C exhibited a drying shrinkage of 0.58 mm/m which increased to 0.92 mm/m as the autoclaving temperature of 165 °C was applied. In general, a comparison of values shows a higher drying shrinkage of the RHA-based AAC compared to the quartz-based AAC.

4. Discussion

4.1 X-ray diffraction analysis (XRD)

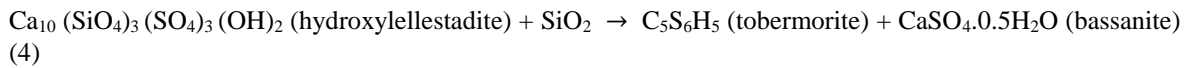
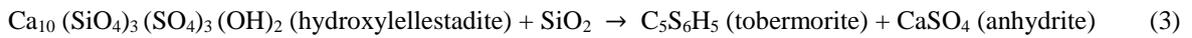
As shown in the results section, for the R75 and R100 mixes, the tobermorite content increased and the amorphous content decreased when the autoclaving temperature of 165 °C was applied instead of 192 °C. This is possibly caused by promoting the transition from non-crystalline C-S-H to tobermorite according to reaction Eq. (2) [15].



The reason for promoting the above transformation could trace back to the lower solubility and dissolution rate of RHA as a result of autoclaving samples at a lower temperature of 165 °C instead of 192 °C [29]. As was expected, applying a lower autoclaving temperature decreases the solubility of RHA which reduces the diffusion of SiO_4^{4-} to the matrix and avoids progressive polymerization of silicate chains. Subsequently, C/S

of non-crystalline C-S-H which are formed at the initial stages of the hydrothermal treatment increases. This means that initial non-crystalline C-S-H formed at the autoclaving temperature of 165 °C have likely higher C/S compared to those formed at the autoclaving temperature of 192 °C. On the other hand, according to literature, C-S-H phases with a higher C/S have short silicate chains and a lower degree of polymerization which implies that they could rearrange to tobermorite at a higher rate [40, 31, 76, 77]. Therefore, the R75 mix autoclaved at 165 °C contains a higher quantity of tobermorite and a lower amorphous content compared to that autoclaved at 192 °C.

There exist other pathways for tobermorite formation which may favor the formation of C-S-H with a higher C/S by applying lower autoclaving temperature. In R100, an increase in the total content of tobermorite was also accompanied by a reduction in the quantity of hydroxyllellstadite and an increase in the total quantity of the sulfate phases, i.e. the sum of bassanite and anhydrite quantities. This might be due to promoting the reaction of dissolved silica with hydroxyllellstadite which generates tobermorite and either or both of the sulfate phases which can be described by the reaction Eqs. (3) and (4) [15, 78].



The main influence of hydrothermal treatment is dissolving silica and speeding up ongoing reactions, such as the C-S-H formation. Moreover, it leads to the formation of new phases including hydroxyllellstadite. Hydroxyllellstadite is a high-lime product which is formed through the reaction of the calcium sulfate phases (anhydrite, gypsum, and bassanite) with lime and SiO₂ according to reaction Eq. (5) [15]. In this study, anhydrite is the main calcium sulfate phase which results in the hydroxyllellstadite formation.



The formed hydroxyllellstadite reacted with the remaining SiO₂ and was further decomposed into tobermorite and either or both of the sulfate phases, i.e. bassanite and anhydrite which was described by the reaction Eqs. (3) and (4) [15, 78]. Factors that determine which of those mentioned sulfate phases will be formed at the end of the reaction are the availability of water in the medium, the temperature, and the salinity of the solution [79, 80]. This is another pathway for crystallization of tobermorite under hydrothermal conditions which might occur in the R100 mix as the lower autoclaving temperature of 165 °C was applied instead of 192 °C. However, this might not be a source of tobermorite formation in the R75 mix since in this mix hydroxyllellstadite quantity and the total quantity of the sulfate phases did not significantly vary as the autoclaving temperature decreased from 192 °C to 165 °C. The probable cause is that the R100 mix contains a higher amount of more soluble silica compared to the R75 mix. Thus, there will be more dissolved silica (SiO₂) available to react with hydroxyllellstadite in the R100 mix. A higher amount of unreacted SiO₂ in the R75 mix autoclaved at 165 °C, i.e. the quantity of cristobalite and quartz at 165 °C in Fig. 6, compared to that in the R100 mix autoclaved at 165 °C, i.e. quantity of cristobalite and quartz at 165 °C in Fig. 7, verifies the above reasoning as well.

Tobermorite was probably formed through the crystallization of C-S-H to tobermorite and also the decomposition of hydroxyllellstadite in the R100 mix when the autoclaving temperature decreased from 192 °C to 165 °C. However, crystallization of C-S-H might be the main source of tobermorite formation in the R75 mix. This can be a possible reason for the higher increase in tobermorite content in the R100 mix (131.9 %) compared to that in the R75 mix (105 %). In the previous study, it was reported that lowering the autoclaving temperature from 192 °C to 165 °C caused an increase of 60 % in the total content of tobermorite in the C-DE-based AAC [40] which is lower than that in RHA-based AAC. The reason could be attributed to the different dissolution properties of the C-DE and RHA. A comparison of amorphous content, SEM images, specific surface areas, as well as water demand of RHA with those of C-DE, indicates that C-DE has a higher solubility and faster dissolution than RHA. This could cause a greater rate of supplying Si at the initial stage of the hydrothermal treatment into the C-DE mix compared to the RHA mix. Lower unreacted cristobalite which

remained in the C-DE-based AAC [40] compared to the RHA-based at all autoclaving temperatures confirms the aforementioned understanding. A higher rate of supplying Si would lead to the initially formed C-S-H with a higher degree of polymerization and as a result a lower increase in tobermorite content in the C-DE-based AAC compared to that in the RHA-based AAC.

As stated in the results section, for the R75 and R100 mixes, the total content of tobermorite decreased and amorphous content increased as the autoclaving temperature was set to 165 instead of 152 °C. For the RHA-based AAC, temperatures below 165 °C might lead to a silica dissolution behavior which does not support the transition to tobermorite. A higher quantity of quartz and cristobalite which remained unreacted in the R75 and R100 samples autoclaved at the temperature of 152 °C, supports the aforementioned explanation. For the C-DE-based AAC, the same temperature range, i.e. $T < 165$ °C, led to a slight reduction in the total content of tobermorite [40]. However, unlike the RHA-based AAC, autoclaving at temperatures below 165 °C did not affect cristobalite content considerably in the C-DE-based AAC [40]. This indicates the higher solubility of C-DE used in the previous study compared to RHA used in the present study.

Moreover, for the R75 and R100 mixes, hydroxyllestadite quantity increased and the total quantity of the sulfate phases decreased as a result of decreasing the autoclaving temperature from 165 to 152 °C. This could be due to the suppression of the hydroxyllestadite decomposition into tobermorite and the sulfate phases as a result of a reduction in the dissolution of silica (Eqs. (3) and (4)).

The above results demonstrate that for the RHA-based AAC, an adequate adaptation of the autoclaving temperature is required to achieve the optimum tobermorite formation. This outcome is in line with the results of the previous study [40], in which adjusting the autoclaving temperature to adequately low values accelerated tobermorite formation in the C-DE-based AAC.

The result of the Q100 mix showed a decrease in the total content of tobermorite and an increase in the amorphous content as the autoclaving temperature was reduced from 192 °C to 152 °C. This implies that non-crystalline C-S-H did not transit to tobermorite at a high rate as lower autoclaving temperatures than the typical one (192 °C) were applied. This result is in accordance with the result of studies carried out by Mitsuda et al. [17] and Chen et al. [23] in which the amount of 1.1-nm tobermorite and crystallinity increased with further autoclaving. Moreover, a decrease in the total content of tobermorite occurred simultaneously with an increase in the quantity of hydroxyllestadite and a decrease in the total quantity of the sulfate phases. The possible cause attributed to this is similar to what was discussed earlier. The decomposition of hydroxyllestadite (Eqs. (3) and (4)) was suppressed since the quartz was not dissolved to a sufficient extent at low autoclaving temperatures. A higher amount of quartz which was left unreacted and did not react with hydroxyllestadite confirms this understanding.

For the RHA-based AAC, the optimum autoclaving temperature for tobermorite formation was $T = 165\text{--}175$ °C with an autoclaving duration of 6 h. This temperature was $T = 152\text{--}165$ °C and $T = 192$ °C with the same duration for the C-DE-based AAC and quartz-based AAC, respectively. This implies that in the case of using a silica material with different dissolution properties from that of quartz sand in the AAC mixture applying the typical autoclaving temperature will not necessarily lead to the optimum tobermorite formation and indeed the optimum autoclaving temperature for tobermorite formation will likely be changed.

4.2 Mechanical properties

As reported in the result section, changing the autoclaving temperature affected the compressive strength of samples for all mixes. In order to compare the compressive strength of several samples with each other, it is needed to consider the effect of density. The bulk density of samples of each mix, e.g. samples of R100 mix autoclaved at various autoclaving temperatures, did not change significantly when different autoclaving temperatures between 152 °C and 192 °C were applied. Therefore, the difference in the compressive strength values of samples of each mix is not because of the difference in bulk density but rather due to the change in the proportion of C-S-H and other hydrothermal products of samples. This agrees with the XRD results where changing the autoclaving temperature affected the hydrothermal products and proportion of C-S-H in all mixes.

For the R75 and the R100 mixes, the highest compressive strength was obtained at the autoclaving temperature of $T = 165\text{--}175$ °C. This shows that in the R75 and the R100 mixes, the microstructure, e.g. the proportion of different C-S-H might approach the optimum effectiveness when the autoclaving temperature is in the range

of $T = 165\text{-}175\text{ }^{\circ}\text{C}$. For the quartz-based AAC, the optimum microstructure might be acquired by autoclaving at $T = 192\text{ }^{\circ}\text{C}$. For all specimens, an increase in compressive strength occurred with an increase in the total content of tobermorite which is in accordance with the results of numerous studies [3, 28, 26, 16, 17] which reported obtaining a higher compressive strength as a result of an increase in tobermorite quantity.

The A-values of the R75 and R100 mixes autoclaved at $165\text{ }^{\circ}\text{C}$ are almost the same as that of the Q100 mix autoclaved at $192\text{ }^{\circ}\text{C}$. This shows that the existing difference in the compressive strength of these samples is simply due to the difference in density since comparison with the subtraction of density effect, i.e. A-value comparison, shows almost equal strength quality. Thus, the strength to density ratio of the R75 and R100 autoclaved at $165\text{ }^{\circ}\text{C}$ are almost the same as that of Q100 autoclaved at $192\text{ }^{\circ}\text{C}$ in spite of the distinct difference in tobermorite content. The R75 and R100 autoclaved at $165\text{ }^{\circ}\text{C}$ contain 24.4 wt. % and 21.1 wt. % tobermorite, respectively. While the tobermorite content of the Q100 mix autoclaved at $192\text{ }^{\circ}\text{C}$ is about two times higher (41.3 wt. %). This indicates that the tobermorite content might not be the only determining factor for compressive strength. In addition to tobermorite, other C-S-H phases also act as the binding phases in the microstructure. Thus, the microstructure, the proportion of tobermorite and other C-S-H, and the way they are interconnected to each other might affect compressive strength considerably. This is in line with the results of other studies [7, 26, 46] which have shown that in addition to a high content of tobermorite, a homogeneous distribution of the tobermorite crystals in the solid structure is required to obtain optimum strength properties. In the R75 and R100 mixes autoclaved at $165\text{ }^{\circ}\text{C}$, around 20-25 wt. % tobermorite and 50-55 wt. % amorphous content resulted in a microstructure which led to a strength equal to that provided by the microstructure of the Q100 mix autoclaved at $192\text{ }^{\circ}\text{C}$ which contains around 41 wt. % tobermorite and 28 wt. % amorphous content. This implies that there might exist an optimum proportion of different C-S-H for each type of the mix which leads to the high compressive strength of the AAC product. On the other hand, an optimum mix in the previous study [40], which had comparatively high compressive strength at 165°C , contained 52 wt. % amorphous content and around 19 wt. % tobermorite. In this study, the R75 and R100 mix autoclaved at $165\text{ }^{\circ}\text{C}$ contain almost the same proportion of C-S-H phases, i.e. around 50-55 wt. % amorphous content including non-crystalline C-S-H and around 20-25 wt. % tobermorite. This implies that the proportion of around 50 wt. % non-crystalline C-S-H and 20 wt. % tobermorite might be close to the optimum proportion for compressive strength of AAC products containing silica materials of a higher solubility, e.g. C-DE and RHA, as the silica raw material. This optimum proportion will be achieved by applying adequately low autoclaving temperature, i.e. a temperature which is significantly lower than that required for autoclaving the quartz-based AAC.

4.3 Scanning electron microscopy (SEM)

As reported in the result section, a high amount of non-crystalline C-S-H with a fibrous felted structure was formed in the R75 and R100 mixes when the autoclaving temperature is $192\text{ }^{\circ}\text{C}$. The formed non-crystalline C-S-H is probably a kind of C-S-H of a low C/S ratio, i.e. $C/S < 0.8$ [3, 81] because RHA has a comparatively high rate of Si dissolution. A comparable result was obtained in other studies [63, 25], in which rice husk ash and slag were used in the AAC mixture. Those studies also pointed out that the C-S-H formed had a very low C/S ratio [63, 25].

In the R75 and R100 mixes autoclaved at $165\text{ }^{\circ}\text{C}$, lath-like tobermorite was formed while tobermorite formed in the Q100 mix autoclaved at $192\text{ }^{\circ}\text{C}$ was a type of needle-like. The difference in the micro-morphology of these crystalline phases is due to the difference in the C/S ratio [3]. It is reported that C-S-H crystallizes to needle-like tobermorite at a C/S ratio > 1 . However, the C/S ratio decreases with the enlargement of tobermorite, e.g. from 1.69 to 0.9, which leads to the formation of plate-like and crumbled foiled tobermorite [3, 82]. Therefore, the C/S of lath-like tobermorite is probably lower than that of needle-like since lath-like tobermorite, which appeared in the R75 and R100 mixes autoclaved at $165\text{ }^{\circ}\text{C}$, exhibits wider crystals compared to needle-like tobermorite formed in the Q100 mix autoclaved at $192\text{ }^{\circ}\text{C}$. This implies that the C/S of the matrix in the R75 and R100 mixes autoclaved at $165\text{ }^{\circ}\text{C}$ might be still lower than that of Q100 autoclaved at $192\text{ }^{\circ}\text{C}$. This shows a higher Si supply in the R75 and R100 mixes autoclaved at $165\text{ }^{\circ}\text{C}$ compared to the Q100 mix autoclaved at $192\text{ }^{\circ}\text{C}$ which could be due to the higher solubility and dissolution rate of RHA even at a lower temperature, i.e. $165\text{ }^{\circ}\text{C}$ compared to that of quartz at the temperature of $192\text{ }^{\circ}\text{C}$. This finding is also confirmed by the results of XRD where a lower amount of unreacted SiO_2 was observed in the R75 and R100 mixes autoclaved at $165\text{ }^{\circ}\text{C}$ (cristobalite + quartz in **Tables 6 and 7**) compared to the Q100 mix autoclaved at $192\text{ }^{\circ}\text{C}$.

4.4 Shrinkage

As reported in the result section, changing the autoclaving temperature affected the shrinkage of samples for all mixes. The drying shrinkage of the quartz-based AAC autoclaved at 165 °C was approximately 59 % higher than that autoclaved at 192 °C. This is an expected behavior since the quartz-based AAC autoclaved at 165 °C contained a lower quantity of tobermorite and a higher amorphous content compared to that autoclaved at 192 °C. It is widely known that the autoclaving process reduces the shrinkage of quartz-based AAC by supporting the formation of well-crystallized C-S-H [83–85, 3].

RHA-based AAC demonstrates a contrary shrinkage behavior to quartz-based AAC. The drying shrinkage of the R75 and R100 mixes autoclaved at 165 °C was approximately 33 % and 19 % lower than those autoclaved at 192 °C. It has been reported that the shrinkage of AAC mainly depends on the volume and the specific surface of micro-pores [86, 87]. The high porosity and the high specific surface of the pores are responsible for the high drying shrinkage of AAC [86, 88]. On the other hand, increasing the degree of crystallinity is accompanied by a lower specific surface area and a lower portion of micro-pores. Therefore, a higher degree of crystallinity and a lower proportion of non-crystalline C-S-H lead to a lower shrinkage [18, 83, 41]. This confirms the findings on the shrinkage behavior of RHA-based AAC considering a higher amount of tobermorite and lower amorphous content at 165 °C compared to 192 °C.

The shrinkage of RHA-AAC improved by virtue of applying lower autoclaving temperature. However, similar shrinkage as that of the quartz-based AAC autoclaved at 192 °C could not be achieved. The reason attributes to the increase in amorphous content as the result of replacing quartz sand with RHA in the AAC mixture. In general, the optimum value of drying shrinkage of the RHA-based AAC was approximately 1.6 times higher than that of the quartz-based AAC. Similar observations have been reported by Ramamurthy et al. [88]. The findings of the aforementioned study demonstrate that the shrinkage of the fly ash-based AAC was 5-7 times higher than that of the quartz-based AAC.

5. Conclusion

This study demonstrates that the RHA-based AAC exhibited a different behavior compared to the quartz-based AAC at different autoclaving temperatures. This implies that the optimum temperature for autoclaving AAC has a direct dependency on the dissolution properties of silica raw materials used in the mixture. In contrast to the quartz-based AAC, the properties of RHA-based AAC have been improved by applying a lower autoclaving temperature compared to the conventional temperature, i.e. 192 °C. For the RHA-based AAC, applying an autoclaving temperature of 165 °C instead of 192 °C (27 °C lower) was followed by

- a maximum increase of 22 % in compressive strength,
- a maximum increase of 131.9 % in the total content of tobermorite,
- a maximum increase of 19 % in the A-value,
- a maximum decrease of 33 % in the total value of drying shrinkage,
- a changing of the surface structure by transforming non-crystalline C-S-H to lath-like tobermorite.

This implies that the opportunity to reduce energy consumption during hydrothermal treatment is not limited to calcined diatomaceous earth (C-DE) material, but can potentially be achieved by other silica raw materials with comparable dissolution properties in alkaline systems.

Moreover, using RHA as an agricultural waste product in the AAC mixture results in an improvement in the material efficiency of the product, the conservation of quartz sand resources as the quarried natural resources, and a reduction in electricity consumption by removing the milling process of quartz sand.

The RHA-based AAC autoclaved at 165 °C had a slightly higher compressive strength to density ratio, which was expressed using A-value, compared to the quartz-based AAC autoclaved at 192 °C. However, the RHA-based AAC autoclaved at 165 °C exhibited a higher total drying shrinkage because it contained a higher proportion of non-crystalline C-S-H compared to the quartz-based AAC autoclaved at 192 °C. This might be an issue for some applications in which it is needed to fulfill shrinkage requirements in addition to the strength and density grades.

Funding and Conflicts of interests

This research was financially supported by the Fraunhofer Institute for Building Physics IBP. The authors have no relevant financial or non-financial interests to disclose.

References

- [1] Nunez E, Nunez SA, Fouad, FH, "Sustainability in Autoclaved Aerated Concrete (AAC) construction," In *Autoclaved Aerated Concrete, Innovation and Development*, C. Mukesh, M. C. Limbachiya, and J. J. Roberts, eds., Taylor & Francis Group, London, pp. 531–537, 2005.
- [2] Lutter J, "New research on the primary energy content of building materials," In *Advances in Autoclaved Aerated Concrete*, Witmann FH, ed., Balkema, Zurich, pp. 277–282, 1992.
- [3] Qu X, Zhao X, "Previous and present investigations on the components, microstructure and main properties of autoclaved aerated concrete – A review," *Constr. Build. Mater.*, V. 135, pp. 505–516, 2017.
- [4] Karakurt C, Kurama H, Topcu IB, "Utilization of natural zeolite in aerated concrete production," *Cement and Concrete Composites*, V. 32, No. 1, pp. 1–8, 2010.
- [5] Stumm A, "Cement and sulphate free autoclaved aerated concrete," In *5th International Conference on Autoclaved Aerated Concrete "Securing a Sustainable Future"*, D. Boroński, ed., University of Technology and Life Sciences Press, pp. 375–381, 2011.
- [6] Chucholowski C, Holger M, Thienel K-C, "Improving the recyclability, environmental compatibility, and CO₂ balance of autoclaved aerated concrete by replacing sulfate carrier and cement with calcined clays," *ce/papers*, V. 2, No. 4, pp. 503–512, 2018.
- [7] Mesecke K, "Untersuchungen zur Phasenbildung und Gefügeentwicklung bei der hydrothermalen Härtung von Porenbeton mittels in situ-Röntgendiffraktometrie mit dem Ziel der Sulfatreduzierung und Prozessoptimierung," 19464 BR / 1, 2020.
- [8] Valore JR, Rudolph C, "Cellular Concretes Part 1 Composition and Methods of Preparation," *Journal Proceedings*, V. 50, No. 5, pp. 773–796, 1954.
- [9] Aroni S, Groot GJ, Robinson MJ, Svanholm G, Wittman FH, "Autoclaved Aerated Concrete - Properties, Testing and Design: RILEM Recommended Practice RILEM Technical Committees 78-MCA and 51-ALC E," Taylor & Francis, 2004.
- [10] Kreft O, "Closed-loop recycling of autoclaved aerated concrete / Geschlossener Recyclingkreislauf für Porenbeton," *Mauerwerk*, V. 20, No. 3, pp. 183–190, 2016.
- [11] Schober G, "The most important aspects of microstructure influencing strength of AAC," In *Autoclaved Aerated Concrete, Innovation and Development*, C. Mukesh, M. C. Limbachiya, and J. J. Roberts, eds., Taylor & Francis Group, London, pp. 145–153, 2005.
- [12] Schober G, "Porosity in autoclaved aerated concrete (AAC): A review on pore structure, types of porosity, measurement methods and effects of porosity on properties," In *5th International Conference on Autoclaved Aerated Concrete "Securing a Sustainable Future"*, D. Boroński, ed., University of Technology and Life Sciences Press, pp. 351–359, 2011.
- [13] Kadashevich I, Schneider HJ, Stoyan D, "Statistical modeling of the geometrical structure of the system of artificial air pores in autoclaved aerated concrete," *Cement and Concrete Research*, V. 35, No. 8, pp. 1495–1502, 2005.
- [14] Ioannou I, Hamilton A, Hall C, "Capillary absorption of water and n-decane by autoclaved aerated concrete," *Cement and Concrete Research*, V. 38, No. 6, pp. 766–771, 2008.
- [15] Schober G, "Chemical transformations during the manufacturing of autoclaved aerated concrete (ACC): Cement, lime, gypsum and quartz sand become cellular concrete: Die chemischen Umsetzungen bei der Herstellung von Porenbeton: Aus Zement, Kalk, Gips und Quarzsand wird Porenbeton," *ZKG international*, V. 58, No. 7, pp. 63–70, 2005.
- [16] Isu N, Ishida H, Mitsuda T, "Influence of quartz particle size on the chemical and mechanical properties of autoclaved aerated concrete (I) tobermorite formation," *Cem. Concr. Res.*, V. 25, No. 2, pp. 243–248, 1995.
- [17] Mitsuda T, Sasaki K, Ishida H, "Phase evolution during autoclaving process of aerated concrete," *Journal of the American Ceramic Society*, V. 75, No. 7, pp. 1858–1863, 1992.
- [18] Alexanderson J, "Relations between structure and mechanical properties of autoclaved aerated concrete," *Cement and Concrete Research*, V. 9, No. 4, pp. 507–514, 1979.
- [19] Mitsuda T, Chan CF, "Anomalous tobermorite in autoclaved aerated concrete," *Cement and Concrete Research*, V. 7, No. 2, pp. 191–194, 1977.
- [20] Taylor HFW, "Cement chemistry," Thomas Telford, 1997, ISBN: 0727725920.
- [21] Taylor HF, "Proposed Structure for Calcium Silicate Hydrate Gel," *Journal of the American Ceramic Society*, V. 69, No. 6, pp. 464–467, 1986.
- [22] SNELL DS, "Review of Synthesis and Properties of Tobermorite, C-S-H(I), and C-S-H Gel," *Journal of the American Ceramic Society*, V. 58, 7-8, pp. 292–295, 1975.

- [23] Chen Y, Chang J, Lai Y, Chou M, “A comprehensive study on the production of autoclaved aerated concrete: Effects of silica-lime-cement composition and autoclaving conditions,” *Construction and Building Materials*, V. 153, pp. 622–629, 2017.
- [24] Kalousek GL, PREBUS AF, “Crystal Chemistry of Hydrous Calcium Silicates: III, Morphology and Other Properties of Tobermorite and Related Phases,” *Journal of the American Ceramic Society*, V. 41, No. 4, pp. 124–132, 1958.
- [25] Mostafa NY, “Influence of air-cooled slag on physicochemical properties of autoclaved aerated concrete,” *Cement and Concrete Research*, V. 35, No. 7, pp. 1349–1357, 2005.
- [26] Isu N, Teramura S, Ishida H, Mitsuda T, “Influence of quartz particle size on the chemical and mechanical properties of autoclaved aerated concrete (II) fracture toughness, strength and micropore,” *Cement and Concrete Research*, V. 25, No. 2, pp. 249–254, 1995.
- [27] Crennan J. M., Dyczek J. R. L., Taylor H.F.W, “Quantitative phase compositions of autoclaved cement-quartz cubes,” *Cement and Concrete Research*, V. 2, No. 3, pp. 277–289, 1972.
- [28] Narayanan N, Ramamurthy K, “Structure and properties of aerated concrete: a review,” *Cem. Concr. Composites*, V. 22, No. 5, pp. 321–329, 2000.
- [29] Iler RK, “The Chemistry of Silica: Solubility, Polymerization, Colloid and Surface Properties and Biochemistry of Silica,” Wiley, London, 1979, ISBN: 978-0-471-02404-0.
- [30] Kalousek G, “Tobermorite and Related Phases in the System CaO-SiO₂-H₂O,” *Journal Proceedings*, V. 51, No. 6, pp. 989–1011, 1955.
- [31] Sato H, Grutzeck M, “Effect of Starting Materials on the Synthesis of Tobermorite | MRS Online Proceedings Library (OPL) | Cambridge Core,” *Material research society*, V. 245, pp. 235–240, 1992.
- [32] Okada Y, Shimoda M, Mitsuda T, Toraya H, “Synthesis of tobermorite: NMR spectroscopy and analytical electron microscopy,” *Journal of research of the Onoda Cement Company*, V. 42, No. 2, pp. 199–206, 1990.
- [33] Okada Y, Ishida E. H., Mitsuda T, “²⁹Si NMR spectroscopy of silicate anions in hydrothermally formed CSH,” *Journal of the American Ceramic Society*, V. 77, No. 3, pp. 765–768, 1994.
- [34] Chan CF, Mitsuda T, “Formation of 11 A Tobermorite from Mixtures of Lime and Colloidal Silica with Quartz,” *Cement and Concrete Research*, V. 8, pp. 135–138, 1978.
- [35] Gundlach H, “Dampfgehärtete Baustoffe,” Wiesbaden, Berlin, 1973.
- [36] Carroll RA, “Hydrothermal performance of pulverised fuel ash and the manufacture of autoclaved aerated concrete,” (Doctoral dissertation, © Robert A. Carroll), 1996.
- [37] Schober G, “Porenbetonherstellung - Ist-Zustand und mögliche Verbesserungen,” *BFT International*, No. 12, pp. 4–11, 2007.
- [38] Matsui K, Kikuma J, Tsunashima M, Ishikawa T, Matsuno S, Ogawa A, Sato M, “In situ time-resolved X-ray diffraction of tobermorite formation in autoclaved aerated concrete: Influence of silica source reactivity and Al addition,” *Cement and Concrete Research*, V. 41, No. 5, pp. 510–519, 2011.
- [39] Kunchariyakun K, Asavapisit S, Sinyoung S, “Influence of partial sand replacement by black rice husk ash and bagasse ash on properties of autoclaved aerated concrete under different temperatures and times,” *Construction and Building Materials*, V. 173, pp. 220–227, 2018.
- [40] Shams T, Schober G, Heinz D, Seifert S, “Production of autoclaved aerated concrete with silica raw materials of a higher solubility than quartz Part II: Influence of autoclaving temperature,” *Construction and Building Materials*, V. 287, pp. 1–9, 2021.
- [41] Hauser A, Eggenberger U, Mumenthaler T, “Fly ash from cellulose industry as secondary raw material in autoclaved aerated concrete,” *Cement and Concrete Research*, V. 29, No. 3, pp. 297–302, 1999.
- [42] Drabik M, Balkovic S, Peteja M, “Durability of autoclaved aerated concrete produced from fluidized fly ash,” In *5th International Conference on Autoclaved Aerated Concrete "Securing a Sustainable Future"*, D. Boroński, ed., University of Technology and Life Sciences Press, pp. 433–441, 2011.
- [43] F Pospisil, J Jambor, J Belko, “Unit weight reduction of fly ash aerated concrete,” In *Advances in Autoclaved Aerated concrete*, Witmann FH, ed., Balkema, Zurich, pp. 43–52, 1992.
- [44] Walczak P, Szymański P, Różycka A, “Autoclaved Aerated Concrete based on Fly Ash in Density 350kg/m³ as an Environmentally Friendly Material for Energy - Efficient Constructions,” *Procedia Engineering*, V. 122, pp. 39–46, 2015.
- [45] Pietersen HS, “Reactivity of Fly Ash and Slag in Cement,” Delft University of Technology, Delft, The Netherlands.
- [46] Shams T, Schober G, Heinz D, Seifert S, “Production of autoclaved aerated concrete with silica raw materials of a higher solubility than quartz part I: Influence of calcined diatomaceous earth,” *Construction and Building Materials*, V. 272, 2021.

- [47] Aroni S, "On energy conservation characteristics of autoclaved aerated concrete," *Materials and Structures*, V. 23, No. 1, pp. 68–77, 1990.
- [48] Frey E, Briesemann D, "Neuere Berechnungen zum Primärenergieinhalt von Gasbeton," *Betonwerk+Fertigteil-Technik*, V. 51, No. 7, pp. 468–472, 1985.
- [49] Ankele K, Steinfeldt M, "Ökobilanz für typische YTONG-Produktanwendungen," Institut für ökologische Wirtschaftsforschung, Berlin, 1996, 3-932092-01-5.
- [50] Thomas BS, "Green concrete partially comprised of rice husk ash as a supplementary cementitious material – A comprehensive review," *Renewable and Sustainable Energy Reviews*, V. 82, pp. 3913–3923, 2018.
- [51] Sadrul A, Ahiduzzam M, "Green Electricity from Rice Husk: A Model for Bangladesh," In *Thermal Power Plants - Advanced Applications*, M. Rasul, ed., InTech, pp. 127–141, 2013.
- [52] Kang SH, Hong SG, Moon J, "The use of rice husk ash as reactive filler in ultra-high performance concrete," *Cement and Concrete Research*, V. 115, pp. 389–400, 2019.
- [53] Venkatanarayanan H, Rangaraju P, "Effect of grinding of low-carbon rice husk ash on the microstructure and performance properties of blended cement concrete," *Cement and Concrete Composites*, V. 55, pp. 348–363, 2015.
- [54] Weretevsckaja I, Sudelainen N, "Extension of the range of primary materials for the production of AAC," In *Advances in Autoclaved Aerated concrete*, Witmann FH, ed., Balkema, Zurich, 1992.
- [55] Hums D, "Ecological aspects for the production and use of autoclaved aerated concrete," In *Advances in Autoclaved Aerated concrete*, Witmann FH, ed., Balkema, Zurich, 1992.
- [56] Givi NA, Rashid SA, Aziz FNA, Salleh MAM, "Assessment of the effects of rice husk ash particle size on strength, water permeability and workability of binary blended concrete," *Construction and Building Materials*, V. 24, No. 11, pp. 2145–2150, 2010.
- [57] Zhang MH, Malhotra VM, "High-performance concrete incorporating rice husk ash as a supplementary cementing material," *ACI materials journal*, V. 93, No. 6, pp. 629–636, 1996.
- [58] Cordeiro GC, Filho RDT, Fairbairn EMR, "Use of ultrafine rice husk ash with high-carbon content as pozzolan in high performance concrete," *Materials and Structures*, V. 42, No. 7, pp. 983–992, 2009.
- [59] Salas A, Delvasto S, Gutierrez RM, Lange D, "Comparison of two processes for treating rice husk ash for use in high performance concrete," *Cement and Concrete Research*, V. 39, No. 9, pp. 773–778, 2009.
- [60] Chao-Lung H, Anh-Tuan BL, Chun-Tsun C, "Effect of rice husk ash on the strength and durability characteristics of concrete," *Construction and Building Materials*, V. 25, pp. 3768–3772, 2011.
- [61] Zerbino R, Giaccio G, Isaia GC, "Concrete incorporating rice-husk ash without processing," *Construction and Building Materials*, V. 25, No. 1, pp. 371–378, 2011.
- [62] Sensale GR, "Strength development of concrete with rice-husk ash," *Cement and Concrete Composites*, V. 28, No. 2, pp. 158–160, 2006.
- [63] Kunchariyakun K, Asavapisit S, Sombatsompop K, "Properties of autoclaved aerated concrete incorporating rice husk ash as partial replacement for fine aggregate," *Cement and Concrete Composites*, V. 55, pp. 11–16, 2015.
- [64] Mitsuda T, "Influence of Starting Materials on the Hydrothermal Reaction in the CaO–SiO₂–H₂O System" *Ganseki Kobutsu Kosho Gakkaishi*, V. 3, pp. 317–329, 1982.
- [65] Assarsson GO, "Hydrothermal Reactions between Calcium Hydroxide and amorphous Silica: The Reactions between 180 and 220°," *The Journal of Physical Chemistry*, V. 61, No. 4, pp. 473–479, 1957.
- [66] DIN EN 772-1, *Prüfverfahren für Mauersteine – Teil 1: Bestimmung der Druckfestigkeit*, 2016.
- [67] Cabrillac R, Fiorio B, Beaucour A, Dumontet H, Ortola S, "Experimental study of the mechanical anisotropy of aerated concretes and of the adjustment parameters of the introduced porosity," *Construction and Building Materials*, V. 20, No. 5, pp. 286–295, 2006.
- [68] Trunk B, Schober G, Helbling AK, Wittmann FH, "Fracture mechanics parameters of autoclaved aerated concrete," *Cement and Concrete Research*, V. 29, No. 6, pp. 855–859, 1999.
- [69] Bish DL, Howard SA, "Quantitative phase analysis using the Rietveld method," *J Appl Crystallogr*, V. 21, No. 2, pp. 86–91, 1988.
- [70] Snellings R, Bazzoni A, Scrivener K, "The existence of amorphous phase in Portland cements: Physical factors affecting Rietveld quantitative phase analysis," *Cement and Concrete Research*, V. 59, pp. 139–146, 2014.
- [71] Zhao P, Lu L, Liu X, La Torre A de, Cheng X, "Error Analysis and Correction for Quantitative Phase Analysis Based on Rietveld-Internal Standard Method: Whether the Minor Phases Can Be Ignored?," *Crystals*, V. 8, No. 3, p. 110, 2018.
- [72] Środoń J, "Quantitative X-Ray Diffraction Analysis of Clay-Bearing Rocks from Random Preparations," *Clays Clay Miner.*, V. 49, No. 6, pp. 514–528, 2001.

- [73] DIN EN 680, *Bestimmung des Schwindens von dampfgehärtetem Porenbeton; Deutsche Fassung EN 680:2005*, 2005.
- [74] Straube B, Schoch T, “The durability of autoclaved aerated concrete, Dauerhaftigkeit von Porenbeton,” *Mauerwerk*, V. 18, 3/4, pp. 239–245, 2014.
- [75] Tada S, “Pore structure and moisture characteristics of porous inorganic building materials,” In *Advances in Autoclaved Aerated concrete*, Witmann FH, ed., Balkema, Zurich, pp. 53–63, 1992.
- [76] Chen JJ, Thomas JJ, Taylor HWF, Jennings HM, “Solubility and structure of calcium silicate hydrate,” *Cement and Concrete Research*, V. 34, No. 9, pp. 1499–1519, 2004.
- [77] Richardson I, “Tobermorite/jennite- and tobermorite/calcium hydroxide-based models for the structure of C-S-H: applicability to hardened pastes of tricalcium silicate, β -dicalcium silicate, Portland cement, and blends of Portland cement with blast-furnace slag, metakaolin, or silica fume,” *Cement and Concrete Research*, V. 34, pp. 1733–1777, 2004.
- [78] Sakiyama M, Oshio Y, Mitsuda T, “Influence of gypsum on the hydrothermal reaction of lime-quartz system and on the strength of autoclaved calcium silicate product,” *Journal of the Society of Inorganic Materials*, V. 7, pp. 685–691, 2000.
- [79] van Driessche AES, Stawski TM, Kellermeier M, “Calcium sulfate precipitation pathways in natural and engineered environments,” *Chemical Geology*, V. 530, No. 119274, 2019.
- [80] Schmid Th, Jungnickel R, Dariz P, “Insights into the CaSO₄–H₂O System: A Raman-Spectroscopic Study,” *Minerals*, V. 10, No. 115, pp. 1–35, 2020.
- [81] Wongkeo W, Chaipanich A, “Compressive strength, microstructure and thermal analysis of autoclaved and air cured structural lightweight concrete made with coal bottom ash and silica fume, 527 (2010) 3676–3684,” *Materials Science and Engineering: A*, V. 527, 16-17, pp. 3676–3684, 2010.
- [82] Papatzani S, Paine K, Calabria-Holley J, “A comprehensive review of the models on the nanostructure of calcium silicate hydrates,” *Construction and Building Materials*, V. 74, pp. 219–234, 2015.
- [83] Tada S, Nakano S, “Microstructural approach to properties of moist cellular concrete,” In *Autoclaved Aerated Concrete, Moisture and Properties*, Witmann FH, ed., Elsevier, Amsterdam, pp. 71–89, 1983.
- [84] Rudolph C, JR, Valore JR, “Cellular Concretes Part 2 Physical Properties,” *Journal Proceedings*, V. 50, No. 6, pp. 817–836, 1954.
- [85] Schubert P., “Shrinkage behaviour of aerated concrete,” In *Autoclaved Aerated Concrete, Moisture and Properties*, Witmann FH, ed., Elsevier, Amsterdam, pp. 207–217, 1983.
- [86] Ziembika H, “Effect of micropore structure on cellular concrete shrinkage,” *Cement and Concrete Research*, V. 7, pp. 323–332, 1977.
- [87] Georgiades A, Ftikos Ch, Marinos J, “Effect of micropore structure on autoclaved aerated concrete shrinkage,” *Cement and Concrete Research*, V. 21, pp. 655–662, 1991.
- [88] Ramamurthy K, Narayanan N, “Influence of composition and curing on drying shrinkage of aerated concrete,” *Materials and Structures*, V. 33, pp. 243–250, 2000.

B

Permission to Reprint Figures in Chapter 2

Permission request

To: Dr.-Ing. Georg Schober

I am the author of a thesis entitled: Production of autoclaved aerated concrete with silica raw materials of a higher solubility than quartz which will be submitted to the central online platform for doctoral candidates at the Technical University of Munich DocGS and will be published electronically on mediaTUM.

I hereby request non-exclusive, perpetual, worldwide rights to reprint the following images in all formats including print and online and in all subsequent editions, any derivative products, and in publisher-authorised distribution by third-party aggregators and other licensees. A full acknowledgment will be given.

Image 1:



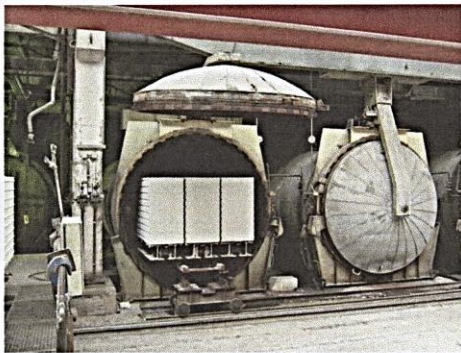
Image 2:



Image 3:



Image 4:



Thank you for your prompt attention to this request.

Yours faithfully,

Taban Shamshejani

I hereby grant permission to use the images requested above

Signature: *Jeany Schich*

Date: *07.06.2022*

List of Figures

Figure 2.1 Casting the AAC mixture into the molds. This figure is reprinted with permission from Schober [72].	6
Figure 2.2 Storing the AAC mixture. This figure is reprinted with permission from Schober [72].	7
Figure 2.3 Demolding (left) and cutting (right) the AAC green cake. This figure is reprinted with permission from Schober [72].	8
Figure 2.4 Removing the AAC blocks out of the autoclave. This figure is reprinted with permission from Schober [72].	8
Figure 2.5 Phase transformation during different steps of the AAC production process [81, 21].	12
Figure 2.6 Variations in peak intensities of main phases formed in AAC during the autoclaving process. T: tobermorite; P: portlandite; Q: quartz; MS: monosulfate; KA: katoite; HE: hydroxyllellstadite; A: anhydrite; C-S-H: non-crystalline calcium silicate hydrate. [75].	12
Figure 2.7 Porous structure of AAC, (a: eye observation of pores on the surface of AAC, line: 4 cm), (b: SEM image of pores on the surface of AAC, line: 200 μm), (c: SEM image of pore wall, line: 50 μm), (d: SEM image of tobermorite crystals formed on the wall of the pore, line: 10 μm).	13
Figure 2.8 Schematic representation of the air pores and the solid structure. This figure is reprinted with permission from Schober [73].	14
Figure 2.9 Influence of the autoclaving process on the specific surface area of AAC [21].	18
Figure 2.10 Stress-strain curves of the AAC samples with a loading direction of parallel and perpendicular to expanding direction [21].	20
Figure 2.11 Solubility of amorphous silica and quartz in water at different temperatures (modified from source [136]).	22
Figure 2.12 Stability ranges of different synthesized C-S-H phases under the saturated steam condition as a function of temperature and C/S of initial synthesized C-S-H gels (modified from source [137]). Pt: portlandite; Rh: pure reinhardbraunsite; H: H ₂ O; X: xonotlite, C-S-H (G): gyrolite-gel, C-S-H (F): faujasite-gel.	24
Figure 2.13 Reaction pathway of quartz and amorphous silica with calcium hydroxide at the autoclaving temperature of 175 °C (modified from source [53]).	26
Figure 3.1 Silica materials used in this study. From left to right, quartz sand, C-DE, and RHA.	36
Figure 3.2 Comparison of the particle size distribution of silica raw materials.	38
Figure 3.3 XRD pattern of quartz sand, C-DE, and RHA.	39
Figure 3.4 SEM micrographs of quartz sand.	40
Figure 3.5 SEM micrographs of C-DE.	40
Figure 3.6 SEM micrographs of RHA.	40
Figure 3.7 The mixing process. This figure is reprinted from Fraunhofer IBP archive.	42
Figure 3.8 From left to right, molding, rising to the final volume, and demolding.	43
Figure 3.9 The autoclave used in this study. The left figure is reprinted from Fraunhofer IBP archive.	43
Figure 3.10 AAC cubes after the cutting process.	44
Figure 3.11 Expansion crack which was observed in the samples.	45

Figure 3.12 Measuring the compressive strength with Zwick Roell Z 100.....	45
Figure 3.13 D2 Phaser diffractometer (from Bruker) which was used to record XRD patterns.	46
Figure 3.14 Phenom Pro X, used to examine the microstructure of samples.....	48
Figure 3.15 SEM sputter coater.	48
Figure 3.16 Malvern Mastersizer 3000, used for determination of particle size for powders.	49
Figure 3.17 AAC prisms for measuring shrinkage (left). Marking measuring points on prisms (right).	49
Figure 3.18 Conditioning AAC prisms in water with a temperature of 20 ± 2 °C for 72 h.	50
Figure 3.19 First measurements of length (L_{c0}).....	50
Figure 4.1 Variation of the relative change in length (ϵ_{csi}) with time for AAC samples autoclaved under the typical condition (192 °C, 9 h) during storage at a temperature of 20 ± 2 °C and relative humidity of 45 ± 5 %.....	56

List of Tables

Table 2.1 The pores volume and the total porosity of AAC with different bulk densities [21].	15
Table 2.2 Relative rate of dissolution for different forms of silica in water at a temperature of 25 °C and a pH of 8.5 [133].	23
Table 2.3 Overview of research studies on the behavior of different silica materials in the lime-silica system (red) and AAC mixture (blue).	30
Table 3.1 Chemical composition of raw materials (wt. %).	38
Table 3.2 Physical properties of raw materials.	38
Table 3.3 Particle size distribution of silica materials.	38
Table 3.4 Amorphous and crystalline content of quartz sand, C-DE, and RHA.	39
Table 3.5 Mix proportions of AAC samples (wt. %).	41
Table 3.6 Measurement parameters used for determination of the compressive strength.	46
Table 3.7 Measurement parameters and settings of the Bruker D2 phaser diffractometer.	47
Table 3.8 PDF number of compounds used for phase identification.	47
Table 4.1 Absolute contents (wt. %) of main phases existing in AAC samples autoclaved under the typical autoclaving condition (192 °C, 9 h). The results were determined by Rietveld refinement using the internal standard method. Standard deviations of the measurement which was repeated 3 times per specimen are given in parentheses.	54
Table 4.2 Characteristic properties of AAC samples under the typical autoclaving condition (192 °C, 9 h). Values in parentheses represent standard deviations of repeated samples.	55
Table 4.3 Absolute contents (wt. %) of main phases existing in the R100 mix autoclaved at different temperatures. The results were determined by Rietveld refinement using the internal standard method. Standard deviations of the measurements which were repeated 3 times per specimen are given in parentheses.	58
Table 4.4 Absolute contents (wt. %) of main phases existing in the Q100 mix autoclaved at different temperatures. The results were determined by Rietveld refinement using the internal standard method. Standard deviations of the measurements which were repeated 3 times per specimen are given in parentheses.	59
Table 4.5 Characteristic properties of AAC samples at autoclaving temperatures of 192 °C and 165 °C. Values in parentheses represent standard deviations of repeated samples.	61

References

- [1]. Qu X, Zhao X, “Previous and present investigations on the components, microstructure and main properties of autoclaved aerated concrete – A review,” *Constr. Build. Mater.*, V. 135, pp. 505–516, 2017, DOI: <https://doi.org/10.1016/j.conbuildmat.2016.12.208>.
- [2]. Karakurt C, Kurama H, Topcu IB, “Utilization of natural zeolite in aerated concrete production,” *Cement and Concrete Composites*, V. 32, No. 1, pp. 1–8, 2010, DOI: <https://doi.org/10.1016/j.cemconcomp.2009.10.002>.
- [3]. Wittmann FH, “Advances in Autoclaved Aerated Concrete,” Proceedings of the 3rd RILEM international symposium, Balkema, Zurich, Zürich. 14-16 October, 1992.
- [4]. Lutter J, “New research on the primary energy content of building materials,” In: *Advances in Autoclaved Aerated Concrete*, Wittmann FH, ed., Balkema, Zurich, pp. 277–282, 1992.
- [5]. Mukesh C, Limbachiya MC, Roberts JJ, “Autoclaved Aerated Concrete, Innovation and Development,” 4th International Conference on Autoclaved Aerated Concrete-Innovation and Development, Taylor & Francis Group, London, 8 pp., Kingston University, London. Jan, 2005.
- [6]. Nunez E, Nunez SA, Fouad, FH, “Sustainability in Autoclaved Aerated Concrete (AAC) construction,” In: *Autoclaved Aerated Concrete, Innovation and Development*, C. Mukesh, M. C. Limbachiya, and J. J. Roberts, eds., Taylor & Francis Group, London, pp. 531–537, 2005.
- [7]. Aroni S, “On energy conservation characteristics of autoclaved aerated concrete,” *Materials and Structures*, V. 23, No. 1, pp. 68–77, 1990, DOI: <https://doi.org/10.1007/BF02472999>.
- [8]. Frey E, Briesemann D, “Neuere Berechnungen zum Primärenergieinhalt von Gasbeton,” *Betonwerk+ Fertigteil-Technik*, V. 51, No. 7, pp. 468–472, 1985.
- [9]. Ankele K, Steinfeldt M, “Ökobilanz für typische YTONG-Produktanwendungen,” Institut für ökologische Wirtschaftsforschung, Berlin, 1996, ISBN: 3-932092-01-5.
- [10]. Gallon N KJ, “Ökobilanz Porenbeton,” 33 pp., 2006.
- [11]. Narayanan N, Ramamurthy K, “Structure and properties of aerated concrete: a review,” *Cem. Concr. Composites*, V. 22, No. 5, pp. 321–329, 2000, DOI: [https://doi.org/10.1016/S0958-9465\(00\)00016-0](https://doi.org/10.1016/S0958-9465(00)00016-0).
- [12]. Isu N, Ishida H, Mitsuda T, “Influence of quartz particle size on the chemical and mechanical properties of autoclaved aerated concrete (I) tobermorite formation,” *Cement and Concrete Research*, V. 25, No. 2, pp. 243–248, 1995.
- [13]. Carroll RA, “Hydrothermal performance of pulverised fuel ash and the manufacture of autoclaved aerated concrete,” (Doctoral dissertation, © Robert A. Carroll), 1996.
- [14]. Pytlik E, Saxena J, “Autoclaved cellular concrete: the building material for the 21st Century,” Proceedings of the 3rd RILEM International Symposium on Autoclaved aerated Concrete, Switzerland. 14-16 October, 1992.
- [15]. Boroński D, “5th International Conference on Autoclaved Aerated Concrete "Securing a Sustainable Future",” 5th International Conference on Autoclaved Aerated Concrete, University of Technology and Life Sciences Press, Bydgoszcz, Poland. September, 14-17, 2011.
- [16]. Hellers BG, Schmidt BR, “Autoclaved aerated concrete (AAC)-the story of a low-weight material,” In: *5th International Conference on Autoclaved Aerated Concrete*

"Securing a Sustainable Future", D. Boroński, ed., University of Technology and Life Sciences Press, pp. 63–71, 2011.

[17]. Bonakdar A, Babbitt F, Mobasher B, "Physical and mechanical characterization of Fiber-Reinforced Aerated Concrete (FRAC)," *Cement and Concrete Composites*, V. 38, pp. 82–91, 2013, DOI: <https://doi.org/10.1016/j.cemconcomp.2013.03.006>.

[18]. Pehlivanlı ZO, Uzun İ, Demir İ, "Mechanical and microstructural features of autoclaved aerated concrete reinforced with autoclaved polypropylene, carbon, basalt and glass fiber," *Construction and Building Materials*, V. 96, pp. 428–433, 2015, DOI: <https://doi.org/10.1016/j.conbuildmat.2015.08.104>.

[19]. Pehlivanlı ZO, Uzun İ, Yücel ZP, Demir İ, "The effect of different fiber reinforcement on the thermal and mechanical properties of autoclaved aerated concrete," *Construction and Building Materials*, V. 112, pp. 325–330, 2016, DOI: <https://doi.org/10.1016/j.conbuildmat.2016.02.223>.

[20]. Aroni S, Groot GJ, Robinson MJ, Svanholm G, Wittman FH, "Autoclaved Aerated Concrete - Properties, Testing and Design: RILEM Recommended Practice RILEM Technical Committees 78-MCA and 51-ALC E," Taylor & Francis, 2004.

[21]. Schober G, "The most important aspects of microstructure influencing strength of AAC," In: *Autoclaved Aerated Concrete, Innovation and Development*, C. Mukesh, M. C. Limbachiya, and J. J. Roberts, eds., Taylor & Francis Group, London, pp. 145–153, 2005.

[22]. Schober G, "Chemical transformations during the manufacturing of autoclaved aerated concrete (ACC): Cement, lime, gypsum and quartz sand become cellular concrete: Die chemischen Umsetzungen bei der Herstellung von Porenbeton: Aus Zement, Kalk, Gips und Quarzsand wird Porenbeton," *ZKG international*, V. 58, No. 7, pp. 63–70, 2005.

[23]. Stumm A, "Cement and sulphate free autoclaved aerated concrete," In: *5th International Conference on Autoclaved Aerated Concrete "Securing a Sustainable Future"*, D. Boroński, ed., University of Technology and Life Sciences Press, pp. 375–381, 2011.

[24]. Matsui K, Ogawa A, Kikuma J, Tsunashima M, Ishikawa T, Matsuno S, "Influence of addition of Al compound and gypsum on tobermorite formation in autoclaved aerated concrete studied by in situ X-ray diffraction," 5th International Conference on Autoclaved Aerated Concrete, Cement Wapno Beton, Poland. September 14-17, 2011.

[25]. Kaminskas R, Barauskas I, "Autoclaved aerated concrete waste as a micro-filler for portland cement," *Romanian Journal of Materials*, V. 49, No. 2, pp. 244–250, 2019.

[26]. Schober G, "AAC Compendium Part III: Process technology and raw materials," 2018.

[27]. Weretevskaia I, Sudelainen N, "Extension of the range of primary materials for the production of AAC," In: *Advances in Autoclaved Aerated Concrete*, Wittmann FH, ed., Balkema, Zurich, 1992.

[28]. Hums D, "Ecological aspects for the production and use of autoclaved aerated concrete," In: *Advances in Autoclaved Aerated Concrete*, Wittmann FH, ed., Balkema, Zurich, 1992.

[29]. Hauser A, Eggenberger U, Mumenthaler T, "Fly ash from cellulose industry as secondary raw material in autoclaved aerated concrete," *Cement and Concrete Research*, V. 29, No. 3, pp. 297–302, 1999, DOI: [https://doi.org/10.1016/S0008-8846\(98\)00207-5](https://doi.org/10.1016/S0008-8846(98)00207-5).

[30]. Drabik M, Balkovic S, Peteja M, "Durability of autoclaved aerated concrete produced from fluidized fly ash," In: *5th International Conference on Autoclaved Aerated Concrete "Securing a Sustainable Future"*, D. Boroński, ed., University of Technology and Life Sciences Press, pp. 433–441, 2011.

- [31]. F Pospisil, J Jambor, J Belko, “Unit weight reduction of fly ash aerated concrete,” In: *Advances in Autoclaved Aerated Concrete*, Wittmann FH, ed., Balkema, Zurich, pp. 43–52, 1992.
- [32]. Kurama H, Topcu IB, Karakurt C, “Properties of the autoclaved aerated concrete produced from coal bottom ash,” *Journal of Materials Processing Technology*, V. 209, No. 2, pp. 767–773, 2009, DOI: <https://doi.org/10.1016/j.jmatprotec.2008.02.044>.
- [33]. Valore JR, Rudolph C, “Cellular Concretes Part 1 Composition and Methods of Preparation,” *Journal Proceedings*, V. 50, No. 5, pp. 773–796, 1954, DOI: <https://doi.org/10.14359/11794>.
- [34]. Schober G, “AAC Compendium Part I: Mixture and Green Cake,” 2018.
- [35]. Ramamurthy K, Narayanan N, “Factors influencing the density and compressive strength of aerated concrete,” *Magazine of Concrete Research*, V. 52, No. 3, 2015, DOI: <https://doi.org/10.1680/mac.2000.52.3.163>.
- [36]. Isu N, Teramura S, Ishida H, Mitsuda T, “Mechanical Property Evolution during Autoclaving Process of Aerated Concrete Using Slag: II, Fracture Toughness and Microstructure,” *Journal of the American Ceramic Society*, V. 77, pp. 2093–2096, 1994.
- [37]. Rózycka A, Pichór W, “Effect of perlite waste addition on the properties of autoclaved aerated concrete,” *Construction and Building Materials*, V. 120, pp. 65–71, 2016.
- [38]. Isu N, Teramura S, Ishida H, Mitsuda T, “Influence of quartz particle size on the chemical and mechanical properties of autoclaved aerated concrete (II) fracture toughness, strength and micropore,” *Cement and Concrete Research*, V. 25, No. 2, pp. 249–254, 1995, DOI: [https://doi.org/10.1016/0008-8846\(95\)00004-6](https://doi.org/10.1016/0008-8846(95)00004-6).
- [39]. Mitsuda T, Sasaki K, Ishida H, “Phase evolution during autoclaving process of aerated concrete,” *Journal of the American Ceramic Society*, V. 75, No. 7, pp. 1858–1863, 1992, DOI: <https://doi.org/10.1111/j.1151-2916.1992.tb07208.x>.
- [40]. Alexanderson J, “Relations between structure and mechanical properties of autoclaved aerated concrete,” *Cement and Concrete Research*, V. 9, No. 4, pp. 507–514, 1979, DOI: [https://doi.org/10.1016/0008-8846\(79\)90049-8](https://doi.org/10.1016/0008-8846(79)90049-8).
- [41]. Taylor HFW, “Cement chemistry,” Thomas Telford, 1997, ISBN: ISBN: 0727725920.
- [42]. Chen Y, Chang J, Lai Y, Chou M, “A comprehensive study on the production of autoclaved aerated concrete: Effects of silica-lime-cement composition and autoclaving conditions,” *Construction and Building Materials*, V. 153, pp. 622–629, 2017, DOI: <https://doi.org/10.1016/j.conbuildmat.2017.07.116>.
- [43]. Sato H, Grutzeck M, “Effect of Starting Materials on the Synthesis of Tobermorite | MRS Online Proceedings Library (OPL) | Cambridge Core,” *Material research society*, V. 245, pp. 235–240, 1992.
- [44]. Okada Y, Shimoda M, Mitsuda T, Toraya H, “Synthesis of tobermorite: NMR spectroscopy and analytical electron microscopy,” *Journal of research of the Onoda Cement Company*, V. 42, No. 2, pp. 199–206, 1990.
- [45]. Mitsuda T, “Influence of Starting Materials on the Hydrothermal Reaction in the CaO–SiO₂–H₂O System (in Japanese),” *Ganseki Kobutsu Kosho Gakkaishi*, V. 3, pp. 317–329, 1982.
- [46]. Okada Y, Ishida E. H., Mitsuda T, “²⁹Si NMR spectroscopy of silicate anions in hydrothermally formed CSH,” *Journal of the American Ceramic Society*, V. 77, No. 3, pp. 765–768, 1994.

- [47]. Chan CF, Mitsuda T, “Formation of 11 A Tobermorite from Mixtures of Lime and Colloidal Silica with Quartz,” *Cement and Concrete Research*, V. 8, pp. 135–138, 1978, DOI: [https://doi.org/10.1016/0008-8846\(78\)90001-7](https://doi.org/10.1016/0008-8846(78)90001-7).
- [48]. Chan C, Sakiyama M, Mitsuda T, “Kinetics of the CaO.quartz .H₂O reaction at 120° to 180°C in suspensions,” *Cement and Concrete Research*, V. 8, No. 1, pp. 1–5, 1978.
- [49]. Chen M, Lu L, Wang S, Zhao P, Zhang W, Zhang S, “Investigation on the formation of tobermorite in calcium silicate board and its influence factors under autoclaved curing,” *Construction and Building Materials*, V. 143, pp. 280–288, 2017, DOI: <https://doi.org/10.1016/j.conbuildmat.2017.03.143>.
- [50]. Aitken A, Taylor HFW, “Hydrothermal reactions in lime-quartz pastes,” *Journal of Applied Chemistry*, V. 10, No. 1, pp. 7–15, 1960, DOI: <https://doi.org/10.1002/jctb.5010100104>.
- [51]. Black L, Garbev K, Stemmermann P, Hallam KR, Allen GC, “Characterisation of crystalline C-S-H phases by X-ray photoelectron spectroscopy,” *Cement and Concrete Research*, V. 33, No. 6, pp. 899–911, 2003, DOI: [https://doi.org/10.1016/S0008-8846\(02\)01089-X](https://doi.org/10.1016/S0008-8846(02)01089-X).
- [52]. El-Hemaly SAS, Mitsuda T, Taylor HFW, “Synthesis of normal and anomalous tobermorites,” *Cement and Concrete Research*, V. 7, No. 4, pp. 429–438, 1977.
- [53]. Kalousek G, “Tobermorite and Related Phases in the System CaO-SiO₂-H₂O,” *Journal Proceedings*, V. 51, No. 6, pp. 989–1011, 1955.
- [54]. Kalousek GL, PREBUS AF, “Crystal Chemistry of Hydrated Calcium Silicates: III, Morphology and Other Properties of Tobermorite and Related Phases,” *Journal of the American Ceramic Society*, V. 41, No. 4, pp. 124–132, 1958, DOI: <https://doi.org/10.1111/j.1151-2916.1958.tb13525.x>.
- [55]. Alujević V, Bezjak A, Glasnović A, “Kinetic study of the hydrothermal reaction in CaO-quartz system,” *Cement and Concrete Research*, V. 16, No. 5, pp. 695–699, 1986, DOI: [https://doi.org/10.1016/0008-8846\(86\)90043-8](https://doi.org/10.1016/0008-8846(86)90043-8).
- [56]. Assarsson GO, “Hydrothermal Reactions between Calcium Hydroxide and amorphous Silica: The Reactions between 180 and 220°,” *The Journal of Physical Chemistry*, V. 61, No. 4, pp. 473–479, 1957, DOI: <https://doi.org/10.1021/j150550a020>.
- [57]. Assarsson GO, “Hydrothermal Reactions between Calcium Hydroxide and Amorphous Silica. The Reactions between 120 and 160°,” *The Journal of Physical Chemistry*, V. 62, No. 2, pp. 223–228, 1958, DOI: <https://doi.org/10.1021/j150560a019>.
- [58]. Assarsson G. O., “Hydrothermal Reactions of Calcium Hydroxide-Quartz at 120–220°,” *Journal of Physical Chemistry*, V. 64, No. 3, pp. 328–331, 1960, DOI: <https://doi.org/10.1021/j100832a010>.
- [59]. Dyczek JRL, Taylor HFW, “X-ray determination of tobermorite, quartz and [alpha]-dicalcium silicate hydrate in autoclaved calcium silicate materials,” *Cement and Concrete Research*, V. 1, No. 6, pp. 589–605, 1971, DOI: [https://doi.org/10.1016/0008-8846\(71\)90015-9](https://doi.org/10.1016/0008-8846(71)90015-9).
- [60]. Gabrovsek R, Kurbus B, Lengar Z, “Comparison of unsubstituted and aluminum containing synthetic tobermorite characterized by different methods,” *Cement and Concrete Research*, V. 16, No. 3, pp. 325–332, 1986.
- [61]. Barnes MW SBE, “The chemistry of Al-tobermorite and its coexisting phases at 175 C,” *Special Cements with Advanced Properties*, Material Research Society Symposium Proceedings, Boston, 1989, DOI: <https://doi.org/10.1557/PROC-179-243>.

- [62]. Isu N, Sasaki K, Ishida H, Mitsuda T, “Mechanical Property Evolution during Autoclaving Process of Aerated Concrete Using Slag: I, Tobermorite Formation and Reaction Behavior of Slag,” *Journal of the American Ceramic Society*, V. 77, No. 8, pp. 2088–2092, 1994, DOI: <https://doi.org/10.1111/j.1151-2916.1994.tb07101.x>.
- [63]. Sakiyama M, Mitsuda T, “Hydrothermal reaction between C₁S/H and kaolinite for the formation of tobermorite at 180°C,” *Cement and Concrete Research*, V. 7, No. 6, pp. 681–685, 1977, DOI: [https://doi.org/10.1016/0008-8846\(77\)90051-5](https://doi.org/10.1016/0008-8846(77)90051-5).
- [64]. Komarneni S, Roy R, Roy MD, Fyfe CA, Kennedy GJ, Bothner-By AA, Dadok J, Chesnick AS, “²⁷Al and ²⁹Si magic angle spinning nuclear magnetic resonance spectroscopy of Al-substituted tobermorites,” *Journal of Materials Science*, V. 20, No. 11, pp. 4209–4214, 1985, DOI: <https://doi.org/10.1007/BF00552416>.
- [65]. Black L, Stumm A, Garbev K, Stemmermann P, Hallam KR, Allen GC, “X-ray photoelectron spectroscopy of aluminium-substituted tobermorite,” *Cement and Concrete Research*, V. 35, No. 1, pp. 51–55, 2005, DOI: <https://doi.org/10.1016/j.cemconres.2004.08.005>.
- [66]. Shaw S, Clark SM, Henderson CM, “Hydrothermal formation of the calcium silicate hydrates, tobermorite (Ca₅Si₆O₁₆(OH)₂·4H₂O) and xonotlite (Ca₆Si₆O₁₇(OH)₂): an in situ synchrotron study,” *Chemical Geology*, V. 167, 1-2, pp. 129–140, 2000, DOI: [https://doi.org/10.1016/S0009-2541\(99\)00205-3](https://doi.org/10.1016/S0009-2541(99)00205-3).
- [67]. Mostafa NY, Shaltout AA, Omar H, Abo-El-Enein SA, “Hydrothermal synthesis and characterization of aluminium and sulfate substituted 1.1 nm tobermorites,” *Journal of Alloys and Compounds*, V. 467, 1-2, pp. 332–337, 2009, DOI: <https://doi.org/10.1016/j.jallcom.2007.11.130>.
- [68]. Mitsuda T, Taylor HFW, “Influence of aluminium on the conversion of calcium silicate hydrate gels into 11 Å tobermorite at 90°C and 120°C,” *Cement and Concrete Research*, V. 5, pp. 203–210, 1975.
- [69]. Sakiyama M, Maeshima T, Mitsuda T, “Synthesis and crystal chemistry of Al-substituted 11 Å tobermorite,” *Journal of the Society of Inorganic Materials*, V. 7, pp. 413–419, 2000.
- [70]. Youssef H, Ibrahim D, Komarneni S, Mackenzie KJD, “Synthesis of 11 Å Al-substituted tobermorite from trachyte rock by hydrothermal treatment,” *Ceramics International*, V. 36, pp. 203–209, 2010.
- [71]. Pachideh G, Gholhaki M, “Effect of pozzolanic materials on mechanical properties and water absorption of autoclaved aerated concrete,” *Journal of Building Engineering*, V. 26, Article No.100856, 2019.
- [72]. Schober G, *personal communication*, , Fraunhofer IBP, November 2018.
- [73]. Schober G, “AAC Compendium Part II: Autoclaving and Products,” 2018.
- [74]. Mostafa NY, “Influence of air-cooled slag on physicochemical properties of autoclaved aerated concrete,” *Cement and Concrete Research*, V. 35, No. 7, pp. 1349–1357, 2005, DOI: <https://doi.org/10.1016/j.cemconres.2004.10.011>.
- [75]. Matsui K, Kikuma J, Tsunashima M, Ishikawa T, Matsuno S, Ogawa A, Sato M, “In situ time-resolved X-ray diffraction of tobermorite formation in autoclaved aerated concrete: Influence of silica source reactivity and Al addition,” *Cement and Concrete Research*, V. 41, No. 5, pp. 510–519, 2011, DOI: <https://doi.org/10.1016/j.cemconres.2011.01.022>.
- [76]. Crennan J. M., Dyczek J. R. L., Taylor H.F.W, “Quantitative phase compositions of autoclaved cement-quartz cubes,” *Cement and Concrete Research*, V. 2, No. 3, pp. 277–289, 1972, DOI: [https://doi.org/10.1016/0008-8846\(72\)90070-1](https://doi.org/10.1016/0008-8846(72)90070-1).

- [77]. Grutzeck M, Benesi A, Fanning B, “Silicon-29 Magic Angle Spinning Nuclear Magnetic Resonance Study of Calcium Silicate Hydrates,” *Journal of the American Ceramic Society*, V. 72, No. 4, pp. 665–668, 1989.
- [78]. Mitsuda T, Kiribayashi T, Sasaki K, Ishida H, “Influence of hydrothermal processing on the properties of autoclaved aerated concrete,” In: *Advances in Autoclaved Aerated Concrete*, Wittmann FH, ed., Balkema, Zurich, pp. 11–18, 1992.
- [79]. Kikuma J, “Formation of Autoclaved Aerated Concrete Studied by In Situ X-ray Diffraction under Hydrothermal Condition,” pp. 142–143, 2009.
- [80]. Kikuma J, Tsunashima M, Ishikawa T, Matsuno S, Ogawa A, Matsui K, Sato M, “In Situ Time-Resolved X-Ray Diffraction of Tobermorite Formation Process Under Autoclave Condition,” *J Am Ceram Soc*, V. 93, No. 9, pp. 2667–2674, 2010, DOI: <https://doi.org/10.1111/j.1551-2916.2010.03815.x>.
- [81]. Schober G, “Production of aircrete,” 2012, <http://www.pb-aac.de/atechny.html>.
- [82]. Mitsuda T, Chan CF, “Anomalous tobermorite in autoclaved aerated concrete,” *Cement and Concrete Research*, V. 7, No. 2, pp. 191–194, 1977, DOI: [https://doi.org/10.1016/0008-8846\(77\)90030-8](https://doi.org/10.1016/0008-8846(77)90030-8).
- [83]. Schober G, “Porosity in autoclaved aerated concrete (AAC): A review on pore structure, types of porosity, measurement methods and effects of porosity on properties,” In: *5th International Conference on Autoclaved Aerated Concrete "Securing a Sustainable Future"*, D. Boroński, ed., University of Technology and Life Sciences Press, pp. 351–359, 2011.
- [84]. Kadashevich I, Schneider HJ, Stoyan D, “Statistical modeling of the geometrical structure of the system of artificial air pores in autoclaved aerated concrete,” *Cement and Concrete Research*, V. 35, No. 8, pp. 1495–1502, 2005, DOI: <https://doi.org/10.1016/j.cemconres.2004.10.010>.
- [85]. Ioannou I, Hamilton A, Hall C, “Capillary absorption of water and n-decane by autoclaved aerated concrete,” *Cement and Concrete Research*, V. 38, No. 6, pp. 766–771, 2008, DOI: <https://doi.org/10.1016/j.cemconres.2008.01.013>.
- [86]. Petrov I, Schlegel E, “Application of automatic image analysis for the investigation of autoclaved aerated concrete structure,” *Cement and Concrete Research*, V. 24, No. 5, pp. 830–840, 1994, DOI: [https://doi.org/10.1016/0008-8846\(94\)90003-5](https://doi.org/10.1016/0008-8846(94)90003-5).
- [87]. Thongtha A, Maneewan S, Punlek C, Ungkoon Y, “Investigation of the compressive strength, time lags and decrement factors of AAC-lightweight concrete containing sugar sediment waste,” *Energy and Buildings*, V. 84, pp. 516–525, 2014, DOI: <https://doi.org/10.1016/j.enbuild.2014.08.026>.
- [88]. Wittmann FH, “Autoclaved Aerated Concrete, Moisture, and Properties,” Proceedings of the 2nd RILEM international symposium on on Autoclaved Aerated Concrete, Elsevier, Amsterdam, Switzerland. March 1982, 1983.
- [89]. Tada S, Nakano S, “Microstructural approach to properties of moist cellular concrete,” In: *Autoclaved Aerated Concrete, Moisture, and Properties*, Wittmann FH, ed., Elsevier, Amsterdam, pp. 71–89, 1983.
- [90]. Cabrillac R, Fiorio B, Beaucour A, Dumontet H, Ortola S, “Experimental study of the mechanical anisotropy of aerated concretes and of the adjustment parameters of the introduced porosity,” *Construction and Building Materials*, V. 20, No. 5, pp. 286–295, 2006, DOI: <https://doi.org/10.1016/j.conbuildmat.2005.01.023>.

- [91]. Janz M, “Moisture diffusivities evaluated at high moisture levels from a series of water absorption tests,” *Materials and Structures*, V. 35, No. 3, pp. 141–148, 2002, DOI: <https://doi.org/10.1007/BF02533582>.
- [92]. Kunchariyakun K, Asavapisit S, Sinyoung S, “Influence of partial sand replacement by black rice husk ash and bagasse ash on properties of autoclaved aerated concrete under different temperatures and times,” *Construction and Building Materials*, V. 173, pp. 220–227, 2018, DOI: <https://doi.org/10.1016/j.conbuildmat.2018.04.043>.
- [93]. Comité euro-international du béton, “Autoclaved aerated concrete CEB manual of design and technology,” Construction Press, Lancaster, 1978, ISBN: 0904406768.
- [94]. Bave G, “Aerated light weight concrete-current technology,” Second International Symposium on Lightweight Concretes, London, 1980.
- [95]. Topçu İB, Uygunoğlu T, “Properties of autoclaved lightweight aggregate concrete,” *Building and Environment*, V. 42, No. 12, pp. 4108–4116, 2007, DOI: <https://doi.org/10.1016/j.buildenv.2006.11.024>.
- [96]. Wongkeo W, Chaipanich A, “Compressive strength, microstructure and thermal analysis of autoclaved and air cured structural lightweight concrete made with coal bottom ash and silica fume,” *Materials Science and Engineering: A*, V. 527, 16-17, pp. 3676–3684, 2010, DOI: <https://doi.org/10.1016/j.msea.2010.01.089>.
- [97]. Wongkeo W, Thongsanitgarn P, Pimraksa K, Chaipanich A, “Compressive strength, flexural strength and thermal conductivity of autoclaved concrete block made using bottom ash as cement replacement materials,” *Materials & Design*, V. 35, pp. 434–439, 2012, DOI: <https://doi.org/10.1016/j.matdes.2011.08.046>.
- [98]. Kreft O, Hausmann J, Hubáľková J, Aneziris CG, Straube B, Schoch T, “Pore size distribution effects on the thermal conductivity of light weight autoclaved aerated concrete,” In: *5th International Conference on Autoclaved Aerated Concrete "Securing a Sustainable Future"*, D. Boroński, ed., University of Technology and Life Sciences Press, pp. 257–264, 2011.
- [99]. Ropelewski L, Neufeld RD, “Thermal Inertia Properties of Autoclaved Aerated Concrete,” *Journal of Energy Engineering*, V. 125, No. 2, pp. 59–75, 1999, DOI: [https://doi.org/10.1061/\(ASCE\)0733-9402\(1999\)125:2\(59\)](https://doi.org/10.1061/(ASCE)0733-9402(1999)125:2(59)).
- [100]. Tada S, “Material design of aerated concrete-An optimum performance design,” *Materials and Structures*, V. 19, No. 1, pp. 21–26, 1986.
- [101]. Gawin D, Kosny J, Wilkes K, “Thermal Conductivity of Moist Cellular Concrete-Experimental and Numerical Study,” ASHRAE Thermal IX Conference. 2004, 2004.
- [102]. Jerman M, Keppert M, Výborný J, Černý R, “Hygic, thermal and durability properties of autoclaved aerated concrete,” *Construction and Building Materials*, V. 41, pp. 352–359, 2013, DOI: <https://doi.org/10.1016/j.conbuildmat.2012.12.036>.
- [103]. Yang R, Zhu J, Wu Z, Wu Z, Li M, Peng C, “Thermal insulation and strength of autoclaved light concrete,” *Journal of Wuhan University of Technology-Mater. Sci. Ed.*, V. 26, No. 1, pp. 132–136, 2011, DOI: <https://doi.org/10.1007/s11595-011-0184-6>.
- [104]. Walczak P, Szymański P, Rózycka A, “Autoclaved Aerated Concrete based on Fly Ash in Density 350kg/m³ as an Environmentally Friendly Material for Energy - Efficient Constructions,” *Procedia Engineering*, V. 122, pp. 39–46, 2015, DOI: <https://doi.org/10.1016/j.proeng.2015.10.005>.
- [105]. Hoff GC, “Porosity-strength considerations for cellular concrete,” *Cement and Concrete Research*, V. 2, No. 1, pp. 91–100, 1972.

- [106]. Kondo R, “Autoclaved Calcium Silicate Building Products,” Symposium on Autoclaved Calcium Silicate Building Products, Society of Chemical Industry, London. 18-21 May, 1967.
- [107]. Taylor HFW, “A Review of Autoclaved Calcium Silicates,” In: *Autoclaved Calcium Silicate Building Products*, R. Kondo, ed., Society of Chemical Industry, pp. 195–205, 1967.
- [108]. Schober G, “Effect of size distribution of air pores in AAC on compressive strength,” In: *Advances in Autoclaved Aerated Concrete*, Wittmann FH, ed., Balkema, Zurich, pp. 77–82, 1992.
- [109]. Odler I, Rößler M, “Investigations on the relationship between porosity, structure and strength of hydrated Portland cement pastes. II. Effect of pore structure and of degree of hydration,” *Cement and Concrete Research*, V. 15, No. 3, pp. 401–410, 1985, DOI: [https://doi.org/10.1016/0008-8846\(85\)90113-9](https://doi.org/10.1016/0008-8846(85)90113-9).
- [110]. Schneider T, Greil P, Schober G, “Strength modeling of brittle materials with two- and three-dimensional pore structures,” *Computational Materials Science*, V. 16, 1-4, pp. 98–103, 1999, DOI: [https://doi.org/10.1016/S0927-0256\(99\)00051-8](https://doi.org/10.1016/S0927-0256(99)00051-8).
- [111]. Taylor HF, “Proposed Structure for Calcium Silicate Hydrate Gel,” *Journal of the American Ceramic Society*, V. 69, No. 6, pp. 464–467, 1986.
- [112]. SNELL DS, “Review of Synthesis and Properties of Tobermorite, C-S-H(I), and C-S-H Gel,” *Journal of the American Ceramic Society*, V. 58, 7-8, pp. 292–295, 1975, DOI: <https://doi.org/10.1111/j.1151-2916.1975.tb11478.x>.
- [113]. Plank J, Schönlein M, Kanchanason V, “Study on the early crystallization of calcium silicate hydrate (C-S-H) in the presence of polycarboxylate superplasticizers,” *Journal of Organometallic Chemistry*, V. 869, pp. 227–232, 2018, DOI: <https://doi.org/10.1016/j.jorganchem.2018.02.005>.
- [114]. Kalousek GL, “High Temperature Curing of Concrete under High Pressure,” Proceedings 5th International Symposium on the Chemistry of Cement, Tokyo, 1968.
- [115]. Purton MJ, “The composition of the binding material in calcium silicate bricks,” *Journal of Applied Chemistry and Biotechnology*, V. 23, No. 12, pp. 871–877, 1973, DOI: <https://doi.org/10.1002/jctb.5020231204>.
- [116]. Walker RC, Purton MJ, “Some observations on calcium silicate brick specimens in the autoclave,” *Journal of Applied Chemistry and Biotechnology*, V. 23, No. 12, pp. 879–886, 1973, DOI: <https://doi.org/10.1002/jctb.5020231205>.
- [117]. Zhao Y, Zhang Y, Chen T, Chen Y, Bao S, “Preparation of high strength autoclaved bricks from hematite tailings,” *Construction and Building Materials*, V. 28, No. 1, pp. 450–455, 2012, DOI: <https://doi.org/10.1016/j.conbuildmat.2011.08.078>.
- [118]. Mitra N, Sarkar PK, Prasad D, “Intermolecular dynamics of ultraconfined interlayer water in tobermorite: influence on mechanical performance,” *Physical chemistry chemical physics: PCCP*, V. 21, No. 21, pp. 11416–11423, 2019, DOI: <https://doi.org/10.1039/C9CP01285K>.
- [119]. Mesecke K, “Untersuchungen zur Phasenbildung und Gefügeentwicklung bei der hydrothermalen Härtung von Porenbeton mittels in situ-Röntgendiffraktometrie mit dem Ziel der Sulfatreduzierung und Prozessoptimierung,” 19464 BR / 1, 2020.
- [120]. Sakiyama M, Oshio Y, Mitsuda T, “Influence of gypsum on the hydrothermal reaction of lime-quartz system and on the strength of autoclaved calcium silicate product,” *Journal of the Society of Inorganic Materials*, V. 7, pp. 685–691, 2000, DOI: <https://doi.org/10.11451/mukimate2000.7.685>.

- [121]. Saumann Z, “Die Hydroxylellestadit-Bildung $[Ca_{10}(SiO_4)_3(SO_4)(OH)_2]$ unter den Bedingungen des Hydrothermalprozesses,” International Symposium über die Beziehungen von Eigenschaften von KS-Produkten und den Bindemittelaufbau, Karlsruhe, 1978.
- [122]. Kunchariyakun K, Asavapisit S, Sombatsompop K, “Properties of autoclaved aerated concrete incorporating rice husk ash as partial replacement for fine aggregate,” *Cement and Concrete Composites*, V. 55, pp. 11–16, 2015, DOI: <https://doi.org/10.1016/j.cemconcomp.2014.07.021>.
- [123]. Trunk B, Schober G, Helbling AK, Wittmann FH, “Fracture mechanics parameters of autoclaved aerated concrete,” *Cement and Concrete Research*, V. 29, No. 6, pp. 855–859, 1999, DOI: [https://doi.org/10.1016/S0008-8846\(99\)00059-9](https://doi.org/10.1016/S0008-8846(99)00059-9).
- [124]. Wagner F, Schober G, Mortel H, “Measurement of the gas permeability of autoclaved aerated concrete in conjunction with its physical properties,” *Cement and Concrete Research*, V. 25, No. 8, pp. 1621–1626, 1995, DOI: [https://doi.org/10.1016/0008-8846\(95\)00157-3](https://doi.org/10.1016/0008-8846(95)00157-3).
- [125]. Ramamurthy K, Narayanan N, “Influence of composition and curing on drying shrinkage of aerated concrete,” *Materials and Structures*, V. 33, pp. 243–250, 2000, DOI: <https://doi.org/10.1007/BF02479334>.
- [126]. Straube B, Schoch T, “The durability of autoclaved aerated concrete, Dauerhaftigkeit von Porenbeton,” *Mauerwerk*, V. 18, 3/4, pp. 239–245, 2014, DOI: <https://doi.org/10.1002/dama.201400630>.
- [127]. Schoch T, Straube B, Stumm A, “Dauerhaftigkeit von Porenbeton bei hoher CO₂-Beaufschlagung,” *Bauphysik*, V. 33, No. 5, pp. 318–322, 2011, DOI: <https://doi.org/10.1002/bapi.201110797>.
- [128]. Tada S, “Pore structure and moisture characteristics of porous inorganic building materials,” In: *Advances in Autoclaved Aerated Concrete*, Wittmann FH, ed., Balkema, Zurich, pp. 53–63, 1992.
- [129]. Ziembika H, “Effect of micropore structure on cellular concrete shrinkage,” *Cement and Concrete Research*, V. 7, pp. 323–332, 1977, DOI: [https://doi.org/10.1016/0008-8846\(77\)90095-3](https://doi.org/10.1016/0008-8846(77)90095-3).
- [130]. Georgiades A, Ftikos Ch, Marinos J, “Effect of micropore structure on autoclaved aerated concrete shrinkage,” *Cement and Concrete Research*, V. 21, pp. 655–662, 1991, DOI: [https://doi.org/10.1016/0008-8846\(91\)90116-Y](https://doi.org/10.1016/0008-8846(91)90116-Y).
- [131]. Chucholowski C, Holger M, Thienel K-C, “Improving the recyclability, environmental compatibility, and CO₂ balance of autoclaved aerated concrete by replacing sulfate carrier and cement with calcined clays,” *ce/papers*, V. 2, No. 4, pp. 503–512, 2018, DOI: <https://doi.org/10.1002/cepa.846>.
- [132]. Schober G, “Porenbetonherstellung - Ist-Zustand und mogliche Verbesserungen,” *BFT International*, No. 12, pp. 4–11, 2007.
- [133]. Iler RK, “The Chemistry of Silica: Solubility, Polymerization, Colloid and Surface Properties and Biochemistry of Silica,” Wiley, London, 1979, ISBN: ISBN: 978-0-471-02404-0.
- [134]. Park GA, “Equilibrium Concepts in Natural Water Systems,” Advances in Chemistry Series, American Chemical Society, Washington, DC, 1967.
- [135]. Stoeber W, “Formation of Silicic Acid in Aqueous Suspensions of Different Silica Modifications,” In: *Equilibrium Concepts in Natural Water Systems*, G. A. Park, ed., American Chemical Society, Washington, DC, pp. 161–182, 1967.
- [136]. Gundlach H, “Dampfgehartete Baustoffe,” Wiesbaden, Berlin, 1973.

- [137]. Garbev K, "Struktur, Eigenschaften und quantitative Rietveldanalyse von hydrothermal kristallisierten Calciumsilikathydraten (C-S-H-Phasen)," Dissertation, Universität Heidelberg, Heidelberg, Germany, 2003.
- [138]. Mitsuda T, Toraya H, Okada Y, Shimoda M, "Synthesis of tobermorite: NMR spectroscopy and analytical electron microscopy," *Ceramic Transactions*, V. 3, pp. 206–213, 1989.
- [139]. Walczak P, Szymański P, Różycka A, "Autoclaved Aerated Concrete based on Fly Ash in Density 350kg/m³ as an Environmentally Friendly Material for Energy - Efficient Constructions," *Procedia Engineering*, V. 122, pp. 39–46, 2015, DOI: <https://doi.org/10.1016/j.proeng.2015.10.005>.
- [140]. Pietersen HS, "Reactivity of Fly Ash and Slag in Cement," Delft University of Technology, Delft, The Netherlands.
- [141]. Carroll R, Payne J, "Autoclaved cementitious products using pulverised fuel ash," In: *Advances in Autoclaved Aerated Concrete*, Wittmann FH, ed., Balkema, Zurich, pp. 297–304, 1992.
- [142]. Carroll R, Guest J, "The use of pulverised fuel ash for the manufacture of Autoclaved Aerated Concrete," In: *Autoclaved Aerated Concrete, Innovation and Development*, C. Mukesh, M. C. Limbachiya, and J. J. Roberts, eds., Taylor & Francis Group, London, pp. 49–57, 2005.
- [143]. Mostafa NY, "Factors effecting the hydrothermal reactions in CaO– SiO₂–H₂O system," Master thesis, Suez Canal university, Egypt, 1995.
- [144]. Schoch T, "Special Issue ICAAC - 6th International Conference on Autoclaved Aerated Concrete," 6th International Conference on Autoclaved Aerated Concrete, ce/papers, University Potsdam. September 4-6, 2018, DOI: <https://doi.org/10.1002/cepa.841>.
- [145]. Černý V, Drochytka R, Šebestová P, "Options for the implementation of new secondary raw materials in autoclaved aerated concrete," In: *Special Issue ICAAC - 6th International Conference on Autoclaved Aerated Concrete*, Schoch T, ed., ce/papers, pp. 431–437, 2018, DOI: <https://doi.org/10.1002/cepa.841>.
- [146]. Wang C, Ni W, Zhang S, Wang S, Gai G, Wang W, "Preparation and properties of autoclaved aerated concrete using coal gangue and iron ore tailings," *Construction and Building Materials*, V. 104, pp. 109–115, 2016.
- [147]. Song Y, Li B, Yang E, Liu Y, Ding T, "Feasibility study on utilization of municipal solid waste incineration bottom ash as aerating agent for the production of autoclaved aerated concrete," *Cement and Concrete Composites*, V. 56, pp. 51–58, 2015.
- [148]. Reka AA, Pavlovski B, Makreski P, "New optimized method for low-temperature hydrothermal production of porous ceramics using diatomaceous earth," *Ceramics International*, V. 43, No. 15, pp. 12572–12578, 2017, DOI: <https://doi.org/10.1016/j.ceramint.2017.06.132>.
- [149]. Gock E, Vogt V, Leußner T, Hoops G, Knauf H, "Mineralische Nebenprodukte und Abfälle: Einführung des Recyclings von Kieselgur in die Praxis der Bierherstellung," Thomé-Kozmiensky Verlag GmbH, Neuruppin, Germany, 2014, ISBN: 978-3944310114.
- [150]. Leußner T, Gock E, "Recycling von Kieselgur-Filterschlämmen aus Brauereien mithilfe von Mini-Hydrozyklonen," *wlb – Wasser, Luft, Boden*, V. 6, pp. 44–47, 2004.
- [151]. Leußner T, "Recycling von Kieselgur-Filterschlämmen aus der Brauindustrie," Dissertation, Technical University of Clausthal, Germany, 2007.

- [152]. Finis P, Galaske H, “Recycling von Brauerei-Filterhilfsmitteln – Tremonis-Verfahren bewährt sich in NRW,” *Sonderdruck aus Brauwelt*, No. 49, pp. 2332–2347, 1988.
- [153]. Ackermann (Rice husk ash supplier) A, *personal communication*, , via email, January 2022.
- [154]. Thomas BS, “Green concrete partially comprised of rice husk ash as a supplementary cementitious material – A comprehensive review,” *Renewable and Sustainable Energy Reviews*, V. 82, pp. 3913–3923, 2018, DOI: <https://doi.org/10.1016/j.rser.2017.10.081>.
- [155]. Rasul M, “Thermal Power Plants - Advanced Applications,” InTech, 2013, ISBN: 978-953-51-1095-8.
- [156]. Sadrul A, Ahiduzzam M, “Green Electricity from Rice Husk: A Model for Bangladesh,” In: *Thermal Power Plants - Advanced Applications*, M. Rasul, ed., InTech, pp. 127–141, 2013, DOI: <https://doi.org/10.5772/55224>.
- [157]. Kang SH, Hong SG, Moon J, “The use of rice husk ash as reactive filler in ultra-high performance concrete,” *Cement and Concrete Research*, V. 115, pp. 389–400, 2019, DOI: <https://doi.org/10.1016/j.cemconres.2018.09.004>.
- [158]. Venkatanarayanan H, Rangaraju P, “Effect of grinding of low-carbon rice husk ash on the microstructure and performance properties of blended cement concrete,” *Cement and Concrete Composites*, V. 55, pp. 348–363, 2015, DOI: <https://doi.org/10.1016/j.cemconcomp.2014.09.021>.
- [159]. DIN 66137-2, “Determination of solid state density - Part 2: Gaspycnometry: Bestimmung der Dichte fester Stoffe - Teil 2: Gaspyknometrie,” 2019.
- [160]. Bruker AXS GmbH, “DIFFRAC.EVA Tutorial,” 2013.
- [161]. Bruker AXS GmbH, “TOPAS Tutorial,” 2016.
- [162]. Aono Y, Shibata S, Matsushita F, “Mechanisms and countermeasures against cavity defectives in AAC during manufacturing,” In: *Autoclaved Aerated Concrete, Innovation and Development*, C. Mukesh, M. C. Limbachiya, and J. J. Roberts, eds., Taylor & Francis Group, London, 2005.
- [163]. DIN EN 772-1, “Prüfverfahren für Mauersteine – Teil 1: Bestimmung der Druckfestigkeit,” 29 pp., 2016.
- [164]. Bish DL, Howard SA, “Quantitative phase analysis using the Rietveld method,” *J Appl Crystallogr*, V. 21, No. 2, pp. 86–91, 1988, DOI: <https://doi.org/10.1107/S0021889887009415>.
- [165]. Snellings R, Bazzoni A, Scrivener K, “The existence of amorphous phase in Portland cements: Physical factors affecting Rietveld quantitative phase analysis,” *Cement and Concrete Research*, V. 59, pp. 139–146, 2014, DOI: <https://doi.org/10.1016/j.cemconres.2014.03.002>.
- [166]. Zhao P, Lu L, Liu X, La Torre A de, Cheng X, “Error Analysis and Correction for Quantitative Phase Analysis Based on Rietveld-Internal Standard Method: Whether the Minor Phases Can Be Ignored?,” *Crystals*, V. 8, No. 3, p. 110, 2018, DOI: <https://doi.org/10.3390/cryst8030110>.
- [167]. Środoń J, “Quantitative X-Ray Diffraction Analysis of Clay-Bearing Rocks from Random Preparations,” *Clays Clay Miner.*, V. 49, No. 6, pp. 514–528, 2001, DOI: <https://doi.org/10.1346/CCMN.2001.0490604>.
- [168]. DIN EN 680, “Bestimmung des Schwindens von dampfgehärtetem Porenbeton; Deutsche Fassung EN 680:2005,” 2005.
- [169]. DIN EN 772-13, “Prüfverfahren für Mauersteine Teil 13: Bestimmung der Netto- und Brutto-Trockenrohichte von Mauersteinen (außer Natursteinen),” 6 pp., 2000.

- [170]. Chen JJ, Thomas JJ, Taylor HWF, Jennings HM, “Solubility and structure of calcium silicate hydrate,” *Cement and Concrete Research*, V. 34, No. 9, pp. 1499–1519, 2004, DOI: <https://doi.org/10.1016/j.cemconres.2004.04.034>.
- [171]. Richardson I, “Tobermorite/jennite- and tobermorite/calcium hydroxide-based models for the structure of C-S-H: applicability to hardened pastes of tricalcium silicate, β -dicalcium silicate, Portland cement, and blends of Portland cement with blast-furnace slag, metakaolin, or silica fume,” *Cement and Concrete Research*, V. 34, pp. 1733–1777, 2004, DOI: <https://doi.org/10.1016/j.cemconres.2004.05.034>.
- [172]. Nonat A, “The structure and stoichiometry of C-S-H,” *Cement and Concrete Research*, V. 34, No. 9, pp. 1521–1528, 2004.
- [173]. H. Weber HH, “Porenbeton Handbuch,” Aufl. Bauverlag, 2002, ISBN: 978-3762535201.
- [174]. Isu N, Ishida H, Mitsuda T, “Influence of quartz particle size on the chemical and mechanical properties of autoclaved aerated concrete (I) tobermorite formation,” *Cem. Concr. Res.*, V. 25, No. 2, pp. 243–248, 1995, DOI: [https://doi.org/10.1016/0008-8846\(95\)00003-8](https://doi.org/10.1016/0008-8846(95)00003-8).
- [175]. Rudolph C, JR, Valore JR, “Cellular Concretes Part 2 Physical Properties,” *Journal Proceedings*, V. 50, No. 6, pp. 817–836, 1954.
- [176]. Schubert P., “Shrinkage behavior of aerated concrete,” In: *Autoclaved Aerated Concrete, Moisture, and Properties*, Wittmann FH, ed., Elsevier, Amsterdam, pp. 207–217, 1983.